EFFECTS OF ANTHROPOGENIC EMISSIONS ON BIOGENIC ORGANIC AEROSOL FORMATION IN THE SOUTHEASTERN UNITED STATES

A Dissertation
Presented to
The Academic Faculty

by

Lu Xu

In Partial Fulfillment
of the Requirements for the Degree
Doctor of Philosophy in the
School of Chemical and Biomolecular Engineering

Georgia Institute of Technology
August 2016

EFFECTS OF ANTHROPOGENIC EMISSIONS ON BIOGENIC ORGANIC AEROSOL FORMATION IN THE SOUTHEASTERN UNITED STATES

Approved by:

Dr. Nge Lee Ng, Advisor
School of Chemical and Biomolecular Engineering and School of Earth and Atmospheric Sciences
Georgia Institute of Technology

Dr. Athanasios Nenes
School of Earth and Atmospheric Sciences and School of Chemical and Biomolecular Engineering
Georgia Institute of Technology

Dr. Christopher W. Jones
School of Chemical and Biomolecular Engineering and School of Chemistry and Biochemistry
Georgia Institute of Technology

Dr. Rodney J. Weber
School of Earth and Atmospheric Sciences
Georgia Institute of Technology

Dr. Greg Huey
School of Earth and Atmospheric Sciences
Georgia Institute of Technology

Date Approved: May 24, 2016

To my family

ACKNOWLEDGEMENTS

Firstly, I would like to sincerely thank my advisor, Dr. Sally Ng, for her continuous and generous support throughout my graduate study. She introduced me to the field of atmospheric science. More importantly, she taught me every single aspects of research, from operating instruments to writing papers, from communication with collaborators to public presentation. I am also grateful to her for encouraging me to pursue the challenging goals and strive for excellence.

I have been fortunate to collaborate with Dr. Rodney Weber and Dr. Athanasios Nenes, whose expertise in different research areas has largely helped my research and tremendously broadened my view. It is always a pleasure to go to field campaigns with Dr. Weber, whose rich experience makes the stressful projects easier to handle. I would also like to thank my other two thesis committee members, Dr. Greg Huey and Dr. Christopher Jones, for their valuable time and providing career advice.

I acknowledge Ng group members not only for their assistance in my research, but also their company. Chris Boyd is my English and American culture teacher. Javier Sanchez shares his workout tips with me. Wing Tuet makes delicious cookies. Yunle Chen recommends good restaurants. I also would like to thank Weber group, Nenes group, and Huey group members. Thanks especially to Hongyu Guo for being such a wonderful collaborator and great friend.

Finally, I thank my parents for their unconditional love and continuous support. They are always there, patiently listening to me and helping me through the difficulties. I thank my wife Jia, for being my best company and inspiring me from her research expertise. Without them, this work would not have been possible.

TABLE OF CONTENTS

LIST OF TABLES

LIST OF FIGURES

LIST OF SYMBOLS AND ABBREVIATIONS

Symbols

bap_{365}	Light absorption coefficient at 365 nm
BrC	Brown Carbon
CO	Carbon monoxide
CO_2	Carbon dioxide
f_{43}	fraction of organic signal at *m/z* 43
f_{44}	fraction of organic signal at *m/z* 44
H:C	atomic hydrogen to carbon ratio
H^+	hydronium ion
H_2O_{ptcl}	particle phase water
$HO_2•$	Hydroperoxy radical
HSO_4^-	Bisulfate ion
K^+	Potassium ion
NH_4^+	Ammonium ion
NO	Nitrogen monoxide
NO_2	Nitrogen dioxide
$NO_3•$	Nitrate radical
NO_3^-	Nitrate ion
NO_x	Nitrogen Oxides ($NO + NO_2$)
O:C	atomic oxygen to carbon ratio
O_3	Ozone
OH•	Hydroxy radical
Org	Organics
$RO_2•$	Organic peroxy radical
SO_2	Sulfur dioxide
SO_4^{2-}	Sulfate ion
κ	Hygroscopicity parameter

Abbreviations

ACSM	Aerosol Chemical Speciation Monitor
BB	Biomass Burning
BBOA	Biomass Burning Organic Aerosol
BC	Black Carbon
BLH	Boundary Layer Height
BVOC	Biogenic Volatile Organic Compound
CIMS	Chemical Ionization Mass Spectrometer
ClearfLo	Clean Air for London
COA	Cooking Organic Aerosol
CTR	Centreville
EC	Elemental Carbon
GT	Georgia Tech site
HOA	Hydrocarbon-like Organic Aerosol
HR-ToF-AMS	High Resolution Time of Flight Aerosol Mass Spectrometer
HULIS	HUmic-Like Substances
IC	Ion Chromatography
IEPOX	Isoprene-derived epoxydiols
isoprene-OA	Isoprene-derived Organic Aerosol
JST	Jefferson Street site
LO-OOA	Less-Oxidized Oxygenated Organic Aerosol
LV-OOA	Low-Volatility Oxygenated Organic Aerosol
LWC	Liquid Water Content
LWCC	Liquid Waveguide Capillary Cell
MFR	Mass Fraction Remaining
MO-OOA	More-Oxidized Oxygenated Organic Aerosol
$NR\text{-}PM_1$	Non-Refractory particulate matter with aerodynamic diameter less than 1μm
OA	Organic Aerosol
OC	Organic Carbon

OM	Organic Matter
ON	Organic Nitrate
OOA	Oxygenated Organic Aerosol
OS	Oxidation State
PAH	Polycyclic Aromatic Hydrocarbon
PILS	Particle-Into-Liquid Sampler
PM_1	Particulate Matter with aerodynamic diameter less than 1μm
$PM_{2.5}$	Particulate Matter with aerodynamic diameter less than 2.5 μm
PMF	Positive Matrix Factorization
POA	Primary Organic Aerosol
RH	Relative Humidity
RS	Roadside site
SCAPE	Southeastern Center for Air Pollution and Epidemiology study
SEARCH	Southeastern Aerosol Research and Characterization
SENEX	Southeast Nexus
SOA	Secondary Organic Aerosol
SOAS	Southern Oxidant and Aerosol Study
SV-OOA	Semi-Volatile Oxygenated Organic Aerosol
TD	Thermal Denuder
VFR	Volume Fraction Remaining
VOC	Volatile Organic Compound
WSOC	Water-Soluble Organic Carbon
YRK	Yorkville site

SUMMARY

Atmospheric particulate matter (PM) has substantial impacts on climate, air quality, and human health. A substantial fraction of atmospheric PM is constituted of secondary organic aerosol (SOA), which is formed in the atmosphere through the oxidation of volatile organic compounds (VOCs). Formulating strategies to control SOA is highly challenging, in part, because of the numerous sources and complex formation mechanisms of SOA. In particular, to what extent human activities alter SOA formation from biogenic emissions? Although a number of mechanisms about the interactions of anthropogenic and biogenic emissions on SOA formation have been proposed from prior laboratory studies, only a few have been directly observed in the ambient environment. Moreover, the extent of such interactions in the atmosphere is unknown. This question is investigated in depth in this dissertation based on comprehensive ambient measurements and complementary laboratories studies.

The southeastern US is an ideal region to study the effects of anthropogenic emissions on biogenic organic aerosol formation because this region is characterized by large emissions from both biogenic and anthropogenic sources. In this study, we applied a suite of instruments, with a focus on a High-Resolution Time-of-Flight Aerosol Mass Spectrometer (HR-ToF-AMS), to extensively characterize the composition of organic aerosol (OA) in the southeastern United States (US). Multiple measurements were obtained during different seasons at both urban sites (Jefferson Street and Georgia Tech Campus in Georgia) and rural sites (Yorkville in Georgia and Centreville in Alabama), as part of Southeastern Center of Air Pollution and Epidemiology Study (SCAPE) and Southern Oxidant and Aerosol Study (SOAS). Positive Matrix Factorization (PMF) analysis was

performed on the high-resolution organic mass spectra obtained by the HR-ToF-AMS for OA source apportionment. We identified various OA sources, the contribution of which to OA concentration depends on location and season. Hydrocarbon-like OA (HOA, surrogate of OA emitted directly from vehicle emissions) and cooking OA (COA) have important, but not dominant, contributions to total OA in urban sites (i.e., 21-38% of total OA depending on site and season). Biomass burning OA (BBOA) concentration shows a distinct seasonal variation with a larger enhancement in winter than summer. Isoprene SOA formed via the reactive uptake of isoprene epoxydiols (denoted as Isoprene-OA) is only resolved in warmer months and contributes 18-36% of total OA. More-oxidized and less-oxidized oxygenated organic aerosol (MO-OOA and LO-OOA, respectively) are dominant fractions (47-79%) of OA in all sites. MO-OOA correlates well with ozone in summer, but not in winter, indicating MO-OOA sources may vary with seasons. LO-OOA, which reaches a daily maximum at night, correlates well with estimated nitrate functionality from organic nitrates. These findings significantly improve our understanding of OA sources in the southeastern US and provide suggestions for implementing effective regulations to reduce ambient PM level.

After identifying OA sources in the southeastern US, we further investigated the effects of anthropogenic influences on SOA formation from biogenic VOCs (denoted as biogenic SOA) based on complementary laboratory studies and ambient measurements. Among various interactions between anthropogenic and biogenic emissions, we probed (1) the effects of NO_x on the SOA formation from isoprene photooxidation, (2) the effects of sulfate on the reactive uptake of isoprene epoxydiols (IEPOX), which are oxidation products of isoprene under low-NO_x oxidation conditions, and (3) the oxidation of

monoterpenes by nitrate radical (a product of anthropogenic NO_x and ozone). Firstly, the effects of NO_x on the SOA from isoprene photooxidation were investigated in laboratory chamber experiments. We found that the yield, volatility, and oxidation state of isoprene SOA are sensitive to and exhibit a non-linear dependence on NO_x levels. The non-linear dependence likely arises from gas-phase organic peroxy radical (RO_2) chemistry and succeeding particle-phase oligomerization reactions. Our results suggest that it is not proper to treat the effects of NO_x on SOA properties as a linear combination of SOA formation under two extremes ("low-NO_x" and "high-NO_x" conditions) as currently done in regional and global atmospheric SOA models. Secondly, based on ambient measurements in the southeastern US, we demonstrated that the isoprene SOA formed via reactive uptake of IEPOX (denoted as isoprene-OA), which accounts for 18-36% of total OA mass in summer time, is directly modulated by the abundance of anthropogenic sulfate. This contradicts with prior laboratory studies, which suggest the process is controlled by the particle water content and/or particle acidity. Based on both surface and flight measurements, we estimate that 1 $\mu g\ m^{-3}$ reduction of sulfate would decrease the isoprene-derived OA by 0.23-0.42 $\mu g\ m^{-3}$. Thirdly, SOA from monoterpenes, which was shown to account for 19-34% of total OA mass throughout the year, was enhanced at night via oxidation of monoterpenes by nitrate radical. Taken together, we present direct observational evidence on the magnitude of anthropogenic influence on biogenic SOA formation in the southeastern US. That is, anthropogenic sulfate and NO_x can potentially modulate 43-70% of total measured OA in the southeastern US during summer.

Long-term measurements (1999-2013) at the Southeastern Aerosol Research and Characterization (SEARCH) network have revealed that the emissions of SO_2 and NO_x

decrease by about 65% and 52%, respectively, in the southeastern US, which is caused by regulations of anthropogenic emissions from power plants and vehicles as well as the switch from coal to natural gas in many power plants. Meanwhile, the OA concentration has also decreased significantly in the same region. Part of the observed decrease in OA concentration can be explained by our proposed mechanisms regarding anthropogenic pollutants modulating biogenic SOA formation. The continual decrease in SO_2 and NO_x emissions may not only reduce the OA burden, but also have impacts on climate and human health, considering biogenic SOA formed under lower sulfate and NO_x environments could have substantially different properties than those formed in polluted environments. At last, updating current modeling frameworks by including anthropogenic-biogenic interactions will also lead to more accurate treatment of aerosol formation and consequently improve air quality and climate simulations.

CHAPTER 1: INTRODUCTION

1.1 Atmospheric Organic Aerosol

Atmospheric aerosols solid or liquid particles suspended in the air. Research in atmospheric aerosols contributes significantly to the understanding of many current and pressing scientific concerns, such as Earth's climate change, reduction of visibility in air quality, and adverse human health effects (Kanakidou et al., 2005). Atmospheric aerosols are a complex mixture of inorganic and organic matter. While the formation of inorganic aerosols is relatively well understood (Hallquist et al., 2009; Kanakidou et al., 2005), the composition and formation of organic aerosols (OA) remain poorly understood due to their chemical complexity, diverse sources, and dynamic formation and evolution processes (Hildebrandt et al., 2010). Based on ambient measurements around the world, OA represents a significant fraction of the submicron particles (Zhang et al., 2007). Thus, increasing our understanding of OA is essential to better assess the impacts of aerosols on many crucial scientific issues.

OA can be classified into primary OA (POA) and secondary OA (SOA). POA refers to organic aerosols directly emitted by a source, such as fossil fuel combustion. SOA refers to organic aerosols generated by oxidation of gaseous precursors which leads to the formation of condensable products. Recent studies show that SOA comprises a large fraction of the total OA burden. Goldstein and Galbally (2007) estimated SOA formation to be approximately 140-910 TgC/yr, while the emission of POA is estimated to be only 35 TgC/yr. This significant difference in OA burden highlights the importance of studying SOA formation. Additionally, SOA accounts for 64%-95% of total OA on average, as

shown by analyzing Aerosol Mass Spectrometer data in 37 field campaigns in the mid-latitudes of the northern hemisphere (Zhang et al., 2007).

The most commonly studied mechanism of SOA formation is the gas-phase oxidation of volatile organic compounds (VOCs) which forms products of lower volatility that subsequently partition into the condensed phase (Kroll and Seinfeld, 2008). SOA yield (mass of SOA formed per mass of hydrocarbon reacted) varies greatly for different VOCs under different reaction conditions (Chan et al., 2010a; Kroll, 2005, 2006; Ng, 2008; Sprengnether et al., 2002; Ng, 2007; Presto, 2005a, b; Griffin et al., 1999). These VOCs can come from anthropogenic emissions, biogenic emissions, or the condensed phase (Robinson et al., 2007). Volatile organic compounds which are emitted into the atmosphere from biogenic sources, mainly from vegetation, are termed biogenic volatile organic compounds (BVOCs). Compared to VOCs from anthropogenic emissions and the condensed phase, BVOCs have larger global emissions and higher reactivity, therefore contributing greatly to total SOA mass. On a global scale, BVOC emissions exceed those of non-methane anthropogenic organic compounds by a factor of 10, according to global emission inventories (Lamb et al., 1993; Lamb et al., 1987). In addition, most BVOCs are highly reactive due to the presence of unsaturated carbon-carbon bonds (Atkinson and Arey, 2003b). The oxidation of BVOCs can form products of lower volatility, leading to the formation of SOA. Therefore, BVOCs are substantial contributors to the global SOA burden because of their large global emissions and high reactivity.

1.2 Source Apportionment of Organic Aerosol in the southeastern US

The southeastern US is an intriguing region to study aerosol formation. Firstly, the fine particulate matter ($PM_{2.5}$) concentration is generally high and often exceeds the National Ambient Air Quality Standards (NAAQS) (Cohan et al., 2007; Blanchard et al., 2013). Secondly, the southeastern US is characterized by large emissions from both biogenic and anthropogenic sources, which makes it an ideal region to study the effects of interactions between biogenic/anthropogenic emissions on organic aerosol formation and air quality. Roughly, half of the land in the southeastern US is covered by forests, which emit large amounts of biogenic volatile organic compounds (VOCs) that are precursors for secondary organic aerosol (SOA) formation (Geron et al., 2000; Guenther et al., 2006). Based on radiocarbon analysis, Schichtel et al. (2008) showed that about 90% of total carbon is biogenic in a rural site in Tennessee. Similarly, Weber et al. (2007) found that 70-80% of the carbon in water-soluble organic carbon (WSOC, a surrogate for SOA) is of biogenic origin in Atlanta, GA. However, recent studies revealed that the formation of SOA from biogenic VOCs is largely controlled by anthropogenic emissions in the southeastern US (Weber et al., 2007; Xu et al., 2015a). Thirdly, a wide range of air quality data has been routinely collected by the SEARCH (SouthEastern Aerosol Research and Characterization) network, including multiple rural and urban sites in the southeastern US from 1999 to 2013 (Edgerton et al., 2005; Hansen et al., 2003; Hidy et al., 2014). Combining short-term field campaigns and long-term measurements is useful because short-term field campaigns with state-of-the-art instruments can better characterize atmospheric processes and provide insights in interpreting the long-term observations. In turn, long-term measurements of

basic air quality parameters are helpful when testing the robustness of short-term field campaign results (Hidy et al., 2014).

A number of field studies have been conducted to understand the sources of OA in the southeastern US. Lim and Turpin (2002) showed that ~50% of OC is secondary in urban Atlanta by using an EC tracer method. Blanchard et al. (2008) applied three different empirical models and estimated that the fraction of secondary OC (SOC) in OC is ~20-60% in the southeastern US, which was higher at rural sites compared to urban sites and higher in summer compared to winter. The authors also showed that the estimated SOC/OC ratio highly depends on the estimation methods. By using WSOC as a surrogate for SOC, Weber et al. (2007) showed that SOC accounts for roughly 75% of OC in Yorkville, a rural site in GA, while the contribution of SOC to OC decreases to about 65% in Georgia Institute of Technology, an urban site. However, these studies were based on bulk properties, such as OC and WSOC, which makes it challenging for OC source apportionment beyond separating it into primary and secondary OC. Attempts have been made to apportion OC into different sources based on molecular makers. For example, by using molecular maker-based chemical mass balance modeling (CMB-MM), Zheng et al. (2006) attributed OC into various primary emission sources such as wood combustion and gasoline engine exhaust. However, limited by the number of molecular markers included in the model, the CMB-MM method is insufficient to resolve SOC and often results in high percentages of unexplained OC (Zheng et al., 2002). Also, filter samples collected on a daily basis have been used in most previous studies, which limits the temporal resolution and could introduce uncertainty due to filter sampling artifacts. The Aerodyne Aerosol Mass Spectrometer (AMS) has been widely used to characterize the chemical composition

of submicron non-refractory species with high temporal resolution (Canagaratna et al., 2007; Jayne et al., 2000). Budisulistiorini et al. (2013) deployed an Aerosol Chemical Speciation Monitor (ACSM) (Ng et al., 2011) at the SEARCH Jefferson Street site in downtown Atlanta, GA. Various OA sources were identified by factor analysis in Budisulistiorini et al. (2013), including one source related to isoprene oxidation. However, due to the lower resolving power of ACSM, PMF analysis on ACSM data can have difficulty in separating different primary sources such as cooking and vehicle emission, which have similar mass spectra (Crippa et al., 2014; Mohr et al., 2009). In addition, measurements at both rural and urban sites are needed in order to investigate the spatial distribution of aerosol and various OA subtypes.

1.3 Effects of Anthropogenic Emissions on Secondary Organic Aerosol Formation from Biogenic Volatile Organic Compounds

1.3.1 The Effects of NO_x on Isoprene Photooxidation

Isoprene is the most abundant non-methane hydrocarbon (NMHC) emitted into the atmosphere with a global emission of ~500 Tg/year(Guenther et al., 2006). Isoprene oxidation by OH radicals plays a critical role in tropospheric ozone (O_3) chemistry and secondary organic aerosol (SOA) formation(Chameides et al., 1988; Claeys et al., 2004b; Carlton et al., 2009; Hallquist et al., 2009). Recent studies have shown that nitrogen oxides (NO_x=NO+NO_2) are highly influential in SOA formation from various hydrocarbon precursors, including isoprene (Tuazon et al., 1990; Kroll et al., 2006; Surratt et al., 2010; Lane et al., 2008; Sato et al., 2011). NO_x effects on SOA formation have been attributed to the chemistry of organic peroxy radicals (RO_2). While the reaction of RO_2 with HO_2 and

NO_2 produces low volatile species, RO_2+NO reaction could form volatile species via fragmentation of the resultant RO radical (Atkinson, 1997; Kroll and Seinfeld, 2008; Hatakeyama et al., 1989). Despite the fact that SOA formation from isoprene has been intensively studied, many observations in both laboratory studies and field measurements cannot be well explained based on our current knowledge of isoprene oxidation chemistry and yield (Lin et al., 2013a; Robinson et al., 2011a; Goldstein et al., 2009; Carlton et al., 2010; Brock et al., 2003). For example, recent aircraft and ground-based studies during the CARES field mission suggested that SOA formation was enhanced when NO_x was mixed with isoprene-rich air masses, though the mechanism for the enhancement remains unclear (Setyan et al., 2012; Shilling et al., 2013).

1.3.2 The Effects of Sulfate on the Reactive Uptake of Isoprene Epoxydiols

Laboratory studies have revealed that the isoprene SOA yield is greatly enhanced in the presence of sulfate seed particles resulting in acidic aqueous particles (Surratt et al., 2010). The enhancement is due to the sulfate induced reactive uptake of isoprene epoxydiols (IEPOX), which are isoprene oxidation products from the peroxy radical (RO_2) + hydroperoxyl radical (HO_2) pathway (Paulot et al., 2009b). Isoprene-derived OA factor (i.e., isoprene-OA) resolved by positive matrix factorization (PMF) analysis of aerosol mass spectrometry data, which is a surrogate for isoprene SOA through IEPOX reactive uptake, has been identified at multiple sampling sites (Robinson et al., 2011a; Slowik et al., 2011; Budisulistiorini et al., 2013; Hu et al., 2015; Chen et al., 2015; Xu et al., 2015a; Xu et al., 2015b). Specifically, PMF analysis of high resolution AMS data showed that

isoprene-OA accounted for 18-36% of OA in summer in the southeastern United States (Xu et al., 2015a; Xu et al., 2015b).

Based on measurements at multiple sites in the southeastern United States, Xu et al. (2015a) showed that isoprene-OA is strongly associated with sulfate, but not associated with particle pH or particle water as suggested by prior laboratory studies. This strong correlation between isoprene-OA and sulfate has been repeatedly observed in many studies (Budisulistiorini et al., 2015; Hu et al., 2015) and reproduced in a chemical transport model (Marais et al., 2015). However, a coherent explanation regarding the relationships between isoprene-OA and sulfate, particle pH, and particle water has not emerged. The model results by Marais et al. (2015) suggest that the correlation between isoprene-OA and sulfate is caused by sulfate's influence on volume and pH, although the role of particle volume is not explicitly discussed and remains unclear. Regarding the repeatedly observed lack of correlation between isoprene-OA and particle pH in ambient measurements (Budisulistiorini et al., 2015; Xu et al., 2015a), some studies suggested that it is due to that isoprene-OA measured at a surface site is affected by transport, during which the particle pH can change (Budisulistiorini et al., 2013). However, Budisulistiorini et al. (2015) modeled the concentration of IEPOX-derived SOA tracers with good accuracy by using local particle pH and particle water at Look Rock, TN, even though the observed isoprene-SOA did not correlate with local particle pH. In addition, in Xu et al. (2015a), where isoprene-OA was largely locally produced at Centreville, AL as indicated by the highly reproducible diurnal variation of isoprene-OA regardless of the origin of air masses, isoprene-OA is still not correlated with particle pH. Thus, transport may not explain the lack of correlation between isoprene-OA and particle pH. Other possible mechanisms of

sulfate on isoprene-OA formation are through the surface accommodation process (Lin et al., 2013a) or nucleophilic effects of sulfate (Xu et al., 2015a).

1.3.3 The Oxidation of Biogenic Volatile Organic Compounds by Nitrate Radical

Nitrate radical ($NO_3^{\bullet}$, a product of NO_x and ozone reaction) is a well-known nocturnal oxidant. $NO_3^{\bullet}$ reacts rapidly with BVOCs containing double bonds (Atkinson and Arey, 2003a) and produce SOA with large yields (Griffin et al., 1999; Hallquist et al., 1999; Spittler et al., 2006; Rollins et al., 2009; Fry et al., 2011; Fry et al., 2014; Ng et al., 2008). Global modeling studies by Pye et al. (2010) showed that $NO_3^{\bullet}$ oxidation can produce 69 to 88 Tg yr^{-1} of OA annually.

The oxidation of BVOCs by $NO_3^{\bullet}$ produces large amount of organic nitrates, which are important atmospheric species as their fate could affect the nitrogen cycle and ozone production (Perring et al., 2013; Mao et al., 2012). Rollins et al. (2012) observed that organic nitrates contribute about 27-40% to the OA growth at night in Bakersfield, CA, by using a Thermal-Dissociation Laser-Induced-Fluorescence technique (TD-LIF) (Day et al., 2002). However, the concentration of organic nitrates in the atmosphere is uncertain due to limited measurement techniques. Multiple approaches have also been proposed to estimate organic nitrates from indirect measurements. For example, Farmer et al. (2010) proposed that the concentration of the nitrate functionality (i.e., $-ONO_2$) in organic nitrates could be estimated based on the nitrate functionality fragmentation pattern in the AMS, or the differences between AMS and ion-chromatography (IC) measurements.

1.4 Scope and Motivations

This dissertation covers several emerging issues of atmospheric OA, with a focus on the sources apportionment and formation mechanisms of OA in the southeastern US. Specifically, in chapter 2, we investigate the sources, seasonal variation, and spatial distribution of OA in the southeastern US. In Chapter 3 – 5, we study three mechanisms of anthropogenic emissions influencing biogenic SOA formation. Chapter 3 discusses the effects of NO_x on the SOA from isoprene oxidation based on systematic laboratory chamber studies. Chapter 4 presents direct observational evidence on the mechanis and magnitude of anthropogenic influence on biogenic SOA formation in the southeastern US based on comprehensive ambient surface measurements. Chapter 5 provides further insights into the effects of sulfate on SOA formation via reactive uptake of IEPOX through airborne measurements. This study acts as a bridge between the idealized laboratory studies and complicated atmospheric process. Finally, chapter 6 summarizes the findings in this dissertation and provides recommendations for future research.

CHAPTER 2: AEROSOL CHARACTERIZATION OVER THE SOUTHEASTERN UNITED STATES USING HIGH RESOLUTION AEROSOL MASS SPECTROMETRY: SPATIAL AND SEASONAL VARIATION OF AEROSOL COMPOSITION AND SOURCES WITH A FOCUS ON ORGANIC NITRATES

2.1 Background

The southeastern US is an intriguing region to study aerosol formation. Firstly, the fine particulate matter ($PM_{2.5}$) concentration is generally high and often exceeds the National Ambient Air Quality Standards (NAAQS) (Cohan et al., 2007; Blanchard et al., 2013). Secondly, the southeastern US is characterized by large emissions from both biogenic and anthropogenic sources, which makes it an ideal region to study the effects of interactions between biogenic/anthropogenic emissions on organic aerosol formation and air quality. Roughly, half of the land in the southeastern US is covered by forests, which emit large amounts of biogenic volatile organic compounds (VOCs) that are precursors for secondary organic aerosol (SOA) formation (Geron et al., 2000; Guenther et al., 2006). Based on radiocarbon analysis, Schichtel et al. (2008) showed that about 90% of total carbon is biogenic in a rural site in Tennessee. Similarly, Weber et al. (2007) found that 70-80% of the carbon in water-soluble organic carbon (WSOC, a surrogate for SOA) is of biogenic origin in Atlanta, GA. However, recent studies revealed that the formation of SOA from biogenic VOCs is largely controlled by anthropogenic emissions in the southeastern US (Weber et al., 2007; Xu et al., 2015a). Thirdly, a wide range of air quality data has been routinely collected by the SEARCH (SouthEastern Aerosol Research and Characterization)

network, including multiple rural and urban sites in the southeastern US from 1999 to 2013 (Edgerton et al., 2005; Hansen et al., 2003; Hidy et al., 2014). Combining short-term field campaigns and long-term measurements is useful because short-term field campaigns with state-of-the-art instruments can better characterize atmospheric processes and provide insights in interpreting the long-term observations. In turn, long-term measurements of basic air quality parameters are helpful when testing the robustness of short-term field campaign results (Hidy et al., 2014).

A number of field studies have been conducted to understand the sources of OA in the southeastern US. Lim and Turpin (2002) showed that ~50% of OC is secondary in urban Atlanta by using an EC tracer method. Blanchard et al. (2008) applied three different empirical models and estimated that the fraction of secondary OC (SOC) in OC is ~20-60% in the southeastern US, which was higher at rural sites compared to urban sites and higher in summer compared to winter. The authors also showed that the estimated SOC/OC ratio highly depends on the estimation methods. By using WSOC as a surrogate for SOC, Weber et al. (2007) showed that SOC accounts for roughly 75% of OC in Yorkville, a rural site in GA, while the contribution of SOC to OC decreases to about 65% in Georgia Institute of Technology, an urban site. However, these studies were based on bulk properties, such as OC and WSOC, which makes it challenging for OC source apportionment beyond separating it into primary and secondary OC. Attempts have been made to apportion OC into different sources based on molecular makers. For example, by using molecular maker-based chemical mass balance modeling (CMB-MM), Zheng et al. (2006) attributed OC into various primary emission sources such as wood combustion and gasoline engine exhaust. However, limited by the number of molecular markers included

in the model, the CMB-MM method is insufficient to resolve SOC and often results in high percentages of unexplained OC (Zheng et al., 2002). Also, filter samples collected on a daily basis have been used in most previous studies, which limits the temporal resolution and could introduce uncertainty due to filter sampling artifacts. The Aerodyne Aerosol Mass Spectrometer (AMS) has been widely used to characterize the chemical composition of submicron non-refractory species with high temporal resolution (Canagaratna et al., 2007; Jayne et al., 2000). Budisulistiorini et al. (2013) deployed an Aerosol Chemical Speciation Monitor (ACSM) (Ng et al., 2011) at the SEARCH Jefferson Street site in downtown Atlanta, GA. Various OA sources were identified by factor analysis in Budisulistiorini et al. (2013), including one source related to isoprene oxidation. However, due to the lower resolving power of ACSM, PMF analysis on ACSM data can have difficulty in separating different primary sources such as cooking and vehicle emission, which have similar mass spectra (Crippa et al., 2014; Mohr et al., 2009). In addition, measurements at both rural and urban sites are needed in order to investigate the spatial distribution of aerosol and various OA subtypes.

Organic nitrates are important atmospheric species as their fate could affect the nitrogen cycle and ozone production (Perring et al., 2013; Mao et al., 2012). Organic nitrates, which are primarily formed from VOCs oxidation by nitrate radicals, or by ozone and hydroxyl radical in the presence of NO_x, have been shown to be an important component of organic aerosol. For example, Rollins et al. (2012) observed that organic nitrates contribute about 27-40% to the OA growth at night in Bakersfield, CA, by using a Thermal-Dissociation Laser-Induced-Fluorescence technique (TD-LIF) (Day et al., 2002). Multiple approaches have also been proposed to estimate organic nitrates from indirect

measurements. For example, Farmer et al. (2010) proposed that the concentration of the nitrate functionality (i.e., -ONO_2) in organic nitrates could be estimated based on the nitrate functionality fragmentation pattern in the AMS, or the differences between AMS and ion-chromatography (IC) measurements.

In this study, we performed measurements by a suite of instrumentation in multiple sites in the greater Atlanta, GA, area, and Centerville, AL, with a focus on a high-resolution time-of-flight aerosol mass spectrometer (HR-ToF-AMS). Positive matrix factorization analysis is performed on HR-ToF-AMS data to identify distinct OA sources. The contribution of organic nitrates to total OA is estimated by different methods based on HR-ToF-AMS measurements. Measurements were performed in both rural and urban sites to investigate the spatial distribution of aerosol in the southeastern US. In addition, measurements spanning over a year allow us to evaluate the seasonal variation of aerosol composition. These results are supported by long-term measurements from the SEARCH network and provide further insights into interpreting historic measurements.

2.2 Method

Measurements were conducted at the following sites as part of two field campaigns:

2.2.1 Southern Oxidant and Aerosol Study (SOAS)

The Southern Oxidant and Aerosol Study (SOAS, http://soas2013.rutgers.edu/) is a collaborative field campaign that took place from 1 June to 15 July 2013. The sampling site (32.94°N, 87.18°W) is a SEARCH network site near Centreville, in rural Alabama, as shown in Figure 2.1. The site is located in a forested area away from large urban cities (55km SE of Tuscaloosa and 84 km SW of Birmingham, AL). Detailed meteorological

conditions of the sampling site can be found in Hidy et al. (2014). In brief, the sampling period was characterized by high relative humidity (>50% all the time), warm temperatures (daily maximum 28.6 °C at 15:00 local time), and light winds (Xu et al., 2015a).

2.2.2 Southeastern Center for Air Pollution and Epidemiology study (SCAPE)

This extensive field study was part of the Southeastern Center for Air Pollution and Epidemiology (SCAPE, http://scape.gatech.edu/), which is an EPA-funded joint research center between Georgia Tech and Emory University, focusing on the study of air quality and the health effects of air pollutants (Verma et al., 2014; Winquist et al., 2014; Russell et al., 2014). Four sampling sites in both rural and urban areas are selected, as shown in Figure 2.1. Detailed description of each sampling site can be found in Verma et al. (2014) and Hansen et al. (2003). Briefly,

Roadside site (RS site) is on the Georgia Tech campus and adjacent (within 5 m) to the Interstate 75/85 (8 lanes each direction). According to Georgia Department of Transportation, about 95% of the traffic fleet on the Interstate 75/85 is light-duty gasoline vehicles.

Georgia Tech site (GT site) is also on the Georgia Tech campus, but 840 m away from the roadside site. The GT site is located on the top floor of the Ford Environmental Science & Technology Building, which is 30-40 m above ground.

Jefferson Street site (JST site) is a central SEARCH network site, which is about 2 km west of the Georgia Tech site. This site is situated in Atlanta's urban area and surrounded by a mixed residential and commercial neighborhood and is considered representative of urban Atlanta.

Yorkville site (YRK site) is the SEARCH rural pair to the JST site located approximately 80 km northwest of JST. This site is situated in a mixed forested – agricultural area and immediately surrounded by pastures for cattle grazing.

We outfitted a trailer with a large suite of instrumentation (described in section 2.3) and conducted measurements from May 2012 to February 2013, with roughly one month at each site, and repeated it in different seasons. The sampling periods are listed in Table 2.1.

While the trailer was rotated between multiple sites, we also deployed an Aerosol Chemical Speciation Monitor (ACSM, described in section 2.3.2) (Ng et al., 2011) at the Georgia Tech site from May 2012 to February 2013. The paired and simultaneous measurements using an ACSM at the Georgia Tech site and a High Resolution Time-of-Flight Aerosol Mass Spectrometer (HR-ToF-AMS, described in section 2.3.1) rotating among four different sites allow for investigating spatial distributions of aerosol loading and composition in the greater Atlanta area. It is noted that from 20 July to 4 September 2012, both the HR-ToF-AMS and the ACSM were deployed at the Georgia Tech site for instrument inter-comparison.

2.2.3 Instrumentation

2.2.3.1 High Resolution Time-of-Flight Aerosol Mass Spectrometer (HR-ToF-AMS)

An Aerodyne High-Resolution Time-of-Flight Aerosol Mass Spectrometer (HR-ToF-AMS) was rotated among different sites in this study to characterize the composition of ambient submicron non-refractory particulate matter (NR-PM_1). A detailed description of the HR-ToF-AMS can be found in the literature (Canagaratna et al., 2007; DeCarlo et

al., 2006). In brief, the HR-ToF-AMS focuses ambient particles with vacuum aerodynamic diameter smaller than 1μm into a narrow beam via an aerodynamic lens. The submicron particles are then impacted on a hot tungsten surface (~600°C), where non-refractory species are flash vaporized. The resultant vapors are ionized using 70eV electron impact ionization and analyzed by a time-of-flight mass spectrometer. During sampling, a PM_1 cyclone was used to remove coarse particles. A nafion-dryer was placed upstream of the HR-ToF-AMS to dry the particles (relative humidity <20%) in order to eliminate the potential influence of relative humidity on particle collection efficiency (CE) at the vaporizer (Matthew et al., 2008). Gas-phase interference was eliminated by subtracting the signals when the HR-ToF-AMS sampled through a HEPA filter, which was performed regularly on a daily basis at different times of the day. Ionization efficiency (IE) calibrations were performed with 300nm ammonium nitrate particles, on a weekly basis. The composition-dependent CE was applied to the data based on Middlebrook et al. (2012). We operated the HR-ToF-AMS in two ion optical modes (V and W) with different sensitivity and spectra resolution, but only V mode data are reported in this study considering the low intensity of W mode data. The average sampling time was set at two minutes. The data analysis was performed using the standard AMS analysis toolkits SQUIRREL v1.53 and PIKA v1.12 in Igor Pro 6.34 (WaveMetrics Inc.). Default RIE values were used for the HR-ToF-AMS data. Elemental ratios, such as atomic oxygen-to-carbon ratio (O:C), hydrogen-to-carbon ratio (H:C), and organic mass-to-organic carbon ratio (OM:OC), are determined by following the latest procedures recommended by Canagaratna et al. (2015). Canagaratna et al. (2015) improved the estimation from Aiken et al. (2008), which has been widely used in the literature to estimate elemental ratios, by

Table 2.1. Sampling sites and periods for the SCAPE and SOAS studies. Campaign average meteorological conditions, mixing ratios of gas-phase species, and mass concentrations of black carbon and NR-PM_1 species for all datasets. Average ± one standard deviation are reported.

AMS sampling site		Jefferson Street	Centreville	Yorkville	Georgia Tech	Jefferson Street	Yorkville	Roadside
Sampling period		5/10/2012 - 6/2/2012	6/1/2013- 7/15/2013	6/26/2012 - 7/20/2012	7/20/2012 - 9/4/2012	11/6/2012 - 12/4/2012	12/5/2012 - 1/10/2013	1/26/2013 - 2/28/2013
Abbreviation		JST_May	CTR_June	YRK_July	GT_Aug	JST_Nov	YRK_Dec	RS_Jan
Met[a]	T (°C)[b]	23.0 ± 4.3	24.7 ± 4.3	26.9 ± 4.5	26.1 ± 3.5	11.3 ± 5.0	7.8 ± 5.5	8.1 ± 4.8
	RH(%)	65.8 ± 19.3	82.9 ± 15.3	61.9 ± 18.5	71.2 ± 17.2	64.5 ± 20.6	74.2 ± 20.1	64.6 ± 25.3
	WS ($m\ s^{-1}$)	1.6 ± 1.1	1.9 ± 0.9	2.3 ± 1.1	1.3 ± 0.8	1.3 ± 0.9	3.4 ± 1.7	2.1 ± 1.4
Gas (ppb)	NO	4.1 ± 13.0	0.1 ± 0.2	0.1 ± 0.1	N/A	32.1 ± 60.2	0.3 ± 0.8	N/A
	NO_2	10.3 ± 10.3	0.6 ± 0.6	1.1 ± 0.8	N/A	18.4 ± 12.8	3.0 ± 3.0	N/A
	SO_2	0.4 ± 0.7	0.3 ± 0.7	0.4 ± 0.5	N/A	1.2 ± 1.7	0.6 ± 1.1	N/A
	O_3	39.0 ± 21.9	26.4 ± 12.4	41.1 ± 17.0	N/A	18.8 ± 14.5	28.8 ± 8.3	N/A
$PM_{2.5}$ ($\mu g\ m^{-3}$)	BC[c]	N/A	0.2 ± 0.2	N/A	0.9 ± 0.7	0.9 ± 1.0	0.4 ± 0.3	1.3 ± 1.0
NR-PM_1 ($\mu g\ m^{-3}$)	SO_4	3.0 ± 1.5	1.9 ± 1.4	3.5 ± 1.8	4.0 ± 2.1	1.7 ± 0.9	1.4 ± 1.0	1.6 ± 1.2
	NO_3	0.4 ± 0.3	0.1 ± 0.1	0.3 ± 0.2	0.4 ± 0.4	1.2 ± 1.1	0.8 ± 0.8	1.4 ± 1.3
	NH_4	1.1 ± 0.5	0.4 ± 0.3	1.1 ± 0.5	1.2 ± 0.6	0.9 ± 0.6	0.6 ± 0.5	0.9 ± 0.6
	Chl	0.03 ± 0.03	0.01 ± 0.01	0.03 ± 0.03	0.02 ± 0.01	0.06 ± 0.07	0.04 ± 0.07	0.06 ± 0.11
	Org	9.1 ± 4.3	5.0 ± 4.0	11.2 ± 6.4	9.6 ± 4.4	7.9 ± 5.1	3.2 ± 2.3	4.7 ± 3.6

[a] Meteorological data at JST and YRK are recorded by Atmospheric Research & Analysis (ARA). Meteorological data at GT and RS are from JST during the same periods.

[b] The numbers reported in the table are campaign-averaged values based on high temporal resolution data (1 - 60min depending on instrument).

[c] Black carbon concentration was measured by a seven-wavelength Aethalometer at GT_Aug and JST_Nov and by a multi-angle absorption photometer (MAAP) at CTR_June, YRK_Dec, and RS_Jan.

including composition-dependent correction factors. Caution is required when comparing the elemental ratios in this study with values reported in the literature, which typically used the Aiken estimation. Nitrate signals (NO^+ and NO_2^+) and sulfate signals (SO^+, SO_2^+, etc) are not included in the elemental ratio calculations. Oxidation state (OS) is calculated as 2*O:C – H:C (Kroll et al., 2011).

2.2.3.2 Aerosol Chemical Speciation Monitor (ACSM)

An Aerosol Chemical Speciation Monitor (ACSM) was stationary at the Georgia Tech site from 10 May 2012 to 28 February 2013. Similar to the HR-ToF-AMS, the ACSM also provides continuous, quantitative measurements of NR-PM_1 (Ng et al., 2011). The mass resolving power of ACSM (~200) is lower than that of the HR-ToF-AMS (~2000 in V mode) due to use of a low cost residual gas analyzer (RGA) quadrupole mass spectrometer in ACSM (Ng et al., 2011). In addition, the time resolution of ACSM (~30min) is longer than that of HR-ToF-AMS (~2min). The response factor (RF) of the ACSM was also determined by using 300nm ammonium nitrate particles (Ng et al., 2011). The relative ionization efficiency (RIE) values used for organics, nitrate, and chloride are 1.4, 1.1, and 1.3, respectively. RIE values of 4.18 and 0.59 were used for ammonium and sulfate, which were determined from IE calibrations by using ammonium nitrate and ammonium sulfate particles.

2.2.3.3 Co-located Instruments

In addition to the HR-ToF-AMS, we deployed various instruments in the trailer while performing measurements at multiple sites (Verma et al., 2014). Instruments of interest to this study include a PILS-LWCC-TOC system (Particle Into Liquid Sampler - Liquid Waveguide Capillary Cell - Total Organic Carbon analyzer), a seven-wavelength

Aethalometer and a multi-angle absorption photometer (MAAP). The PILS-LWCC-TOC system continuously (i.e., 15min resolution) measured the light absorption spectra of water-soluble organic components. The detailed working principle of the PILS-LWCC-TOC system can be found in Hecobian et al. (2010). In brief, water-soluble species are first dissolved in water in a PILS (Weber et al., 2001). The liquid sample from the PILS is then injected into a Liquid Waveguide Capillary Cell, where the absorption spectra are collected over wavelengths of 200 to 800nm. The average light absorption between 360 to 370 nm is used as a measure of brown carbon light absorption. Black carbon concentration was measured by either a seven-wavelength Aethalometer or a multi-angle absorption photometer (MAAP). For the Aethalometer, measurements at 660nm were chosen to represent the black carbon concentration, because 660nm is closest to the wavelength utilized by the MAAP. The measured data were corrected for loading effects (Virkkula et al., 2007). The temporal resolutions are 2 min and 1 min for Aethalometer and MAAP, respectively.

At the Jefferson Street (JST) and Yorkville (YRK) sites, a suite of instruments was operated by the SEARCH Network. Detailed descriptions about the collocated instruments can be found in Hansen et al. (2003) and Edgerton et al. (2005). In brief, O_3 concentration was measured by a UV-absorption analyzer with a temporal resolution of 1min. NO and NO_x were measured by a chemilumnescence analyzer (1min temporal resolution), where the NO_2 concentration was calculated by subtracting NO from the total NO_x. $PM_{2.5}$ sulfate and OC were continuously measured by a Fe reduction/UV-fluorescence analyzer and an oxidative combustion (R&P 5400) analyzer, respectively. The temporal resolution is 5min

and 60min for $PM_{2.5}$ sulfate and OC, respectively. Meteorological conditions, such as temperature, relative humidity (RH), solar radiation, and wind speed were also recorded.

2.2.4 Positive Matrix Factorization (PMF) Analysis

Positive Matrix Factorization (PMF) is a mathematical technique to solve bilinear unmixing problems (Paatero, 1997; Paatero and Tapper, 1994). PMF analysis has been widely applied in the aerosol community for source apportionment (Ulbrich et al., 2009; Jimenez et al., 2009; Zhang et al., 2010; Lanz et al., 2007; Ng et al., 2010; Beddows et al., 2015; Jaeckels et al., 2007; Visser et al., 2015a). For the data measured by AMS, PMF analysis represents the observed data matrix as a linear combination of various factors with constant mass spectra but varying concentrations across the dataset (Ulbrich et al., 2009; Zhang et al., 2011). To determine the sources of organic aerosol, PMF analysis was performed on the high-resolution organic mass spectra (*m/z* 12 - 200) obtained by the HR-ToF-AMS for each sampling dataset. We generated the organic data matrix and error matrix from PIKA v1.12 and pretreated the error matrix by using PMF Evaluation Toolkit (PET) software following the procedure described in Ulbrich et al. (2009). Variables (i.e., *m/z*'s) with a signal-to-noise ratio less than 0.2 are removed and variables with a signal-to-noise ratio ranging between 0.2 and 2 are downweighted by a factor of 2. We downweighted the errors of O^+, HO^+, H_2O^+, and CO^+, which are related to CO_2^+ signal, to avoid excessive weighting of CO_2^+. In addition, for four datasets (JST_May, CTR_June, YRK_July, and GT_Aug), the error of CHO^+ is downweighted by a factor of 4. This is because that PIKA v1.12 appears to underestimate CHO^+ error, possibly caused by the overlap of the CHO^+ (*m/z* 29.0027) ion with its adjacent N_2 isotope ion (j15NN, *m/z*

29.0032). For the other three datasets (JST_Nov, YRK_Dec, and RS_Jan), CHO^+ is not included in the PMF analysis due to its occasional negative signal, which is likely caused by a low CHO^+ signal in winter. At times, the CHO^+ concentration is near the detection limit, so a shift in threshold might cause the CHO^+ signal to be treated as noise. PMF solutions were carefully evaluated according to the procedure outlined in Zhang et al. (2011). For each dataset, the optimal solution was determined after examining the residuals of PMF fits, interpretability of factor's diurnal trend, factor correlation with external tracers, and characteristic signatures of factor mass spectrum. The rotational ambiguity of solutions was examined by changing the parameter FPEAK and the robustness of solutions were evaluated by starting PMF with different initial conditions (parameter SEED). The key diagnostic plots for all datasets are shown in Fig. S1. An FPEAK value of 0 is used for all datasets in our PMF analysis on organic mass spectra, because the use of FPEAK values that are different from 0 do not improve the correlations between PMF factors with external tracers.

2.2.5 Estimation of organic nitrates contribution to ambient OA

As direct measurements of organic nitrates are not available, we estimate the concentration of particle-phase organic nitrates at each site based on HR-ToF-AMS measurements in this study. It is important to note that total nitrates measured by the HR-ToF-AMS (denoted as $NO_{3,meas}$) is the nitrate functionality ($-ONO_2$), which could arise from both inorganic and organic nitrates. Here, we apply two independent methods in separating the measured total nitrates into nitrate functionality from inorganic and organic nitrates. In the following discussion, we use the subscripts $_{meas,}$ $_{inorg,}$ and $_{org}$ to denote nitrate

functionality ($-ONO_2$) or fragments (NO^+ and NO_2^+) from total nitrates (measured), inorganic nitrates (calculated), and organic nitrates (calculated), respectively.

The first method is based on the NO^+/NO_2^+ ratio (denoted as NO_x^+ ratio method for discussions hereafter) in the AMS mass spectra (Farmer et al., 2010). Due to the extensive fragmentation caused by 70eV electron ionization in the HR-ToF-AMS, the nitrate functionality ($-ONO_2$) fragments to produce NO^+ and NO_2^+ ions. Previous laboratory studies have shown that the NO^+/NO_2^+ ratio in the aerosol mass spectrum is substantially higher for organic nitrates than ammonium nitrate (AN) (Bruns et al., 2010; Fry et al., 2009; Sato et al., 2010; Farmer et al., 2010; Boyd et al., 2015), which is the major source of PM_1 inorganic nitrates in the southeast US that can be detected by the AMS (Guo et al., 2015; Allan et al., 2004). For example, while the NO^+/NO_2^+ ratio is about 2.4 for ammonium nitrate, the ratio ranges from 5 to 10 for SOA derived from isoprene+$NO_3^\bullet$ and β-pinene+$NO_3^\bullet$ reactions, respectively (Bruns et al., 2010; Boyd et al., 2015). In addition to organic nitrates produced from biogenic VOC oxidation, Sato et al. (2010) showed that the NO_x^+ ratio of organic nitrates from the photooxidation of aromatic hydrocarbons is also clearly higher than that of ammonium nitrate (3.8-5.8 vs 1.1-2.8). Based on the differences in NO_x^+ ratio between organic and inorganic nitrates, Farmer et al. (2010) proposed that the concentrations of NO_{org} and $NO_{2,org}$ can be estimated from NO_{meas} and $NO_{2,meas}$ by Eq. 2.1 and 2.2.

$$NO_{2,org} = \frac{NO_{2,meas} \times (R_{meas} - R_{AN})}{R_{ON} - R_{AN}} \qquad \text{Eq. 2.1}$$

$$NO_{org} = R_{ON} \times NO_{2,org} \qquad \text{Eq. 2.2}$$

R_{meas} is the NO_x^+ ratio from observation. R_{AN} is the NO_x^+ ratio for pure ammonium nitrate (AN), which has been reported to depend on instrument performance and vary between different instruments (Farmer et al., 2010; Rollins et al., 2010). In this study, we determine the R_{AN} of each dataset from Ionization Efficiency (IE) calibrations using 300nm ammonium nitrate particles. We find that R_{AN} varies between 1.73 and 2.93 (Table 2.2), which is within the range (1.1 – 3.5) reported in the literature (Sato et al., 2010; Farmer et al., 2010; Sun et al., 2012b; Fry et al., 2013). R_{ON} is the NO_x^+ ratio for organic nitrates. Similar to R_{AN}, R_{ON} also varies between instruments (Boyd et al., 2015; Bruns et al., 2010; Fry et al., 2009). Thus, the R_{ON} values reported in the literature cannot be directly applied in our datasets. In order to circumvent this issue, Fry et al. (2013) assumed that the R_{ON}/R_{AN} value is instrument independent. The authors further obtained R_{ON} by multiplying R_{AN} determined from in-field IE calibrations with R_{ON}/R_{AN} determined from six organic nitrate standards (average value = 2.25) . However, the reported R_{ON}/R_{AN} values in the literature vary for different organic nitrates. For example, while the average R_{ON}/R_{AN} value is 2.25 for the organic nitrate standards in Farmer et al. (2010), the R_{ON}/R_{AN} ranges from 3.70 to 4.17 for organic nitrates produced from β-pinene oxidation by nitrate radicals (Boyd et al., 2015; Bruns et al., 2010; Fry et al., 2009). Considering the large variations in R_{ON}/R_{AN} values and unknown contributions from different organic nitrates, we apply the NO_x^+ ratio method to obtain an estimation range by using extreme R_{ON} values. We select organic nitrates formed from isoprene and β-pinene oxidation as representative because of their large abundance in the southeastern US, potential to produce organic nitrates, and because that they cover a wide range of R_{ON}/R_{AN} values (i.e., 2.08 for isoprene and 3.70-4.17 for β-pinene) (Boyd et al., 2015; Bruns et al., 2010; Fry et al., 2009). The organic nitrates

Table 2.2. A summary of organic nitrates estimation from NO_x^+ ratio method. R_{AN} represents the NO_x^+ ratio (=NO^+/NO_2^+) for pure ammonium nitrate (AN). R_{meas} represents the NO_x^+ ratio from observation. $NO_{3,meas}$ represents the total nitrate functionality (from both organic and inorganic nitrates) as measured by the HR-ToF-AMS. $NO_{3,org}$ represents the nitrate functionality from organic nitrates, which is estimated from the NO_x^+ ratio method. ON and OA represent organic nitrate and organic aerosol, respectively.

Site	R_{AN}[a]	R_{meas}	R with LO-OOA		$NO_{3,org}$ conc. ($\mu g\ m^{-3}$)[d]		$NO_{3,org}/NO_{3,meas}$		ON/OA[e]	
			$NO_{3,meas}$	$NO_{3,org}$[b]	lower	upper	lower	upper	lower	upper
JST_May	1.73	4.47	0.68	0.78	0.19	0.27	0.55	0.76	0.07	0.14
CTR_June[c]	2.93	7.10	0.76	0.84	0.06	0.08	0.80	1.00	0.06	0.10
YRK_July	2.24	5.45	0.66	0.83	0.18	0.28	0.63	1.00	0.05	0.12
GT_Aug	2.26	6.17	0.56	0.70	0.21	0.33	0.64	0.99	0.07	0.16
JST_Nov	1.95	3.12	0.14	0.63	0.23	0.25	0.19	0.21	0.09	0.15
YRK_Dec	2.24	3.16	0.29	0.08	0.09	0.16	0.11	0.21	0.09	0.25
RS_Jan	2.62	2.78	0.46	-0.22	0.13	0.13	0.10	0.10	0.09	0.13

[a] R_{AN} is determined from IE calibrations at each site.
[b] The Pearson's correlation coefficient (R) between LO-OOA and $NO_{3,org}$ are obtained by using R_{ON} = 10 in the NO_x^+ ratio method.
[c] For CTR_June, only 6/24 - 7/15 data are reported in order to compare with results from AMS-IC method where a PM_1 cyclone was used.
[d] For CTR_June and YRK_July, the NO_x^+ ratio method with R_{ON} = 10 and PMF method define the lower and upper bound for $NO_{3,org}$, respectively; for JST_Nov, YRK_Dec, the PMF method and NO_x^+ ratio method with R_{ON} = 10 define the lower and upper bound, respectively; for RS_Jan, the PMF method defines both the lower and upper bound; for JST_May and GT_Aug, the NO_x^+ ratio method with R_{ON} = 10 and 5 defines the lower and upper bound, respectively.
[e] The lower and upper bounds correspond to an assumed MW of organic nitrates of 200 and 300 g mol^{-1}.

derived from other biogenic VOCs (i.e., α-pinene, limonene, 3-carene, etc) are not considered due to either their lower ambient concentrations in the SE US or lower organic nitrate yields compared to isoprene and β-pinene (Xu et al., 2015a). Though the photooxidation of aromatic VOCs could also produce organic nitrates, their R_{ON}/R_{AN} ratio is close to that of isoprene organic nitrates (Sato et al., 2010). Multiplying the average R_{AN} (i.e., 2.28±0.40) of all datasets in this study by the average R_{ON}/R_{AN} ratio of isoprene (i.e., 2.08) and β-pinene organic nitrates (i.e., 3.99±0.25) in the literature (Boyd et al., 2015; Bruns et al., 2010; Fry et al., 2009), within one standard deviation we selected 5 (i.e.,

4.74±0.83) and 10 (i.e., 9.10±1.69) as the lower and upper values of R_{ON}. It is important to note that R_{ON} values of 5 and 10 likely correspond to upper and lower bounds of the $NO_{3,org}$ concentrations estimated by the NO_x^+ ratio method. The assumption that R_{ON}/R_{AN} is instrument independent warrants further study.

The second method is based on PMF analysis (denoted as PMF method). In addition to PMF analysis on organic mass spectra (denoted as PMF_{org}), we have also performed PMF analysis on organic mass spectra together with NO^+ and NO_2^+ ions (denoted as $PMF_{org+NO3}$). Such analysis could provide useful insights regarding the relative contributions of organic and inorganic nitrates. For instance, Sun et al. (2012b) and Hao et al. (2014) performed PMF analysis on merged mass spectra with both organic and inorganic signals from HR-ToF-AMS measurements. The authors showed that the NO^+ and NO_2^+ fragments are distributed among a nitrate inorganic aerosol (NIA) factor and other organic aerosol factors.

In this study, the selection of optimal solutions for PMF analysis on the merged mass spectra (i.e., $PMF_{org+NO3}$) is discussed in detail in the Supplement. In brief, in addition to examining the typical diagnostic plots (Fig. S3), the optimal solutions are selected by comparing the time series (Fig. S5), mass spectrum (Fig. S5), and mass concentration (Fig. S6) with results from PMF_{org}. After determining the optimal solution of $PMF_{org+NO3}$, the concentrations of "nitrate functionality from organic nitrates" (i.e., $NO_{3,org}$) are calculated by summing up the nitrate signals (i.e., NO^+ and NO_2^+) from all OA factors by the following equations.

$$[NO^+_{org}]=\sum([\text{OA factor}]_i \times f\_NO_i) \qquad \text{Eq. 2.3}$$

$$[NO_{2,org}^{+}] = \sum([\text{OA factor}]_i \times f\_NO_{2,i}) \qquad \text{Eq. 2.4}$$

where $[\text{OA factor}]_i$ is the mass concentration of the *i*th OA factor, f_NO_i and $f\_NO_{2,i}$ are the mass fraction of NO^+ and NO_2^+, respectively, in the *i*th OA factor. For both the NO_x^+ ratio method and PMF method, we calculate the concentration of $NO_{3,inorg}$ (i.e., nitrate functionality from inorganic nitrates) by subtracting $NO_{3,org}$ (i.e., nitrate functionality from organic nitrates) from $NO_{3,meas}$ (i.e., total measured nitrates).

2.3 Results

Table 2.1 lists the meteorology parameters (temperature, relative humidity, and wind speed), gas-phase concentrations of NO, NO_2, and O_3, and aerosol composition of the seven datasets reported in this study. The average RH is above 60% for all the datasets, with little seasonal variation, which is consistent with previous observations (Ford and Heald, 2013). The high RH in the southeastern US has direct impacts on particle water content and particle acidity. Recently, Guo et al. (2015) showed that particle water and acidity are mainly driven by the variability of RH, although particle composition also plays a role. The average wind speed is relatively constant (1.3–3.4 m s^{-1}) throughout the year at all sites. NO_x (NO and NO_2) and black carbon (BC), which are tracers for anthropogenic emissions, are lower in the rural Yorkville (YRK) site than the urban Jefferson Street (JST) site. In YRK, the NO_x level is low (i.e., average concentration < 0.3 ppb) in all seasons. In contrast, at the urban JST site, the NO_x level is elevated in winter compared to summer, indicating more anthropogenic emissions, or less dispersion, in winter at urban sites.

Figure 2.2 shows the composition of non-refractory submicron particulate matter ($NR\text{-}PM_1$) for all datasets. Organics are the dominant components, which account for more

than 50% of NR-PM_1 mass at all sites throughout the year. Although dominant, the concentration of organic aerosol varies substantially among sites and seasons. The seasonal variation of OA mass concentration is small for the urban JST site (9.1 μg m^{-3} in May vs 7.9 μg m^{-3} in November); however, the OA concentration is about 4 times higher in summer than winter for the rural YRK site (11.2 μg m^{-3} in July vs 3.2 μg m^{-3} in December). The difference in seasonality of OA between urban and rural sites is likely due to the varying strength of different OA sources, which will be discussed in detail in section 4.4.2. In terms of diurnal variation, the OA diurnal trend is relatively flat in summer and peaks at night in winter (Figure 2.3). The diurnal variation of OA is largely influenced by the changes in planetary boundary layer height and changes in contributions to total OA from various sources, which will be discussed in detail in section 4.4.1. The campaign-average mass spectra of OA from all datasets are similar, as shown in Fig. S7. In order to assess the degree of oxidation of OA, average f_{44} (the ratio of *m/z* 44 to total OA signal) and f_{43} (the ratio of *m/z* 43 to total OA signal) of each dataset is plotted in the triangular space as defined by Ng et al. (2010) in Figure 2.4. The OA from all datasets locate in the middle part of the triangle, indicating they are moderately oxidized and have a similar degree of oxidation.

Following organics, sulfate (SO_4) has the second largest contribution to total NR-PM_1 mass at all sites (Figure 2.2). Average SO_4 concentration varies between 3.0 to 4.0 μg m^{-3} at different sites in summer and decreases to 1.4~1.7 μg m^{-3} in winter. The SO_4 concentration at most sites (except JST_Nov and RS_Jan) reaches a daily maximum in the afternoon (Figure 2.3), which is likely caused by the strong photooxidation of SO_2 or sulfate entrainment from aloft when the boundary layer height is the highest in the afternoon (Weber, 2003). In contrast to SO_4, where the concentration is higher in summer, total nitrate

concentration is elevated in winter. While the average concentration of total nitrates is 0.3-0.4 μg m^{-3} (2-3% of total NR-PM_1, Figure 2.2) in summer, it almost triples in winter (0.8-1.4 μg m^{-3}) with elevated mass fraction in total NR-PM_1 (10-16%). The reason for the seasonal variation of the total nitrates will be discussed in section 4.2.2.

2.4 Discussion

2.4.1 OA source apportionment

In this section, we focus on the OA source apportionment based on results from PMF analysis on organic mass spectra only (i.e., PMF_{org}). We resolved various factors, including hydrocarbon-like OA (HOA), cooking OA (COA), biomass burning OA (BBOA), isoprene-derived OA (Isoprene-OA), more-oxidized oxygenated OA (MO-OOA), and less-oxidized oxygenated OA (LO-OOA) at multiple sites in different seasons. Based on the inferred volatility from O:C ratios, the two oxygenated OA factors (i.e., MO-OOA and LO-OOA) are typically named as low-volatility OOA (higher O:C and lower volatility) and semi-volatile OOA (lower O:C and higher volatility) (Ng et al., 2010; Jimenez et al., 2009). However, recent studies showed that O:C ratios are not always well-correlated with aerosol volatility (Hildebrandt et al., 2010; Xu et al., 2014). Thus, in this study, we use the terms "more-oxidized OOA" (MO-OOA, O:C ranges between 0.66 and 1.05, with an average of 0.87) and "less-oxidized OOA" (LO-OOA, O:C ranges between 0.44 and 0.62, with an average of 0.54) (Fig. S10). This terminology has been used in several previous studies (Setyan et al., 2012; Xu et al., 2015a).

2.4.1.1 HOA

Hydrocarbon-like organic aerosol (HOA) is a surrogate of primary OA from vehicle emissions. Among all the OA factors, HOA is the least oxidized with oxidation state (OS) ranging from -1.86 to -1.39 (Figure 2.4). The mass spectrum of HOA is characterized by hydrocarbon-like ions (C_xH_y family) as shown in Fig. S2, which is similar to the mass spectrum of freshly emitted traffic aerosol (Zhang et al., 2005). HOA is only identified at urban sites with evident morning and evening rush hour peaks (Figure 2.5). HOA also shows good correlation with black carbon (R ranges from 0.70 to 0.83) (Fig. S2), further supporting the primary nature of this OA subtype.

For the sites where HOA is identified, HOA accounts for 9-15% (daily average) of total OA (Figure 2.6). Even for the roadside (RS) site, which is within 5 meter of the Interstate 75/85, HOA only contributes 15% of total OA. Low contributions of HOA to total OA near highways have been observed in several prior studies (Sun et al., 2012a; DeWitt et al., 2014). For example, DeWitt et al. (2014) found that HOA only comprised 20% of total OA based on HR-ToF-AMS measurements in a high diesel environment (near a highway) in Paris, France. The small contribution of HOA could arise from the types of vehicles on road, the rapid dilution of vehicle emissions, or the high level of regional background OA. Firstly, roughly 95% of the traffic fleet on I75/85 is light-duty gasoline vehicles, according to Georgia Department of Transportation. Unlike diesel vehicles which have large emissions of POA and BC, gasoline vehicles have a larger emission of VOCs (e.g., toluene and benzene) (Platt et al., 2013). Secondly, in addition to vehicle type, the evaporation of POA emitted from vehicles would further decrease its mass concentration. Robinson et al. (2007) showed that POA from vehicle emissions is indeed semi-volatile,

which would evaporate substantially upon dilution from tailpipe to ambient conditions (a dilution ratio of 10^3 to 10^4). Thirdly, HOA tends to contribute a small fraction of OA because of the high level of regional background OA in the greater Atlanta area. For example, OOA factors (i.e., LO-OOA and MO-OOA) compromise 47-79% of OA as shown in Figure 2.6. The effect of wind direction on HOA concentration is expected to be small considering the close proximity of the roadside sampling site to the highway.

2.4.1.2 COA

The mass spectrum of cooking organic aerosol (COA) is characterized by prominent signals at ions $C_3H_5^+$ (*m/z* 41) and $C_4H_7^+$ (*m/z* 55) (Fig. S2), which could arise from the heating of seed oil (Allan et al., 2010). Another feature of COA is its unique diurnal trend. For three out of four datasets (except JST_Nov) where a COA factor is identified, the COA factor exhibits a small peak at lunch time and a large peak at dinner time (Figure 2.5). The COA factor is identified in urban sites (JST, GT, and RS) throughout the year, with the average mass fraction varying from 12-20%. A prior study by Zheng et al. (2002) estimated that meat cooking accounts for 5-12% of $PM_{2.5}$ organic carbon in the southeastern US by using a chemical mass balance receptor model. The range reported by Zheng et al. (2002) is similar to our study, considering the differences in sampling periods, particle size range, and estimation method. The COA factor has also been detected in many megacities around the world (Huang et al., 2010; Allan et al., 2010; Slowik et al., 2010; Mohr et al., 2012; Crippa et al., 2013), indicating cooking is an important OA source in megacities.

We note that the COA factor was not resolved in Budisulistiorini et al. (2013), in which the authors performed PMF analysis on the data collected by an Aerosol Chemical Speciation Monitor (ACSM) at the JST site in 2011 summer and fall. The lack of a COA factor in the analysis by Budisulistiorini et al. (2013) could be a result of the lower resolution (unit mass resolution) of the ACSM compared to HR-ToF-AMS. Previous studies have suggested that COA is not easily differentiated from HOA due to the similarity of their mass spectra in unit mass resolution data (Crippa et al., 2014; Mohr et al., 2009).

2.4.1.3 Isoprene-OA

The Isoprene-OA factor is characterized by prominent signals at $C_4H_5^+$ (*m/z* 53) and $C_5H_6O^+$ (*m/z* 82) in its mass spectrum (Fig. S2), which resembles that of isoprene SOA formed via isoprene epoxydiols (i.e., IEPOX) uptake in the presence of hydrated sulfate in laboratory experiments (Lin et al., 2012; Budisulistiorini et al., 2013; Nguyen et al., 2014; Liu et al., 2015b). For our datasets, Isoprene-OA is only identified in warmer months (May - August) and accounts for 18-36% of total OA (Figure 2.6). The seasonal variation of Isoprene-OA factor is consistent with that of isoprene emissions, which are high in summer and nearly zero in winter (Guenther et al., 2006). The identification of the Isoprene-OA factor is further supported by its correlation with methyltetrols, which are products formed from isoprene oxidation and likely via IEPOX uptake. For the Centreville dataset where methyltetrols were continuously measured by a semi-volatile thermal desorption aerosol gas chromatograph (SV-TAG) (Isaacman et al., 2014), the correlation coefficient (Pearson's R) between the Isoprene-OA factor and methyltetrols is found to be 0.68 (Xu et al., 2015a).

The f_{C5H6O+} (the ratio of $C_5H_6O^+$ to total signal) in isoprene-OA factor, which is used as a characteristic marker for SOA formed via IEPOX uptake in the literature, ranges from 0.9% - 2.3% in this study. This range is similar to the values from other ambient data (Budisulistiorini et al., 2013; Chen et al., 2014; Robinson et al., 2011a; Slowik et al., 2011), but lower than that from laboratory-generated fresh SOA from IEPOX uptake (3.6% from Liu et al. (2015b)). We note that the f_{C5H6O+} is higher at rural sites (1.9% for YRK_July and 2.3% for CTR_June) than urban sites (0.9% for JST_May and 1.4% for GT_Aug). Similarly, Liu et al. (2015b) observed that the mass spectrum of laboratory-generated SOA from IEPOX uptake has a stronger correlation with that of Isoprene-OA factor from remote regions (Amazon and Borneo) than urban regions (Atlanta, US). The identification of an Isoprene-OA factor at urban sites in the current study has interesting implications. The compound IEPOX is thought to be an oxidation product of isoprene where the organic peroxy radicals react with hydroperoxy radicals (Paulot et al., 2009b). In urban areas, one would expect the majority of organic peroxy radicals to react with NO_x, considering the relatively high NO_x level (~15.4 ppb for JST_May in Table 2.1). However, a recent laboratory study by Jacobs et al. (2014) found that the oxidation of isoprene-derived hydroxynitrates in the presence of NO_x could also produce IEPOX. Thus, Isoprene-OA observed in urban sites could be locally produced. Another possible source for Isoprene-OA at urban sites is advection from rural sites. This could explain the lower f_{C5H6O+} in the Isoprene-OA factor in urban sites, because the compounds which give rise to the $C_5H_6O^+$ signal can be further oxidized during transport. However, the lifetime of the Isoprene-OA factor and the changes in its mass spectral features with chemical aging are largely uncertain. The contribution of advection is probably small as it is unlikely that advection

would result in a consistent diurnal profile of Isoprene-OA, which reaches a daily maximum in the afternoon observed not only in this study (Figure 2.5), but also in other regions, such as Amazon (Chen et al., 2014) and Borneo forest (Janssen et al., 2013; Robinson et al., 2011a). In addition, Robinson et al. (2011a) only observed the Isoprene-OA factor in data obtained from afternoon flights, but not in morning flights through airborne measurements in the Borneo forest, implying that the Isoprene-OA formation is rapid and local. Another possibility for the lower f_{C5H6O+} at the urban sites is that Isoprene-OA factor from the urban sites may contain isoprene SOA produced via other pathways, in addition to the IEPOX uptake pathway. Isoprene SOA formed via RO_2+NO pathway only has a negligible signal at $C_5H_6O^+$ (Kroll et al., 2006; Xu et al., 2014), so that the mixing of Isoprene SOA via different pathways may lower the f_{C5H6O+} in the Isoprene-OA factor. Moreover, seasonality may also have an influence on the lower f_{C5H6O+} at the urban sites since the sampling periods at the urban sites are May and August, when the isoprene concentration is relatively lower than that during the sampling periods at the rural sites (i.e., June and July).

For all the sites where an Isoprene-OA factor is resolved, the Isoprene-OA factor is found to be well-correlated with sulfate (R ranging from 0.73 to 0.88, Fig. S2). Xu et al. (2015a) showed that the formation of isoprene-OA in the southeastern US is largely controlled by the abundance of sulfate, instead of the particle water content and/or particle acidity. While many prior laboratory studies show that particle acidity plays an important role in IEPOX uptake (Gaston et al., 2014; Surratt et al., 2007), results from ambient observations suggest that particle acidity is critical, but not the limiting factor in isoprene OA formation in the southeastern US, which is likely due to the consistently high particle

acidity in the southeastern US (Guo et al., 2015; Xu et al., 2015a). Guo et al. (2015) showed that the daily average particle pH throughout the southeastern US ranges between 1.1 and 1.3 in summer time. In the afternoon, when the isoprene mixing ratio is highest and photochemistry is strongest, the particle pH is even lower, ranging between 0 and 0.75 due to lower particle water content. A recent chamber study (Gaston et al., 2014) showed that decreasing pH from 4.63 to 0.5 could greatly enhance IEPOX uptake by up to 150 times, but the enhancement is much weaker (a factor of 2) when furthering decreasing the pH from 0.5 to -0.27, the range of which is relevant to ambient particle pH (0-0.75) in the summer afternoon in the southeastern US (Guo et al., 2015). Similarly, another laboratory study also showed that the effect of particle acidity on IEPOX uptake is minor when the particle pH is low (Nguyen et al., 2014). By comparing the reactive uptake of IEPOX by using wet $(NH_4)_2SO_4$ seed (pH ~3.5) and wet $MgSO_4$+H_2SO_4 mixture seed (pH~0-1 with large uncertainty), Nguyen et al. (2014) found that the reactive partitioning coefficient of IEPOX increases by only 1.5 times as pH decreases from 3.5 to 1 ($H^+_{(aq)}$ increases by two or three orders of magnitude). Taken together, laboratory studies revealed that while increasing particle acidity could greatly enhance IEPOX uptake when pH is high, the sensitivity of IEPOX uptake to particle acidity is minor when pH is low. This is likely caused by isoprene OA formation from IEPOX uptake being limited by nucleophiles instead of catalyst activity under low pH (Eddingsaas et al., 2010; Piletic et al., 2013), although a low pH is needed to enhance these reactions. We also note that the co-variation between particle acidity and sulfate is not considered in previous laboratory studies (Gaston et al., 2014; Surratt et al., 2007), so the effect of particle acidity could possibly be confounded with the effect of sulfate and warrants further investigation.

2.4.1.4 BBOA

The mass spectrum of biomass burning organic aerosol (BBOA) is characterized by prominent signals at ion $C_2H_4O_2^+$ (*m/z* 60) and $C_3H_5O_2^+$ (*m/z* 73). These two ions are largely produced by levoglucosan, which is formed from the breakdown of cellulose in biomass burning (Schneider et al., 2006). In addition, Heringa et al. (2011) showed that SOA produced during the aging of primary biomass burning emissions could contribute to these two ions. In this study, BBOA accounts for 9-22% of the OA (Figure 2.6). The BBOA factor is mainly resolved in winter datasets, which is consistent with the EPA reported Georgia fire season in late winter (January – March) (Hidy et al., 2014) and the large enhancement in levoglucosan concentrations in winter compared to summer in Georgia (Zhang et al., 2010). BBOA is also identified in JST_May, which may arise from residential wood burning near JST site. The contribution of BBOA to total OA is slightly smaller than the values reported in other studies. Zhang et al. (2010) estimated that biomass burning accounted for 27% of $PM_{2.5}$ mass in winter over the southeastern US by performing PMF analysis on 10 species extracted from filter samples. The differences in biomass burning contribution to OA between this study and Zhang et al. (2010) are likely due to different estimation methods, sampling years (i.e., 2012-2013 vs. 2007), and sample size cut (i.e., PM_1 vs. $PM_{2.5}$).

It is important to note that the BBOA reported in this study likely only represents the relatively fresh OA from biomass burning. For example, laboratory studies revealed that the oxidation of levoglucosan is fast in both the gas and aqueous phases (Zhao et al., 2014; May et al., 2012; Hennigan et al., 2011). The fast oxidation of levoglucosan can result in the rapid decay of signals at $C_2H_4O_2^+$ (*m/z* 60) and $C_3H_5O_2^+$ (*m/z* 73), causing the

mass spectrum of BBOA to lose its characteristic signature. In addition, laboratory studies by Hennigan et al. (2011) and Grieshop et al. (2009a) showed that the mass spectrum of OA from biomass burning becomes increasingly similar to that of MO-OOA after photochemical aging. Ambient measurements in the eastern Mediterranean by Bougiatioti et al. (2014) showed evidence that BBOA could be rapidly converted to OOA in less than a day. Thus, aged OA from biomass burning could be apportioned to the MO-OOA factor.

Recent studies have revealed that OA from biomass burning is an important source for brown carbon (Washenfelder et al., 2015; Andreae and Gelencsér, 2006; Zhang et al., 2010; Lack et al., 2013), which has important impacts on climate (Feng et al., 2013; Liu et al., 2014). For four (out of five) datasets where BBOA is resolved by PMF analysis in this study, the Pearson's correlation coefficient (R) between BBOA and brown carbon is greater than 0.69, with the best correlation observed at JST_Nov (R=0.90) (Figure 2.7). The correlation coefficient between BBOA and brown carbon is only 0.47 for YRK_Dec, which is likely caused by other brown carbon sources at the YRK site. This hypothesis is supported by summer measurements at YRK. In YRK_July, we observed a large abundance of brown carbon, which reached a daily maximum at around 2pm (Fig. S8); however, a BBOA factor is not resolved for YRK_July, indicating that brown carbon, in this case, could arise from sources other than biomass burning. Hecobian et al. (2010) suggested that SOA from aqueous phase reactions may be an important source for brown carbon in summer based on analysis of ~900 filters collected in 2007 in the southeastern US. A recent laboratory study showed that SOA from IEPOX reactive uptake could be light-absorbing and potentially an important source for brown carbon (Lin et al., 2014). However, Isoprene-OA factor, which is related to the IEPOX uptake pathway studied in

Lin et al. (2014), only shows weak correlation (R ranges from 0.22 to 0.50) with brown carbon, as shown in Fig. S9. As suggested by Washenfelder et al. (2015), the difference between ambient observation and laboratory studies is possibly caused by the fact that the IEPOX-derived absorbing chromophores do not dominate the Isoprene-OA mass. However, further studies are warranted to resolve this difference.

2.4.1.5 MO-OOA

Two oxygenated OA factors (MO-OOA and LO-OOA) with high, but differing O:C ratios, were identified in both rural and urban sites throughout the year. MO-OOA contributes 24-49% of total OA mass (Figure 2.6). This factor has the highest O:C ratio, indicating that it is highly oxidized. It has been shown that as OA ages in the atmosphere, the mass spectra of OA from different sources become increasingly similar to each other and resemble that of MO-OOA (Jimenez et al., 2009; Ng et al., 2010). Thus, MO-OOA likely represents a highly aged organic aerosol from multiple sources, which causes the identification of specific sources of MO-OOA to be challenging. In addition to a high degree of oxidation, other notable features of MO-OOA are its diurnal profile and ubiquitous presence. As shown in Figure 2.5, in most datasets except RS_Jan, the diurnal profile of MO-OOA reaches a daily maximum in the afternoon. The daytime increase in MO-OOA would become more prominent after considering the dilution caused by boundary layer height expansion during the day. The similar diurnal profile has also been observed in a number of studies (Aiken et al., 2009; DeWitt et al., 2014; Hildebrandt et al., 2010; Huang et al., 2010; Setyan et al., 2012). Moreover, not only in this study in which MO-OOA is identified in different sites and seasons, MO-OOA (or the OOA factor in

general) was also identified in datasets obtained at multiple sites around the world, pointing to the ubiquitous nature of this OA subtype (Jimenez et al., 2009; Ng et al., 2010).

Possible sources of this factor have been proposed in the literature. Firstly, a number of studies proposed that the source for MO-OOA is long-range transport (Li et al., 2015; Hayes et al., 2013; Robinson et al., 2011b; Raatikainen et al., 2010). This proposed mechanism could explain the high degree of oxidation of MO-OOA because the aerosol gets progressively more oxidized during advection, but it is unlikely to explain the well-defined diurnal profile of MO-OOA (peaks in the afternoon). Secondly, humic-like substances (HULIS) are proposed to be synonymous with MO-OOA because the mass spectrum and the degree of oxidation of HULIS resembles those of MO-OOA (Ng et al., 2010; El Haddad et al., 2013). A recent study by Paglione et al. (2014) performed factor analysis on NMR measurements of water-soluble organic carbon extracted from filters collected in the Netherlands and resolved a factor with mass spectral features that are similar to HULIS. Further, the authors showed that this HUILS factor correlates with the most-oxidized OOA factor (O:C = 0.98) resolved from PMF analysis of their HR-ToF-AMS measurements, providing a linkage between HULIS and MO-OOA. Thirdly, the oxidation of vehicle emission or fuel combustion in general might also contribute to MO-OOA mass, but such contribution is uncertain. On one hand, multiple studies have shown that the photooxidation of gas-phase species from direct vehicle emissions or POA evaporation could rapidly produce secondary OA, which resembles the mass spectrum of oxygenated OA factors and could be 1-2 orders of magnitude higher than the primary OA emissions (Nordin et al., 2013; Presto et al., 2014; Jathar et al., 2014; Platt et al., 2013). In addition, a previous study by Liu et al. (2011) showed that the carboxylic acids measured

by FTIR are exclusively associated with fossil fuel combustion and correlate with the PMF resolved OOA factor from HR-ToF-AMS measurements in coastal California. On the other hand, Zotter et al. (2014) showed that >69% of MO-OOA originated from non-fossil sources in LA basin based on a combination of radiocarbon analysis and AMS PMF analysis. By using the same method, DeWitt et al. (2014) showed that the majority of carbon in OOA is non-fossil even in an environment heavily influenced by traffic emissions, suggesting the source of MO-OOA is not vehicle emissions. Lastly, aged biomass burning is also a possible source for MO-OOA as discussed above in section 4.1.4. One interesting observation in this study is that MO-OOA is well-correlated with ozone in summer (R = 0.73 for JST_May and YRK_July), but not in winter (R = -0.059 and -0.27 for JST_Nov and YRK_Dec, respectively) (Figure 2.8), implying that the sources of MO-OOA may vary with seasons. Considering the large biogenic VOC emissions in summer, the summer MO-OOA may be related to the oxidation of biogenic VOCs. Recently, Ehn et al. (2014) for the first time observed that monoterpene oxidation could produce large quantities of compounds with extremely low vapor pressure. As these compounds have very high O:C (~0.7), it is possible that they serve as an important source for MO-OOA. The identification of the sources of winter MO-OOA could be aided by the radiocarbon analysis. For example, if the majority of MO-OOA in winter has non-fossil sources, it could suggest that aged OA from biomass burning is an important source for MO-OOA, because biomass burning is enhanced and the emissions of biogenic VOCs are low in winter.

2.4.1.6 LO-OOA

Similar to MO-OOA, less-oxidized oxygenated organic aerosol (LO-OOA) is also observed in both rural and urban sites throughout the year. LO-OOA comprises 19-34% of total OA (Figure 2.6). A key feature of LO-OOA is that it consistently exhibits a daily maximum at early morning and at night, in all datasets (Figure 2.5). The similar diurnal variation of LO-OOA has also been observed in previous field measurements and thought to be primarily driven by the semi-volatile nature of LO-OOA. The LO-OOA factor identified in multiple prior field measurements has been observed to correlate with ammonium nitrate, a semi-volatile species which mainly partitions into the particle phase at night when the temperature is relatively low (Jimenez et al., 2009; Sun et al., 2012a; Zhang et al., 2011; Ulbrich et al., 2009). However, in this study, LO-OOA only shows moderate correlation with total NO_3 (i.e., $NO_{3,meas}$) measured by the HR-ToF-AMS in summer datasets (R ranges between 0.56 and 0.76) and is not correlated in winter datasets (R ranges between 0.14 and 0.46) (Figure 2.9 and Table 2.2).

While LO-OOA is only moderately, or sometimes poorly correlated, with $NO_{3,meas}$ in this study, we find improved correlation between LO-OOA and "nitrate functionality from organic nitrates" (i.e., $NO_{3,org}$) (Figure 2.9 and Table 2.2). $NO_{3,org}$ is estimated by using the NO_x^+ ratio method, as described in section 2.5. An R_{ON} value of 10 is applied in this case since different R_{ON} values would only affect the estimated concentration of $NO_{3,org}$, but not the correlation between LO-OOA and $NO_{3,org}$. For most datasets, LO-OOA correlates better with $NO_{3,org}$ than total nitrates. The biggest improvement is seen in JST_Nov, where the correlation coefficient increases from 0.14 to 0.63. However, we also note that the correlation becomes worse for YRK_Dec and RS_Jan, which is likely caused

by the small contribution of organic nitrates to total nitrates, resulting in a larger uncertainty in the NO_x^+ ratio method (Bruns et al., 2010). In addition, the correlations between LO-OOA and $NO_{3,org}$ for YRK_Dec and RS_Jan are weakened by the negative $NO_{3,org}$ concentration estimated from the NO_x^+ ratio method (Figure 2.9). The negative values are a result of smaller R_{meas} than R_{AN}, at times (see Eq. 2.1), which is likely caused by variations in instrument performance (Farmer et al., 2010; Rollins et al., 2010).

2.4.2 Nitrates source apportionment

2.4.2.1 Estimation of organic nitrates

The NO_x^+ ratio method and PMF method are applied to estimate the concentration of "nitrate functionality from organic nitrates" (i.e., $NO_{3,org}$) at different sites. The concentration of $NO_{3,org}$ and the mass fraction of $NO_{3,org}$ in total measured NO_3 (i.e., $NO_{3,meas}$) estimated from both methods are shown in Figure 2.10. Both the NO_x^+ ratio method and the PMF method show a similar seasonality in the contribution of $NO_{3,org}$ to $NO_{3,meas}$ (denoted as $NO_{3,org}/NO_{3,meas}$), which is higher in summer than winter. However, we observe noticeable differences between the two methods. In the following, we first discuss the uncertainties associated with NO_x^+ ratio method and PMF method. Then, we discuss how the uncertainties affect the comparison between the two methods, and provide a "best estimate" range of $NO_{3,org}$ based on the two methods. Lastly, we use the "best estimate" range of $NO_{3,org}$ to calculate the contribution of organic nitrates to OA by assuming the molecular weight (MW) of organic nitrates.

For the PMF method, the uncertainty is mainly associated with the identification of a nitrate inorganic aerosol (NIA) factor. The NIA factor is resolved in most datasets, except

CTR_June and YRK_July. The mass spectrum of the NIA factor is similar to the corresponding factor in Sun et al. (2012b) (Fig. S4). Specifically, it is dominated by NO^+ and contains some organic signals such as CO_2^+ and $C_2H_3O^+$, indicating the NIA factor has a potential interference from organics. The mass fraction of organic signals in the NIA factor varies across sites, with a higher value in warmer months (~70% in JST_May and GT_Aug) than colder months (16%-38% in JST_Nov, YRK_Dec, and RS_Jan) (Fig. S11). The fact that the NO^+/NO_2^+ ratio of the NIA factor resolved from warmer months is higher than that of pure ammonium nitrate (Fig. S12) is also indicative of organic nitrate interference in the NIA factor. Conversely, the NO^+/NO_2^+ ratio of the NIA factor resolved from colder months is closer to that of pure ammonium nitrate, suggesting less interference from organics. Thus, for the sites where a NIA factor is identified, the presence of organic nitrates in the NIA factor would result in an underestimation of $NO_{3,org}$, and the underestimation is larger for warmer months (i.e., JST_May and GT_Aug). For CTR_June and YRK_July, the NIA factor is not resolved from $PMF_{org+NO3}$ analysis, likely due to a small concentration of inorganic nitrates. For example, the concentrations of organics and total nitrates (i.e., $NO_{3,meas}$) are 5.0 and 0.1 μg m^{-3}, respectively, for CTR_June. Even if one assumes that all the measured nitrates arise from inorganic nitrates, the nitrates/organics ratios is only 2%, making it difficult for PMF to retrieve the NIA factor accurately (Ulbrich et al., 2009). Thus, for CTR_June and YRK_July, the small amount of $NO_{3,inorg}$, which is not retrievable by PMF, was attributed to OA factors so that the PMF method would slightly overestimate $NO_{3,org}$.

For the NO_x^+ ratio method, considering the large variation in NO_x^+ ratio for different organic nitrates, the largest uncertainty is associated with the value of R_{ON}.

Ideally, the time-dependent R_{ON} values should be applied. However, this is challenging because the determination of time-dependent R_{ON} requires measurements of every ambient organic nitrate species, which are not available. Knowing this, we apply R_{ON} values of 5 and 10 in our analysis to provide the upper and lower bounds of the estimated $NO_{3,org}$ concentration for the NO_x^+ ratio method as discussed in section 2.5. It is noted that for Centreville, we applied a third method to calculate the concentration of $NO_{3,org}$, which is based on the differences between HR-ToF-AMS measurements (NO_3 from both organic and inorganic species) and PILS-IC measurements (NO_3 from inorganic species only) (Xu et al., 2015a; Bae et al., 2007; Orsini et al., 2003). This method, denoted as AMS-IC method, is only applied for Centreville because the PILS-IC was not deployed in the SCAPE study. In order to match the HR-ToF-AMS particle cut size (i.e., PM_1), a PM_1 cyclone was deployed at the inlet of PILS-IC. However, due to the transmission efficiency of PM_1 cyclone, PILS-IC measurements might include contributions from particles larger than 1μm (i.e., inorganic NO_3 in mineral dust). Interferences from water-soluble refractory particles (e.g., calcium or sodium nitrate) are likely small given the concentration of sodium measured by the PILS-IC with a PM_1 cyclone, for example, was negligible and mostly below its detection limit (0.07 μg m^{-3}) (Fig. S13). As shown in Figure 2.11, The $NO_{3,org}$ estimated by the AMS-IC method falls within the range of NO_x^+ ratio method, which is defined by R_{ON} values of 5 and 10, indicating the feasibility of using these two values as the upper and lower bounds to estimate $NO_{3,org}$ for the NO_x^+ ratio method.

Based on the uncertainties of the PMF method and the NO_x^+ ratio method, we could explain the differences between the two methods and further combine them in order to narrow the estimation range. According to the extent of agreement between the two

methods, all seven datasets are grouped into three categories: summer months (CTR_June and YRK_July), transition months (JST_May and GT_Aug), and winter months (JST_Nov, YRK_Dec, and RS_Jan).

For winter months, the PMF method shows good agreement with the NO_x^+ ratio method with a R_{ON} value of 10 for JST_Nov and YRK_Dec. This is consistent with the observations that the interference of organic nitrates in the NIA factor is small in winter datasets (Figs. S11 and S12) and isoprene emission is negligible in winter (Guenther et al., 2006). Thus, results from the NO_x^+ ratio method with R_{ON} = 5 (i.e., isoprene organic nitrates) are likely unrealistic. With this in mind, we combine the results from the PMF method and the NO_x^+ ratio method with R_{ON} = 10 as the "best estimate" range of organic nitrates for JST_Nov and YRK_Dec. For RS_Jan, the NO_x^+ ratio method predicts negative $NO_{3,org}$ due to R_{meas} being smaller than R_{AN} at times (Eq. 2.1). In this case, the PMF method is selected as the "best estimate". Taken together, the mass fraction of organic nitrates (i.e., $NO_{3,org}/NO_{3,meas}$) is 0.19-0.21, 0.11-0.21, and ~0.10 for JST_Nov, YRK_Dec, and RS_Jan, respectively.

For summer months, the PMF method predicts that all the measured nitrates are from organic nitrates (i.e., $NO_{3,org}/NO_{3,meas}$ = 1, Figure 2.10), because a NIA factor is not resolved from PMF analysis and all the measured NO_3 are distributed in the OA factors. The $NO_{3,org}$ estimated from the PMF method falls within the upper (i.e., R_{ON} = 5) and lower bound (i.e., R_{ON} = 10) of the NO_x^+ ratio method (Figure 2.10). For CTR_June, the NO_x^+ ratio method with R_{ON} value of 5 predicts a $NO_{3,org}/NO_{3,meas}$ ratio that is greater than 1, which results from the assumed R_{ON} value (i.e., 5) being smaller than R_{meas}, at times (Eq. 2.1). Thus, the PMF method and the NO_x^+ ratio method with R_{ON} = 10 define the upper

and lower bound, respectively. Accordingly, the "best estimate" range of $NO_{3,org}/NO_{3,meas}$ is 0.80-1 and 0.63-1 for CTR_June and YRK_July, respectively.

For transition months (i.e., JST_May and GT_Aug), the PMF method and the NO_x^+ ratio method show large discrepancies. Compared to the PMF method, the NO_x^+ ratio method predicts 1.5–2.5 times higher $NO_{3,org}$ concentration depending on the site and R_{ON} value. This is likely caused by the PMF method under-predicting $NO_{3,org}$, owing to the attribution of some organic nitrates to the NIA factor. Thus, we select the NO_x^+ ratio method with R_{ON} values of 5 and 10 as the "best estimate" range. Accordingly, $NO_{3,org}/NO_{3,meas}$ ranges 0.55-0.76 and 0.64-0.99 for JST_May and GT_Aug, respectively.

We also calculate the contribution of organic nitrate molecules to OA from the "best-estimate" range of nitrate functionality (i.e., $NO_{3,org}$). We assume that particle-phase organic nitrates have an average molecule weight of 200 and 300 g mol^{-1} (Rollins et al., 2012), which provides an lower and upper bound for estimating concentrations of organic nitrates. As shown in Figure 2.10, organic nitrates contribute about 5-12% to total OA for summer datasets (CTR_June and YRK_July) and 9-25% to total OA for winter datasets (JST_Nov, YRK_Dec, and RS_Jan), suggesting that organic nitrates are important components of total OA in the southeastern US.

Figure 2.12 shows the diurnal variation of $NO_{3,org}$ based on the NO_x^+ ratio method with an R_{ON} value of 10. For most of the datasets, $NO_{3,org}$ starts increasing after sunset, which is mainly caused by the oxidation of VOCs by nitrate radical at night. The daily maximum of $NO_{3,org}$ appears in mid-morning (i.e., ~8am), which is likely because photooxidation of VOCs in the presence of NO (i.e., RO_2+NO pathway) also contributes to organic nitrate when the NO concentration is highest.

2.4.2.2 Nitrate seasonal variation

As shown in table 2.1 and Figure 2.2, the total nitrate concentration is higher in winter (0.8-1.4 μg m^{-3}, 10-16% of total NR-PM_1) than in summer (0.3-0.4 μg m^{-3}, 2-3% of total NR-PM_1). Based on the NO_x^+ ratio method, $NO_{3,inorg}$ is greatly enhanced in winter relative to summer. For example, the concentration of $NO_{3,inorg}$ increases from 0.22 μg m^{-3} (average of upper and lower bound of the NO_x^+ ratio method) in May to 1.6 μg m^{-3} in November for the JST site. Similarly, $NO_{3,inorg}$ shows a 10-fold increase for YRK_Dec compared to YRK_July.

The seasonal variation of inorganic nitrates could possibly be caused by its semi-volatile nature and varying NO_x emissions. Based on volatility measurements by a thermal denuder, Huffman et al. (2009a) showed that ammonium nitrate is very volatile and its gas/particle partitioning is largely affected by temperature. The average temperature in summer is about 15 °C higher than that in winter (Table 2.1). According to laboratory measurements of ammonium nitrate volatility, a 15°C increase in temperature would lead to the evaporation of 60% of nitrate mass (Huffman et al., 2009a). In addition to volatility, the winter enhancement of inorganic nitrates is related to higher NO_x levels, which is the major source for inorganic nitrates and largely elevated in winter in the southeastern US (Blanchard et al., 2013). For example, as shown in Table 2.1, the NO_x concentration in JST_Nov (50.5 ppb) is 3.5 times higher than that in JST_May (14.4 ppb). Thus, the lower temperature and higher NO_x levels in winter than summer likely compensate for the weaker photooxidation and result in the increase in inorganic nitrates. Interestingly, we observe a rush hour peak (around 9am) in the diurnal trend of total nitrates at urban sites in winter (JST_Nov and RS_Jan). This rush hour peak is primarily from inorganic nitrates supported

by the following evidence: 1) the R_{meas} is close to R_{AN} during the rush hour period (Fig. S15); 2) the rush hour peak only exists in the diurnal profile of $NO_{3,inorg}$ (Figure 2.12); and 3) the coincident peak in the diurnal trend of NH_4 (Figure 2.3). Early morning peaks in inorganic nitrates were also consistently seen by a variety of online instruments as part of the Atlanta Supersite Experiment at the JST site (Weber et al., 2003). In Mexico City, Hennigan et al. (2008) attributed the fast production of inorganic nitrates mainly to secondary formation from photooxidation of NO_x and subsequent partitioning of HNO_3. The rush hour peak of inorganic nitrates disappears rapidly, which is likely caused by evaporation and dilution as the planetary boundary layer height increases (Hennigan et al., 2008).

The concentration of $NO_{3,org}$ is slightly higher in summer, but its seasonal variation is not as strong as $NO_{3,inorg}$ (Table 2.2 and Figure 2.10). This is likely due to the compensating effects of source strength and gas/particle partitioning. The organic nitrates mainly originate from VOC oxidation by the nitrate radical and/or photooxidation in the presence of NO_x. The VOC concentrations are higher in summer due to stronger biogenic emissions, which would provide sources for organic nitrates. However, the temperature is higher in summer than winter, which would hinder the partitioning of organic nitrates into the particle phase.

2.4.3 Aerosol Spatial Variability

The spatial variability of organics, sulfate, ammonium, and total nitrate in the greater Atlanta area is investigated by comparing ACSM measurements (stationary at the Georgia Tech site) with HR-ToF-AMS measurements (rotating among different sites).

Figure 2.13 shows the correlation coefficients for NR-PM_1 species between ACSM measurements (stationary at the Georgia Tech site) and HR-ToF-AMS measurements (rotating among different sites). Detailed comparisons, in terms of time series and scatter plots, are shown in Fig. S14. The ACSM and HR-ToF-AMS are compared side-by-side at the Georgia Tech (GT) site from 20 July to 4 September, 2012 and the time series of the species measured by the two instruments are well correlated (R=0.95, 0.93, 0.82, 0.85 for organics, sulfate, ammonium, and total nitrate, respectively) and agree within instrument uncertainty (i.e., 20-35%) (Bahreini et al., 2009).

As expected, the correlation gets weaker as the distance between the GT site and other sampling sites increases. Surprisingly, the organic correlation coefficient in July is 0.92 between GT and YRK sites, which have considerable spatial separation (i.e., 70 km), indicating that the organics are uniformly distributed in the greater Atlanta area in summer time. In contrast, the organic correlation coefficient between GT and YRK decreases to 0.66 in winter. Unlike organics, the correlation in SO_4 between GT and YRK is similarly good in both summer and winter (R=0.7 and 0.85 for summer and winter, respectively). Our observation is generally consistent with the previous study by Zhang et al. (2012), who showed that WSOC, and to a less extent SO_4, are spatially homogeneous in the southeastern US based on results from daily-average filter measurements (one filter in every six days) in 2007. The authors attributed the uniform distribution of WSOC and SO_4 largely to stagnant air masses in southeastern US during summer time and both long-lived secondary WSOC and SO_4 eventually spread across the region, although somewhat higher WSOC spatial correlations compared to sulfate were thought to be due to widely distributed SOA precursor emissions compared to point sources for SO_2. Hidy et al. (2014) also showed

that secondary species, like SO_4, have weaker rural and urban contrast in the southeastern US, though only yearly average data were considered in that study.

Although meteorology plays an important role in the spatial variability of aerosol, it alone cannot explain the seasonality of the OA spatial variability. For example, meteorology should have the same effect on the regional variability of SO_4 and OA. However, while SO_4 is uniformly distributed in both summer and winter, OA is more uniform in summer than winter, suggesting other factors also influence the spatial variability of OA. The seasonality of OA spatial variability (i.e., more spatially homogeneous in summer compared to winter) is probably affected by the seasonal variation of OA sources in addition to meteorology. As shown in Figure 2.6, SOA is the dominant source for total OA (69-100% of OA) in summer for both rural and urban sites. This likely arises from the fact that biogenic VOCs, which are important precursors for SOA, are abundant and widely distributed in the southeastern US during summer time (Guenther et al., 2006). Thus, SOA is regional and the dominant component of OA, leading to the uniform distribution of OA. In contrast, POA concentration varies greatly between urban and rural sites. In winter, while the SOA still dominates total OA at rural sites, the POA is comparable with SOA at urban sites (Figure 2.6). This is because that the concentration of regional SOA decreases due to weaker photochemical activity and lower biogenic VOCs emissions in winter, but the concentration of POA (HOA+BBOA+COA) is relatively constant, or even increases. This is likely due to elevated emission from biomass burning and reduced evaporation and dispersion, which are associated with lower temperatures in winter (Figure 2.6). Thus, the facts that POA is not uniformly distributed

and that the concentration of POA is comparable to SOA possibly lead to the spatial non-uniformity of OA in winter.

2.4.4 Interpretation of long-term measurements

In this section, we compare our observations from short-term detailed aerosol chemical measurements with those from long-term and more basic measurements to test the validity of our conclusions. Further, based on our extensive measurements, we attempt to provide insights into interpreting long-term observations.

2.4.4.1 OA Diurnal Variation

By investigating the diurnal pattern of organic carbon (OC) from 1 June – 15 July of each year (from 2000 to 2013) in Centreville, rural Alabama, Hidy et al. (2014) observed that OC shows consistently weak diurnal variability. Similarly, Zhang et al. (2012) observed that water-soluble organic carbon (WSOC), which is a surrogate for SOA (in summer), only shows a moderate increase in the daytime in Jefferson Street and Yorkville, GA, during 2008 summer. In this study, we find that OA shows little diurnal variability in summer datasets (Figure 2.3), which is consistent with long-term observations and previous studies.

The lack of a prominent daytime increase in the OA in summer could appear to discount the role of photochemistry-driven secondary OA formation. However, a number of factors need to be considered, such as the changes in planetary boundary layer height, contribution of various sources to OA, and temperature-dependent gas/particle partitioning. Firstly, the rapid expansion of the boundary layer during the day may dilute the OA concentration. In Centreville, the boundary layer height (BLH) was measured by a

ceilometer. The diurnal variation of BLH is shown in Figure 2.14. The BLH typically peaks (i.e., 1300m) at 17:00 and exhibits a daily minimum (i.e., 375m) at 07:00. In order to remove the effect of BLH-driven dilution on the diurnal variation of OA, we multiply the OA diurnal profile by BLH. The interpretation of the product of the concentration of OA (i.e., $\mu g\ m^{-3}$) times BLH (i.e., m) is the integrated column concentration of OA (i.e., $\mu g\ m^{-2}$) from ground to the top of boundary layer over a unit surface area, assuming the OA is well-mixed in the boundary layer. The value of OA*BLH would be conserved if there is no gain or loss of OA in the column regardless of the change of BLH. Thus, this value could indicate the net gain or loss of OA in the column without the effect of BLH-driven dilution. As shown in Figure 2.3d, the OA*BLH increases rapidly starting at ~7:00 and reaches a daily maximum at ~17:00. The evident peak in the diurnal variation of OA*BLH suggests a substantial OA production in the day, and that the relatively flat OA diurnal variation (i.e., $\mu g\ m^{-3}$) is largely caused by the BLH-driven dilution. For the cases where boundary layer height data are not available, normalizing OA by CO is often utilized in the literature to minimize the effect of dilution, considering CO as an inert species. By using this method, Blanchard et al. (2011) and Zhang et al. (2012) showed that OC/CO and WSOC/CO exhibit pronounced daytime increase, suggesting that the expansion of boundary layer would weaken the OA diurnal variation. The fact that both OC/CO and WSOC/CO peaks in the day implies that photochemistry-driven SOA production is an important source of OA.

Secondly, the time-dependent contributions of various sources to total OA could also affect its diurnal profile. As shown in Figure 2.5, the various OA sources resolved by PMF analysis have distinctly different diurnal trends, indicating that their contributions to

total OA vary throughout the day. Primary sources, such as HOA and COA, peak during rush hours and meal-time, respectively. The contributions of Isoprene-OA and MO-OOA to total OA are largest in the afternoon and decrease after sunset. In contrast, another SOA source, LO-OOA, peaks in the early morning and at night, as the formation of LO-OOA is proposed to mainly correspond to nocturnal nitrate radical oxidation of biogenic VOCs in summer (Xu et al., 2015a). Therefore, different diurnal trends of various OA sources compensate each other, which possibly results in the weak diurnal variation of total OA.

Specifically, LO-OOA, which exhibits a daily maximum at night, compensates for the decrease of other OA sources after sunset and results in the relatively flat total OA diurnal profile. This has important implication in interpreting non-speciated OC measurements. For example, Hennigan et al. (2009) observed a substantial nocturnal increase of gas-phase WSOC, but not an accompanied increase in particle-phase WSOC in Atlanta during summer. The authors hypothesized that the differences between gas-phase and particle-phase WSOC are caused by the oxidation of α-pinene and isoprene by $NO_3^{\bullet}$ radical producing substantial amount of gas-phase WSOC but little particle-phase WSOC. Though it is plausible that α-pinene+$NO_3^{\bullet}$ and isoprene+$NO_3^{\bullet}$ reactions produce more volatile products than low-volatility products, our study shows that there is indeed substantial nocturnal SOA production (i.e., LO-OOA), which likely corresponds to the nocturnal increase in gas-phase WSOC in Hennigan et al. (2009), but not clearly discernible in particle-phase WSOC due to the compensation by the decreasing concentrations of other OA sources at night.

In addition, temperature-dependent gas/particle partitioning also plays a role in OA diurnal variation. As the temperature is higher during day, the gas/particle partitioning

would favor the gas-phase and hence lower the particle-phase concentration. Taken together, the weak diurnal variation of OA in summer is likely caused by changes in boundary layer height and the varying contribution of various OA sources throughout the day, which does not contradict the importance of photochemistry-driven SOA production. Especially, LO-OOA, which is likely related to $NO_3^{\bullet}$ chemistry, peaks at night and compensates the nocturnal decrease of other SOA sources. In fact, the importance of photochemistry can be gained by comparing OA diurnal profile of summer and winter. As the photochemistry is relatively weaker in winter, daytime SOA production is suppressed, which results in OA reaching a daily minimum during daytime in winter datasets (Figure 2.3).

2.4.4.2 Urban and rural contrast of OA seasonality

In this study, we observed that the seasonality of OA behaves differently between urban and rural sites. For example, while the OA concentration is relatively constant between summer and winter for the urban JST site (9.1 μg m^{-3} in May vs 7.9 μg m^{-3} in November), the OA concentration is ~4 times higher in summer than winter for the rural YRK site (11.2 μg m^{-3} in July vs 3.2 μg m^{-3} in December). Our observations are consistent with the long-term measurements from the SEARCH network. Figure 2.15 shows the seasonal average OC concentration measured in JST and YRK from 1999 to 2013. Despite the decreasing trend of OC in the past 14 years, which has been noted and discussed extensively in Hidy et al. (2014), we note that the OC concentration is similar between summer and winter at the JST site, but OC is elevated in summer compared to winter for the YRK site. The urban and rural contrast of OA seasonality is likely caused by the fact

that OA sources are different at urban and rural sites. As shown by PMF analysis on our short-term measurements, the total OA at the rural YRK site is dominant by SOA in both summer and winter (SOA/OA = 100% and 78% for summer and winter, respectively, Figure 2.6), but the concentration of SOA is lower in winter when the SOA formation is depressed due to low biogenic VOCs emissions and weak photochemical activity. For the urban JST site, in contrast, POA accounts for a large fraction of total OA (30-48%, depending on the month). Though the SOA formation is also depressed in winter at urban sites, the decrease in SOA concentration is compensated by the increase in POA concentration from vehicles and cooking (Figure 2.6). Thus, the OA at JST is relatively constant between summer and winter. The changing composition of the OA also implies differing aerosol toxicity and health impacts, not discernible from measurements of total OA (or OC) (Verma et al., 2015). The fairly flat seasonal trend in OA or OC at urban sites has not been captured by current models. All 31 models reviewed in a recent study by Tsigaridis et al. (2014) predicted higher OC concentration in summer than winter for urban monitoring sites in Georgia. One possible reason is that the anthropogenic emission inventories applied in current models do not take seasonal variation into account, resulting in an under-prediction of the pollution levels in urban area.

2.4.4.3 Correlation between OC and sulfate

Based on the OC and sulfate measurements (2005 – 2010) from three SEARCH network sites (Centreville, Jefferson Street, and Yorkville), we find that regardless of the sampling sites, the correlation between OC and sulfate has a distinct seasonal variation, with the best correlation in summer (R ranging 0.47-0.69) and worst in winter (R ranging

0.01-0.33) (Figure 2.16). Since sulfate is mostly secondary in the southeastern US, one possible explanation for the seasonality of the correlation between OC and sulfate is that the majority of OC is secondary in summer, but not in winter, which is supported by the OA source apportionment in this study. It is also likely that sulfate is directly involved in the OA production in summer. Specifically, Xu et al. (2015a) found that sulfate directly and largely mediates the formation of isoprene OA (18-36% of total OA in summer) in the southeastern US, instead of particle water content and/or particle acidity, as previous studies have suggested.

2.5 Conclusion

Nearly one-year of measurements were performed across multiple sites in the southeastern US with a variety of online instruments, with the focus on HR-ToF-AMS data in this study. We find that organics are the dominant components of the NR-PM_1 at both rural and urban sites throughout the year. The OA diurnal profile shows little variation in summer and peaks at night in winter datasets. The lack of midday enhancement in OA diurnal profile is likely caused by the expansion of boundary layer in the day and compensating effects of various OA factors. The OA measured at different sampling sites and seasons has a similar degree of oxidation. Sulfate contributes the second highest to NR-PM_1. Sulfate concentration is higher in summer (3.0 to 4.0 μg m^{-3}) than winter (1.4 to 1.7 μg m^{-3}), probably due to stronger photochemistry in summer. In contrast to sulfate, the inorganic nitrate concentration is estimated to be three times higher in winter than summer. This is likely caused by higher NO_x levels in winter, which serves as the source for

inorganic nitrates and the semi-volatile nature of inorganic nitrates, which tend to partitions into the particle phase when the temperature is low.

Positive Matrix Factorization (PMF) analysis revealed that the organic aerosol has various sources in the southeastern US, which changes between seasons and sampling sites (rural vs urban). Hydrocarbon-like organic aerosol (HOA) and cooking organic aerosol (COA), which arise from primary vehicle emissions and cooking, respectively, are important but not dominant OA sources for urban sites. Biomass burning OA (BBOA) concentrations shows clear enhancements in winter compared to summer. In addition, biomass burning is found to be an important, but not exclusive, source for brown carbon in the southeastern US. Isoprene-derived OA (Isoprene-OA), which is from the reactive uptake of isoprene epoxides in the presence of hydrated sulfate, only exists in warmer months (May-August) when isoprene emissions are substantial. In addition to rural sites, Isoprene-OA is resolved from urban sites where the majority of peroxy radicals are believed to react with NO_x. We note that f_{C5H6O+}, which has been used as a marker for Isoprene-OA, ranges from 0.9-2.3% and is higher in the Isoprene-OA factor from rural sites than urban sites. One possible source of Isoprene-OA in urban sites is transport. However, transport would not likely result in the reproducible diurnal profile of Isoprene-OA, which peaks in early afternoon. Instead, Isoprene-OA in urban sites more likely comes from local production, as a recent study showed that IEPOX could be produced in the presence of NO_x (Jacobs et al., 2014). Less-oxidized oxygenated OA (LO-OOA) and more-oxidized oxygenated OA (MO-OOA) are resolved from both rural and urban sites throughout the year. LO-OOA shows improved correlation with estimated "nitrate functionality from organic nitrates" (i.e., $NO_{3,org}$) than total nitrates. In addition, both LO-

OOA and estimated $NO_{3,org}$ peaks at night (Figures 2.5 and 2.12), implying that LO-OOA could arise from nighttime oxidation of biogenic VOCs by nitrate radicals. Unlike isoprene, monoterpene emissions occur year-around and continue into the night. The prevalence of the LO-OOA factor at all sites year-around points to the important contribution of monoterpene SOA to the total OA budget in the southeastern US. As the most oxidized OA factor, MO-OOA reaches a daily maximum in the afternoon and likely contains aged OA from various sources, such as vehicle emission, biomass burning, and aged OA from biogenic VOCs. We find that the correlation between MO-OOA and ozone is substantially better in summer than winter, suggesting that the sources of MO-OOA might vary with season.

In order to estimate the organic nitrate contribution to OA, we applied and evaluated three methods, i.e, NO_x^+ ratio method, PMF method, and AMS-IC method. Despite the uncertainty of the NO_x^+ ratio method (i.e., the values of R_{ON} and R_{AN}) and the PMF method (i.e., the separation of pure NIA factor), both methods provide reasonable results in separating the measured total nitrates into nitrate functionality from inorganic and organic nitrates. The "nitrate functionality from organic nitrates" (i.e., $NO_{3,org}$) accounts for about 63–100% and 10-20% of total measured nitrate (i.e., $NO_{3,meas}$) in summer and winter, respectively. Further, we estimate the contribution of organic nitrates to total OA based on estimated $NO_{3,org}$ and assumed molecular weigth of bulk organic nitrates. Depending on location, season and estimation method, organic nitrates account for about 5-25% of total OA, which indicates that organic nitrates are important components in the ambient aerosol.

The spatial distribution of OA is investigated by comparing ACSM measurements (stationary at the Georgia Tech site) and HR-ToF-AMS measurements (rotating among different sites). In summer, OA is spatially homogeneous as suggested by the good correlation (R=0.92) in July between the GT and YRK sites, which are 70km apart. The spatial homogeneity of OA in summer is likely caused by SOA being the dominant source of OA for both urban and rural sites. The parameters such as temperature, solar radiation, and precursor VOCs, which have great influences on SOA formation, are similar between urban and rural sites. Compared to summer, the OA is less spatially homogenous in winter. The correlation coefficient of OA between GT and YRK decreases to 0.66 in winter. This is likely due to the elevated contribution from POA to total OA in winter and the spatially inhomogeneous distribution of POA. Meteorology also plays a role in the OA spatial distribution, but alone is unlikely to explain the observation.

We show that short-term and extensive measurements can help interpret long-term basic measurements. For example, consistent with long-term (1999 – 2013) OC measurements from the SEARCH network, we also observed that the seasonal variation of OA has some urban and rural contrasts. While the OA concentration is similar between summer and winter for the urban JST site, it increases by a factor of 4 from winter to summer for the rural YRK site, according to our year-long observations. PMF analysis suggests that the different OA seasonality between urban and rural sites is likely due to the varying strength of OA sources. For rural sites, SOA represents the dominant fraction of OA in both summer and winter, but SOA concentration is much lower in winter. For urban sites, in contrast, the decrease in SOA concentration in winter is compensated by the increase in POA concentration due to less dispersion from lower boundary layer heights,

leading to a relatively constant total OA concentration compared to summer. In addition, analysis of long-term OC and sulfate measurements from the SEARCH network shows that the correlation between OC and sulfate is substantially better in summer than winter, consistent with our source apportionment results that show the majority of OA is secondary in summer. The better correlation of OC and sulfate in summer also supports that sulfate directly mediates the formation of isoprene SOA (Xu et al., 2015), which is only present in warmer months.

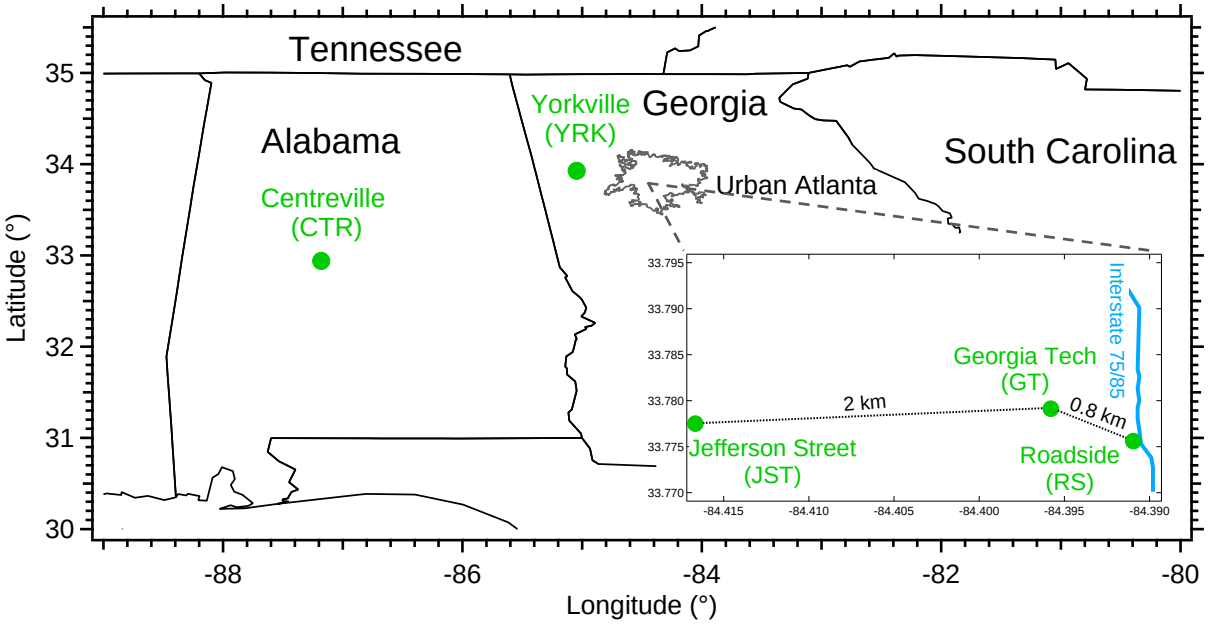

Figure 2.1. Sampling sites for SCAPE and SOAS studies. The gray circled region represents urban Atlanta.

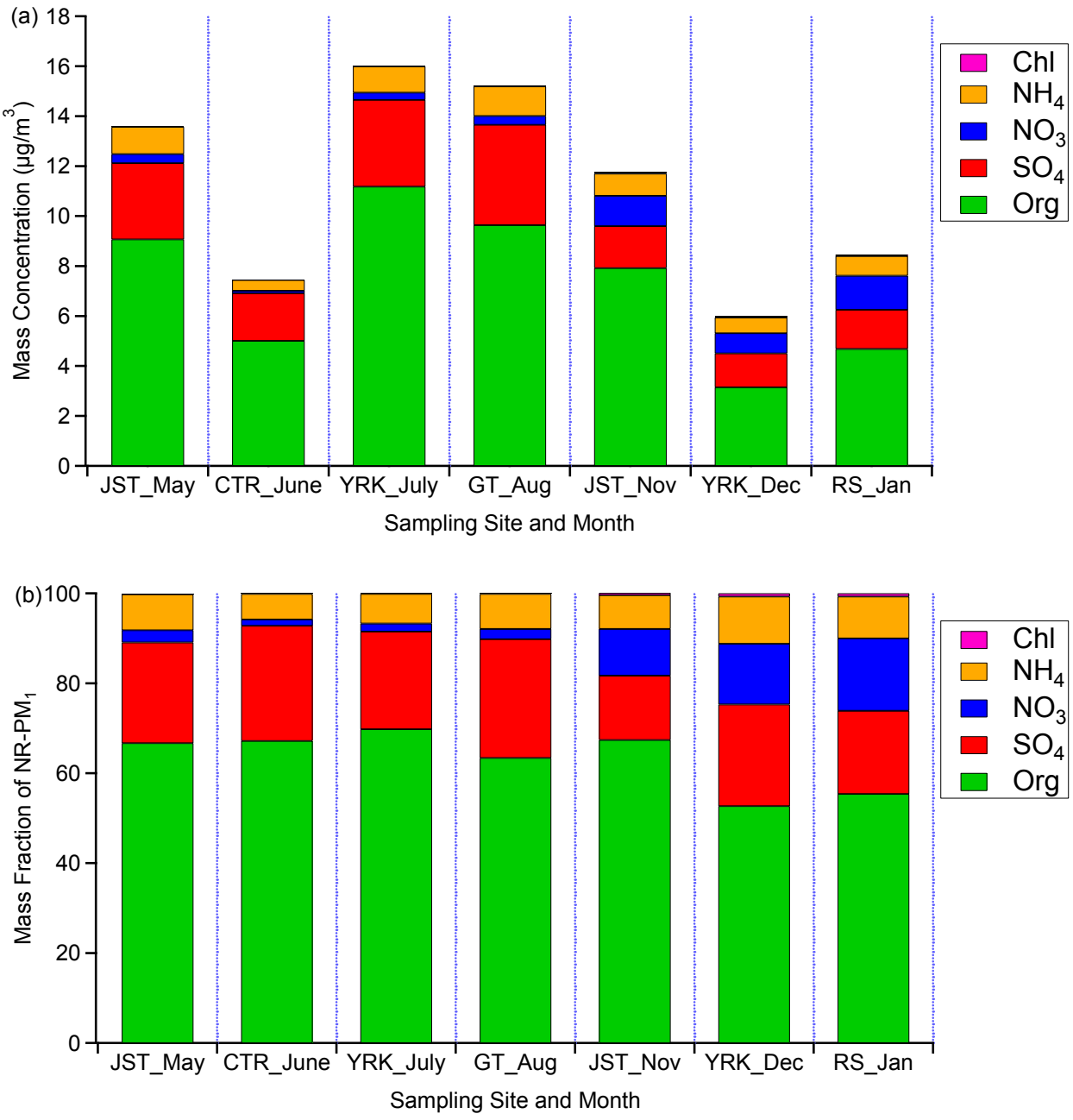

Figure 2.2. Mass concentrations (a) and mass fractions (b) of non-refractory PM_1 (NR-PM_1) species measured by HR-ToF-AMS.

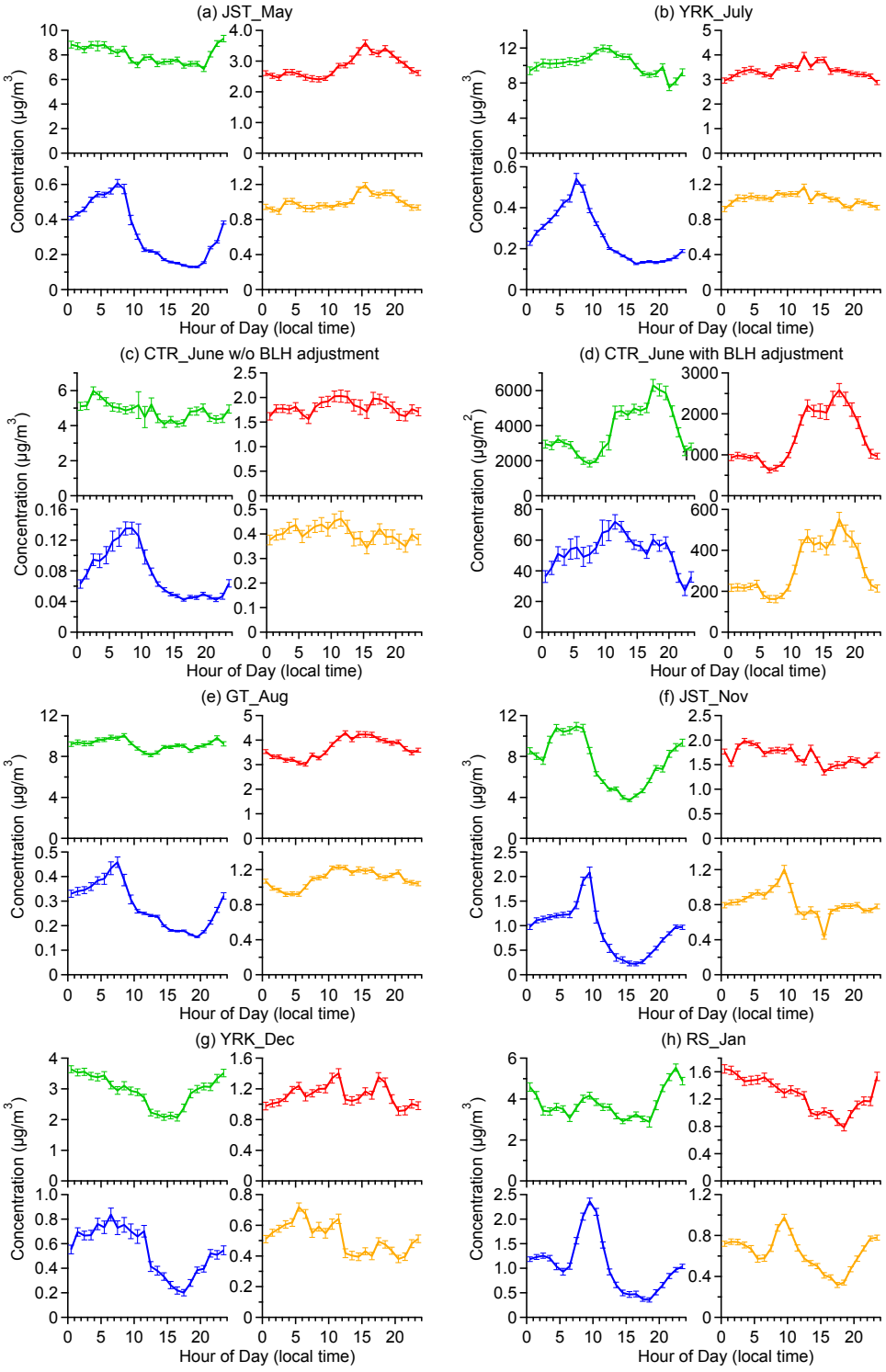

Figure 2.3. Diurnal profiles of non-refractory PM_1 (NR-PM_1) species measured by HR-ToF-AMS. Panel (d) shows the diurnal profiles of NR-PM_1 species after multiplying by the boundary layer height for the Centreville (CTR) site. The solid lines indicate the median concentration and the error bars indicate the standard error.

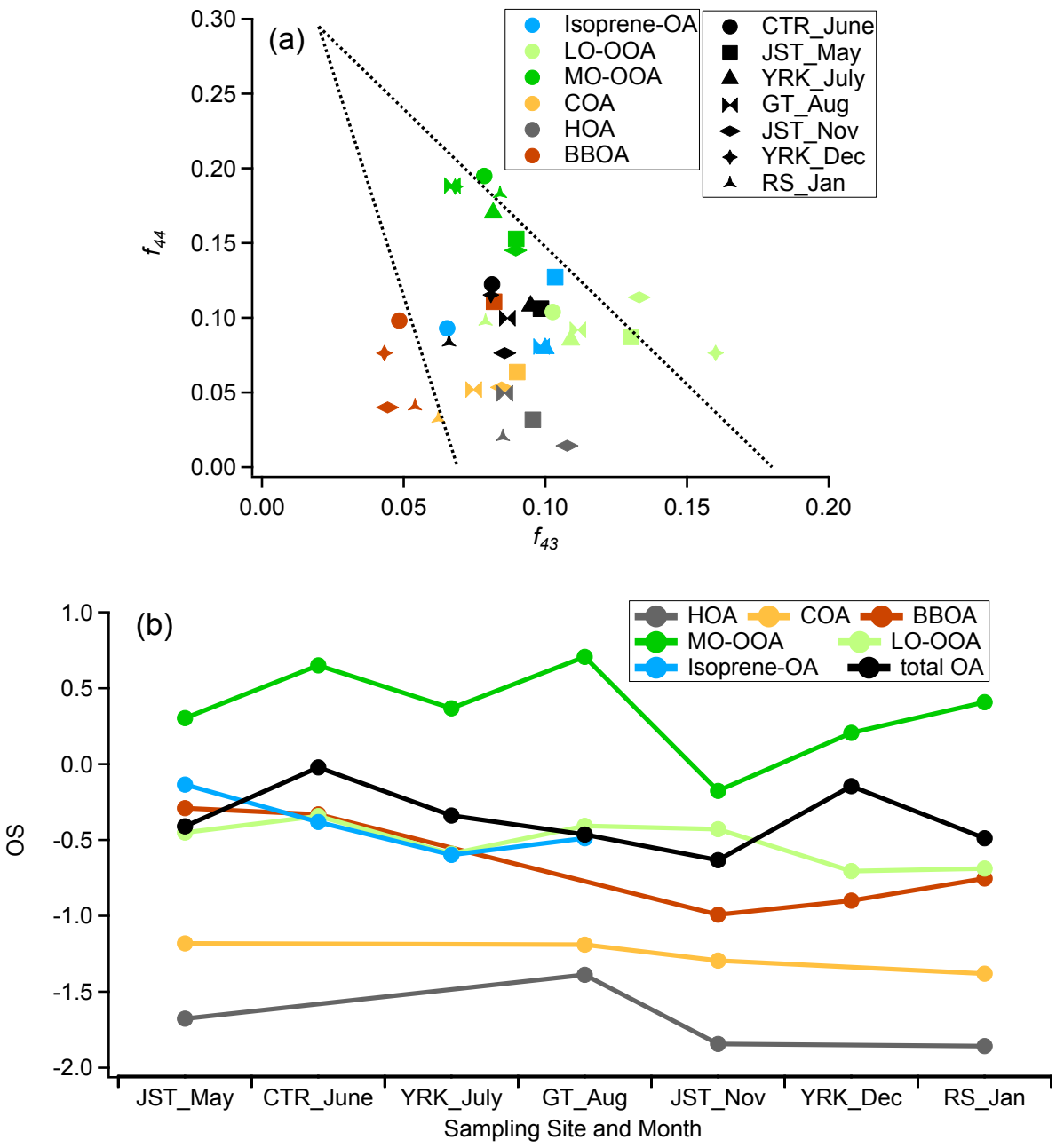

Figure 2.4. (a) f_{44} vs. f_{43} for total OA and OA factors resolved from PMF analysis. (b) The oxidation state of OA factors.

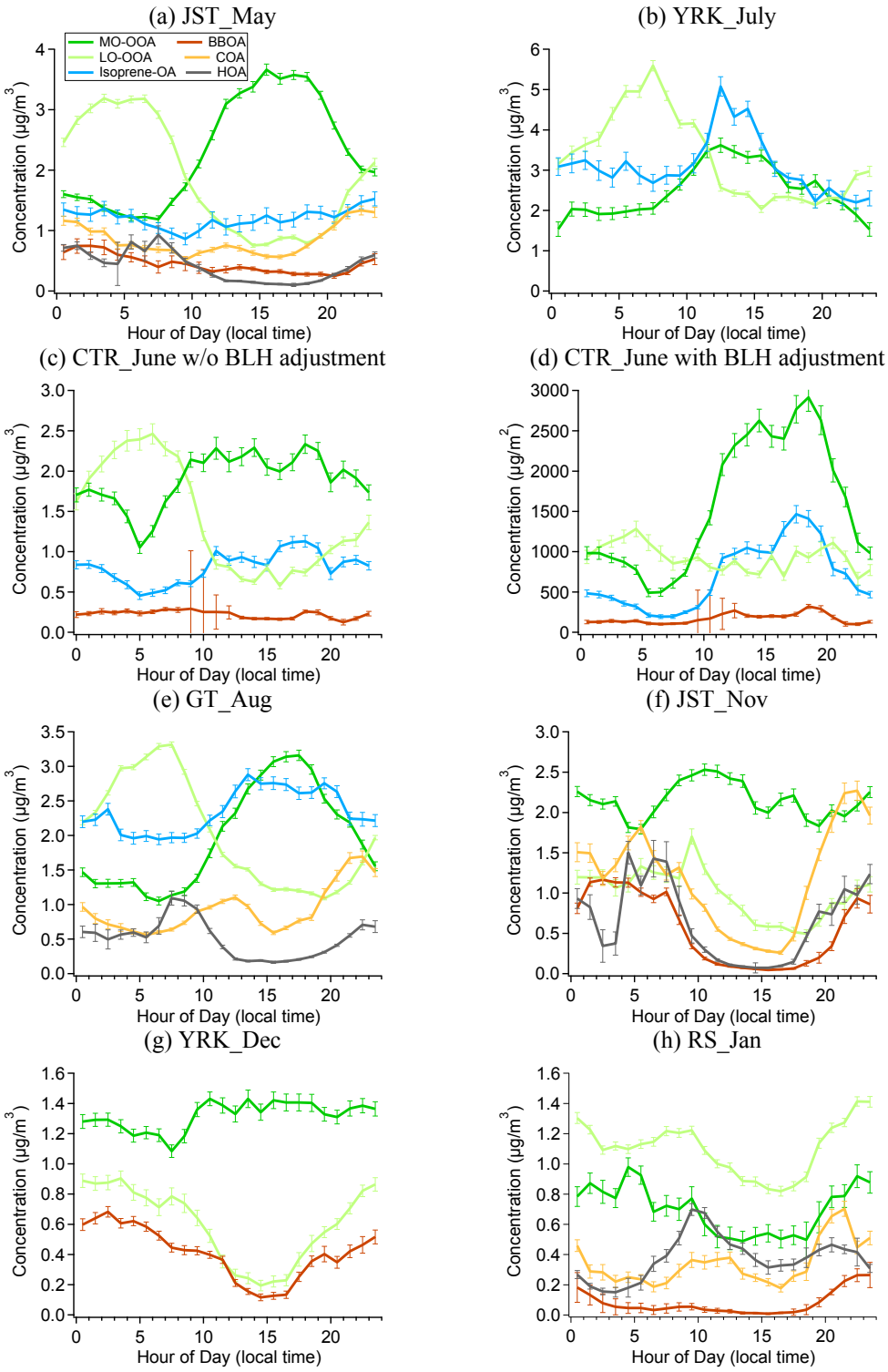

Figure 2.5. Diurnal profiles of OA factors resolved from PMF analysis on organic mass spectra. Panel (d) shows the diurnal profiles of OA factors after multiplying by the boundary layer height for the Centreville (CTR) site. The solid lines indicate the median concentration and the error bars indicate the standard error.

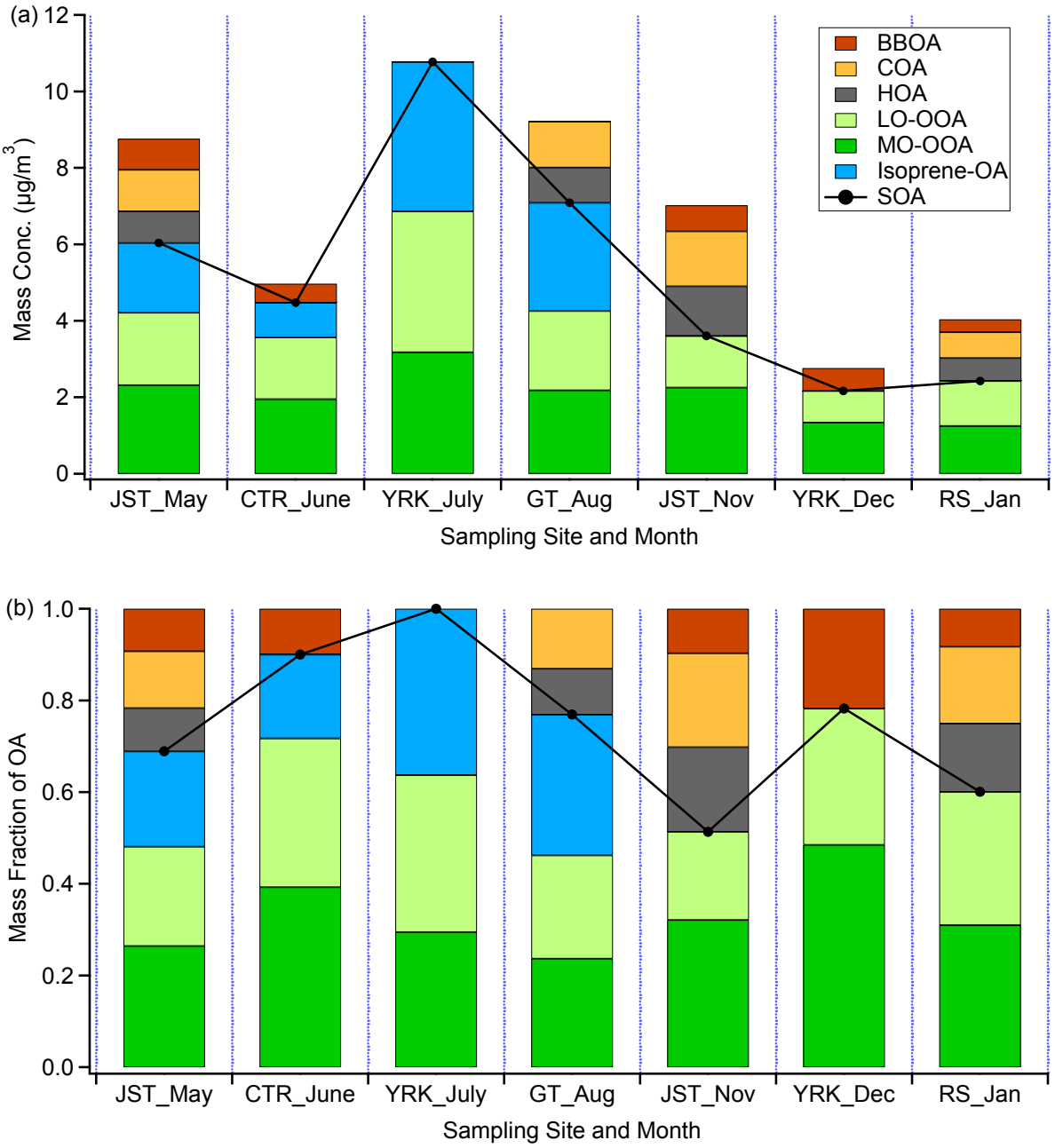

Figure 2.6. (a) Campaign-averaged mass concentrations of OA factors resolved from PMF analysis on organic mass spectra. (b) Campaign-averaged mass fractions of OA factors resolved from PMF analysis on organic mass spectra. SOA is the sum of Isoprene-OA, MO-OOA, and LO-OOA. POA is the sum of HOA, COA, and BBOA.

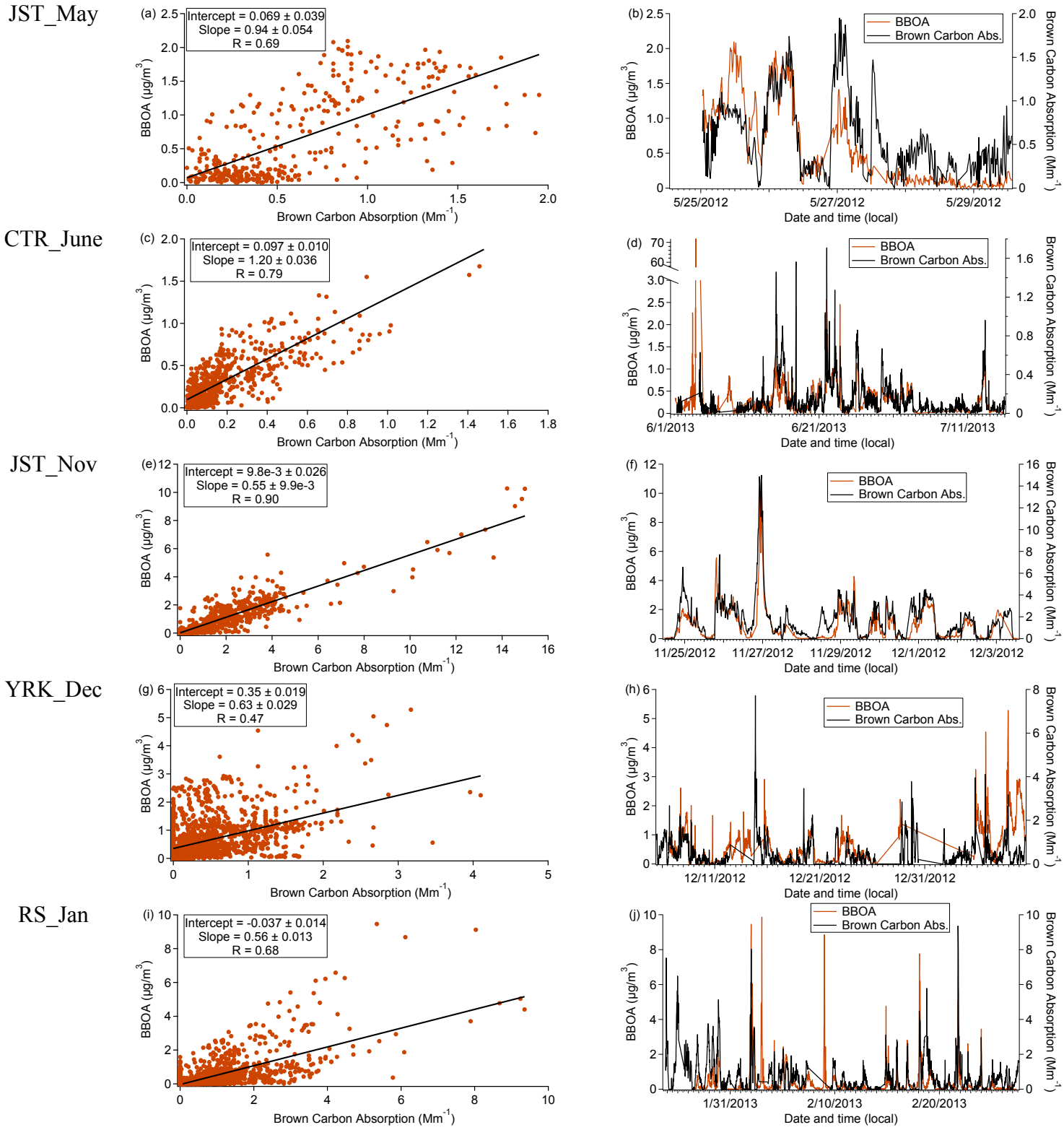

Figure 2.7. Scatter plot (left panel) and the time series (right panel) of BBOA and brown carbon light absorption for the datasets where a BBOA factor was resolved.

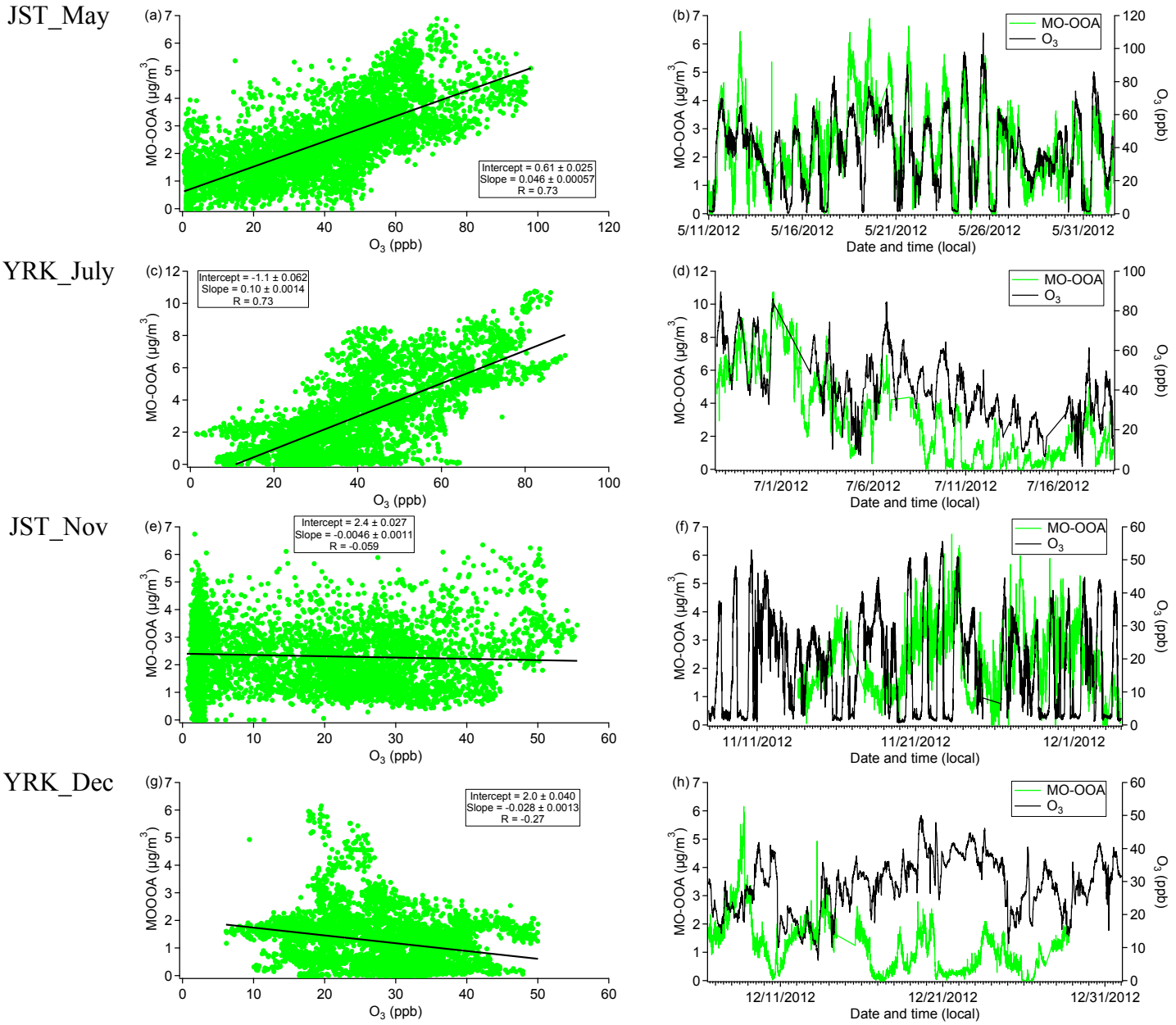

Figure 2.8. Scatter plot (left panel) and the time series (right panel) of MO-OOA and ozone.

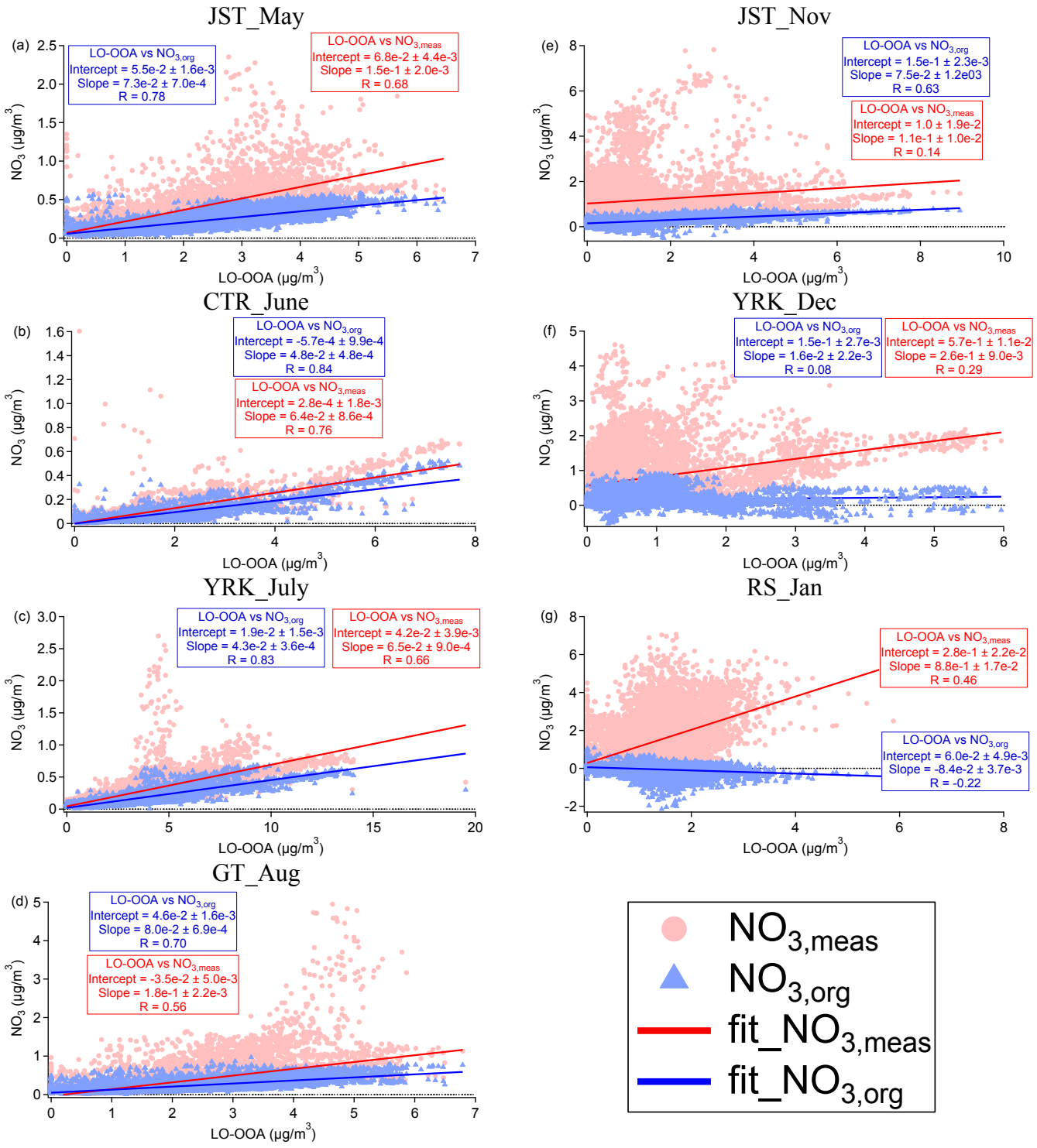

Figure 2.9. Scatter plot of LO-OOA vs. the total measured nitrates (i.e., $NO_{3,meas}$) and LO-OOA vs. estimated concentration of "nitrate funcionality from organic nitrates" (i.e., $NO_{3,org}$) by using R_{ON} = 10 in the NO_x^+ ratio metod.

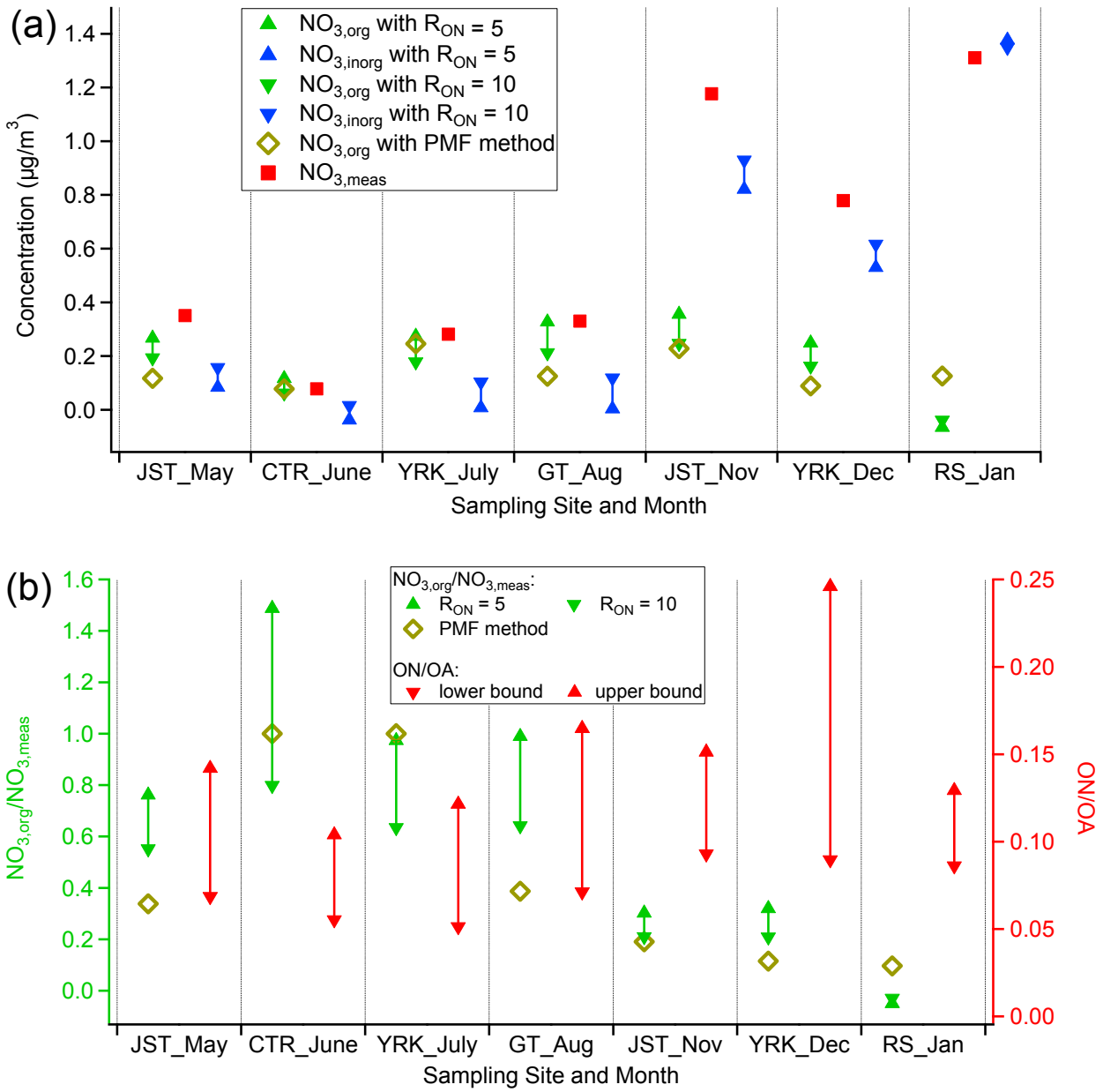

Figure 2.10. (a) Concentrations of total measured NO_3 (i.e., $NO_{3,meas}$), estimated "nitrate functionality from organic nitrates" (i.e., $NO_{3,org}$) by the NO_x^+ ratio method and the PMF method. (b) The contribution of $NO_{3,org}$ to $NO_{3,meas}$ (i.e., $NO_{3,org}/NO_{3,meas}$) from the NO_x^+ ratio method and the PMF method. Also shown are the estimated contribution of organic nitrates to total OA from the "best estimate" range of $NO_{3,org}$ and by assuming a MW of 200 and 300 g mol^{-1} for organic nitrates.

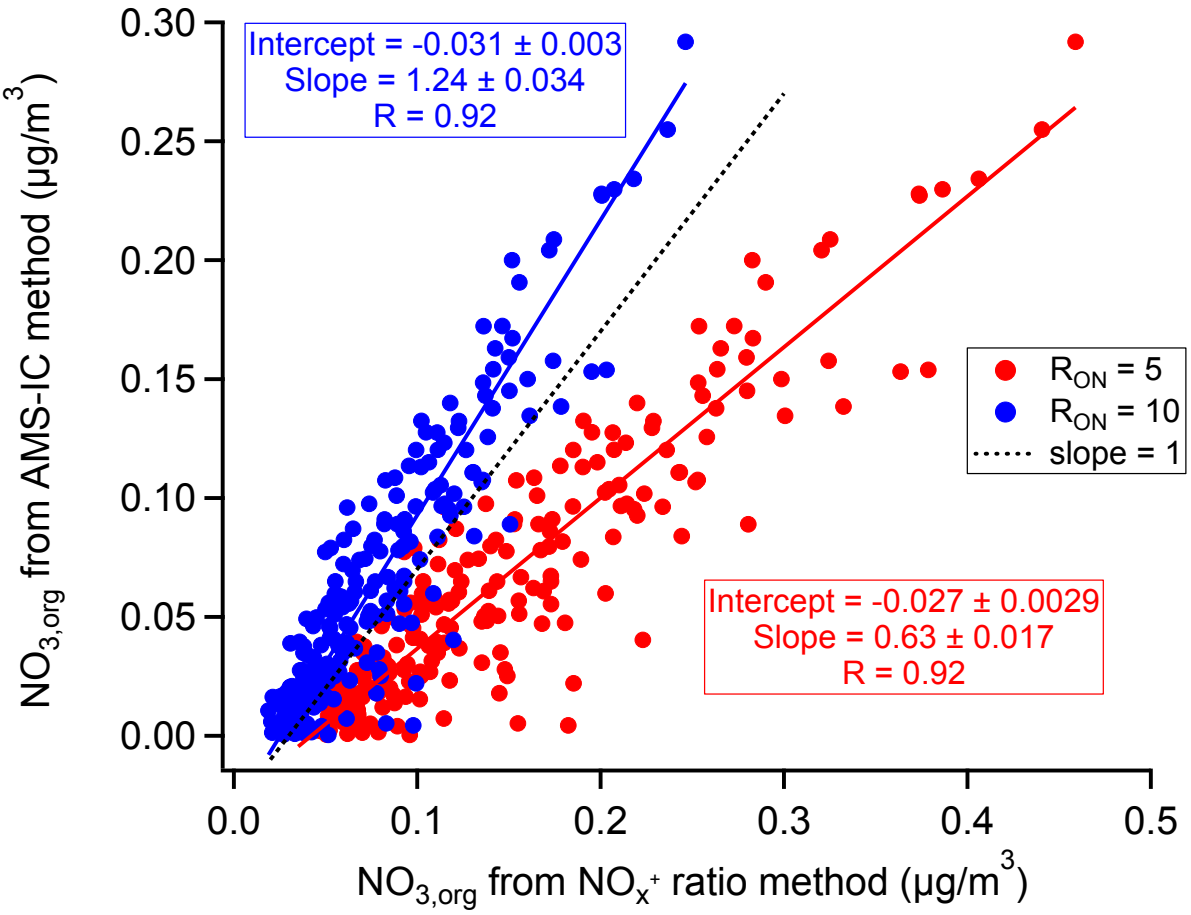

Figure 2.11. Comparion of estimated concentration of "nitrate functionality from organic nitrates" (i.e., $NO_{3,org}$) at the Centreville (CTR) site between the AMS-IC method and NO_x^+ ratio method with R_{ON} values of 5 and 10. The intercept and slope are obtained by orthogonal fit, which considers measurement errors in both dependent and independent variables. The correlation coefficient R is obtained by linear least-squares fit. Intercepts are within the detection limit of PILS-IC nitrate (i.e., 0.03 µg m^{-3}). The 1:1 line is offset by the detection limit of PILS-IC nitrate (i.e., -0.03 µg m^{-3}) for visual clarity. The uncertainty of PILS-IC measurements is about 10% according to Weber et al. (2001).

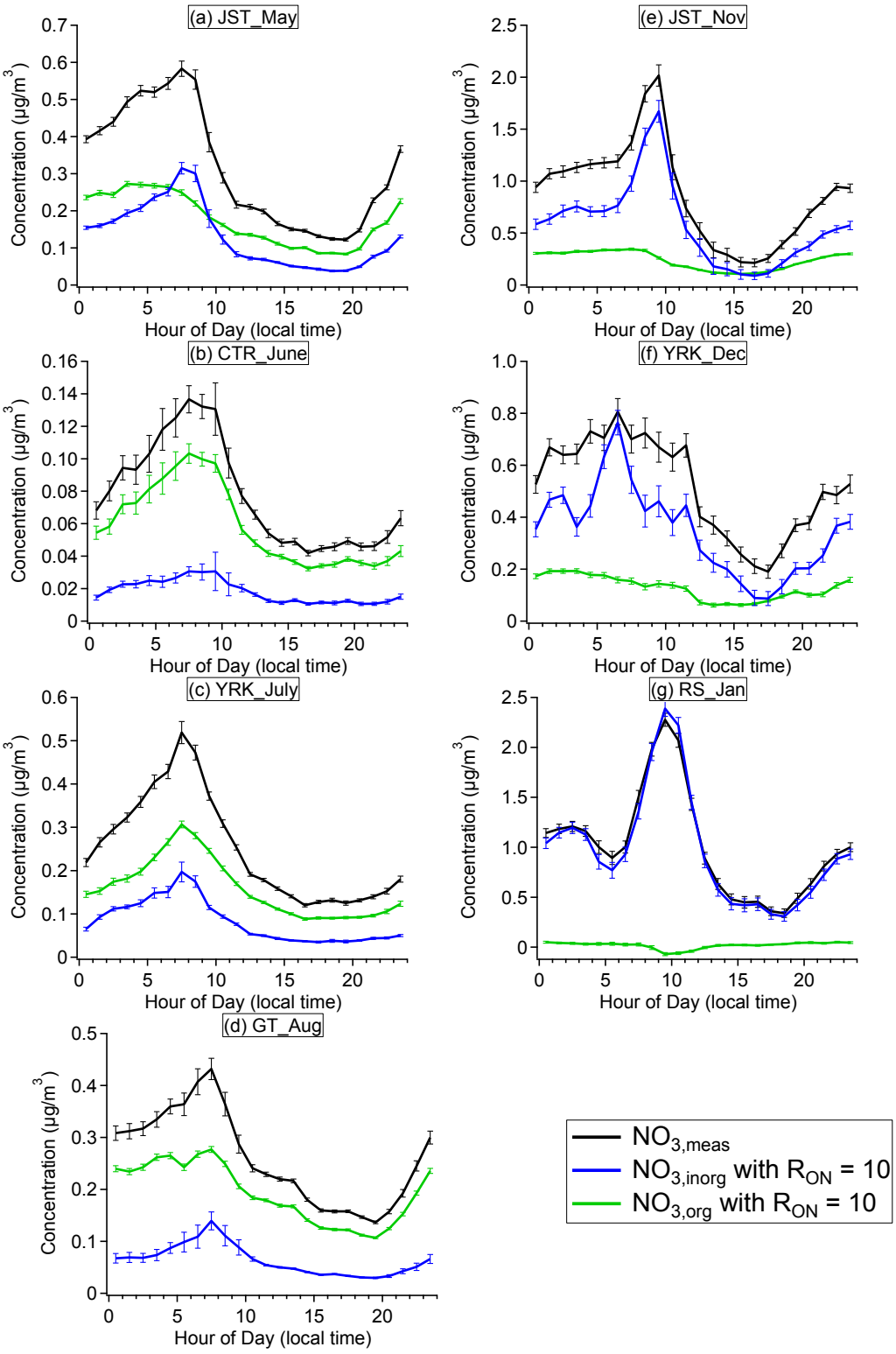

Figure 2.12. Diurnal variation of $NO_{3,meas}$, $NO_{3,org}$, and $NO_{3,inorg}$ for all datasets. $NO_{3,org}$, and $NO_{3,inorg}$ are estimated by the NO_x^+ ratio method with an R_{ON} value of 10. The solid lines indicate the median concentration and the error bars indicate the standard error.

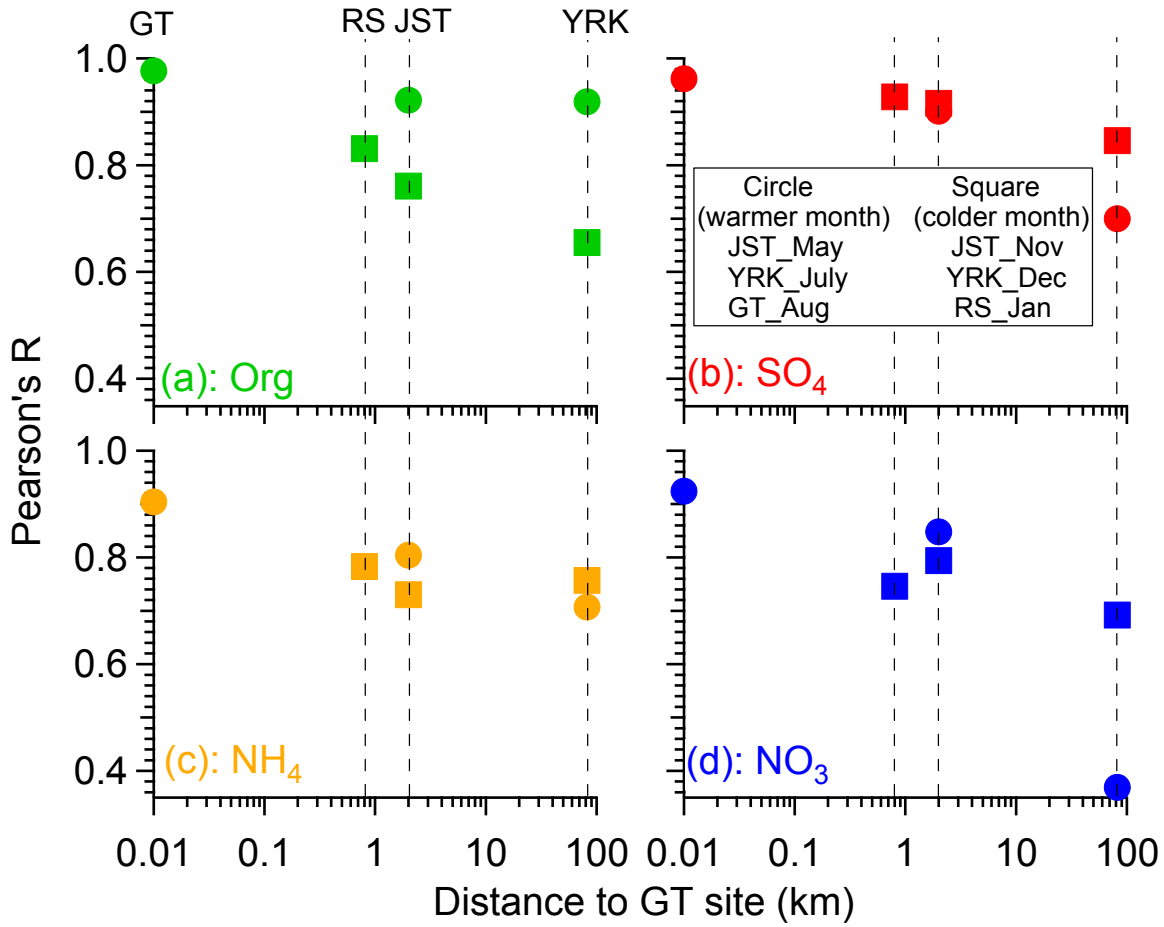

Figure 2.13. Correlation coefficients for NR-PM_1 species between ACSM measurements (stationary at the Georgia Tech site) and HR-ToF-AMS measuremens (rotating among different sites). Values are plotted vs. the relevant distance of the measurement site from the GT site, where the dotted lines represent the sampling sites where the HR-ToF-AMS measurements were made.

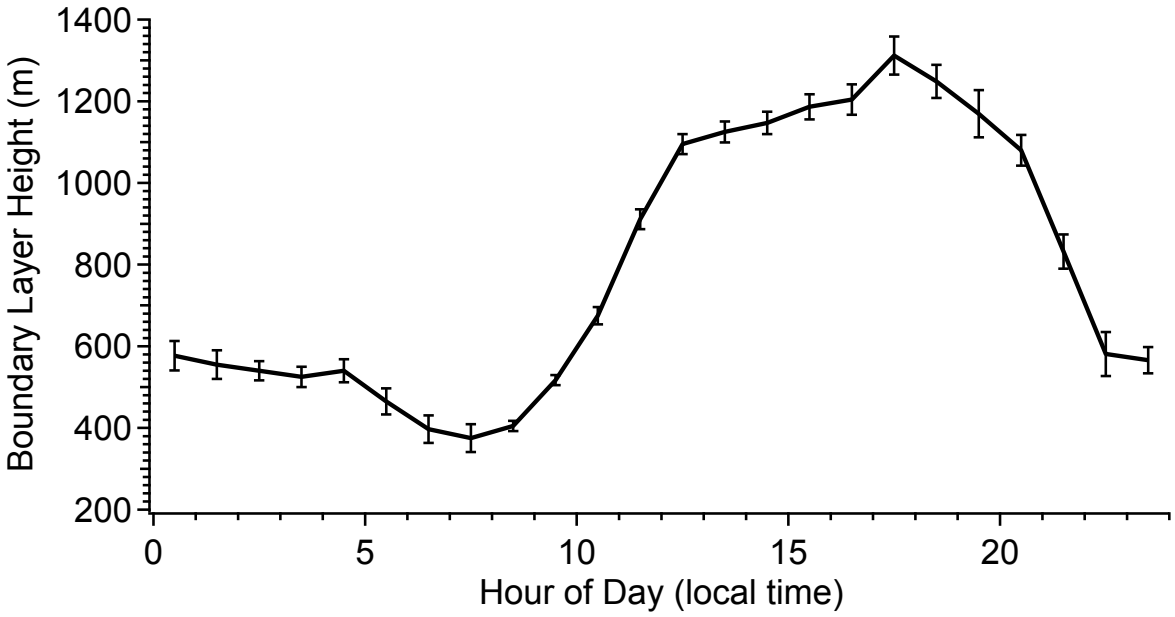

Figure 2.14. Diurnal variation of boundary layer height for CTR_June. The solid line indicates the median concentration and the error bars indicate the standard error.

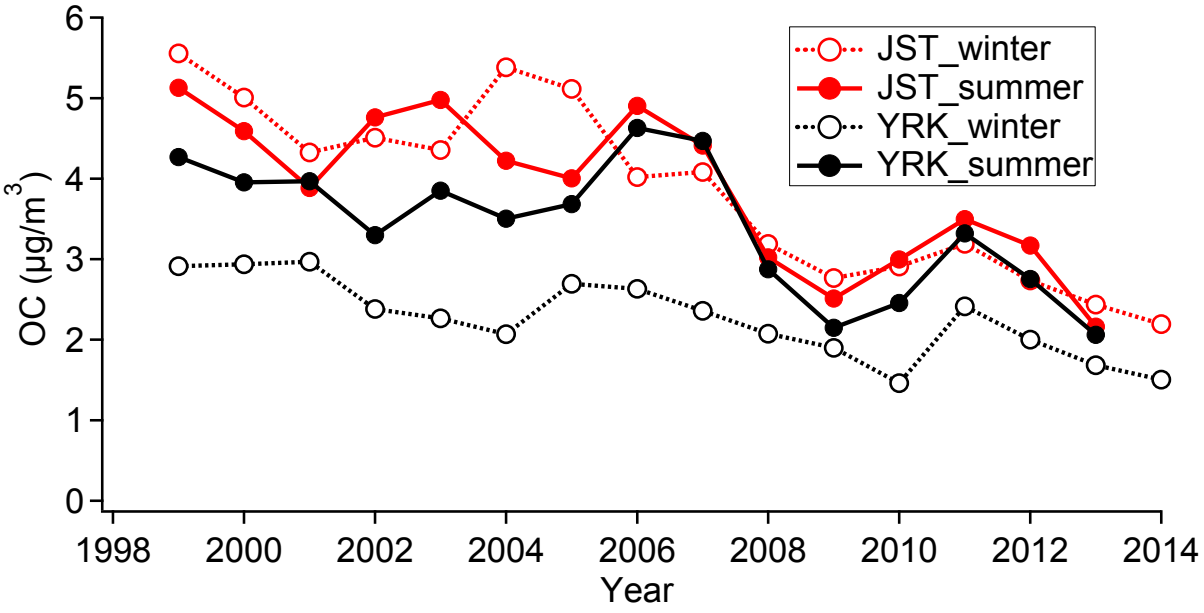

Figure 2.15. Mean seasonal concentrations of organic carbon at the Jefferson Street (JST) and the Yorkville (YRK) sites. Summer: June – August. Winter: December – Februry.

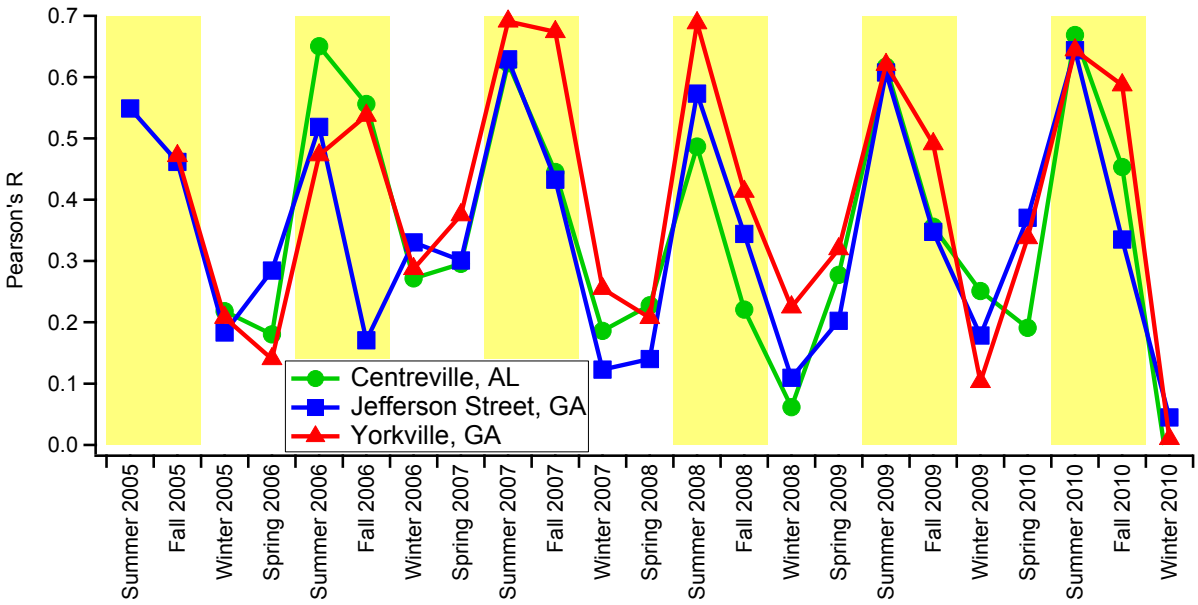

Figure 2.16. The seasonality of the correlation between organic carbon and sulfate at the Jefferson Street (JST), Yorkville (YRK), and Centreville (CTR) sites. Seasons are by grouped by calendar months (Spring: March–May, Summer: June–August, Fall: September–November, and Winter: December–February).

CHAPTER 3: EFFECTS OF NOX ON THE VOLATILITY OF SECONDARY ORGANIC AEROSOL FORMATION FROM ISOPRENE PHOTOOXIDATION

3.1 Background

Isoprene is the most abundant non-methane hydrocarbon (NMHC) emitted into the atmosphere with a global emission of ~500 Tg/year (Guenther et al., 2006). Isoprene oxidation by OH radicals plays a critical role in tropospheric ozone (O_3) chemistry and secondary organic aerosol (SOA) formation (Chameides et al., 1988; Claeys et al., 2004b; Carlton et al., 2009; Hallquist et al., 2009). Recent studies have shown that nitrogen oxides (NO_x=NO+NO_2) are highly influential in SOA formation from various hydrocarbon precursors, including isoprene (Tuazon et al., 1990; Kroll et al., 2006; Surratt et al., 2010; Lane et al., 2008; Sato et al., 2011). NO_x effects on SOA formation have been attributed to the chemistry of organic peroxy radicals (RO_2). While the reaction of RO_2 with HO_2 and NO_2 produces low volatile species, RO_2+NO reaction could form volatile species via fragmentation of the resultant RO radical (Atkinson, 1997; Kroll and Seinfeld, 2008; Hatakeyama et al., 1989). Despite the fact that SOA formation from isoprene has been intensively studied, many observations in both laboratory studies and field measurements cannot be well explained based on our current knowledge of isoprene oxidation chemistry and yield (Lin et al., 2013a; Robinson et al., 2011a; Goldstein et al., 2009; Carlton et al., 2010; Brock et al., 2003). For example, recent aircraft and ground-based studies during the CARES field mission suggested that SOA formation was enhanced when NO_x was mixed

with isoprene-rich air masses, though the mechanism for the enhancement remains unclear (Setyan et al., 2012; Shilling et al., 2013).

Volatility is a key property of organic aerosol because it determines the partitioning between the gas and particle phases, and thus SOA formation. Most of the aerosol volatility studies focused on SOA generated from monoterpene ozonolysis (Li et al., 2007; Kostenidou et al., 2009; Lee et al., 2011; An et al., 2007). Limited studies have been conducted on the volatility of isoprene SOA and the results from these studies are inconclusive. King et al. (2010) observed that isoprene SOA volatility was not affected by NO_x. However, Kleindienst et al. (2009) reported that the effective enthalpies of vaporization (ΔH_{vap}^{eff}) were 38.4 kJ*mol^{-1} and 43.2 kJ*mol^{-1} for SOA from isoprene photooxidation in the absence and presence of NO_x, respectively, indicating that isoprene SOA formed in the presence of NO_x was less volatile. Thus, the effects of NO_x on the volatility of isoprene SOA are highly uncertain.

In this study, we systematically investigate the effects of NO_x on the volatility of SOA from isoprene photooxidation in a series of chamber experiments. With a thermal denuder (TD) set at predefined temperatures, we focus on the measurement of the volatility of both the bulk organic aerosol and key chemical properties of that aerosol. Two types of experiments are conducted with a wide range of NO_x conditions, in which the fate of RO_2 radicals varies and leads to differences in SOA yield, volatility, and oxidation state.

3.2 Experimental Section

Experiments were conducted in the Pacific Northwest National Laboratory (PNNL) dual 10.6 m^3 Teflon environmental chambers (Liu et al., 2012). Before each experiment,

the chambers were flushed with purified air until the particle concentration was less than 10 cm^{-3} and NO_x and O_3 concentrations were less than 1ppbv. Isoprene was injected into the chamber by passing a stream of pure air over a measured volume of the pure compound (Sigma-Aldrich, 99.8%). H_2O_2 was used as OH radical precursor in this study. For each experiment, H_2O_2 (Sigma-Aldrich, 50wt.% in H_2O) was introduced into the chamber by passing pure air over 50μl of the H_2O_2 solution in a gently-heated glass bulb. The concentration of H_2O_2 in the chamber was not directly measured, but it was estimated to be about 1ppm based on the injected H_2O_2 volume and chamber volume. After all of the components were injected and well-mixed in the chamber, UV lights were turned on to initiate photooxidation reactions. All of the experiments were conducted at ~25°C and under dry conditions (RH< 5%). No seed particles were used in this study.

A suite of on-line instruments were used to characterize both the gas- and particle-phase composition. A High Resolution Time-of-Flight Aerosol Mass Spectrometer (HR-ToF-AMS, Aerodyne) was used to continuously characterize the chemical composition of non-refractory aerosol particles (DeCarlo, 2006; M.R.Canagaratna, 2007). A Scanning Mobility Particle Sizer (SMPS, TSI) was used to measure the particle size distribution, number concentration, and total aerosol volume. A Proton Transfer Reaction Mass Spectrometer (PTR-MS) was used to monitor the concentration of isoprene and its major oxidation products in the gas phase. A UV absorption O_3 analyzer (Thermo Environmental Instruments model 49C) allowed for the measurement of O_3 concentration. A chemilumnescence $NO/NO_2/NO_x$ analyzer (Thermo Environmental model 42) was used to measure concentration of NO and NO_x. NO_2 concentration can be calculated by subtracting

NO from the total NO_x, though this calculation may be complicated by detection of NO_y species (e.g. HNO_3) as NO_2 in the instrument.

A thermal denuder (TD), the design of which was based on Fierz et al. (2007) (Fierz et al., 2007), was used in this study to investigate aerosol volatility. The TD consists of a 60cm long, 11.4mm ID stainless steel tube and has a residence time of 12s at the experimental flow rate of 0.31 LPM. In this study, the TD temperature was stepped from 30 to 200°C with a temperature program of 30 /50 /70 /100 /150 /200 /180 /130 /110 /85 /65 / 40°C. Both sections of the TD were set to the same temperature and the entire length contained heated activated carbon absorbent. The TD was placed upstream of the SMPS and HR-ToF-AMS. The aerosol was sampled through the TD at each temperature setting for five minutes, the valve was then switched to a bypass line for another five minutes, during which the TD temperature was ramped to the subsequent temperature setting. A full temperature cycle took two hours. The volatility of the SOA was inferred from the differences in composition and total aerosol volume between bypass and thermal-denuded data from HR-ToF-AMS and SMPS.

Two types of experiments were conducted in this study. The first type was referred to as "HO_2-dominant" experiments (Expt. 1-3, Table 1), in which the NO_x concentration was below the detection limit (1ppb) and organic peroxy radicals (RO_2) primarily reacted with HO_2 radicals. In the second type of experiment, NO was injected into the chamber from a gas cylinder (500ppm in N_2) in addition to H_2O_2. Under these conditions, RO_2 radicals can react through multiple pathways, including with HO_2, NO, NO_2, and other RO_2 radicals. Herein, the second type experiment was referred to as "mixed" experiments (Expt. 4-8, Table 1).

Table 3.1. Experimental conditions and results

Expt.	$[Isoprene]_0$ (ppb)	$[NO]_0$ (ppb)	[OH] (10^6molec^{-1}*cm^3)	SOA ($\mu g/m^3$)[a,c]	SOA Yield (%)[a,c]
1	45.5	<1	1.04	6.3±0.2[b]	5.0±0.1[b]
2	78.4	<1	0.82	14.7±0.3	6.7±0.2
3	144.7	<1	0.44	30.2±1.4[b]	7.5±0.4[b]
4	97.7	68.1	4.64	19.7±0.4	7.2±0.2
5	91.4	114.8	4.40	19.7±0.8	7.7±0.3
6	114.6	338.2	3.58	27.0±1.0	8.5±0.3
7	105.5	466.2	3.35	10.9±1.5	3.7±0.5
8	100.6	738.1	2.72	4.2±0.4	1.5±0.2

a) Both SOA mass concentration and SOA yield are wall-loss corrected unless noted otherwise. Size-dependent wall loss rates are determined from "$(NH_4)_2SO_4$ only" wall-loss experiments (Keywood et al., 2004). The particle mass concentration of SOA is calculated by multiplying the SOA volume by the SOA density. SOA volume is measured by the SMPS. SOA density is calculated from the AMS-measured vacuum aerodynamic diameter and the SMPS-measured mobility diameter. An average density of 1.3 g*cm^{-3} and 1.4 g*cm^{-3} are obtained in HO_2-dominant and mixed experiments, respectively. SOA yield is defined as the ratio of the mass concentration of SOA particles to the mass concentration of reacted isoprene. Stated uncertainties (1σ) are calculated from the scatter in the particle volume measurements.
b) Data are not wall-loss-corrected.
c) Both SOA mass concentration and SOA yield correspond to aerosol growth at equivalent OH exposures of approximately 2*10^7 molecule*hour*cm^{-3}. OH concentration is estimated from the measured isoprene decay.

3.3 Results

3.3.1 Aerosol Growth Dynamics

Table 3.1 shows the experimental conditions and results. Shown in Figure 3.1 are the time series of NO, NO_2, isoprene, methacrolein (MACR, C_4H_6O) + methyl vinyl ketone (MVK, C_4H_6O), and organic aerosol of a typical HO_2-dominant (Expt. 2) and a typical mixed experiment (Expt. 6). In HO_2-dominant experiments, NO and NO_2 concentrations are below 1ppb throughout the experiment. In mixed experiments, NO and NO_2 concentration vary over the course of the experiment. After the lights are turned on, NO is

converted to NO_2 via reaction with RO_2, HO_2, and O_3, so the NO_2 concentration initially increases. After NO is completely consumed, the NO_2 concentration decreases steadily by reaction with RO_2 to form secondary organic products and with OH to form HNO_3. As all of the experiments are conducted under dry conditions (RH<5%), it is expected that the partitioning of HNO_3 into the partition phase is negligible. O_3 formation from NO_2 photolysis is observed in mixed experiments. O_3 concentration was below 200ppb at the time when isoprene was completely consumed. Based on the reaction rate constants of isoprene with O_3 and OH ($1.28*10^{-17}$ and $1.01*10^{-10}$ $cm^3*molecule^{-1}*s^{-1}$, respectively (Atkinson, 1997)) and the inferred OH concentration (~$4*10^6$ $molecule*cm^{-3}$) from the measured isoprene decay, it is estimated that the isoprene+OH reaction is at least one order of magnitude faster than isoprene+O_3 reaction. In addition, according to Kleindienst et al. (2007), ozonolysis of isoprene does not produce an appreciable amount of SOA. Hence, we do not expect the isoprene and O_3 reaction to contribute to aerosol formation in this study. As MACR and MVK have the same molecular weight, they cannot be separated by PTR-MS (Langford et al., 2010; Murphy et al., 2010). Here, they are reported as the sum of the two at *m/z* 71, referred to as MACR+MVK.

(a)

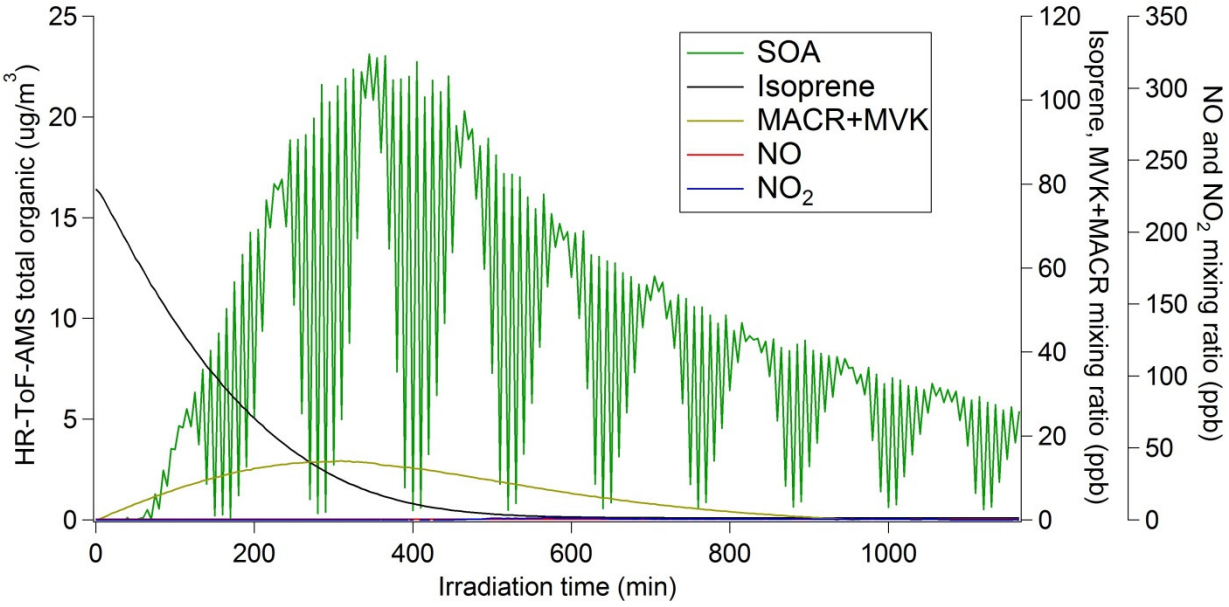

(b)

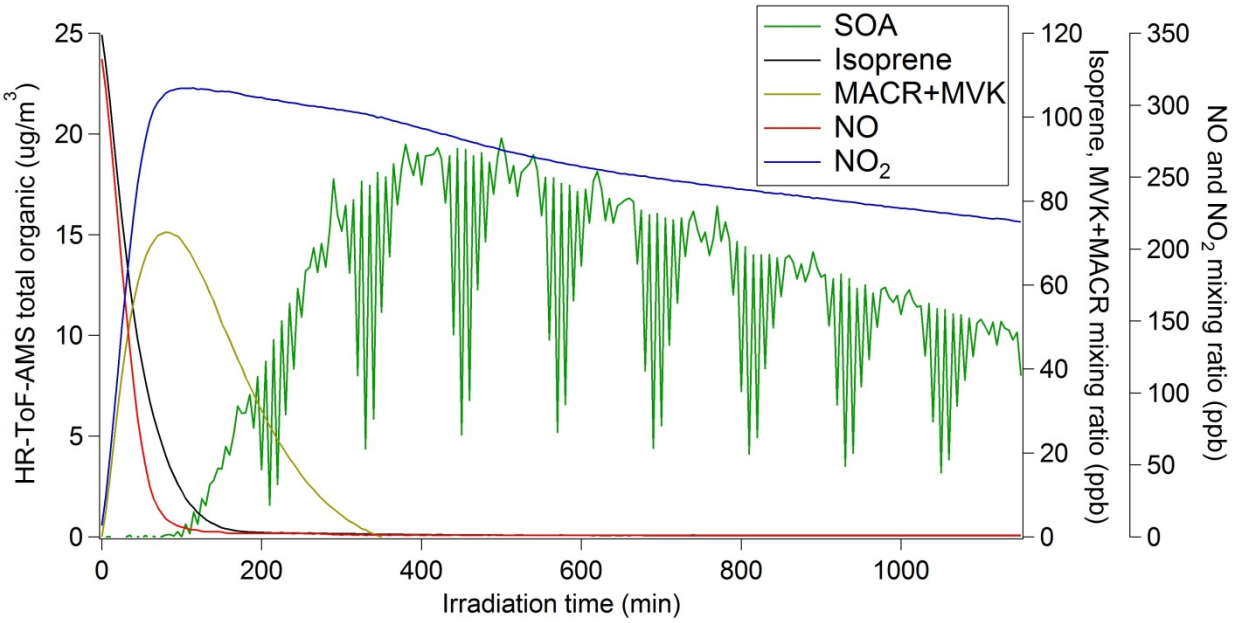

Figure 3.1. Time profiles for a typical (a) HO_2-dominant experiment (Expt.2) and (b) mixed experiment (Expt.6). Note that SOA mass is not wall-loss corrected in these two figures. The large fluctuations in SOA mass concentration are caused by the aerosol alternately passing through the TD at different temperatures and bypassing the TD.

The aerosol growth dynamics can be examined further by plotting the time dependent growth curves under different experimental conditions (Ng et al., 2006) . Shown in Figure 3.2 are the normalized growth curves (i.e., fraction of maximum OA concentration vs. fraction of isoprene reacted). In HO_2-dominant experiments, SOA growth ceases once all of the isoprene is consumed. In mixed experiments, however, SOA continues to grow even after all of the isoprene is consumed, indicated by the vertical section in the growth curve. Furthermore, the vertical section becomes more pronounced as the initial NO/isoprene ratio increases.

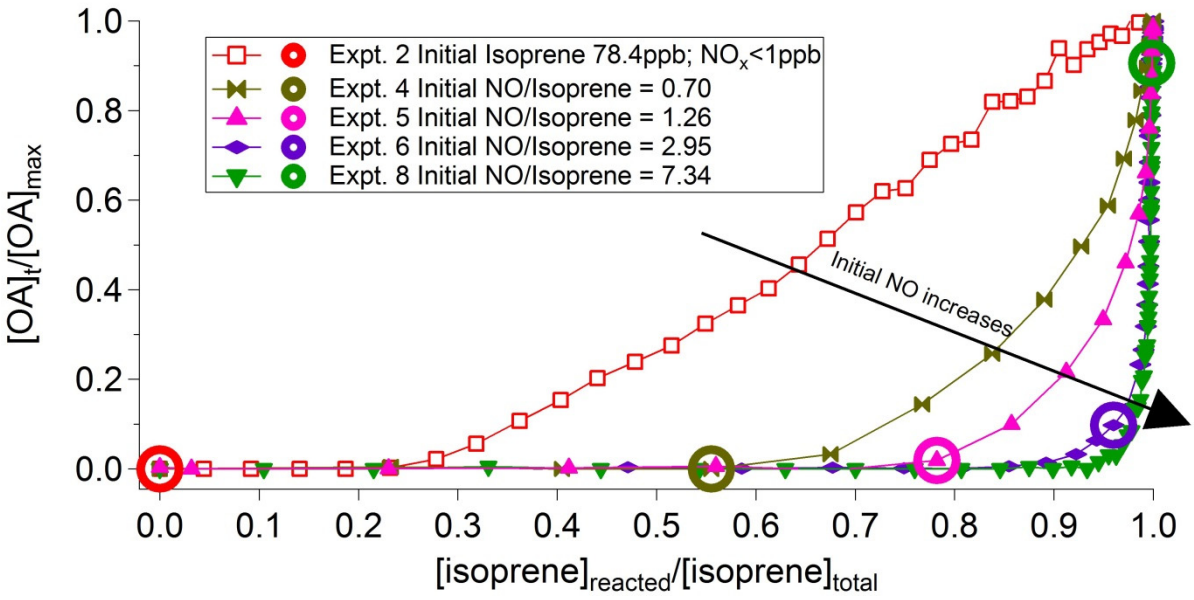

Figure 3.2. Normalized time-dependent growth curves. Circles show the fraction of isoprene consumed by the time NO concentration decreased below the detection limit.

3.3.2 Aerosol Volatility

Aerosol volatility is inferred by plotting the volume fraction remaining (VFR) or mass fraction remaining (MFR) as a function of TD temperature (i.e., "thermograms"). In this study, VFR is calculated as the ratio of the aerosol total volume measured by SMPS through the TD to the average volume of the preceding and succeeding bypass runs.

Similarly, MFR is obtained from HR-ToF-AMS measurement. Chamber particle wall-loss correction is not applied when calculating VFR or MFR, since VFR and MFR are ratios of measurements spaced closely in time and are therefore unaffected by chamber wall-loss. The loss of gas-phase species to chamber wall is not considered in this study, though recent studies suggested it may be significant for some species and therefore could have an effect on SOA composition (Matsunaga and Ziemann, 2010; Loza et al., 2010).

As TD temperature increases, the VFR decreases primarily due to the vaporization of semi-volatile components from the particles (Figure 3.3). The TD used in this study follows the design of Fierz et al. (2007), who observed minimal loss (<5%) of particles larger than 20 nm at temperatures of up to 200°C at a flow rate of 0.32 LPM. Given the short residence time in the TD, the thermal decomposition of species such as organic peroxides, carboxylic acids, and polyols in the TD is likely to be negligible compared to vaporization. For example, Hiatt and Strachan (1963) measured a decomposition rate of $7*10^{-5}$ s^{-1} at 176°C for 1-phenyl-2-methylproply-2-hydroperoxide. This decomposition rate would lead to only 1% decomposition of species during the TD residence time. SOA generated in both HO_2-dominant and mixed experiments shows similar VFR below 70°C. The differences in SOA volatility between HO_2-dominant and mixed experiments become evident above 80°C. Comparing the VFR at each temperature between all experiments, VFR increases with an initial NO/isoprene ratio up to 3. Beyond this ratio, increasing initial NO/isoprene ratio leads to a decrease in VFR. For example, at a TD temperature of 130 °C, the VFR is 0.35 at a NO/isoprene ratio of 0.69, increases to 0.48 at a NO/isoprene ratio of 2.95 and then decreases to 0.30 at a NO/isoprene ratio of 7.34. The observation that VFR

varies nonlinearly with the initial NO/isoprene ratio indicates that the volatility of isoprene SOA is very sensitive to the NO_x level.

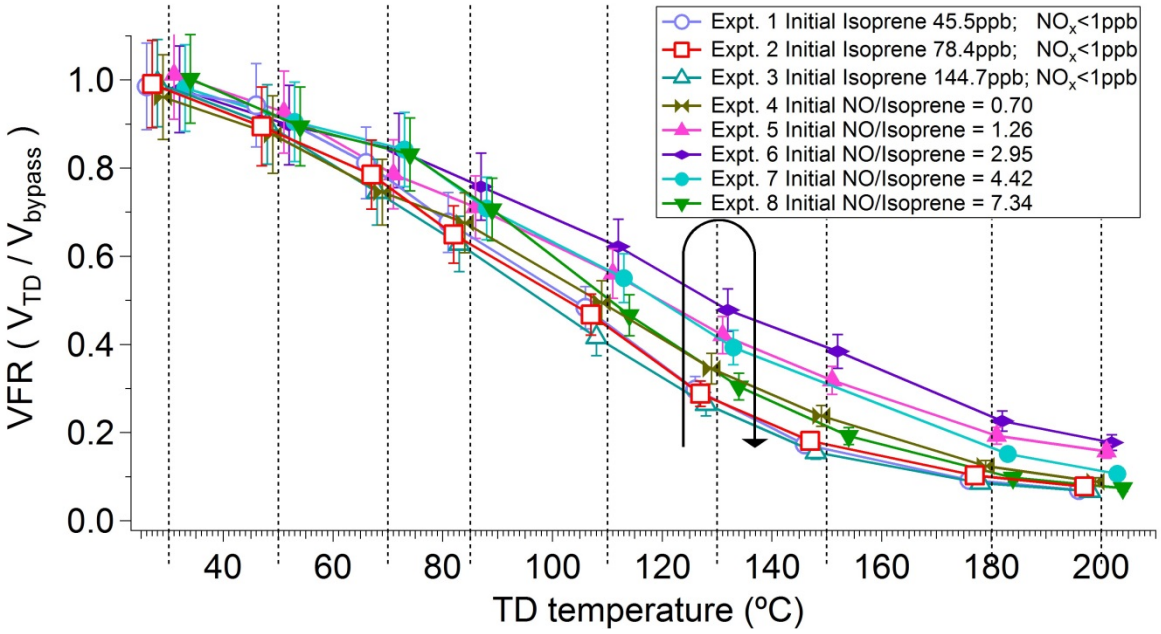

Figure 3.3. SMPS volume-based thermograms for the experiments described herein. VFR is calculated for all experiments at equivalent OH exposures of approximately $2*10^7$ molecule*hour*cm^{-3}. The solid black arrow highlights the observation that VFR first increases and then decreases as NO/isoprene increases. Error bars are based on the variability of the SMPS volume measurements. Data are not corrected for any temperature dependent losses in the TD, which a previous study suggested to be minor (Fierz et al., 2007). Data correspond to the TD temperatures (30 /50 /70 /85 /110 /130 /150 /180 /200°C, indicated by the dashed lines) and data are offset from the TD temperature for visual clarity. The VFR at 40, 65, and 100°C are consistent with shown data, but are omitted for clarity.

3.3.3 SOA Temporal Evolution

Figure 3.4 shows the time evolution of the VFR at various TD temperatures, SOA O/C and H/C ratios, and SOA oxidation state (Kroll et al., 2011) (=2*O/C-H/C) of a typical HO_2-dominant (Expt. 2) and a typical mixed experiment (Expt. 6). The presence of hydroperoxide group and organic nitrate groups (NO^+ and NO_2^+) introduces slight deviations from this calculation. The uncertainty in oxidation state of HO_2-dominant experiments is estimated to be 0.1 based on Kroll et al. (2011). The deviation caused by

organic nitrate groups would be negligible, considering that the mass fraction of NO^+ and NO_2^+ in total SOA is only about 5% in mixed experiments. In the HO_2-dominant experiment, both the VFR at 130°C and the oxidation state continuously increase from 0.10 to 0.29 and from -0.66 to -0.37, respectively, over 18 hours, indicating that the aerosol becomes less volatile and more oxidized as oxidation progresses. In the mixed experiment the VFR remains relatively constant over time. Interestingly, the temporal evolution of the VFR varies with initial NO/isoprene ratios, which is shown in Figure S4 in the supporting information.

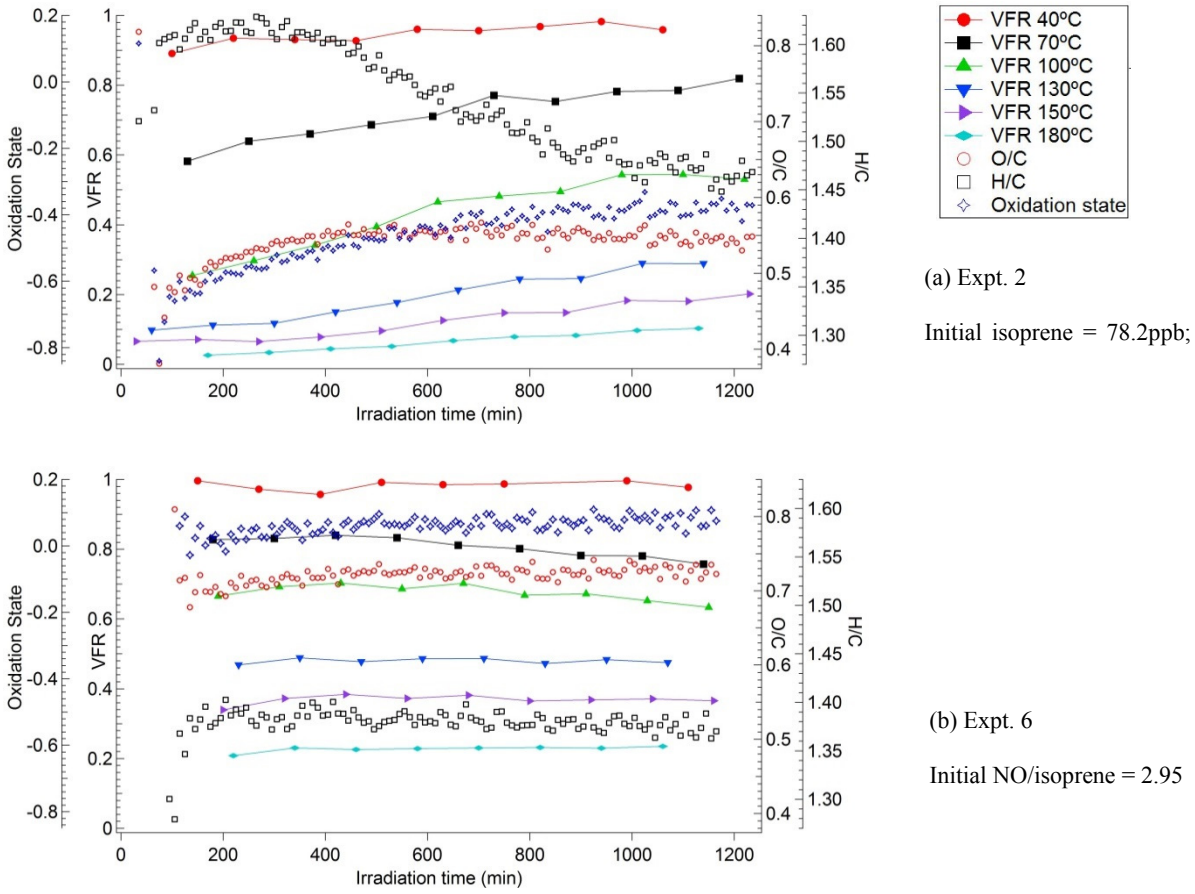

Figure 3.4. Evolution of key SOA chemical and physical properties for a representative (a) HO_2-dominant experiment (Expt.2) and (b) mixed experiment (Expt.6).

3.4 Discussion

3.4.1 NO_x Effects on Volatility of Isoprene SOA

It has been established that the NO_x level plays an important role in SOA formation from isoprene photooxidation (Kroll et al., 2006; Hatakeyama et al., 1991; Lin et al., 2013a) and has been attributed to the chemistry of organic peroxy radicals (RO_2) (Kroll and Seinfeld, 2008; Presto, 2005a) . A simplified mechanism of isoprene photooxidation is shown in Figure 3.5. Generally, reactions of RO_2 with HO_2 form hydroperoxide species (ROOH) of low volatility. Reaction of RO_2 with NO generates RO radicals, which fragment readily due to their small sizes (Atkinson, 1997; Ng et al., 2007). RO_2 may react with NO_2 to form peroxynitrates, which can be relatively low in volatility (Bertman and Roberts, 1991; Tuazon and Atkinson, 1990). RO_2 can also undergo self- and cross-reactions to form alcohols and carbonyls. For clarification, in the following discussions we use ISO_2 to denote the peroxy radical formed from isoprene+OH, $MACRO_2$ to denote the peroxy radical formed from MACR+OH, and RO_2 to denote generic peroxy radicals.

The dependence of SOA yield, VFR, and oxidation state on the initial NO/isoprene ratio is shown in Figure 3.6. SOA yield increases with initial NO/isoprene up to a ratio of 3, beyond which it decreases with increasing initial NO/isoprene ratio. This trend is consistent with previous studies on isoprene photooxidation (Dommen et al., 2006; Kroll, 2006). The VFR and oxidation state also exhibit a similar non-linear dependence on the initial NO/isoprene ratio as SOA yield, indicating that SOA yield is highly related to the volatility and degree of oxidation of the aerosol. It is noted that the aerosol oxidation state observed in Expt. 8 does not follow the general trend observed in the other experiments.

One possible explanation for the higher oxidation state of the aerosol in Expt. 8 is the effect of aerosol mass loading. The loading of suspended particles for Expt. 8 is only 2.5 μg*m^{-3}; however, loadings are between 8 and 9.6 μg*m^{-3} for the other mixed experiments. With a smaller organics mass loading, only the more oxidized species can partition into the aerosol phase, resulting in a higher degree of oxidation of the aerosol in this particular experiment (Odum, 1996; Shilling et al., 2009; Ng et al., 2010; Loza et al., 2012).

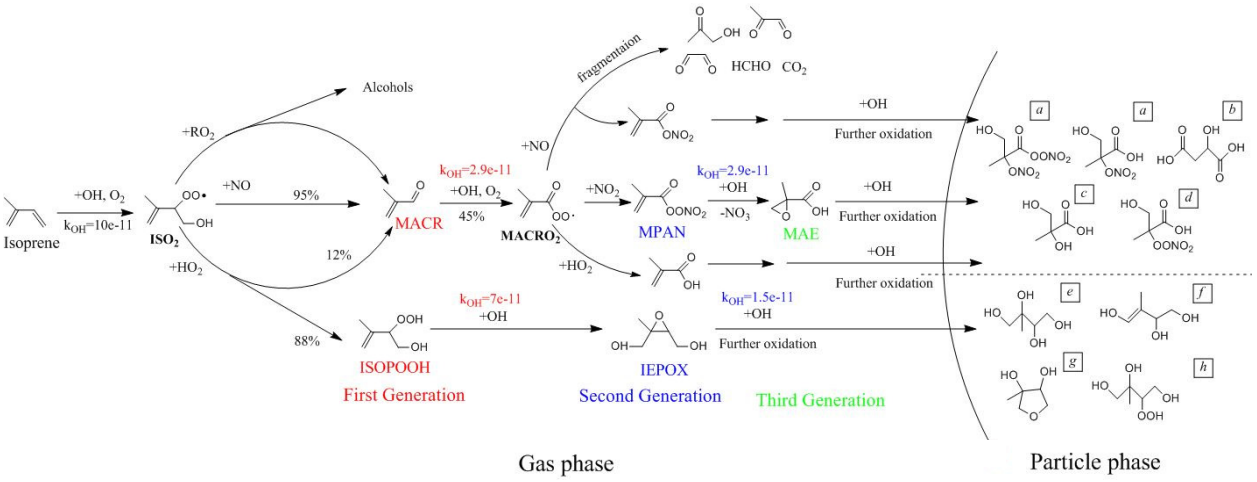

Figure 3.5. Simplified reaction mechanism of isoprene photooxidation. The reaction rate constants listed are from MCMv3.2 in units of cm^3*molecule^{-1}*s^{-1}. Letter labels on particle phase species correspond to literature references as follows: (a) Surratt et al. (2010) (b) Nguyen et al. (2010) (c) Ion et al. (2005) (d) Proposed in this study (e) Claeys et al. (2004a) (f) Wang et al. (2005) (g) Lin et al. (2012) (h) Kleindienst et al. (2009). Note that oligomers are not shown in this figure.

The dependence of SOA yield, volatility, and oxidation state on NO_x level likely arises from gas-phase RO_2 chemistry and succeeding particle-phase oligomerization reactions. In HO_2-dominant experiments, hydroxyhydroperoxides (ISOPOOH) formed via reaction of ISO_2 with HO_2 are the major first generation products. Previous studies showed that the ISOPOOH yield could be as large as ~70% (Paulot et al., 2009b).The decomposition of the OH adduct of ISOPOOH can produce dihydroxyepoxides (IEPOX),

the yield of which exceeds 75% (Paulot et al., 2009b). It is worth noting that no wet/acidic seeds were used in this study, so that the uptake of IEPOX is not expected to be appreciable (Nguyen et al., 2013; Lin et al., 2012). The volatility of SOA generated from heterogeneous reactions of IEPOX in the presence of seed particles could be of lower volatility and this warrants future investigation. In the absence of seed particles in this study, the further oxidation of IEPOX proceeds mainly via H abstraction by OH. The RO_2 formed after this H abstraction and subsequent ring opening can react with HO_2 to form ROOH (Paulot et al., 2009b). In brief, organic peroxides and polyols are major products of RO_2 chemistry in HO_2-domiant experiments (Surratt et al., 2010; Surratt et al., 2006). Previous studies observed oligomers in HO_2-domiant experiments (Nguyen et al., 2011; Surratt et al., 2006). Further, Nguyen et al. (2011) showed that oligomers in HO_2-dominant experiments are dominated by dimers, which are thought to form from aldehydes and polyols through addition chemistry.

In mixed experiments, the RO_2 radical chemistry is more complex and various reaction pathways can contribute to SOA formation. MACR and MVK from the ISO_2 + NO reaction, are the main first generation product, though only MACR is thought to lead to further SOA formation (Surratt et al., 2006; Chan et al., 2010a; Crounse et al., 2012). MACR can be further oxidized by OH via either abstraction of the aldehyde hydrogen (~45%) or addition to the double bond (~55%) (Orlando et al., 1999). An acylperoxy (RC(O)OO) radical is formed after the abstraction of aldehydic hydrogen and reaction with oxygen. RC(O)OO may react with HO_2, RO_2, or NO_2. The reaction of RC(O)OO with HO_2 and RO_2 can form carboxylic acids (Kroll et al., 2009; Atkinson, 2007; Villenave et al., 1998), while the reaction of RC(O)OO with NO_2 can form methacryloylperoxynitrate

(MPAN). It has been suggested that the further oxidation of MPAN by OH can generate methacrylic acid epoxide (MAE) or α-lactone, both of which can lead to 2-methylglyceric acid (2-MG) formation (Lin et al., 2013b; Kjaergaard et al., 2012). Therefore, it is likely that multifunctional acids are primary products of RO_2 chemistry in mixed experiments. This is consistent with our observations of higher f_{CO2} (fraction of CO_2^+ ion signal intensity relative to the total OA signal intensity, indicative of highly oxidized acids (Alfarra et al., 2004)) in mixed experiments than in the HO_2-dominant experiments (Figure S1 and S2 in supporting information). Previous studies found oligomerization to be significant in the isoprene/NO_x photooxidation system (Surratt et al., 2006; Lin et al., 2013b; Nguyen et al., 2011). For instance, Surratt et al. (2006) report that 17% of the SOA mass is oligomers and 2-MG as a key monomeric unit in oligomerization under similar conditions as our mixed experiments.

The highest yield and VFR is achieved in Expt. 6 (initial NO/isoprene ~ 2.95). MACR reaches its maximum concentration approximately when NO decreases to < 1ppb (Figure 3.1b). Thus, $MACRO_2$ mainly reacts with HO_2, and NO_2, rather than NO, which results in the formation of 2-MG as discussed above. Nguyen et al. (2011) showed that oligomerization is more extensive in mixed experiments than in HO_2-dominant experiments and that while dimers are the most abundant oligomers in HO_2-dominant experiments, oligomers with three and four monomer units are the most prominent in mixed experiments. In addition to the longer length of oligomer, the individual monomers have lower volatility in mixed experiments than in HO_2-dominant experiments (Nguyen et al., 2011). Nguyen et al. (2011) observed that 2-MG ($C_4H_8O_4$) is the most frequent repeating monomer in mixed experiments, which is less volatile than the most dominant

acetaldehyde monomer ($C_2H_6O_2$) observed in HO_2-dominant experiments. Unlike other experiments in this study, the thermograms of COH^+, $C_2H_3O^+$, and CO_2^+ (important HR-ToF-AMS ions, Figure S3 in SI) in Expt. 6 are similar and the MFR of these ions remains relatively stable at 0.9 until a TD temperature of > 80°C, indicating the SOA is multifunctional and of lower volatility than in all other experiments. In summary, the NO_x level in Expt. 6 favors the formation of 2-MG and extensive oligomer formation, resulting in the generation of the least volatile and most oxidized SOA with the highest SOA yield.

The dependence of aerosol volatility and oxidation state on NO_x concentration is highly nonlinear, as evident by the trends in Figure 3.6. SOA yield decreases when the initial NO/isoprene is lower than 3. In Expt. 4 (initial NO/isoprene ~ 0.68), NO decreases below 1ppb in 30 min. At that time, half of the initial isoprene still exists and ISOPOOH-related oxidation products contribute to SOA. Thus, SOA generated under this NO_x level has features similar to the HO_2-dominant experiments. However, the presence of NO enhances the formation of MACR, the yield of which is much higher than that in HO_2-dominant experiments. The continued reaction of MACR proceeds mainly through $MACRO_2$+HO_2/RO_2 /NO_2 pathways to form acids and SOA efficiently. Hence, the SOA VFR and yield are higher than in the HO_2-dominant experiments.

Higher NO_x levels cause the RO_2+NO pathway to become more competitive which in turn inhibits SOA formation. In Expt.8 (initial NO/isoprene ~ 7.34), the NO concentration is 60ppb at the time when isoprene is completely consumed and ISO_2 reacts exclusively with NO as a result. When MACR reaches a maximum, the NO/NO_2 ratio is about 0.4. Considering the rate constants for the $MACRO_2$ reaction with NO and NO_2 are similar ($9.04*10^{-12}$ vs. $9.0*10^{-12}$ $cm^3*mole^{-1}*s^{-1}$ (Yee et al., 2012)), a fraction of $MACRO_2$

reacts with NO, the products of which fragment to form volatile species, such as hydroxyacetone and methylglyoxal (Orlando et al., 1999; Paulot et al., 2009a). Therefore, formation of 2-MG is suppressed and more volatile species are generated, leading to less SOA formation at this higher NO level.

It has been suggested that OH concentration could affect SOA formation and yield in laboratory experiments (Song et al., 2007; Healy et al., 2009; Chan et al., 2007). Generally, the OH concentrations in mixed experiments are ~3-4 times higher than in HO_2-dominant experiments (Table 3.1), due to rapid regeneration of OH from the HO_2+NO reaction. However, the effect of OH concentration alone is unlikely to explain our observations of the dependence of SOA properties on NO_x levels. For example, the OH concentration in Expt.7 is only 7% lower than that in Expt. 6, but the SOA yield decreases by more than 50%.

3.4.2 NO_x Effects on Aerosol Growth

Substantial insight into NO_x effects on SOA formation can be gained by examining time-dependent SOA growth under different NO_x conditions. As seen in Figure 3.2, the growth curves in mixed experiments exhibit a vertical section, which becomes more pronounced as the initial NO concentration increases. The vertical section in growth curves can be attributed to the competition between the isoprene consumption rate and the SOA formation rate. In HO_2-dominant experiments, the most important pathway of SOA formation is via ISOPOOH and IEPOX formation and SOA is mainly formed by the oxidation of second-generation products. However, the NO_x reaction pathway requires even higher-generation products to generate SOA (e.g., through MACR, MPAN, and

finally MAE), so that the SOA formation is expected to take longer in the mixed experiments than in the HO_2-dominant experiments. In addition, the high level of NO can further inhibit the SOA formation rate by favoring the $MACRO_2$+NO pathway, which leads to formation of highly volatile species. Therefore, the vertical section in growth curve becomes more evident as the initial NO concentration increases.

Reactions between higher generation products may also contribute to the vertical section observed in the growth curve. Previous studies have shown that aldehydes may react with hydroperoxides to form peroxyhemiacetals (Ng et al., 2007; Johnson et al., 2004; Yee et al., 2012; Bin Lim and Ziemann, 2009). In mixed experiments, the presence of NO enhances aldehyde formation. After the NO concentration goes to zero, the reaction of RO_2 with HO_2 is competitive, which produces hydroperoxides. Thus, the formation of peroxyhemiacetals may be enhanced in mixed experiments and contribute to further aerosol growth after isoprene is consumed.

The absence of vertical sections in HO_2-dominant experiments may be caused by the rapid loss of SOA mass as discussed in the next section. As illustrated in Figure 3.1a, the SOA mass starts decreasing when the isoprene concentration reaches zero. Therefore, SOA growth ceases when isoprene is completely consumed and no vertical section is observed in the growth curve.

3.4.3 Aerosol Aging

The temporal evolution of SOA mass is also different in the two types of experiments (Figure 3.1). After reaching peak growth, SOA mass decreases much faster in HO_2-dominant than that in mixed experiments, even after correcting for particle chamber

wall-loss. The faster decay in SOA mass in the HO_2-dominant experiments has been observed in previous studies (Lee et al., 2000; Surratt et al., 2006; Kroll et al., 2006) and could be attributed to the photolysis of hydroperoxides. Surratt et al. (2006) observed that the peroxide contribution to the total SOA mass decreases from 59% to 26% in 12 hours of irradiation. Recently, Henry and Donahue (2012) observed rapid aerosol evaporation after exposing α-pinene ozonolysis SOA to additional H_2O_2 and UV lights. They attributed the aerosol volatilization to photolysis of hydroperoxides, which were produced after introducing the H_2O_2.

Although SOA mass decreases rapidly in the HO_2-dominant experiments, the remaining SOA becomes less volatile and more oxidized over time (Figure 3.4). The increase in aerosol VFR and oxidation state could arise from the formation of carboxylic acids, which are of low volatility and highly oxidized. In Expt. 2, f_{CO2} increases from 3.6% to 8.5% during the reaction (Figure S5 in SI), suggesting that organic acids contribute more to the total aerosol mass over time. One possible source of carboxylic acids is the oxidation of polyols. Surratt et al. (2010) showed that gas-phase 2-methyltetrols and IEPOX in HO_2-dominant experiments reached a maximum 4 hours after irradiation, but decreased rapidly over the next 8 hours, indicating the further oxidation of polyols. It is likely that hydroxyl groups are oxidized to form aldehyde groups (Bethel et al., 2003), which can then be further oxidized to carboxylic acids (Hasson et al., 2004). Another possible source of carboxylic acids is the photolysis of hydroperoxides, which is expected to be significant as discussed above. The photolysis most likely severs the O-OH bond in hydroperoxides and results in the formation of an alkoxy radical (Baasandorj et al., 2010). Due to the small size of the alkoxy radical in the isoprene oxidation products, fragmentation will occur and likely form

aldehydes, the further oxidation of which can generate carboxylic acids (Hasson et al., 2004). In summary, as the formation of carboxylic acids from alcohol oxidation and hydroperoxide photolysis involves cleavage of C-C bond and addition of oxygen atom, these conversions likely cause the increase in SOA oxidation state over time in the HO_2-dominant experiments (Bethel et al., 2003).

The temporal evolution of VFR in mixed experiments shows the same complex dependence on NO_x level as the SOA yield. For the experiment with the highest yield (Expt. 6, initial NO/isoprene ~ 3), VFR remains relatively constant over time (Figure 3.4b). However, an increase in VFR is observed in mixed experiments when the initial NO/isoprene is above or below 3. For Expt. 4 (initial NO/isoprene ~0.7), the increase in VFR (Figure S4a) may be caused by the fact that products from the RO_2+HO_2 pathway contribute to SOA and SOA formed under low NO_x levels has features similar to the HO_2-dominant experiments. For Expt. 8 (initial NO/isoprene ~7.4), the increase in VFR (Figure S4b) may be attributed to the formation of low volatile species by further oxidation of volatile species, which are generated via the RO_2+NO reaction.

Results from previous studies have suggested that aerosol volatility is generally inversely correlated to the bulk O/C ratio (Jimenez et al., 2009; Lanz et al., 2007; Aiken et al., 2008). However, some recent studies revealed that aerosol with similar volatility can have fairly different O/C ratios (Hildebrandt et al., 2010; Setyan et al., 2012). In this study, VFR is generally well correlated with the O/C ratio in the mixed experiments. In the HO_2-dominant experiments, however, VFR increases over time and the O/C ratio decreases slightly from 0.6 to 0.55 10 hours into the experiment (Figure 3.4a). The oxidation state, reflecting the changes in both O/C and H/C, follows the trend of VFR in both types of

experiments. Thus, this study suggests that particle oxidation state is a better indicator of volatility than O/C ratio for the isoprene photooxidation system.

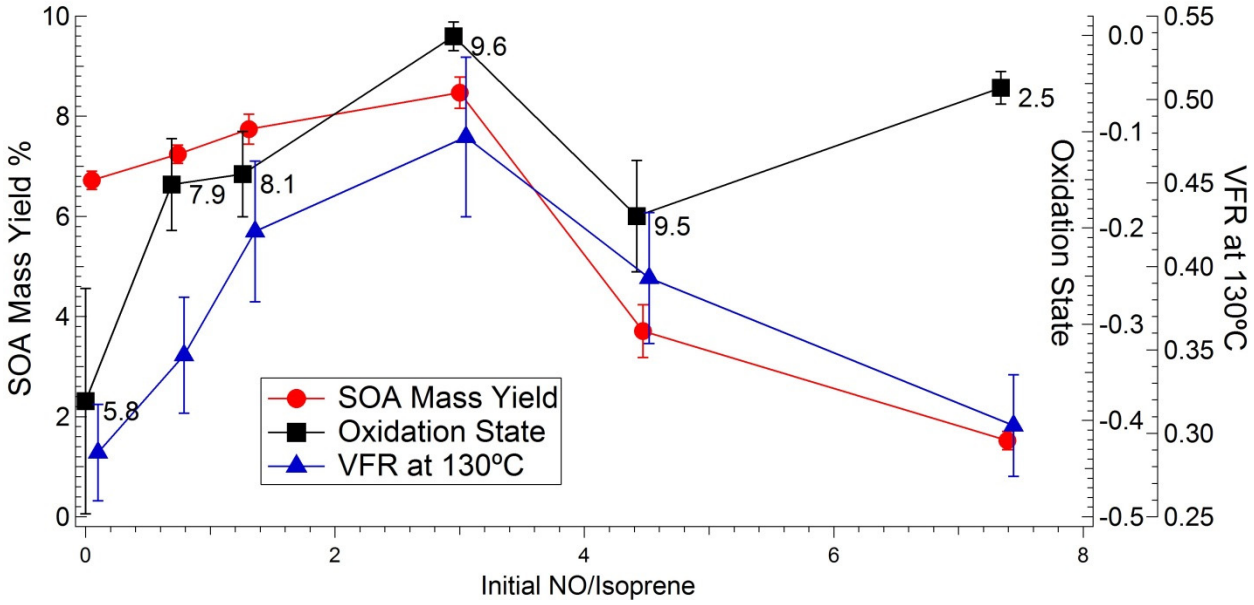

Figure 3.6. Dependence of SOA particle mass yield, VFR, and oxidation state on initial NO/isoprene ratio. The NO-free point (far left of figure) is from Expt. 2, where the initial isoprene concentration is close to that in mixed experiments. Values of all three parameters shown here are calculated at equivalent OH exposures of approximately $2*10^7$ molecule*hour*cm^{-3}. VFR is calculated at a TD temperature of 130°C, which is representative of the trends in all the data at TD temperatures greater than 80°C. Uncertainties in the yield and VFR are the same as in Table 3.1 and Figure 3.3, respectively. Uncertainties in the oxidation state are estimated by propagating the error of O/C (30%) and H/C (7%) measurements (Aiken et al., 2007). Oxidation state (black square) is labelled with loading of suspended particles ($\mu g/m^3$). Most experiments have comparable aerosol loadings, suggesting that the oxidation state trend shown here is not caused by the aerosol loading effect.

3.5 Atmospheric Implications

Previous experiments have been performed under extreme NO_x conditions by the selective use of OH precursors to saturate the system with either NO/NO_x ("high-NO_x" condition) or HO_2 radicals ("low-NO_x" condition). While "high-NO_x" and "low-NO_x" have traditionally been used to describe photochemical conditions, these terms may not

adequately describe the complexity of the reaction pathways. Recently, Wennberg (2013) suggested that instead of characterizing reaction conditions as either high or low NO_x, one should explicitly specify the fate of RO_2 radicals. In this study, we highlight the different roles of NO and NO_2 in SOA formation, dynamic changes between NO and NO_2, and competitive chemistry of RO_2 among various pathways and their effects on aerosol composition and volatility.

We find that SOA volatility is sensitive to NO_x and varies with NO_x level in a non-linear manner. Depending on the NO_x level and reaction pathways of peroxy radicals, the SOA formed in mixed experiments could be of similar or lower volatility compared to that formed in HO_2-dominant experiments. This observation might help to reconcile the seemingly contradictory observations of the NO_x effect on isoprene SOA volatility reported in previous literature studies. While King et al. (2010) observed that isoprene SOA volatility was not affected by NO_x, Kleindienst et al. (2009) reported that isoprene SOA formed in the presence of NO_x was less volatile. It is noted that different NO_x levels were investigated in these two studies. The NO_x/isoprene ratio was maintained at 0.76 in King et al. (2010), so that RO_2+NO reaction was relatively more competitive throughout their experiment. However, in Kleindienst et al. (2009), it appears that 2-31% of isoprene was still present by the time NO had reacted completely. It is possible that difference between these two studies is a result of reactions occurring at different NO/isoprene ratios. In addition to volatility, isoprene SOA yield and oxidation state also exhibit a non-linear dependence on NO_x levels. Current regional and global atmospheric SOA models treat the effects of NO_x on SOA properties as a linear combination of SOA formation under two

extremes ("low-NO_x" and "high-NO_x" conditions) (Presto and Donahue, 2006; Pye et al., 2010). From the time dependent growth curves, it is clear that there is a vertical section at the end of the mixed experiments, indicating the presence of different rate determining steps in SOA formation and/or the enhancement of higher-generation oxidation chemistry when RO_2 reacts through various pathways. Taken together, it is evident from the present work and previous studies that the nonlinear effects of NO_x on SOA formation need to be included in the next generation of models in order to accurately predict the dynamics of SOA formation and composition in ambient environments where the fate of RO_2 varies considerably.

It has been argued previously that the discrepancies between laboratory and ambient SOA could arise from limited oxidation aging in laboratory experiments. This study reveals that SOA aging in laboratory chamber studies is highly dependent on NO_x levels. SOA formed in HO_2-dominant experiments become more oxidized and less volatile as oxidation progresses. On the contrary, the composition of SOA in mixed experiments does not change substantially over time. Therefore, NO_x effects need to be taken into account in future laboratory aging studies.

CHAPTER 4: EFFECTS OF ANTHROPOGENIC EMISSIONS ON AEROSOL FORMATION FROM ISOPRENE AND MONOTERPENES IN THE SOUTHEASTERN UNITED STATES

4.1 Background

Organic aerosol (OA) is an important atmospheric component that influences climate, air quality, and human health (Hallquist et al., 2009). A large fraction of OA is secondary organic aerosol (SOA), which is formed through oxidation of volatile organic compounds (VOCs) emitted from human activities (anthropogenic) and vegetation (biogenic). In particular, biogenic VOCs (BVOCs), such as isoprene (C_5H_8) and monoterpenes ($C_{10}H_{16}$), are key precursors for global SOA formation owing to their larger emissions and higher reactivity with atmospheric oxidants compared to anthropogenic VOCs (Hallquist et al., 2009). However, the extent to which anthropogenic pollutants mediate the formation of SOA from biogenic VOCs (referred to as biogenic SOA) in the ambient environments is poorly understood and highly uncertain. For example, while radiocarbon analysis repeatedly indicated that more than half of carbon in SOA is of modern (biogenic) origin in the southeastern (SE) US (Schichtel et al., 2008; Weber et al., 2007), aircraft measurements in the same region showed that SOA correlates with anthropogenic tracers, such as CO (Weber et al., 2007).

One possible explanation to reconcile the seemingly contradictory results from radiocarbon studies and ambient measurements is that the majority of SOA is produced from naturally emitted BVOCs, but its formation processes also involve pollutants originated from anthropogenic emissions (Weber et al., 2007; Spracklen et al., 2011).

Laboratory studies have recently revealed that biogenic SOA formation can be largely affected by anthropogenic pollutants such as NO_x and SO_2 (Hallquist et al., 2009; Kroll and Seinfeld, 2008). According to 2011 US national emission inventory (http://www.epa.gov/ttn/chief/net/2011inventory.html), 90% of NO_x and 97% of SO_2 are anthropogenically emitted. NO_x can alter SOA formation by influencing peroxy radical chemistry in BVOCs oxidation mechanisms (Kroll and Seinfeld, 2008). The reaction of NO_2 with O_3 forms nitrate radicals, which can oxidize BVOCs to form condensable products that often have high SOA yields (Fry et al., 2009; Ng et al., 2008). The effect of SO_2 was investigated but often explained in the context of particle acidity in laboratory studies (Surratt et al., 2010). Despite intense laboratory investigations, only few proposed mechanisms are consistent with ambient observations (Rollins et al., 2012) and the reasons for the observed enhancement of biogenic SOA formation in certain polluted environments remain unclear (Shilling et al., 2013; Goldstein et al., 2009). For instance, while some laboratory studies found that particle acidity can enhance isoprene SOA formation (Surratt et al., 2010), only weak correlations have been observed in the atmosphere between tracers of isoprene SOA and particle acidity (Worton et al., 2013; Lin et al., 2013a; Budisulistiorini et al., 2013; Tanner et al., 2009). Thus, a coherent understanding of the enhancement of biogenic SOA in polluted environments has not emerged and these proposed mechanisms from laboratory studies have not been quantitatively established in ambient environments.

Here, we provide direct observational evidence and quantification of anthropogenically-enhanced biogenic SOA formation in the Southern Oxidant and Aerosol Study (SI *Appendix, SOAS*) field campaign in June and July 2013. In addition, we also conducted ambient measurements from May 2012 to February 2013 at multiple rural and

urban sites in the greater Atlanta area as part of the Southeastern Center of Air Pollution and Epidemiology study (SCAPE, EPA Clean Air Center, *SI Appendix*). The SE US is ideal for studying anthropogenic-biogenic interactions due to high natural emissions and the proximity to anthropogenic pollution sources. Here, we investigate the sources of OA employing factor analysis of high-time-resolution mass spectrometry data coupled with a suite of comprehensive and collocated measurements (*SI Appendix, Instrumentation*). We have also performed complementary laboratory studies to examine possible chemical mechanisms to interpret results from ambient measurements. From these integrated ambient and laboratory studies, we show that anthropogenic SO_2 and NO_x emissions substantially mediate SOA formation from BVOCs such as isoprene and monoterpenes in the SE US.

4.2 Organic Aerosol Source Apportionment

We obtain quantitative, real-time measurements of five non-refractory submicron particulate matter (PM_1) components (organics, sulfate, nitrate, ammonium, and chloride) with High Resolution Time-of-Flight Aerosol Mass Spectrometer (HR-ToF-AMS) from June 1 to July 15, 2013 (*SI Appendix, Fig.S2*) at the SEARCH (SouthEastern Aerosol Research and Characterization) network site near Centreville in rural Alabama, which served as the SOAS ground site. The measured campaign-average of non-refractory PM_1 mass is 7.5±5.3 μg m^{-3} (average ± one standard deviation), which is similar to the campaign-average $PM_{2.5}$ mass of 7.8±4.6 μg m^{-3} (average ± one standard deviation), considering the detection differences in particle size range and particle composition (refractory species are not detected by HR-ToF-AMS) between two methods. We find that

organics are the dominant components in PM_1 with a mass fraction of 67%, followed by sulfate at 26%.

To determine the sources of organic aerosols (OA) measured at Centreville during SOAS, we perform multivariate factor analysis with positive matrix factorization (PMF) and identify four subtypes of OA (*SI Appendix, PMF*). Figure 4.1 shows the unique mass spectrum and time series of each of these factors. The first two factors are oxygenated OA (OOA) with high but differing atomic oxygen-to-carbon (O:C) ratio. We refer to the OOA factor with higher O:C ratio as "more-oxidized OOA (MO-OOA, O:C=0.80)" and the one with lower O:C ratio as "less-oxidized OOA (LO-OOA, O:C=0.46)". MO-OOA and LO-OOA represent 39% and 33% of OA, respectively. The mass spectrum of the third factor is characterized by ions at *m/z* 60 ($C_2H_4O_2^+$) and 73 ($C_3H_5O_2^+$), which are known to be produced by levoglucosan, a tracer for biomass burning (Schneider et al., 2006) and indeed correlates with the third factor (R=0.65, Figure 4.1f) in Centreville. In addition, the third factor shows good correlation with brown carbon (R=0.8) (*SI Appendix, PILS-LWCC-TOC*), which appears to be significant in biomass combustion emissions (Hecobian et al., 2010). Thus, we identify this factor as biomass burning OA (BBOA), which represents 10% of OA.

A fourth factor, characterized by tracer ions at *m/z* 53 ($C_4H_5^+$) and *m/z* 82 ($C_5H_6O^+$) in its mass spectrum, contributes 18% of OA. This same factor has been observed in several recent field studies (Robinson et al., 2011a; Budisulistiorini et al., 2013; Slowik et al., 2011) and has been linked to isoprene, given its mass spectral similarity to laboratory-generated isoprene SOA via the reactive uptake of epoxydiols (IEPOX), an important oxidation product of isoprene when organic peroxy radicals mainly react with hydroperoxy

radicals (Paulot et al., 2009b). Previous ambient measurements (Budisulistiorini et al., 2013) showed that this factor correlated with 24h integrated filter-based 2-methylerythritol and 2-methylthreitol (collectively referred to as methyltetrols), which are known isoprene SOA tracers likely formed from IEPOX uptake (Claeys et al., 2004a; Surratt et al., 2010). In Centreville, we continuously measure particle-phase methyltetrols with a semi-volatile thermal desorption aerosol gas chromatograph (SV-TAG) and find that the fourth factor indeed correlates with methyltetrols (R=0.65, Figure 4.1h), which provides further evidence that this factor is related to isoprene. Additionally, isoprene is the most abundant BVOC (highest mixing ratio) during daytime in Centreville and exhibits a similar diurnal trend as the fourth OA factor (*SI Appendix, Fig.S4*). PMF analysis of our six SCAPE datasets (*SI Appendix, SCAPE*, EPA Clean Air Center) also revealed a factor of similar mass spectral features (i.e., prominent signals at $C_4H_5^+$ and $C_5H_6O^+$) only in the warmer months, from May to September (Figure 4.2) when isoprene emissions are strongest and methyltetrols concentrations are highest (Guenther et al., 2006; Ding et al., 2008). Based on all of this evidence, we name the fourth factor, which is likely related to isoprene SOA formed via reactive uptake of IEPOX, as isoprene-derived organic aerosol (Isoprene-OA).

In this work, we aim at quantifying the extent of anthropogenically mediated biogenic SOA in the SE US. We focus on the discussion of Isoprene-OA and less-oxidized oxygenated organic aerosol (LO-OOA), as these two OA subtypes could originate from biogenic isoprene and monoterpenes, respectively, and be greatly mediated by anthropogenic emissions. We note that the more-oxidized oxygenated organic aerosol (MO-OOA) accounts for 24-49% of measured organic aerosol in the SE US (Figure 4.2), though the sources of this OA subtype is currently unclear and warrants future

investigations. As MO-OOA has the highest O:C ratio among all OA factors, it likely represents highly aged organic aerosol from multiple origins (Ng et al., 2010).

4.3 Effects of Sulfate on Isoprene-derived Organic Aerosol

A striking feature of the Centreville aerosol is a strong association (R=0.77) between Isoprene-OA and sulfate (SO_4^{2-}). This feature appears to be common throughout the SE US based on our SCAPE datasets in the greater Atlanta area (range of R between Isoprene-OA and sulfate is 0.73-0.88). For instance, in Centreville, a spike in Isoprene-OA and known isoprene oxidation product methyltetrols was observed from about noon to 18:00 on June 26 when the site was influenced by a sulfate-rich plume (Figure 4.1h). Similarly, in Yorkville (SEARCH site in Georgia), when a dramatic decrease in sulfate concentration occurred on July 6, 2012, among three OA factors, only the Isoprene-OA showed a corresponding decrease (*SI Appendix, Fig.S5*). These observations, and other observed similar events highlight the importance of sulfate in isoprene SOA formation in the SE US. However, how exactly and to what extent sulfate mediates isoprene SOA formation in the ambient environments remains elusive. Recent laboratory studies proposed that isoprene SOA formation from IEPOX requires particle water (H_2O_{ptcl}) for IEPOX uptake, proton donors (e.g., H^+ or NH_4^+) for catalyzing IEPOX ring-opening, and nucleophiles (e.g., H_2O, SO_4^{2-}, NO_3^-) to facilitate further particle-phase reactions (Surratt et al., 2010; Nguyen et al., 2014). A simplified mechanism of this process is shown in Figure 4.3a. The highly convoluted interactions among particle water, particle acidity, and sulfate present a challenge in elucidating the roles of each of these parameters in isoprene SOA formation (Figure 4.3a). For example, the direct effect of sulfate on SOA formation

(possibly through nucleophilic addition) may be "misinterpreted" as the effect of particle water and acidity because they are typically driven by sulfate (Fountoukis and Nenes, 2007).

Another critical challenge to elucidate the effects of each parameter is the determination of particle water content ([H_2O_{ptcl}], [ ] denotes μg m^{-3} of air) and particle acidity ($H^+_{(aq)}$, $_{(aq)}$ denotes mol L^{-1} of H_2O). For Centreville and all SCAPE datasets, we comprehensively calculate [H_2O_{ptcl}] by including the contribution from organics based on measured organic hygroscopicity (Cerully et al., 2015) and contribution from inorganics based on the thermodynamic model ISORROPIA II (Fountoukis and Nenes, 2007). Detailed calculations of [H_2O_{ptcl}] can be found in (Guo et al., 2015). The calculated [H_2O_{ptcl}] agrees with our indirect measurements of particle water content (Guo et al., 2015). Further, we calculate particle pH based on [H_2O_{ptcl}] and ISORROPIA II output [H^+] (μg m^{-3} air). The ISORROPIA equilibrium calculations accurately predict the measured gas-phase ammonia concentrations, providing a strong validation for our particle acidity calculation (Guo et al., 2014). Our results show that aerosol throughout the SE US is very acidic (pH ranging between 0 and 2) and contains high particle water contents (average [H_2O_{ptcl}] ranging between 5.1 and 8.4 μg m^{-3}) in the summer time (Guo et al., 2015).

In the SE US, H^+ is a more efficient proton donor than NH_4^+ since NH_4^+ is an effective catalyst only for pH>4 (Nguyen et al., 2014). Bisulfate (HSO_4^-) could also act as proton donor, which may provide electrostatic stabilization of partially formed intermediate (Whalen, 1973). Although the efficiency of bisulfate in catalyzing IEPOX ring opening is uncertain, it is expected to be lower than H^+ under the low pH condition in the SE US. Regarding nucleophiles, SO_4^{2-} is the most important because of its high particle

concentration and stronger nucleophilic strength (Piletic et al., 2013) compared to other species (NO_3^- and H_2O). Together, these results indicate that H_2O_{ptcl}, H^+, and SO_4^{2-} are the most important parameters affecting isoprene SOA formation from IEPOX uptake in the SE US.

We perform multivariate linear regression analysis on Centreville data to gain quantitative insights into the effects of particle water ($[H_2O_{ptcl}]$), particle acidity ($H^+_{(aq)}$), and sulfate ($[SO_4^{2-}]$) (*SI Appendix, Multivariate Linear Regression*) on isoprene SOA formation (i.e., Isoprene-OA factor). Importantly, we find that SO_4^{2-} has a statistically significant ($p<0.0001$) positive linear relationship with Isoprene-OA factor with a regression coefficient of 0.42 (*SI Appendix, Table S2*). These results suggest that a 1 μg m^{-3} increase in SO_4^{2-} will (on average) increase Isoprene-OA by an estimated 0.42 μg m^{-3}, when holding the other covariates constant. In contrast, the estimated effects of H_2O_{ptcl} and H^+ are not statistically significant, suggesting that particle water and acidity are not the limiting parameters in isoprene SOA formation.

To visualize this important finding, nine scatter plots of H^+ vs H_2O are generated by sorting all data points into nine bins based on a 0.5 μg m^{-3} increment in $[SO_4^{2-}]$ and representing [Isoprene-OA] by the size of data points (Figure 4.3b). These plots are useful because they offer a clear view of the effect of one parameter on Isoprene-OA while holding the other two covariates constant. We note that in each subplot (similar $[SO_4^{2-}]$), the data point size ([Isoprene-OA]) appears to be independent of $H^+_{(aq)}$ and $[H_2O_{ptcl}]$, indicating that varying $H^+_{(aq)}$ or $[H_2O_{ptcl}]$ under similar $[SO_4^{2-}]$ causes little change in [Isoprene-OA]. In contrast, the data point size ([Isoprene-OA]) tends to increase appreciably with increasing $[SO_4^{2-}]$, indicating that sulfate could greatly mediate isoprene

OA formation directly through its abundance. We perform the same analysis on our SCAPE datasets where Isoprene-OA factor is identified (*SI Appendix, Fig.S6*) and arrive at the same conclusion that isoprene OA formation over broad regions of the SE US is directly controlled by the abundance of sulfate.

One possible explanation for the remarkable control of isoprene SOA by sulfate might be the concerted nucleophilic addition to the IEPOX ring. Both experimental and computational studies (Eddingsaas et al., 2010; Piletic et al., 2013) have revealed that this step is the rate determining step in OA formation from IEPOX. Thus, an increase in [SO_4^{2-}] may effectively facilitate the ring-opening reaction of IEPOX and subsequent OA formation, especially the formation of organosulfates (Surratt et al., 2010), which have been detected previously in the SE US (Surratt et al., 2008) and could hydrolyze to form methyltetrols (Hu et al., 2011) (Figure 4.3a). To a less extent than sulfate, water could also react with IEPOX by acting as a nucleophile, which forms methyltetrols (Surratt et al., 2010). Sulfate may also affect isoprene-OA formation through salting-in effect. Salting-in refers to the effect that increasing salt concentration in aqueous solution would increase the solubility of polar organic compounds. For example, Kampf et al. (2013) found that the effective Henry's law coefficient of glyoxal increases exponentially with $SO_4^{2-}{}_{(aq)}$ until glyoxal uptake is kinetically limited. Considering that IEPOX is also highly water soluble as glyoxal, sulfate may also cause salting-in effect on IEPOX. Once IEPOX is in the particle phase, further reactions such as ring-opening and subsequent nucleophilic attack by sulfate prevent the reversible partitioning of IEPOX back to the gas phase. However, no systematic study about the salting-in effect of IEPOX uptake is currently available and this warrants further study.

Our finding that particle acidity does not influence isoprene SOA formation in the SE US is striking and contrasts with several previous laboratory and modeling studies, which suggested the importance of particle acidity in isoprene SOA formation (Pye et al., 2013; Surratt et al., 2010). The weak correlation between IEPOX-derived SOA tracers and particle acidity has been observed in prior field measurements, but the explanations are rather inconclusive (Lin et al., 2013a; Worton et al., 2013). For example, Lin et al. (2013a) attributed the weak correlation as SOA not being formed locally and that the particle acidity could change as the aerosol is advected to the sampling site from other regions. However, isoprene OA measured in Centreville, or the SE US in general, is expected to be formed locally (*SI Appendix, Backtrajectory Analysis and Fig.S10*) owing to regionally abundant isoprene emissions in summer time (Pye et al., 2013) and the short lifetime of isoprene (~1.4 hour at 25°C assuming [OH] ~ $2*10^6$ molecule cm^{-3}), consistent with our observations of similar processes at different sites. Here, we hypothesize that the weak influence of particle acidity on isoprene OA is a result of consistently high particle acidity in the SE US (Guo et al., 2015). A recent chamber study (Nguyen et al., 2014) showed that the reactive partitioning coefficient of IEPOX increases by only 1.5 times as $H^+_{(aq)}$ increases by many orders of magnitude (in the pH range relevant to our study). Our ambient measurements show that the particle pH throughout the SE US is very low (ranging between 0 and 2, the average value is 0.94±0.59 for Centreville) (Guo et al., 2015), which means that isoprene OA formation is insensitive to H^+ in the SE US. Moreover, as the isoprene OA formation is limited by nucleophiles instead of catalyst activity (Piletic et al., 2013; Eddingsaas et al., 2010), increasing particle acidity (within pH range 0-2) may not facilitate the isoprene OA formation rate and hence the association between $H^+_{(aq)}$ and

[Isoprene-OA] is not significant. Therefore, although our analysis does not discount the important role of particle acidity in isoprene OA formation via IEPOX uptake, it suggests that particle acidity is not the limiting parameter given the acidic nature of aerosol in the SE US.

The weak influence of particle water on isoprene OA formation, which is surprising, could be a result of the competition between particle water abundance and dilution of ions at high relative humidity typically found in these regions. Increasing particle water content would provide more medium for gas-phase water-soluble species to dissolve and potentially increase SOA (Carlton and Turpin, 2013); increasing water, however, reduces $SO_4^{2-}{}_{(aq)}$ (mol L^{-1} of H_2O) by diluting the particle concentration of sulfate. This dilution could not only reduce the reaction rate due to lower nucleophile concentration, but also suppress IEPOX uptake due to weakening ionic strength and salting-in effect. Thus, increasing water could potentially decrease SOA. In Centreville, [H_2O_{ptcl}] reached a daily minimum at about 16:00 local time when $SO_4^{2-}{}_{(aq)}$ is highest and isoprene is near its maximum (*SI Appendix, Fig.S4 and Fig.S7*), indicating that the two opposing effects of particle water are competing with each other when IEPOX is abundant.

As particle water content correlates with sulfate, we perform additional multivariate linear regression by considering water uptake by organics only (Org-H_2O), which is not related to sulfate and contributes about 36% of total particle water (Guo et al., 2015), in order to deconvolute the interaction between sulfate and particle water on isoprene OA formation. In contrast to total particle water, which is not significantly associated with Isoprene-OA, Org-H_2O shows a significantly positive relationship with Isoprene-OA ($p=0.002$, *SI Appendix, Table S2*). Even though significant, Org-H_2O still does not have a

dominant effect on isoprene OA formation as its β-coefficient is 80 times smaller than that of sulfate. Further, the contrasting regression results between total particle water vs. Org-H_2O indicate that increasing [H_2O_{ptcl}] under low particle water levels (i.e., Org-H_2O) would enhance Isoprene-OA formation. However, under high particle water levels (i.e., total particle water), which is typical in the SE US, particle water is not a limiting parameter for isoprene-OA formation.

4.4 Effects of NO_x on Less-Oxidized Oxygenated Organic Aerosol

Similar to the spatial uniformity of the association between Isoprene-OA and sulfate during summer, LO-OOA factor shows consistently similar diurnal patterns *(SI Appendix, Fig.S8*) in Centreville and SCAPE datasets at various rural and urban sites, but in this case LO-OOA factor is observed throughout the year (Figure 4.2). To determine whether LO-OOA is locally produced or from long-range transport, we focus on Centreville where auxiliary data are available. Measurements in Centreville are split into four subsets based on 72hr back trajectories of air mass geographical origins relative to the location of measurement site: NW, NE, SW, and SE (*SI Appendix, Backtrajectory Analysis, Fig.S9 and Fig.S10*). The diurnal patterns of LO-OOA are similar regardless of the origin of the air masses. Combined with similar diurnal patterns at multiple sites suggests that the source of LO-OOA is local. As seen in Figure 4.1i, the LO-OOA concentration shows a diurnal maximum at night and a minimum at around 17:00. From 17:00 to sunrise, the LO-OOA concentration increases by nearly four times. This increase still exists after the LO-OOA concentration is adjusted by the boundary layer height,

indicating that the nighttime increase in LO-OOA is likely caused by nighttime aerosol production instead of the nocturnal boundary layer becoming shallow.

Since the $NO_3^{\bullet}$ radical (a product of NO_x and ozone reaction) is a well-known nocturnal oxidant, we hypothesize that $NO_3^{\bullet}$ oxidation of BVOCs contributes to the nighttime increase in LO-OOA. Laboratory studies have revealed that organic nitrates make up a substantial fraction of the SOA from BVOC+$NO_3^{\bullet}$ (Ng et al., 2008; Fry et al., 2009). To examine the role of organic nitrates in LO-OOA formation, we calculate the mass concentration of the nitrate functional groups in organic compounds ($NO_{3,org}^-$) from the difference between HR-ToF-AMS measurements (NO_3^- from both organic and inorganic species) and PILS-IC measurements (NO_3^- from inorganic nitrate only) (*SI Appendix, Organic Nitrate Estimation*). We find a good correlation (R=0.81) between LO-OOA and $NO_{3,org}^-$, which supports that LO-OOA is most likely related to nighttime $NO_3^{\bullet}$ chemistry. Further, we calculate that organic nitrates contribute 40-60% of LO-OOA in early morning based on the concentration of nitrate functional groups and the assumption that the average molecular weight of organic nitrates ranges from 200 to 300 g mol^{-1} (Rollins et al., 2012) (*SI Appendix, Fig.S11*).

To quantitatively constrain the contribution of $NO_3^{\bullet}$ chemistry to LO-OOA, we estimate aerosol formation from isoprene, α-pinene, and β-pinene, which are the most abundant biogenic SOA precursors measured in Centreville, via various oxidation pathways. We estimate [$NO_3^{\bullet}$] to be about 7.6×10^{-2} ppt (*SI Appendix, [$NO_3^{\bullet}$] estimation*) with a corresponding lifetime of 8 s. We further calculate that NO_3 chemistry at night accounts for 17%, 20%, and 38% of the reacted isoprene, α-pinene, and β-pinene, respectively (*SI Appendix, Table S4*). The contribution of each BVOC and reaction

pathway to total nighttime SOA formation would depend on their respective SOA yields at mass loadings relevant to Centreville (i.e., ~8 μg m^{-3}), which are available in the literature (*SI Appendix, Table S5 and herein*), except for β-pinene+$NO_3^•$. To this end, we performed comprehensive laboratory chamber studies to investigate SOA formation from β-pinene+$NO_3^•$ under conditions relevant to Centreville and SE US (*SI Appendix, Laboratory chamber experiments*). The SOA yield is found to be 50%, which is ~17 times higher than β-pinene SOA yields from ozonolysis and photooxidation for a mass loading of ~8 μg m^{-3}. This implies that β-pinene could still form aerosol in the absence of $NO_3^•$, although the amount of aerosol formed would be substantially smaller. Based on our β-pinene SOA yields, and yields for other BVOCs via various oxidation pathways from prior chamber studies, we calculate that 0.7 μg m^{-3} of SOA would be produced, which agrees within a factor of three to the measured nighttime LO-OOA production (1.7 μg m^{-3} from 17:00 to sunrise).

According to model estimation, 64% of total nighttime OA production arises from the $NO_3^•$ oxidation pathway (*SI Appendix, Table S5 and Fig.S12*), which is consistent with the estimated contribution of organic nitrates to LO-OOA. For the amount of OA produced from $NO_3^•$ oxidation pathway, 80% originates from monoterpenes, which is much greater than the contribution from isoprene (20%) as suggested by our model. Taken together, monoterpenes+$NO_3^•$ chemistry accounts for 50% of total nighttime OA production. The large contribution is likely due to the large abundance of monoterpenes at night, which exhibit the same diurnal pattern as LO-OOA (*SI Appendix, Fig.S4*), as well as the high SOA yield from β-pinene+$NO_3^•$ as revealed by our chamber studies. Additionally, the

presence of LO-OOA throughout the year in the greater Atlanta area (Figure 4.2) is in agreement with the fact that monoterpenes emissions exist in all seasons in the SE US (Ding et al., 2008). Therefore, we conclude from our integrated ambient observations and laboratory studies that nighttime monoterpenes+$NO_3^{\bullet}$ chemistry contributes substantially to LO-OOA.

Our results highlight the important role of BVOC composition in evaluating their contribution to ambient OA via $NO_3^{\bullet}$ oxidation. A recent study (Rollins et al., 2012) observed that high [BVOC] can suppress SOA formation from $NO_3^{\bullet}$ oxidation in Bakersfield (CA), where $NO_3^{\bullet}$ activity is dominated by limonene. The authors attributed the suppression to high concentrations of limonene depleting [$NO_3^{\bullet}$], thus inhibiting the further oxidation of their first-generation products and subsequent aerosol formation. Nevertheless, our study shows that BVOCs+$NO_3^{\bullet}$ can still be an important pathway for OA production in the SE US. In contrast to limonene, BVOCs like β-pinene, whose first-generation oxidation products are condensable (Fry et al., 2009), could lead to substantial nighttime aerosol production.

4.5 Implications

We provide direct evidence from ambient measurements to show that anthropogenic pollution can greatly mediate SOA formation from biogenic VOCs under current conditions in the SE US. Being strongly influenced by the $NO_3^{\bullet}$ radical and sulfate, LO-OOA (mainly from monoterpenes oxidation by $NO_3^{\bullet}$) and Isoprene-OA (isoprene SOA formed via reactive uptake of IEPOX in the presence of hydrated sulfate) account for 19-34% and 18-36% (May-September only) of OA, respectively, in Centreville and the greater

Atlanta area (Figure 4.2). In the SE US, the majority of sulfate (photochemical reactions of SO_2) and $NO_3^{\bullet}$ radical (a product of NO_x and ozone reaction) is of anthropogenic origin (Carlton et al., 2010). Using measurement at Centreville (SEARCH site) from 2006 to 2010, we find that the correlation between organic carbon (OC) and sulfate (hourly average data) is substantially better in summer (June-August) than winter (December-February) (*SI Appendix, Fig.S13*). As isoprene emission is higher in warmer months, our proposed interaction between sulfate and Isoprene-OA provides a possible explanation for the seasonal variation in the correlation between OC and sulfate, though we cannot rule out other possibilities. In addition, over the past 15 years, the OC at rural SEARCH sites in the SE US declined by about 38% as calculated from the trends shown in (Hidy et al., 2014). During the same period, the emission of SO_2 and NO_x have also decreased by about 65% and 52%, respectively (Hidy et al., 2014), suggesting that our proposed mechanism about anthropogenic emissions mediating biogenic SOA formation contributes in a potentially significant way to the decrease in OC. As SO_2 and NO_x emissions continue to fall, other biogenic SOA formation pathways (e.g., isoprene SOA formation in the absence of sulfate and monoterpenes SOA from ozonolysis and photooxidation) may become more important, though these pathways have relatively lower SOA yields compared to the mechanisms discussed in this study (Surratt et al., 2010). The decreasing SO_2 and NO_x emissions may not only reduce the biogenic SOA burden, but also have impacts on climate and health. For example, while SOA from IEPOX uptake in the presence of sulfate (i.e., Isoprene-OA factor) is found to have the highest hygroscopicity (tendency to absorb water vapor) of all OA components (Cerully et al., 2015), biogenic SOA formed under lower

sulfate and NO_x environments could have substantially different properties than those formed in polluted environments and warrants further studies.

Although isoprene OA formation via IEPOX uptake has been reported in several field campaigns, our study performs detailed analyses of particle water, particle acidity, and sulfate, and then provides comprehensive assessment to deconvolute their individual effects on isoprene OA formation in the atmosphere (Cerully et al., 2015; Guo et al., 2015). Our observation in Centreville and the greater Atlanta area shows that it is sulfate, instead of particle water and acidity, that controls isoprene OA formation in the SE US during summer, though the exact mechanisms of this direct sulfate effect need further investigation. The influence of these parameters can vary regionally and globally. Therefore, SOA models need to carefully consider the fate of IEPOX and the complexity of isoprene OA formation under various atmospheric conditions. Moreover, our results reveal that the direct effect of sulfate may complicate the role of particle water in the partitioning of water-soluble organics. Finally, these findings emphasize the importance of careful calculations of both particle water content and particle acidity when investigating these SOA formation processes.

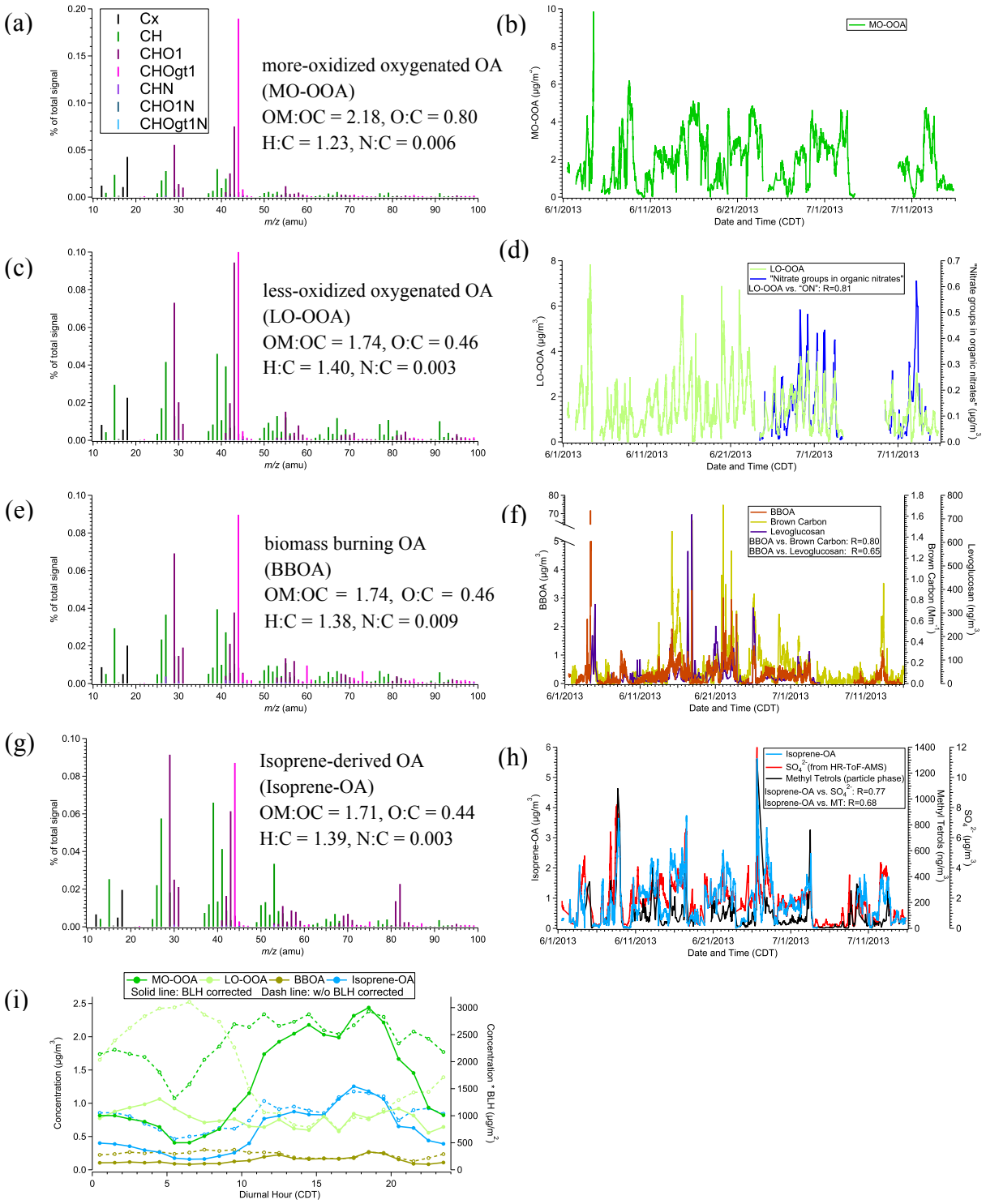

Figure 4.1. (a,c,e,g) Normalized high-resolution mass spectra (colored by the ion type) and elemental ratios of the PMF factors. (b,d,f,h) Time series of the PMF factors and tracer compounds, along with their correlation coefficient. (i) Diurnal trends of PMF factors with (solid line) and without (dash line) multiplying by boundary layer height (BLH).

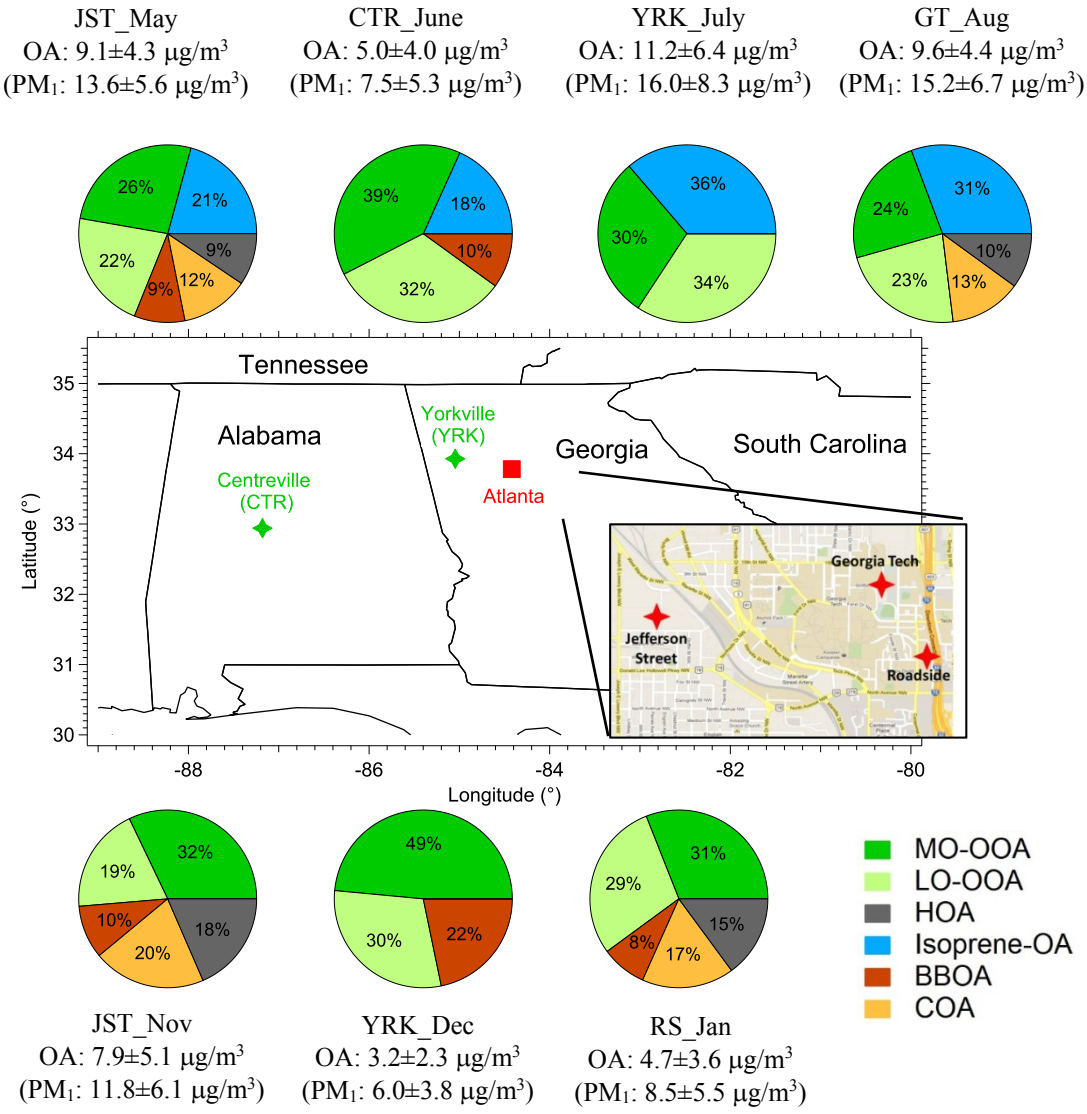

Figure 4.2. Geographical locations and organic aerosol characterization of SOAS and SCAPE field campaigns in the southeastern US. The inset shows a detailed map of Atlanta (adapted from Google Maps). Abbreviations correspond to Centerville (CTR), Yorkville (YRK), Jefferson Street (JST), Georgia Institute of Technology (GT), and Roadside (RS). Details about sampling period at each site are listed in Table. S1. Measurement sites are classified based on their locations as urban (red star) and rural (green star). The pie charts report the source apportionment of organic aerosol. The mass concentrations ± one standard deviation of organics and PM_1 as measured by HR-ToF-AMS are also reported. The identified OA subtypes are: MO-OOA (more-oxidized oxygenated OA), LO-OOA (less-oxidized oxygenated OA), Isoprene-OA (isoprene-derived OA), BBOA (biomass burning OA), HOA (hydrocarbon-like OA), and COA (cooking OA). Isoprene-OA is only identified in the warmer months (from May to September) and LO-OOA is identified at various rural and urban sites throughout the year. Isoprene-OA and LO-OOA account for 43-70% of total measured OA in summer time.

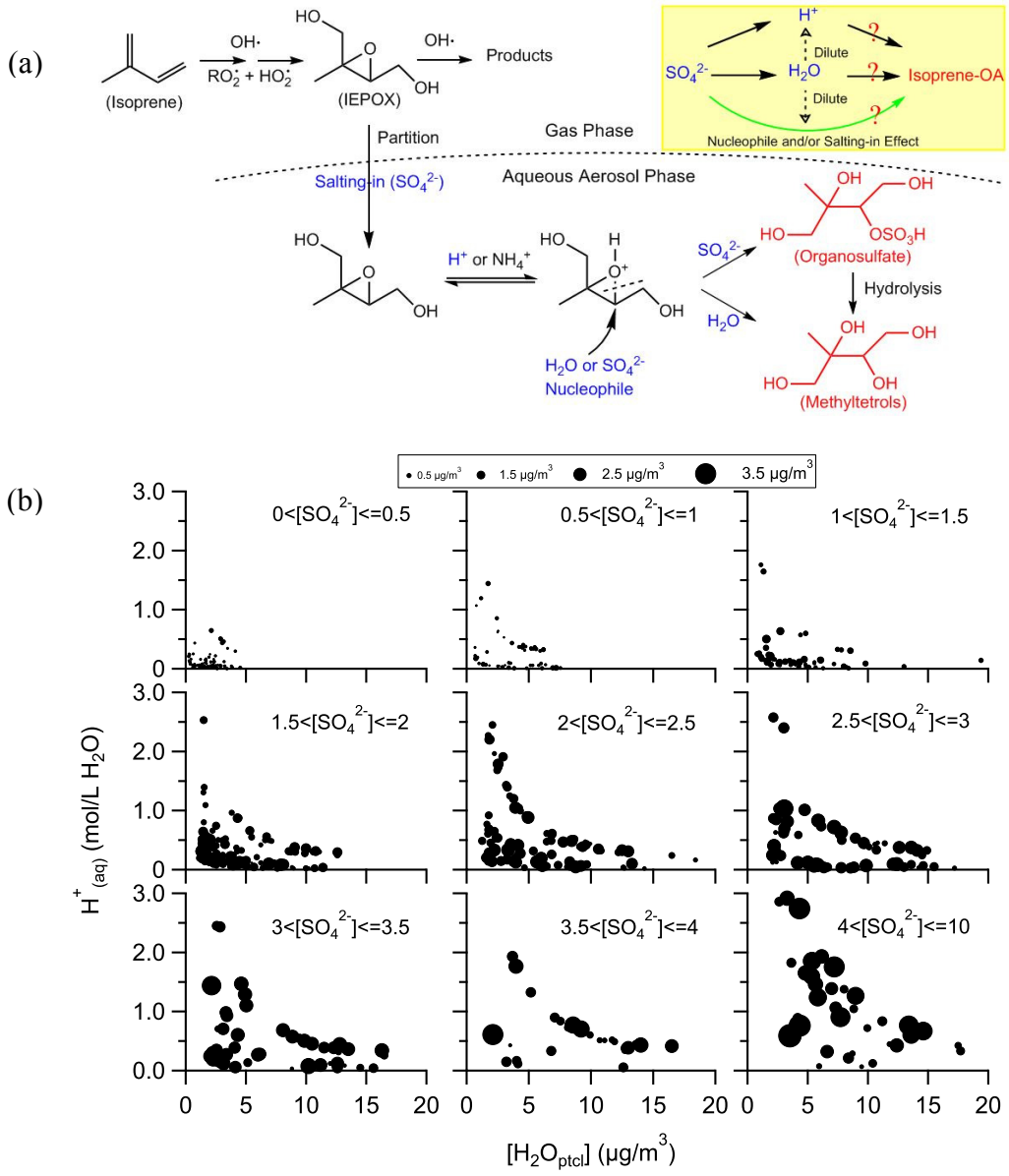

Figure 4.3. (a) A simplified mechanism of isoprene SOA formation via reactive uptake of IEPOX based on refs. (8) and (25). Only one IEPOX isomer is shown in the figure. Compounds colored blue are the parameters we investigate in this study. Compounds colored red are two representative species for isoprene SOA. The inset shows a schematic explaining the relationship between particle water (H_2O_{ptcl}), particle acidity (H^+), sulfate (SO_4^{2-}), and Isoprene-OA. The direct role of SO_4^{2-} on isoprene OA formation is colored green. The indirect role of SO_4^{2-} through H_2O_{ptcl} and/or H^+ is colored black. (b) $H^+_{(aq)}$ (mol L^{-1} H_2O) as a function of [H_2O_{ptcl}] (µg m^{-3}). All data points are grouped into nine subplots based on a 0.5 µg m^{-3} increment in [SO_4^{2-}] and the size of data points represents [Isoprene-OA]. In some cases, a range of $H^+_{(aq)}$ is observed for the same [H_2O_{ptcl}], which is likely due to difference in gas-phase [NH_3] (*SI Appendix, Fig. S6*).

CHAPTER 5: ENHANCED FORMATION OF ISOPRENE-DERIVED ORGANIC AEROSOL IN SULFUR-RICH POWER PLANT PLUMES DURING SOUTHEAST NEXUS (SENEX)

5.1 Background

Secondary organic aerosol (SOA), which is formed in the atmosphere via the oxidation of volatile organic compounds (VOC), accounts for a large fraction of submicron particulate matter globally (Hallquist et al., 2009; Jimenez et al., 2009). In the southeastern United States, a large fraction of SOA originates from biogenic VOCs in summer (Weber et al., 2007; Spracklen et al., 2011; Liao et al., 2007; Xu et al., 2015b; Xu et al., 2015a). However, the SOA formation process is largely mediated by anthropogenic pollutants, such as nitrogen oxides (NO_x) and aerosol sulfate (Carlton et al., 2010; Xu et al., 2015a; Hoyle et al., 2011; Xu et al., 2015b). Long-term measurements (1999-2013) at the Southeastern Aerosol Research and Characterization (SEARCH) network have revealed a significant decreasing trend in ambient concentrations of sulfur dioxide (SO_2) and NO_x, which is caused by regulations of anthropogenic emissions from power plants and vehicles (Hidy et al., 2014), as well as the switch from coal to natural gas in many power plants (de Gouw et al., 2014). Meanwhile, the concentration of organic carbon (OC) has also decreased significantly in the same region as shown in Hidy et al. (2014). However, the causes for the OC reduction were less clear. Blanchard et al. (2015) estimated that about 45% of OC in the southeastern United States derives from combustion sources (vehicles and biomass burning), which contributes the most to the OC reduction. In addition to the reduction in primary OC from combustion sources, secondary OC from biogenic VOCs also likely

decreases, due to the reduction in NO_x and SO_2 and their interactions with biogenic emissions. For example, Blanchard et al. (2015) observed an association between OC and sulfate based on a statistical analysis of the long-term SEARCH data. The amount of sulfate-associated OC accounted for ~25% of average OC concentration from 1999 to 2013. Also, as shown in Xu et al. (2015b), the correlation between OC and sulfate in the SEARCH data is substantially better in summer than in winter.

One possible explanation for the association between OC and sulfate arises from the effect of sulfate on isoprene SOA formation. Globally, isoprene is the single most contributing compound to VOC emissions from vegetation (Guenther et al., 2006). Laboratory studies have revealed that the isoprene SOA yield is greatly enhanced in the presence of sulfate seed particles resulting in acidic aqueous particles (Surratt et al., 2010). The enhancement is due to the sulfate induced reactive uptake of isoprene epoxydiols (IEPOX), which are isoprene oxidation products from the peroxy radical (RO_2) + hydroperoxyl radical (HO_2) pathway (Paulot et al., 2009b). Isoprene-derived OA factor (i.e., isoprene-OA) resolved by positive matrix factorization (PMF) analysis of aerosol mass spectrometry data, which is a surrogate for isoprene SOA through IEPOX reactive uptake, has been identified at multiple sampling sites (Robinson et al., 2011a; Slowik et al., 2011; Budisulistiorini et al., 2013; Hu et al., 2015; Chen et al., 2015; Xu et al., 2015a; Xu et al., 2015b). Specifically, PMF analysis of high resolution AMS data showed that isoprene-OA accounted for 18-36% of OA in summer in the southeastern United States (Xu et al., 2015a; Xu et al., 2015b).

Based on measurements at multiple sites in the southeastern United States, Xu et al. (2015a) showed that isoprene-OA is strongly associated with sulfate, but not associated

with particle pH or particle water as suggested by prior laboratory studies. This strong correlation between isoprene-OA and sulfate has been repeatedly observed in many studies (Budisulistiorini et al., 2015; Hu et al., 2015) and reproduced in a chemical transport model (Marais et al., 2015). However, a coherent explanation regarding the relationships between isoprene-OA and sulfate, particle pH, and particle water has not emerged. The model results by Marais et al. (2015) suggest that the correlation between isoprene-OA and sulfate is caused by sulfate's influence on volume and pH, although the role of particle volume is not explicitly discussed and remains unclear. Regarding the repeatedly observed lack of correlation between isoprene-OA and particle pH in ambient measurements (Budisulistiorini et al., 2015; Xu et al., 2015a), some studies suggested that it is due to that isoprene-OA measured at a surface site is affected by transport, during which the particle pH can change (Budisulistiorini et al., 2013). However, Budisulistiorini et al. (2015) modeled the concentration of IEPOX-derived SOA tracers with good accuracy by using local particle pH and particle water at Look Rock, TN, even though the observed isoprene-SOA did not correlate with local particle pH. In addition, in Xu et al. (2015a), where isoprene-OA was largely locally produced at Centreville, AL as indicated by the highly reproducible diurnal variation of isoprene-OA regardless of the origin of air masses, isoprene-OA is still not correlated with particle pH. Thus, transport may not explain the lack of correlation between isoprene-OA and particle pH. Other possible mechanisms of sulfate on isoprene-OA formation are through the surface accommodation process (Lin et al., 2013a) or nucleophilic effects of sulfate (Xu et al., 2015a).

In this study, we investigate the mechanisms and kinetics of anthropogenic emissions on isoprene SOA formation based on airborne measurements in the southeastern

United States, a region with large emissions from both anthropogenic and biogenic sources. We sampled downwind from power plants in Georgia. The power plant studies serve as a unique perturbation experiment in the atmosphere by injecting anthropogenic emissions (NO_x and SO_2) into isoprene-rich air masses. We use measurements made downwind from two power plants with differing SO_2 emissions, which provides an opportunity to examine the sensitivity of isoprene SOA to varying amounts of particle sulfate in otherwise nearly identical ambient conditions.

5.2 Measurements and Models

Measurements were performed as part of the Southeast Nexus (SENEX) campaign in June and July, 2013 (Warneke et al., 2016). In the SENEX campaign, the NOAA WP-3D aircraft flew 20 research flights over the southeastern United States. In the current study, we focused on the flight on 16 June, 2013, when the aircraft flew over Georgia. The flight track is shown in figure 5.1. We focus our analysis on the measurements at different downwind distances of two power plants, Scherer and Harllee Branch, the locations of which are shown in figure 5.1. Both Scherer and Harllee Branch are coal-fired power plants, but they have different emissions of NO_x and SO_2. As shown in figure S1, the daytime NO_x and SO_2 emissions of Scherer are only about 1/3 and 1/6 of those of Harllee Branch, respectively, which is a result of the installation of different emissions reduction equipment in Scherer compared to Harllee Branch according to Continuous Emissions Monitoring System (http://www3.epa.gov/ttn/emc/cem.html). The wind direction for this flight was constantly from the southwest, resulting in a well-defined plume of emissions that was advected to the northeast. We note that there was a biomass burning source located

upwind of the two power plants and the plume from this source advected between the power plants. As will be discussed below, portions of this plume mixed with the Scherer plume in some transects. The gas-phase chemistry in these plumes is described in a parallel paper that focuses on the effect of NO_x on oxidation rates and the formation of isoprene products such as formaldehyde (de Gouw et al., 2016).

A suite of instruments were deployed aboard the aircraft. The instruments of interest to our study are summarized in Table S1 and discussed briefly below. A compact time-of-flight aerosol mass spectrometer (cToF-AMS) was deployed to measure the composition of non-refractory submicron particles (Canagaratna et al., 2007; Bahreini et al., 2008; Bahreini et al., 2009). Positive Matrix Factorization (PMF) analysis was performed on the organic mass spectra of the whole flight for OA source apportionment (supporting information). The collection efficiency (CE) for the AMS data was determined according to the composition-dependent algorithm proposed by Middlebrook et al. (2012) (figure S2a). We validated the application of composition-dependent CE (CDCE) by converting the mass concentrations of non-refractory species (measured by AMS) and refractory black carbon (measured by single-particle soot photometer) to volume concentration (denoted as composition-based volume) (supporting information). Then we compared the composition-based volume with Ultra-High Sensitivity Aerosol Size spectrometer (UHSAS) measurements, which reports the particle size distribution in the range of 70 – 1000 nm (Brock et al., 2015). As shown in figure S2b, the composition-based volume for this flight agrees well with the UHSAS volume (slope = 1.01±0.06). Even in the plume where the particle composition changes largely and there is an increase in smaller-sized particles, they still show excellent agreement (slope = 0.97±0.04). Depending

on the organic aerosol density, the accuracy of the AMS mass relative to the mass calculated from the UHSAS for this flight is ±16% (figure S2c).

A high-resolution time-of-flight chemical ionization mass spectrometer (HR-CIMS) using iodide-adducts was deployed to measure a suite of oxygenated volatile organic compounds (oVOCs) at high frequency (1 Hz). Detailed working principles and sampling protocol can be found in Lee et al. (2014). The instrument is able to elucidate the chemical composition of 100's of molecular ions from the high mass accuracy and resolution, but it does not provide structural information nor isomer separation. Among all the oVOCs detected by the CIMS, the signal for $C_5H_{10}O_3$ species which has contribution from two isomers, isoprene hydroxyhydroperoxides (ISOPOOH) and isoprene epoxydiols (IEPOX), is of interest to our study.

The particle liquid water content (H_2O_{ptcl}) was calculated based on water uptake by both organics and inorganics (Guo et al., 2015) and the measured ambient meteorological data (Warneke et al., 2016). The H_2O_{ptcl} uptake by organics was calculated based on the organic concentration (measured by AMS) and hygroscopicity (i.e., κ_{org}) (Petters and Kreidenweis, 2007). Considering uncertainties in κ_{org} from previous measurements under different saturation states (Brock et al., 2015; Cerully et al., 2015), we performed sensitivity tests by varying κ_{org} from 0 to 0.2, which has negligible effects on the conclusions. An average value of 0.1 was selected for κ_{org}. The particle-phase H^+ and H_2O_{ptcl} uptake by inorganics were predicted using the thermodynamic model ISORROPIA II (Fountoukis and Nenes, 2007). In addition to the particle-phase inorganic ions (i.e., sulfate, nitrate, ammonium, and chloride measured by AMS), gas-phase HNO_3 and NH_3

measured from the aircraft were also included in the model prediction of H^+ and pH (Hennigan et al., 2015). The particle-phase pH was calculated by

$$pH = -\log_{10} a_{H}^{+} = -\log_{10}\left(\frac{H^+}{LMass} \times \rho_{particle} \times 1000\right) \qquad \text{Eq. 5.1}$$

where H^+ and LMass are the mass concentrations of particle hydronium ion and total aqueous phase output from ISORROPIA II ($\mu g\ sm^{-3}$), $\rho_{particle}$ is the particle density ($g\ cm^{-3}$), and a_{H^+} is the H^+ activity in the aqueous phase ($mol\ L^{-1}$). The modeled HNO_3, NH_3, and particle NH_4^+ agree within 20% of the measurements (figure S3), which supports the accuracy of our pH calculation. The details about the calculation of particle water and particle acidity are discussed in the supporting information.

5.3 Results and Discussion

5.3.1 Evolution of species downwind of the power plants.

Plumes from the two power plants, Scherer and Harllee Branch, were each intercepted five times at different downwind distances, which allows us to investigate the evolution of plume composition, with a focus on organic aerosol. In order to compare the species concentration inside and outside the plume, for each intercept, we calculate the average plume concentration of a certain species based on 1-minute measurements in the center of the plume (defined by peak NO_2 concentration) and we calculate the average concentration outside the plume based on 2-minute measurements before and after the plume intercepts (see figure S4 for details). Figure 5.2 shows the evolution of species of interest and figure S5 shows the evolution of auxiliary species. While the SO_2 concentration is enhanced in both plumes compared to outside the plume (figure 5.2a), the

enhancement magnitude is larger in the Harllee Branch plume due to larger emissions of SO_2. The oxidation of SO_2 causes the enhancement of sulfate downwind of the power plants (figure 5.2b). Figure 5.2c shows that enhancements in OA are observed at all intercepts of the Harllee Branch plume. The largest enhancement occurred at the fourth intercept (i.e., 62.8 km downwind of Harllee Branch), where the OA increased by 1.8 μg sm^{-3} after correcting for the particle collection efficiency in AMS. In contrast, the OA was only enhanced for the first two intercepts of Scherer plume. Below, we address the causes for OA enhancement in both plumes, with a focus on the Harllee Branch plume.

5.3.2 Reasons for OA enhancement in the plumes

The OA enhancement for the first two intercepts of Scherer plume is likely caused by a biomass burning plume that partly merged with the Scherer plume. Black carbon (figure S6) and other tracers for biomass burning (e.g., CO and acetonitrile) are enhanced in the first two intercepts of Scherer plume. This biomass burning plume has negligible influence on the Harllee Branch as neither black carbon nor acetonitrile is enhanced in the Harllee Branch plume (figure S6).

To examine the reasons for the OA enhancement in the Harllee Branch plume, we firstly investigate the composition of OA formed in the plume. For each intercept, we subtract the OA mass spectra outside the plume from the OA mass spectra inside the plume and then normalize the difference mass spectra to the total difference signal. As shown in figure 5.3, the composition of OA formed in the Harllee Branch is distinctly different from that outside the plume. Outside the plume, the most prominent signal is *m/z* 44 (mainly CO_2^+, a tracer for carboxylic acids (Canagaratna et al., 2015; Ng et al., 2010)). Inside the

Harllee Branch plumes, we note a substantial signal at *m/z* 53 and *m/z* 82, which are attributed to isoprene SOA via the reactive uptake of IEPOX (Robinson et al., 2011a; Lin et al., 2012; Liu et al., 2015b; Allan et al., 2014). *m/z* 82 accounts for about 2.1 - 3.5% of the OA formed in the Harllee Branch plume. The enhancement of *m/z* 82 suggests that the formation of isoprene SOA contributes to the OA enhancement in the Harllee Branch plume. Although the cToF-AMS used in this study cannot separate the ions at *m/z* 82 ($^{34}SO_3^+$, $C_4H_2O_2^+$, $C_5H_6O^+$, and $C_6H_{10}^+$), the mass resolution is sufficient to indicate that the signal at *m/z* 82 is distinctly not solely due to $^{34}SO_3^+$ or $C_6H_{10}^+$. It is likely dominated by $C_5H_6O^+$ based on high resolution AMS data obtained in surface measurements in the southeastern United States (Xu et al., 2015a; Xu et al., 2015b).

To further investigate the reasons for OA enhancement in the plumes, we perform PMF analysis on organic mass spectra for source apportionment. Two OA factors, oxygenated OA (OOA) and isoprene-derived OA (isoprene-OA), are resolved for this flight. The mass spectra and time series of these two factors are shown in figure 5.4. The mass spectrum of OOA is characterized by high f_{44} (ratio of *m/z* 44 to total OA signal), which indicates that this factor is highly oxidized (Ng et al., 2010). For the entire flight on 16 June, OOA accounts for 76% of OA on average. The time series of OOA correlates well with CO (R = 0.92, figure 5.4b), which is consistent with previous field studies (Sullivan et al., 2006; Worton et al., 2011; Bahreini et al., 2009; Weber et al., 2007).

The mass spectrum of the isoprene-OA factor is characterized by peaks at *m/z* 53 and 82 (figure 5.4a). As discussed above, *m/z* 53 and 82 have been used as a tracer for SOA formed via IEPOX reactive uptake based on current knowledge. However, we cannot rule out the possibility that this factor also includes contribution from isoprene OA formed via

other pathways, or the possibility that isoprene oxidation products other than IEPOX are taken up by acidic sulfate particles to generate *m/z* 53 and 82 (Schwantes et al., 2015). Thus, we name the factor as isoprene-OA (Xu et al., 2015a; Xu et al., 2015b). The time series of isoprene-OA correlates well with sulfate (R = 0.73), which is consistent with surface measurements in the southeastern United States (Xu et al., 2015a; Budisulistiorini et al., 2015; Xu et al., 2015b) . Isoprene-OA accounts for 24% of OA on average, with enhanced mass fraction in the Harllee Branch plume (figure 5.4c).

Figure 5.5 shows the vertical profiles of the concentrations and mass fractions of OOA and isoprene-OA. The concentrations of both factors are relatively constant from the bottom of the profile to 2 km. Above 2 km, their concentrations decrease rapidly with altitude. At high altitude (i.e., > 3 km), isoprene-OA concentration falls nearly to 0 and OOA dominates the OA (i.e., >90%). The vertical profile of isoprene-OA in this study is similar to the vertical profile of IEPOX sulfate ester over the southeastern United States (Liao et al., 2015; Froyd et al., 2010) and the vertical profile of isoprene SOA tracer ion *m/z* 82 over the Amazon (Allan et al., 2014) and tropical forest (Robinson et al., 2011a).

PMF analysis shows that the OA enhancement for the first two intercepts of Scherer plume is mainly due to an increase in OOA concentration. This OOA enhancement is likely caused by a biomass burning plume that partly merged with the Scherer plume (figure S6). A biomass burning OA factor is not resolved from this flight, which is likely caused by that the OA from biomass burning is aged and hence may be apportioned OOA factor by PMF analysis (Xu et al., 2015b; Grieshop et al., 2009a; Hennigan et al., 2011). It is also possible that the contribution from biomass burning OA to total OA is less than 5% so that PMF cannot retrieve the biomass burning OA factor (Ulbrich et al., 2009). According to

PMF analysis, isoprene-OA is the main reason for the OA enhancement in the Harllee Branch plume. As shown in figure 5.2e, isoprene-OA factor is substantially enhanced in the Harllee Branch plume, which is consistent with a large increase at signal *m/z* 82 inside the plume (figure 5.3). In contrast, the isoprene-OA factor is not enhanced in the Scherer plume.

5.3.3 Reasons for isoprene-OA enhancement in Harllee Branch plume

Next, we investigate the possible causes for the isoprene-OA enhancement in the Harllee Branch plume. Isoprene is depleted rapidly in the Harllee Branch plume (de Gouw et al., 2016). The gas-phase chemistry in these plumes was investigated by de Gouw et al. (2016), who concluded that hydroxyl radical (OH) concentrations in both plumes were enhanced due to the presence of NO_x. The enhancements in OH concentration led to lower isoprene concentrations and increased concentration of isoprene products like formaldehyde in both plumes. Nevertheless, the oxidation of isoprene inside the Harllee Branch plume is unlikely the reason for the isoprene-OA enhancement. This is because of the high concentration of NO_x in the plume, which dominates the fate of RO_2 and inhibits the formation of IEPOX via the RO_2+HO_2 pathway (supporting information). Although Jacobs et al. (2014) showed that the RO_2+NO pathway could also produce IEPOX, the IEPOX yield from that reaction is very small. For example, the largest reduction in isoprene observed in the third intercept of the Harllee Branch plume (i.e., ~1 ppb) would produce only 0.01 ppb IEPOX (~0.03 $\mu g/m^3$), which is too low to explain the magnitude of isoprene-OA enhancement. In addition, formaldehyde (HCHO), a product of isoprene oxidation via fragmentation (Paulot et al., 2009a), is enhanced in the plume, which is likely

due to enhanced OH concentration and NO dominating the fate of RO_2 in the plume (de Gouw et al., 2016; Wolfe et al., 2015). Thus, based on current understanding on IEPOX formation mechanisms, it is unlikely that enhanced isoprene oxidation in the plume can produce enough IEPOX to explain the magnitude of isoprene-OA enhancement.

Background IEPOX, rather than IEPOX produced in the plume, likely dominated the isoprene-OA enhancement when it interacted with the sulfate-rich power plant plume. We perform a rough mass closure analysis to demonstrate that the reactive uptake of already-existing IEPOX in the atmosphere could explain the isoprene-OA enhancement in the plume. Since IEPOX and ISOPOOH were measured as the same cluster ion at *m/z* 245 ($C_5H_{10}O_3I^-$) by I^- CIMS in this study, we apply a previously measured IEPOX/ISOPOOH concentration ratio to estimate IEPOX from the $C_5H_{10}O_3I^-$ signal using Eq. 5.2

$$C_5H_{10}O_3I^- \text{ signal} = [\text{IEPOX}] \times \text{IEPOX sensitivity} + [\text{ISOPOOH}] \times \text{ISOPOOH sensitivity} \quad \text{Eq. 5.2}$$

In Eq. 5.2, $C_5H_{10}O_3I^-$ signal (in unit of counts per second, cps) is measured by I^- CIMS in this study. The HR-CIMS sensitivities to IEPOX and ISOPOOH are 0.39 and 3.32 (cps ppt^{-1}), respectively. [IEPOX] and [ISOPOOH] are the concentration of IEPOX and ISOPOOH (ppt), respectively, which are to be determined. The IEPOX/ISOPOOH concentration ratio is estimated to be 1.04±0.54 (average ± 1 standard deviation), based on the IEPOX and ISOPOOH measurements by a triple quadrupole CIMS during the Southeastern Oxidant and Aerosol Study (SOAS) and the Studies of Emissions and Atmospheric Composition, Clouds and Climate Coupling by Regional Surveys (SEAC4RS), which occurred over a similar region of the southeastern United States a few months after the SENEX project. After applying the estimated IEPOX/ISOPOOH concentration ratio to Eq. 5.2 and propagating uncertainties, we estimate that the IEPOX

concentration is about 750±546 ppt outside the Harllee Branch plume. Details about the estimation can be found in the supporting information. Then, assuming that all the IEPOX is taken up by the acidic particles in the plume and assuming a SOA yield of 20% from IEPOX reactive uptake (Riedel et al., 2015), the IEPOX reactive uptake would produce about 0.7±0.51 μg sm^{-3} SOA, which is similar to the observed isoprene-OA enhancements in the plume (about 1 μg sm^{-3} in figure 5.2e). Despite large uncertainties in estimating IEPOX concentration, SOA yield, and IEPOX fate in the plume, this analysis demonstrates that the isoprene-OA enhancement in the plume could be explained by reactive uptake of IEPOX.

5.3.4 Parameterization of IEPOX heterogeneous reactions

To quantitatively support our argument that IEPOX reactive uptake process is fast and contributes to the OA enhancement in the Harllee Branch plume, we calculate the pseudo-first-order heterogeneous reaction rate constant for IEPOX reactive uptake (k_{het}, s^{-1}). The k_{het} can be calculated by following Eq. 5.3, neglecting the gas phase diffusion which has a minor effect on k_{het} (Gaston et al., 2014).

$$k_{het} = \frac{\gamma \upsilon S_a}{4} \qquad \text{Eq. 5.3}$$

In Eq. 5.3, γ is the uptake coefficient of IEPOX, ν is the mean molecular speed of IEPOX (231 m s^{-1} at 298 K), and S_a is the surface area of wet particles at ambient RH, which is calculated from the measured dry particle size distribution and κ-Köhler theory (supporting information). γ is parameterized based on a resistor model, which includes the mass accommodation at the surface (i.e., the first term in Eq. 5.4) and aqueous-phase diffusion and reactions (i.e., the second term in Eq. 5.4) (Pye et al., 2013).

$$\frac{1}{\gamma} = \frac{1}{\alpha} + \frac{\nu}{4H_{IEPOX}RT\sqrt{D_a k_{aq}}} \frac{1}{f(q)} \quad \text{Eq. 5.4}$$

$$f(q) = \coth(q) - \frac{1}{q} \quad \text{Eq. 5.5}$$

$$q = r_p \sqrt{\frac{k_{aq}}{D_a}} \quad \text{Eq. 5.6}$$

$$k_{aq} = \sum_{i=1}^{N} \sum_{j=1}^{M} k_{i,j} [nuc_i][acid_j] \quad \text{Eq. 5.7}$$

In Eqs. (4)-(7), the mass accommodation coefficient, α, is estimated to be 0.1 by Gaston et al. (2014); the diffusivity of IEPOX in the aqueous phase, D_a, is estimated to be 10^{-9} m^2 s^{-1} by Gharagheizi et al. (2011); r_p is the effective particle radius. The pseudo-first-order aqueous-phase rate constant, k_{aq}, is based on an acid-catalyzed ring-opening A-2 mechanism (Eddingsaas et al., 2010). [nuc] and [acid] represent the molarity (mol L^{-1}) of nucleophiles (SO_4^{2-} and H_2O) and acids (HSO_4^- and H^+), respectively. $k_{i,j}$ are the reaction rate coefficients between IEPOX and nucleophiles (H_2O and SO_4^{2-}). We applied the values of $k_{i,j}$ from Riedel et al. (2016), who estimated the $k_{i,j}$ values using a box model with experimental constraints. H_{IEPOX} is the Henry's Law coefficient of IEPOX. There are large uncertainties in many model parameters. For example, the H_{IEPOX}, which has been determined by model calculations and laboratory measurements, spans two orders of magnitude (Chan et al., 2010b; Eddingsaas et al., 2010; Gaston et al., 2014; Nguyen et al., 2014; Pye et al., 2013). Here, we apply the values of 3×10^7 and 1.7×10^8 M atm^{-1} based on measurements by Nguyen et al. (2014) and Gaston et al. (2014) for a sensitivity analysis.

All the values of the parameters used in the calculation are summarized in Table S2. The parameterization is illustrated in figure 5.6. k_{aq} describes the IEPOX aqueous-phase reaction rate constant; γ evaluates the probability of gas-particle collisions that leads to reaction; k_{het} describes the overall heterogeneous reaction rate constant of IEPOX, which includes two steps, IEPOX uptake to particles and subsequent aqueous-phase reactions.

In addition to the pseudo-first-order heterogeneous reaction rate constant for IEPOX reactive uptake (i.e., k_{het}), we also calculate the pseudo-first-order oxidation rate constant for IEPOX by OH radical (i.e., k_{ox}, s^{-1}). k_{ox} is estimated by the product of OH concentration and the rate coefficient for the reaction of IEPOX and OH ($k_{OH+IEPOX}$) (Eq. 5.8). The OH concentration in the power plant plumes is estimated by a Lagrangian plume dispersion model with photochemistry (Sillman, 2000; Brock et al., 2002; Wert et al., 2003). There are two measured $k_{OH+IEPOX}$ values in the literature (i.e., 1.51×10^{-11} and 3.52×10^{-11} cm^3 $molecule^{-1}$ s^{-1} at 298K in Bates et al. (2014) and Jacobs et al. (2013), respectively), both of which are applied in this study for a sensitivity analysis.

$$k_{ox} = k_{IEPOX+OH}[OH] \qquad \text{Eq. 5.8}$$

Figure 5.7 shows the calculated k_{het} and k_{ox} for each intercept. In the Harllee Branch plume, the k_{het} is greater than 1.4×10^{-3} s^{-1}, which corresponds to an IEPOX lifetime shorter than 12 min (figure S7), suggesting the heterogeneous reaction is very fast. Also, the IEPOX heterogeneous reaction rate is 3-10 times faster than its gas phase oxidation rate, which indicates that the heterogeneous reaction is the major fate of IEPOX in the Harllee Branch plumes. Compared to Harllee Branch, the heterogeneous reaction rate is slower in

Scherer, which is essentially caused by the smaller enhancement of sulfate in the Scherer plume. In Scherer, the IEPOX gas phase oxidation rate is comparable with its heterogeneous reaction rate (figure 5.7), which implies that a portion of IEPOX may undergo OH oxidation, instead of heterogeneous reaction. This may explain the lack of isoprene-OA enhancement in Scherer.

5.3.5 Roles of sulfate on isoprene-OA formation

The rapid heterogeneous reaction of IEPOX is a result of sulfate enhancements in the Harllee Branch plume, which is consistent with the finding that sulfate plays an important role in isoprene-OA formation in Xu et al. (2015a). As shown in figure 5.2b, the sulfate concentration is enhanced in the Harllee Branch plume by a factor of 2 – 5 compared to outside the plume, which is caused by the oxidation of SO_2. As a consequence of the sulfate enhancement, particle acidity, particle water, and particle surface area in the plume are increased and correlated with each other (figure 5.2). All these changes facilitate the IEPOX heterogeneous reaction. However, since these changes occur simultaneously, the separate effects (i.e., nucleophile vs. acid catalyst vs. uptake medium) are difficult to quantify. As shown in Eq. 5.3 and figure 5.6, k_{het} is proportional to both surface area and γ (which is affected by particle acidity). The relative importance of surface area and particle acidity on k_{het} will be systematically assessed below.

Firstly, we find that the nucleophilic effect of SO_4^{2-} is likely small. Although the absolute amount of SO_4^{2-} concentration in air (i.e., $[SO_4^{2-}]$, [] indicates unit $\mu g\ m^{-3}$ air) increases in the plume (figure S8e), its aqueous-phase concentration (i.e., $SO_4^{2-}{}_{(aq)}$, $_{(aq)}$ indicates unit mol L^{-1}) is not enhanced in the plume (figure S8f). This is because for the

same RH, higher [SO_4^{2-}] leads to higher [H_2O_{ptcl}], which dilutes the aqueous phase SO_4^{2-} concentration and limits $SO_4^{2-}{}_{(aq)}$ enhancement. This suggests that the SO_4^{2-} nucleophilic effect is not likely the reason for the isoprene-OA enhancement in the plumes. We note that the $SO_4^{2-}{}_{(aq)}$ in the third Harllee Branch plume intercept is lower in the plume compared to outside. This is because the low particle pH in this intercept shifts the SO_4^{2-}-HSO_4^- equilibrium towards HSO_4^-, which results in lower $SO_4^{2-}{}_{(aq)}$ and higher $HSO_4^-{}_{(aq)}$ (figure S8).

Particle acidity (i.e., $H^+{}_{(aq)}$) could affect k_{het} by influencing the IEPOX aqueous-phase reactions (k_{aq}) and hence γ (Eq. 5.7 and 5.4, respectively). In order to test the magnitude of this effect in the Harllee Branch plume, we first calculate k_{het} by using all the species concentration outside the plume (denoted as $k_{het,out}$) and k_{het} by using all the species concentration inside the plume (denoted as $k_{het,in}$). We then calculate a new k_{het} by using all the species concentration outside the plume but replacing only $H^+{}_{(aq)}$ with the concentration inside the plume (denoted as $k_{het,H+}$). By comparing the values of these different k_{het}, we can evaluate the effect of changing particle acidity alone on k_{het}. Figure 5.8 shows that $k_{het,H+}$ is larger than $k_{het,out}$, suggesting that increasing particle acidity contributes to k_{het} enhancement in the Harllee Branch plume. However, comparing $k_{het,H+}$ with $k_{het,in}$ shows that $k_{het,H+}$ accounts for 40-65% or 42-66% of $k_{het,in}$ using an H_{IEPOX} value of 3.0×10^7 or 1.7×10^8 M atm^{-1}, respectively. This suggests that increasing particle acidity alone does not fully explain the enhanced magnitude of k_{het} in the plume according to the model.

Enhanced particle surface area also contributes to enhanced k_{het} in the Harllee Branch plume. Unlike particle acidity which affects k_{het} by influencing aqueous-phase

reactions, particle surface area affects k_{het} by influencing the gas-particle collision frequency and hence the amount of IEPOX uptake to particles. Figure 5.8 shows that $k_{het,SA}$ (calculated in the similar way as $k_{het,H+}$ discussed above) accounts for 30-51% or 70-80% of $k_{het,in}$ using an H_{IEPOX} value of 3.0×10^7 or 1.7×10^8 M atm^{-1}, implying that increasing particle surface area alone could possibly explain a large fraction of enhanced k_{het} in the plume.

Despite the uncertainties in H_{IEPOX}, it is clear that sulfate enhances isoprene-OA formation in the Harllee Branch plume due to both enhanced particle surface area (i.e., IEPOX uptake to particles) and particle acidity (i.e., aqueous-phase reactions).

5.3.6 Insights into the relationships between isoprene-OA, sulfate, particle acidity and water.

Xu et al. (2015a) observed a strong association between isoprene-OA and sulfate but a lack of correlation between isoprene-OA and particle water and acidity. Other studies have reported similar relationships (Worton et al., 2013; Budisulistiorini et al., 2015; Lin et al., 2013a). The reason for these observations may arise from the competition between IEPOX uptake to particles and subsequent aqueous-phase reactions (summarized in Table 5.1 and figure 5.6). Regarding the sulfate, its increase will not only enhance the aqueous-phase reaction but also enhance IEPOX uptake rate to particles as the case in Harllee Branch. Therefore, the overall IEPOX heterogeneous reaction rate is enhanced and the correlation between isoprene-OA and sulfate is expected. Increasing other factors (such as particle acidity and particle water), however, may only affect one aspect of k_{het} or have trade-off effects on k_{het}.

Table 5.1. The effects of increasing H^+ (μg/m^3), particle water (μg/m^3), or sulfate (μg/m^3) on k_{het} while holding the other covariates constant.

Increase in	Resulting changes	Uptake to particles	Aqueous-phase reaction	Overall effect on k_{het}
[sulfate]	$H^+_{(aq)}$ increases. Surface area increases.	increase	increase	always increase
$[H^+]$	$H^+_{(aq)}$ increases	no change	increase	may be small when k_{aq} is sufficiently large
$[H_2O_{ptcl}]$	$H^+_{(aq)}$ and $SO_4^{2-}{}_{(aq)}$ decrease. Surface area increases.	increase	decrease	may offset

Increasing particle acidity will increase the aqueous-phase reaction rate constant (i.e., k_{aq}) and hence γ. Laboratory studies by Gaston et al. (2014) showed that particle acidity has the strongest effect on γ. It is important to note that γ only evaluates the probability of gas-particle collisions that lead to reaction, but the IEPOX heterogeneous reaction lifetime (i.e., $1/k_{het}$) and isoprene-OA concentration depend not only on γ but also on the particle surface area (Eq. 5.3). If the aqueous-phase reaction is sufficiently fast, γ saturates at the mass accommodation coefficient and the overall heterogeneous rate constant (i.e., k_{het}) is limited by particle surface area. Thus, increasing particle acidity may not increase the amount of isoprene-OA.

The observed lack of correlation between $[H_2O_{ptcl}]$ and isoprene-OA, even when other covariates are held constant, may be due to the trade-off effects of particle water on k_{het}. Higher $[H_2O_{ptcl}]$ increases particle surface area to potentially enhance IEPOX uptake. However, higher $[H_2O_{ptcl}]$ also dilutes the aqueous-phase concentration of compounds (i.e., $H^+_{(aq)}$, $SO_4^{2-}{}_{(aq)}$, $HSO_4^-{}_{(aq)}$), which decreases the aqueous-phase reaction rate constant (i.e., k_{aq}). To quantitatively evaluate the effects of particle water, we calculate the k_{het} by only changing $[H_2O_{ptcl}]$ and holding other covariates constant and similar to values measured at

the Centreville, Alabama during SOAS (supporting information). As shown in figure 5.9, increasing [H_2O_{ptcl}] dilutes particle phase concentrations which decreases γ, consistent with laboratory studies by Nguyen et al. (2014) and Gaston et al. (2014). We note that the effect of [H_2O_{ptcl}] on k_{het} is affected by H_{IEPOX} value. The k_{het} is insensitive to change in [H_2O_{ptcl}] if an H_{IEPOX} value of 3.0×10^7 M atm^{-1} is used, which is due to the increase in surface area compensating the decrease in γ; however, k_{het} increases with [H_2O_{ptcl}] if an H_{IEPOX} value of 1.7×10^8 M atm^{-1} is used. Nevertheless, this analysis quantitatively shows that the opposing effects of particle water could potentially explain the lack of association between [H_2O_{ptcl}] and isoprene-OA. Regarding the role of particle water on SOA formation, Carlton and Turpin (2013) used a photochemical transport model and showed that the particle water largely controls the partitioning of water-soluble gas and subsequent SOA formation by providing partitioning medium in the southeastern US. However, since the dilution effect was not considered in Carlton and Turpin (2013), the role of particle water may be overestimated.

These competing effects may explain the observed relationships between isoprene-OA and different factors in previous studies. We note that the parameter values in the IEPOX heterogeneous reaction parameterization are uncertain (such as α, H_{IEPOX}, and $k_{i,j}$'s in Eq. 5.4-5.7), which highly limits quantitative understanding of the role of each factor. Further studies that constrain these parameters will improve predictions of isoprene OA.

5.4 Implications

Although the rapid reactive uptake of IEPOX to acidic particles has been observed in laboratory studies (Gaston et al., 2014; Surratt et al., 2010; Liu et al., 2015b), we report,

for the first time, the rapid isoprene-OA formation via the IEPOX reactive uptake based on ambient measurements. We show that the sulfate, which is an oxidation product of SO_2 emitted from power plants, can enhance IEPOX uptake and facilitate the subsequent SOA formation, because sulfate enhances both IEPOX uptake to particles (i.e., through particle surface area) and aqueous-phase reactions (i.e., through particle acidity).

Airborne measurements of power plant plumes provide an opportunity to elucidate the magnitude of sulfate influence on isoprene-OA formation. As the isoprene-OA was formed rapidly in the plumes that were sampled shortly after emission, we avoid challenges encountered in the interpretation of surface measurements, such as long-range transport and chemical aging of aerosol. For the Harllee Branch plume, we find that 1 μg sm^{-3} decrease in sulfate is associated with 0.23±0.08 μg sm^{-3} decrease in isoprene-OA (figure 5.10). The uncertainty is estimated by propagating the uncertainties of the linear correlation (26%), AMS measurement on this flight (18%), and isoprene-OA concentration from PMF analysis (13% by bootstrapping runs (Ulbrich et al., 2009)). The magnitude of the sulfate effect on isoprene-OA formation observed here is consistent with Blanchard et al. (2015), who estimated that the future decrease in sulfate concentration by 1 μg m^{-3} would reduce OA concentration by 0.2 to 0.35 μg m^{-3} (assuming OA/OC = 1.4) based on statistical analysis on 14 years of data collected at multiple sites in the southeastern United States. The magnitude in our study is also similar to Xu et al. (2015a), who reported that 1 μg m^{-3} decrease in sulfate would lead to 0.42 μg m^{-3} reduction of isoprene-OA at the ground site of the SOAS. However, it is important to note that the magnitude of sulfate on isoprene-OA reported in this study (i.e., 0.23 μg sm^{-3}) depends on the OH level. Plume OH is enhanced and reacts with IEPOX, which competes with IEPOX heterogeneous reaction.

For example, while the sulfate concentration is enhanced in the Scherer plume (though weaker than Harllee Branch), the isoprene-OA is not enhanced, which is likely due to gas phase OH oxidation of IEPOX competing with IEPOX heterogeneous reaction.

The contrast in isoprene-OA concentration evolution between Harllee Branch (representative of older, inefficient, high NO_x and SO_2 emitting coal plants) and Scherer (representative of modern, more-efficient, lower NO_x and SO_2 emitting coal plants) shows one benefit to air quality by implementing the emission control system and subsequent reducing SO_2 emission. This benefit should be considered in the perspective of the environmental impacts of electric power generation (de Gouw et al., 2014). Hidy et al. (2014) showed that sulfate concentration in the southeastern United States has reduced by ~3 μg m^{-3} (average of all SEARCH sites) in summer during the past 15 years. This sulfate reduction could cause ~0.7 μg m^{-3} reduction in OA by applying the magnitude of sulfate effect on isoprene-OA obtained from this study. Considering that OA decreases by 2.8 μg m^{-3} (average of all SEARCH sites and assuming OA/OC ratio of 1.4) (Hidy et al., 2014), ~25% of the OA reduction could arise from the sulfate control over isoprene-OA formation. However, this estimation serves as an upper bound because the IEPOX concentration is expected to be lower in the past than the present, considering that ambient NO_x levels were substantially higher in the past and likely dominated the fate of RO_2. In the future, as the NO_x concentration is expected to keep decreasing due to emission regulations (Pye et al., 2015), the formation of IEPOX would be enhanced and could potentially increase the importance of sulfate in terms of mediating isoprene-OA formation during the summer.

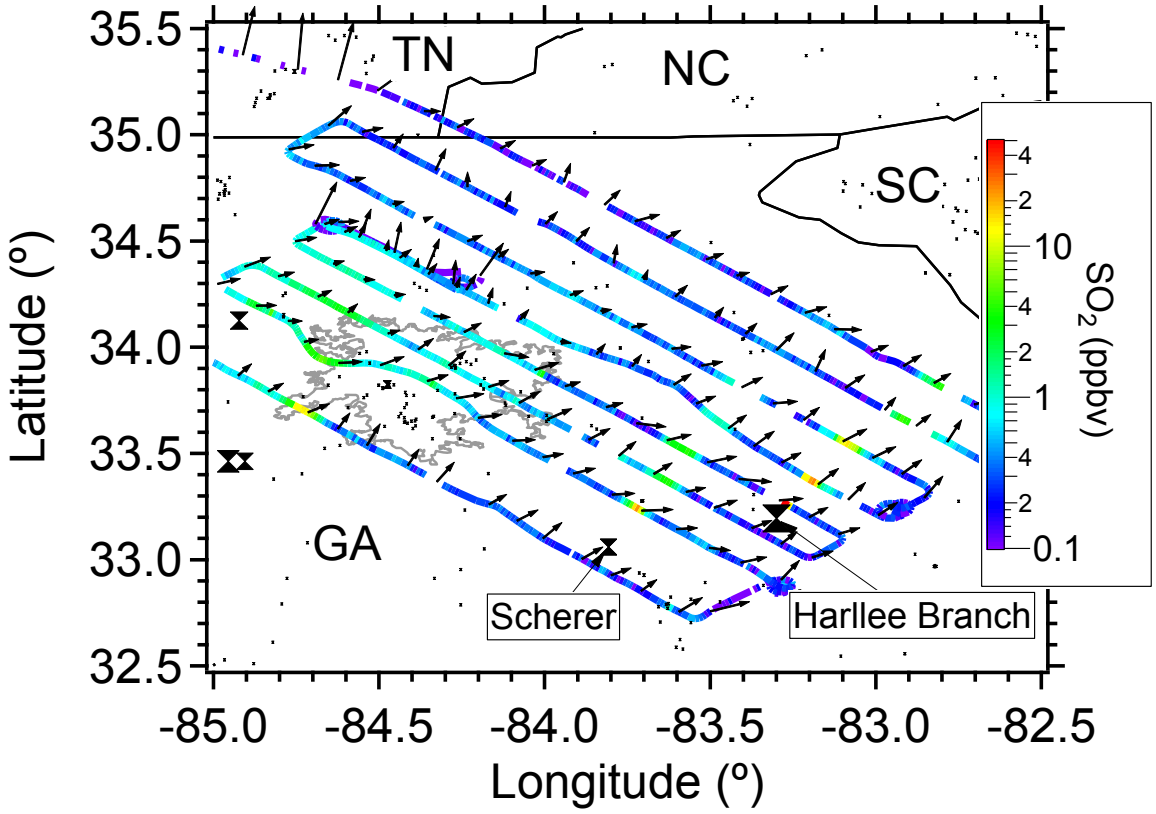

Figure 5.1. Flight track of the NOAA WP-3D aircraft presented in this study. The flight track is colored by SO_2 concentration. The direction of arrows represents wind direction and the length of arrow is proportional to wind speed. The power plants are marked in the figure and sized by its SO_2 emission. The two power plants of interest to this study, Scherer and Harllee Branch, are labelled in the figure. The gray circled region represents urban Atlanta.

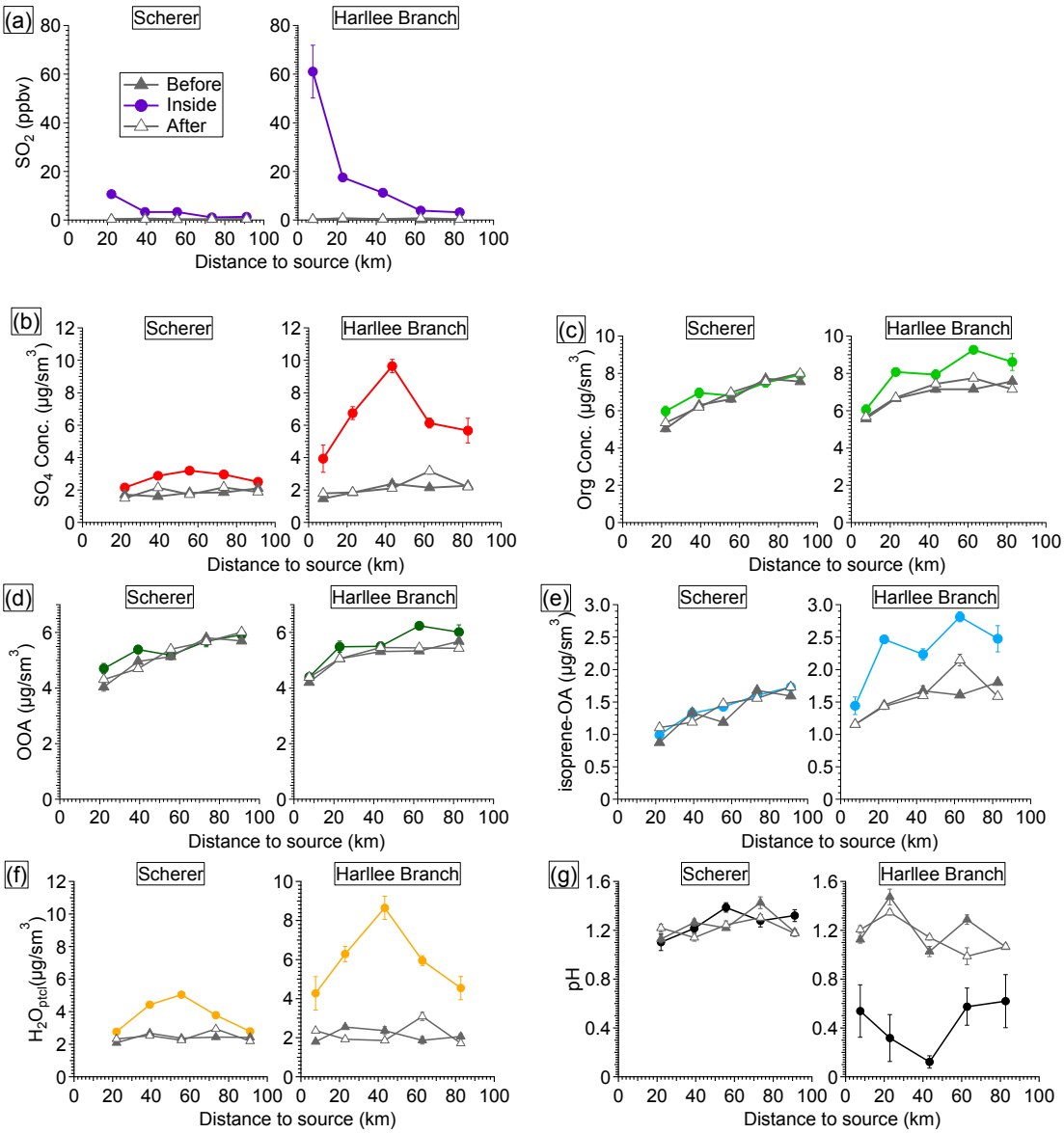

Figure 5.2. Evolution of (a) SO_2, (b) sulfate, (c) organics, (d) oxygenated organic aerosol (OOA), (e) isoprene-derived organic aerosol (isoprene-OA), (f) particle water, and (g) particle pH. The error bars represent the standard error. The error bars of some data points are smaller than the symbol size of the data points. Details about the particle water and pH calculation can be found in the supporting information. The sulfate concentration reported here is measured by AMS, which include both SO_4^{2-} and HSO_4^-. The ISORROPIA calculated concentrations of SO_4^{2-} and HSO_4^- are shown in figure S8.

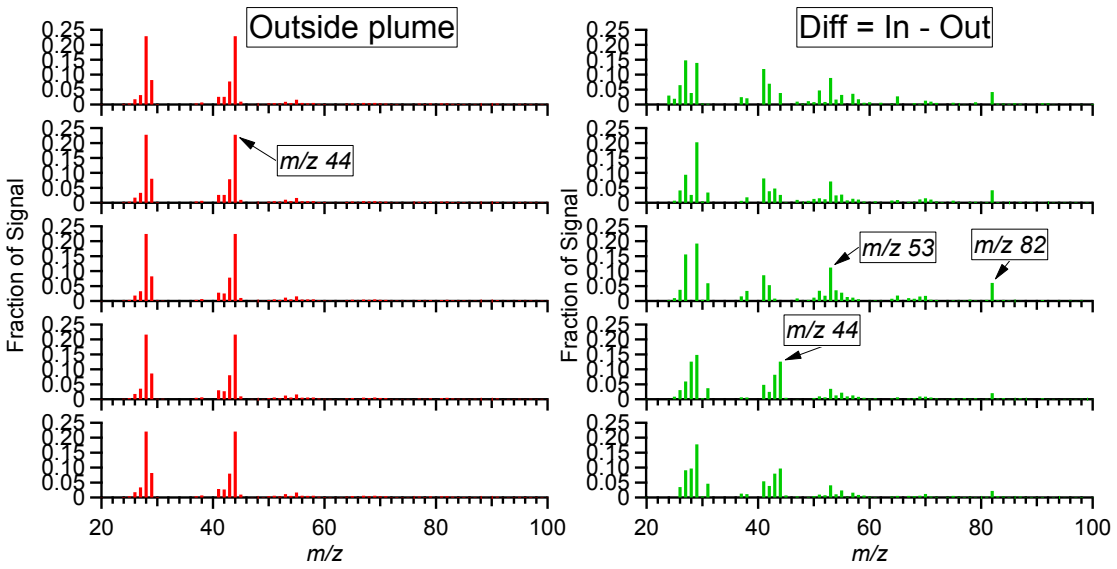

Figure 5.3. Left panels: normalized mass spectra of OA outside the Harllee Branch plume. Right panels: normalized mass spectra of OA formed inside the Harllee Branch plume, which are calculated by subtracting the OA mass spectra outside the plume from that inside the plume and then normalize the difference mass spectra to the total difference signal.

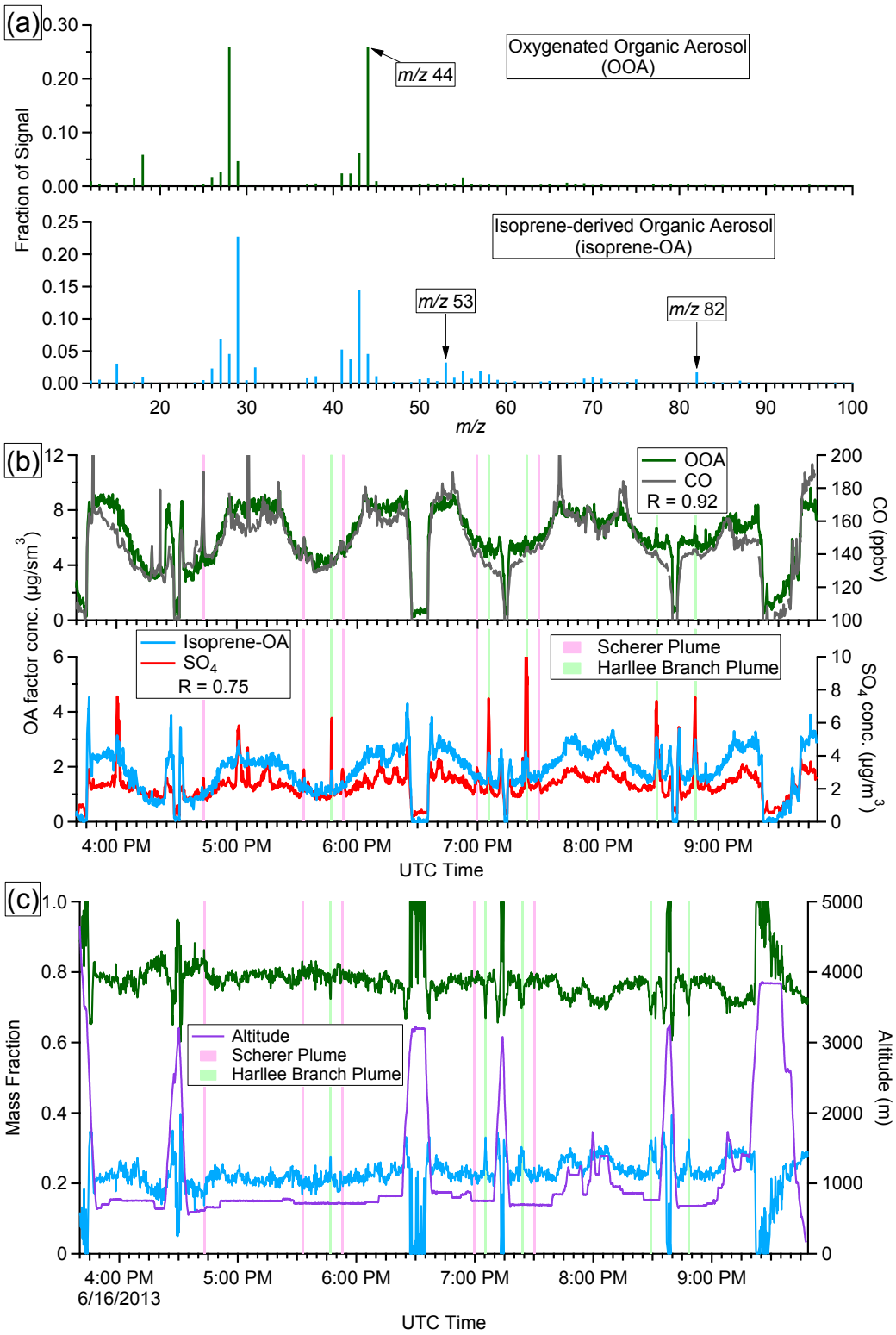

Figure 5.4. (a) Mass spectra, (b) time series, and (c) mass fractions of OA factors resolved from PMF analysis on the whole flight. The time series of corresponding external tracers are also shown in panel (b).

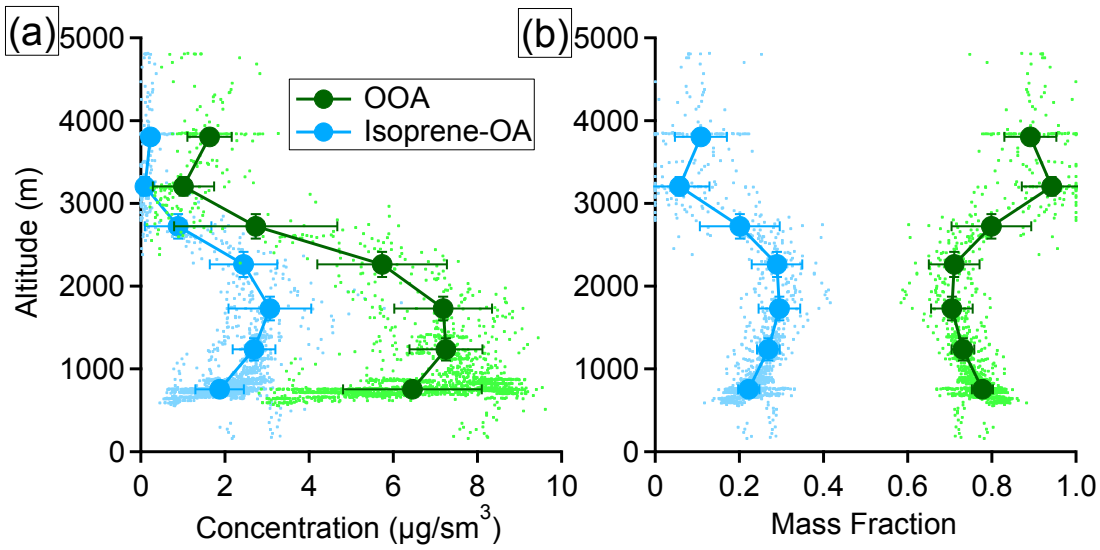

Figure 5.5. Vertical profile of (a) concentration and (b) mass fraction of OOA and isoprene-OA. The data are grouped based on 500m increment in altitude. The error bars represent one standard deviation.

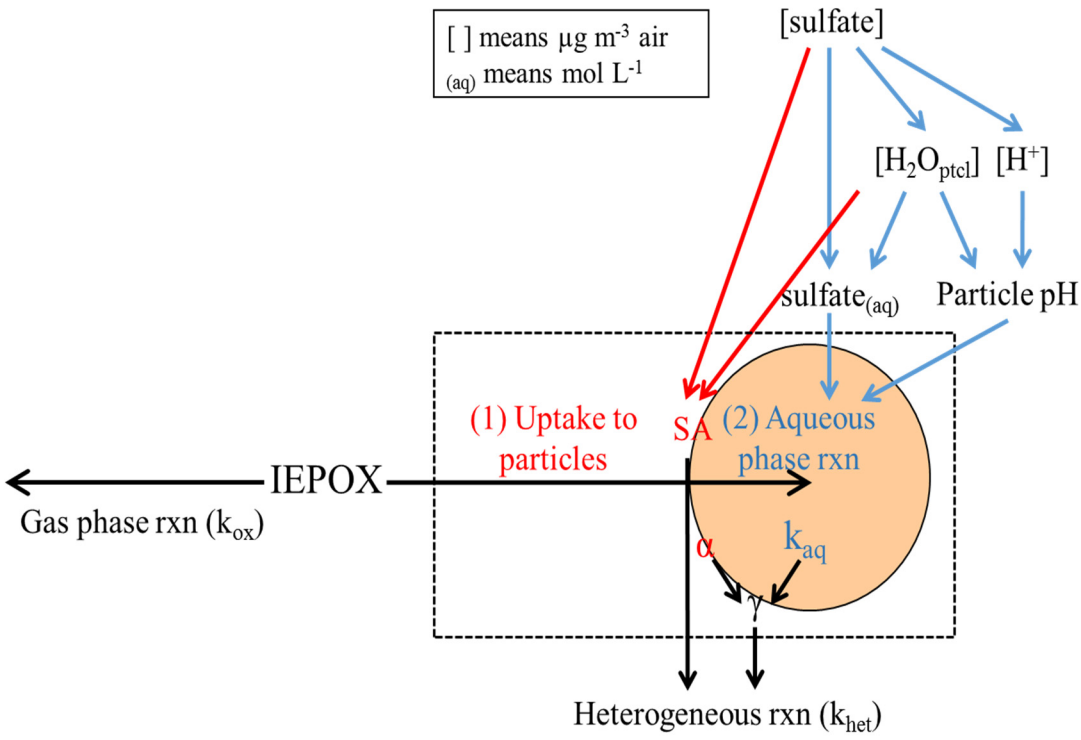

Figure 5.6. A schematic representation of the processes involved in the heterogeneous reaction of IEPOX and the effects of sulfate on the processes.

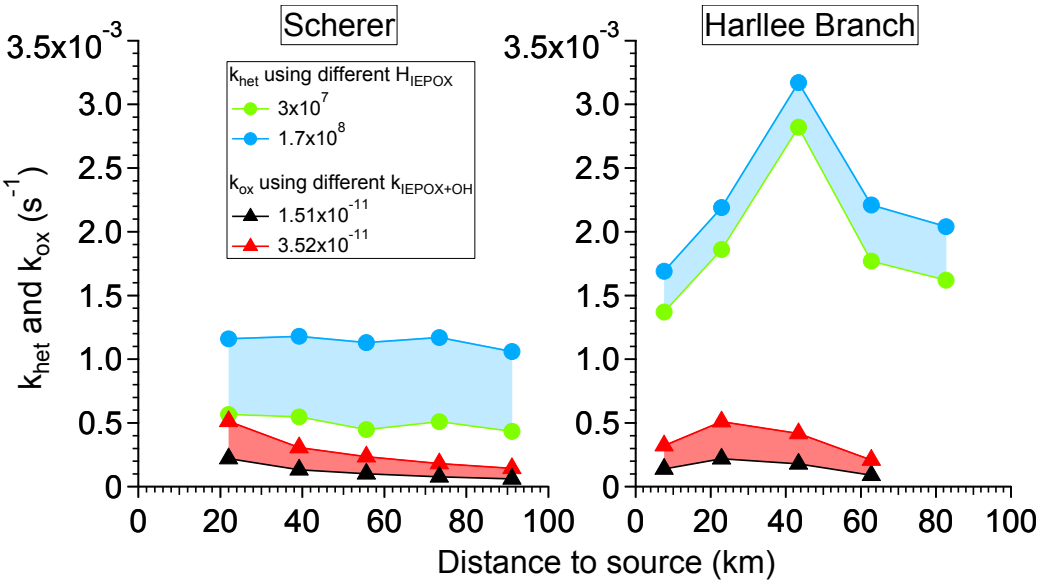

Figure 5.7. The pseudo-first-order reaction rate constants of IEPOX with respect to heterogeneous reaction and OH oxidation. Henry's law constants of IEPOX (H_{IEPOX}, in the unit of M atm^{-1}) are from Nguyen et al. (2014) and Gaston et al. (2014). The rate coefficients for the reaction of IEPOX and OH ($k_{IEPOX+OH}$, in unit of cm^3 $molecule^{-1}$ s^{-1}) are from Bates et al. (2014) and Jacobs et al (2013). The lifetime of IEPOX with respect to heterogeneous reaction and OH oxidation are shown in figure S7.

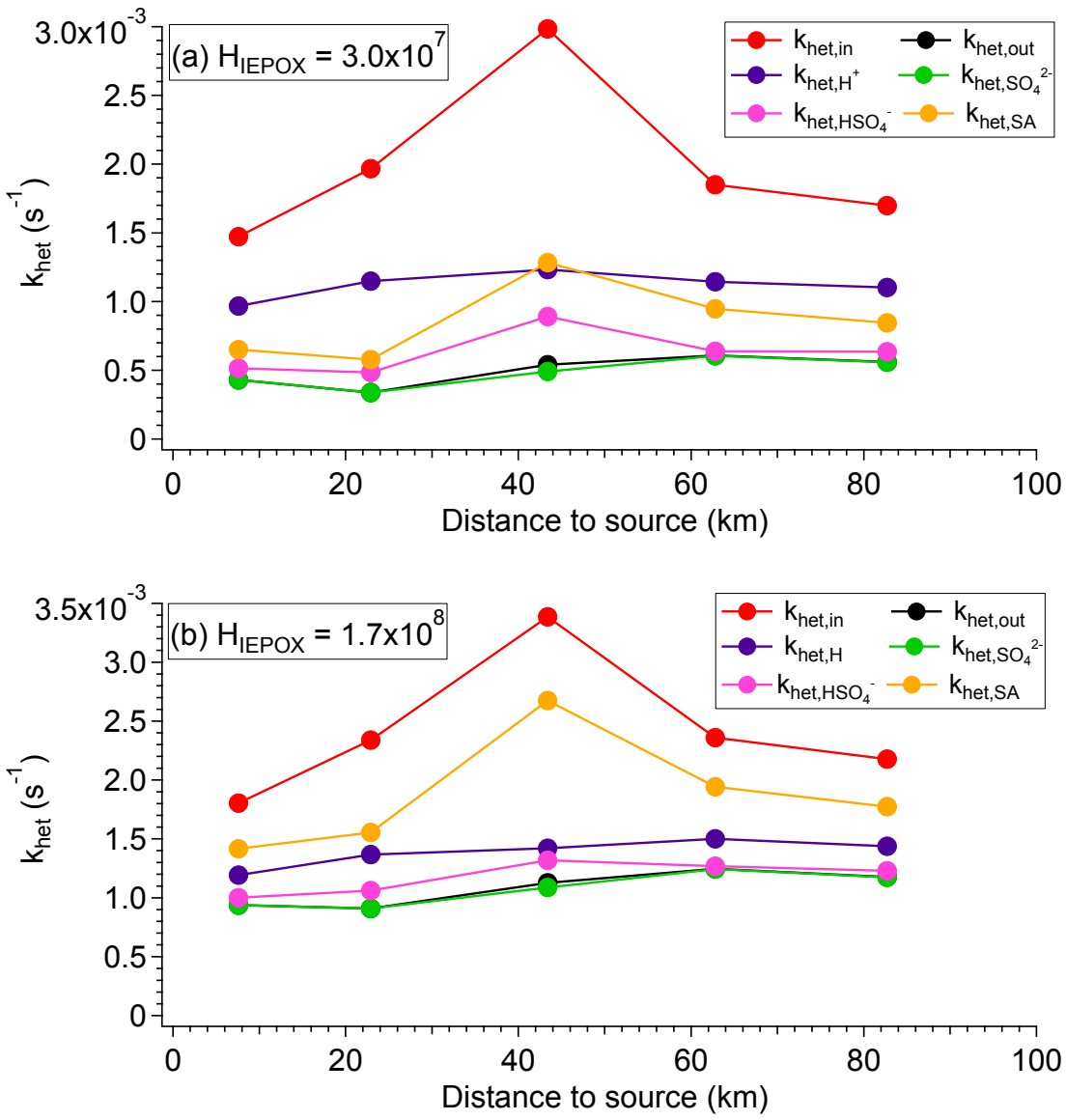

Figure 5.8. The pseudo-first-order heterogeneous reaction rate constant of IEPOX (k_{het}) inside and outside the plume. $k_{het,X}$ is calculated by using species concentrations outside the plume but only substituting the concentration of species X (X = H^+, SO_4^{2-}, HSO_4^-, and SA) with the value inside the plume. Different H_{IEPOX} values (M atm^{-1}) are used in panel (a) and (b).

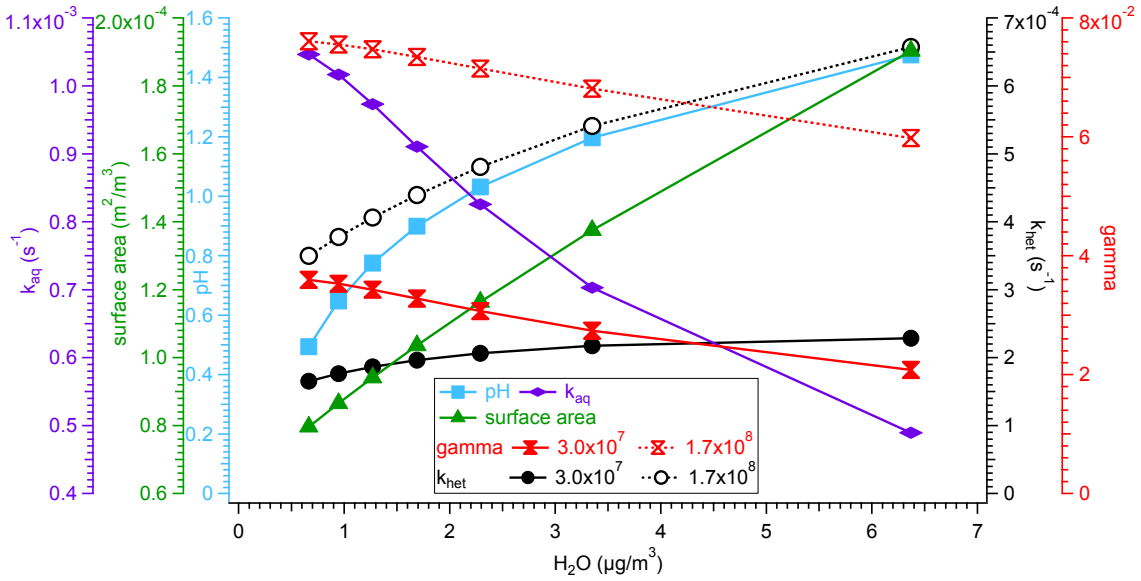

Figure 5.9. The effect of H_2O (µg/m^3) on particle pH, k_{aq}, γ, surface area, and k_{het} while holding the other covariates (sulfate and H^+) constant. Different H_{IEPOX} values (in unit of M atm^{-1}) are used.

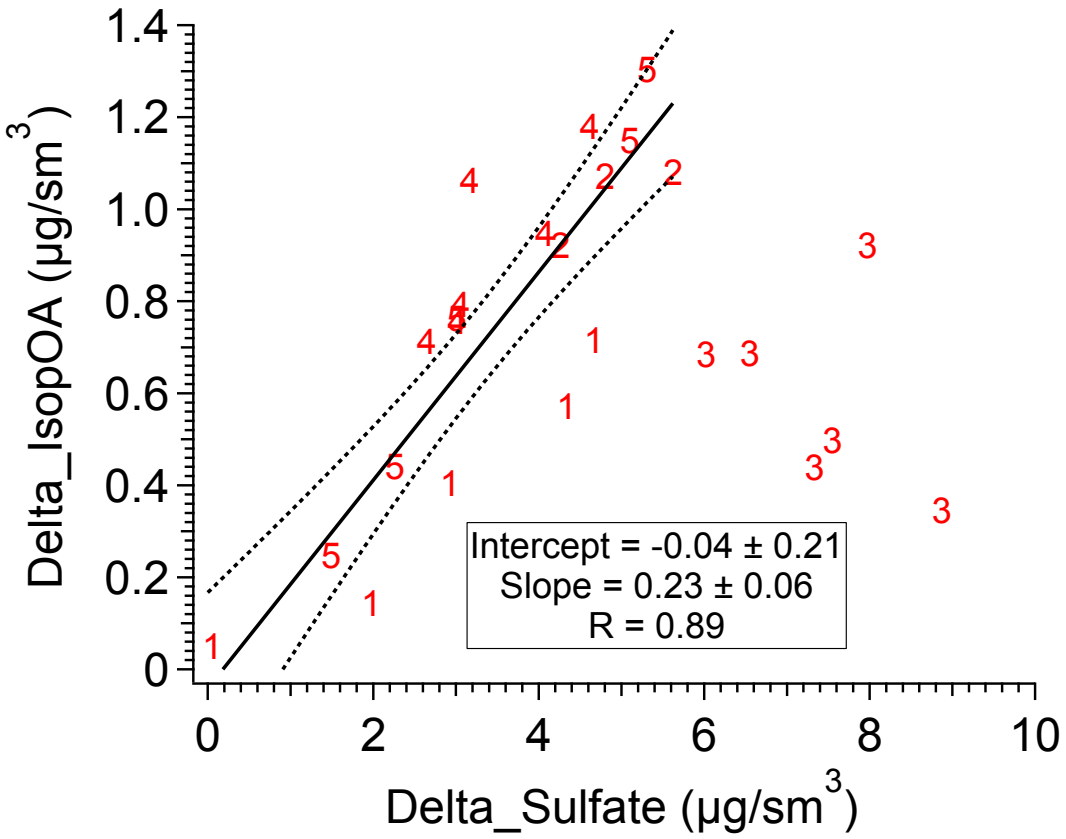

Figure 5.10. Scatter plot of the isoprene-OA enhancement (delta_isopOA) and the sulfate enhancement (delta_SO_4) in the Harllee Branch plume. The "delta" = concentration inside the plume - the average concentration of before and after the plume. The data points are labeled by the intercept number of Harllee Branch plume. The Intercept and slope are obtained by the orthogonal distance regression. The Pearson's R is from the linear least-square fitting. The dashed lines represent the 95% confidence level of orthogonal distance regression. The data from the third transect of Harllee Branch plume are not included in the fitting. The reason that the third transect of Harllee Branch plume does not follow the linear trend is not clear, but may be due to differing background IEPOX concentration compared to other transects.

CHAPTER 6: SUMMARY AND FUTURE WORKS

6.1 Summary of major findings

6.1.1 Sources and spatial distribution of OA in the southeastern US

Nearly one-year of measurements were performed across multiple sites in the southeastern US with a variety of online instruments, with the focus on HR-ToF-AMS data in this study. We find that **organics are the dominant components of the NR-PM_1 at both rural and urban sites throughout the year**. The OA diurnal profile shows little variation in summer and peaks at night in winter datasets. The lack of midday enhancement in OA diurnal profile is likely caused by the expansion of boundary layer in the day and compensating effects of various OA factors. Sulfate contributes the second highest to NR-PM_1. Sulfate concentration is higher in summer (3.0 to 4.0 μg m^{-3}) than winter (1.4 to 1.7 μg m^{-3}), probably due to stronger photochemistry in summer. In contrast to sulfate, the inorganic nitrate concentration is estimated to be three times higher in winter than summer. This is likely caused by higher NO_x levels in winter, which serves as the source for inorganic nitrates and the semi-volatile nature of inorganic nitrates, which tend to partitions into the particle phase when the temperature is low.

Positive Matrix Factorization (PMF) analysis revealed that the **organic aerosol has various sources in the southeastern US**, **which changes between seasons and sampling sites (rural vs urban).** Hydrocarbon-like organic aerosol (HOA) and cooking organic aerosol (COA), which arise from primary vehicle emissions and cooking, respectively, are important but not dominant OA sources for urban sites. Biomass burning OA (BBOA) concentration shows clear enhancements in winter compared to summer. In addition,

biomass burning is found to be an important, but not exclusive, source for brown carbon in the southeastern US. Isoprene-derived OA (Isoprene-OA), which is from the reactive uptake of isoprene epoxydiols in the presence of hydrated sulfate, only exists in warmer months (May-August) when isoprene emissions are substantial. Less-oxidized oxygenated OA (LO-OOA) and more-oxidized oxygenated OA (MO-OOA) are resolved from both rural and urban sites throughout the year. LO-OOA shows improved correlation with estimated "nitrate functionality from organic nitrates" (i.e., $NO_{3,org}$) than total nitrates. In addition, both LO-OOA and estimated $NO_{3,org}$ peaks at night, implying that LO-OOA could arise from nighttime oxidation of biogenic VOCs by nitrate radicals. Unlike isoprene, monoterpene emissions occur year-around and continue into the night. The prevalence of the LO-OOA factor at all sites year-around points to the important contribution of monoterpene SOA to the total OA budget in the southeastern US. As the most oxidized OA factor, MO-OOA reaches a daily maximum in the afternoon and likely contains aged OA from various sources, such as vehicle emission, biomass burning, and aged OA from biogenic VOCs. We find that the correlation between MO-OOA and ozone is substantially better in summer than winter, suggesting that the sources of MO-OOA might vary with season.

In order to estimate the particulate organic nitrate contribution to OA, we applied and evaluated three methods, i.e, NO_x^+ ratio method, PMF method, and AMS-IC method. Despite the uncertainty of the NO_x^+ ratio method (i.e., the values of R_{ON} and R_{AN}) and the PMF method (i.e., the separation of pure NIA factor), both methods provide reasonable results in separating the measured total nitrates into nitrate functionality from inorganic and organic nitrates. The "nitrate functionality from organic nitrates" (i.e., $NO_{3,org}$)

accounts for about 63–100% and 10-20% of total measured nitrate (i.e., $NO_{3,meas}$) in summer and winter, respectively. Further, we estimate the contribution of organic nitrates to total OA based on estimated $NO_{3,org}$ and assumed molecular weight of bulk organic nitrates. **Depending on location, season and estimation method, particulate organic nitrates account for about 5-25% of total OA**, which indicates that organic nitrates are important components in the ambient aerosol.

The spatial distribution of OA is investigated by comparing ACSM measurements (stationary at the Georgia Tech site) and HR-ToF-AMS measurements (rotating among different sites). **In summer, OA is spatially homogeneous** as suggested by the good correlation (R=0.92) in July between the GT and YRK sites, which are 70km apart. The spatial homogeneity of OA in summer is likely caused by SOA being the dominant source of OA for both urban and rural sites. The parameters such as temperature, solar radiation, and precursor VOCs, which have great influences on SOA formation, are similar between urban and rural sites. **Compared to summer, the OA is less spatially homogenous in winter**. The correlation coefficient of OA between GT and YRK decreases to 0.66 in winter. This is likely due to the elevated contribution from POA to total OA in winter and the spatially inhomogeneous distribution of POA. Meteorology also plays a role in the OA spatial distribution, but alone is unlikely to explain the observation.

We show that **short-term and extensive measurements can help interpret long-term basic measurements**. For example, consistent with long-term (1999 – 2013) OC measurements from the SEARCH network, we also observed that the seasonal variation of OA has some urban and rural contrasts. While the OA concentration is similar between summer and winter for the urban JST site, it increases by a factor of 4 from winter to

summer for the rural YRK site, according to our year-long observations. PMF analysis suggests that the different OA seasonality between urban and rural sites is likely due to the varying strength of OA sources. For rural sites, SOA represents the dominant fraction of OA in both summer and winter, but SOA concentration is much lower in winter. For urban sites, in contrast, the decrease in SOA concentration in winter is compensated by the increase in POA concentration due to less dispersion from lower boundary layer heights, leading to a relatively constant total OA concentration compared to summer. In addition, analysis of long-term OC and sulfate measurements from the SEARCH network shows that the correlation between OC and sulfate is substantially better in summer than winter, consistent with our source apportionment results that show the majority of OA is secondary in summer. The better correlation of OC and sulfate in summer also supports that sulfate directly mediates the formation of isoprene SOA, which is only present in warmer months.

6.1.2 Effects of NO_x on the volatility of secondary organic aerosol from isoprene photooxidation

Previous experiments have been performed under extreme NO_x conditions by the selective use of OH precursors to saturate the system with either NO/NO_x ("high-NO_x" condition) or HO_2 radicals ("low-NO_x" condition) (Kroll and Seinfeld, 2008). While "high-NO_x" and "low-NO_x" have traditionally been used to describe photochemical conditions, these terms may not adequately describe the complexity of the reaction pathways. Recently, Wennberg (2013) suggested that instead of characterizing reaction conditions as either high or low NO_x, one should explicitly specify the fate of RO_2 radicals. In this study, **we investigate the different roles of NO and NO_2 in SOA formation, dynamic changes**

between NO and NO_2, and competitive chemistry of RO_2 among various pathways and their effects on aerosol composition and volatility. We find that **SOA volatility is sensitive to NO_x and varies with NO_x level in a non-linear manner.** Depending on the NO_x level and reaction pathways of peroxy radicals, the SOA formed in mixed experiments could be of similar or lower volatility compared to that formed in HO_2-dominant experiments. This observation might help to reconcile the seemingly contradictory observations of the NO_x effect on isoprene SOA volatility reported in previous literature studies. While King et al. (2010) observed that isoprene SOA volatility was not affected by NO_x, Kleindienst et al. (2009) reported that isoprene SOA formed in the presence of NO_x was less volatile. It is noted that different NO_x levels were investigated in these two studies. The NO_x/isoprene ratio was maintained at 0.76 in King et al. (2010), so that RO_2+NO reaction was relatively more competitive throughout their experiment. However, in Kleindienst et al. (2009), it appears that 2-31% of isoprene was still present by the time NO had reacted completely. It is possible that difference between these two studies is a result of reactions occurring at different NO/isoprene ratios. **In addition to volatility, isoprene SOA yield and oxidation state also exhibit a non-linear dependence on NO_x levels.** Current regional and global atmospheric SOA models treat the effects of NO_x on SOA properties as a linear combination of SOA formation under two extremes ("low-NO_x" and "high-NO_x" conditions) (Presto and Donahue, 2006; Pye et al., 2010). From the time dependent growth curves, it is clear that there is a vertical section at the end of the mixed experiments, indicating the presence of different rate determining steps in SOA formation and/or the enhancement of higher-generation oxidation chemistry when RO_2 reacts through various pathways. Taken together, it is evident from the present work and previous studies

that the nonlinear effects of NO_x on SOA formation need to be included in the next generation of models in order to accurately predict the dynamics of SOA formation and composition in ambient environments where the fate of RO_2 varies considerably.

It has been argued previously that the discrepancies between laboratory and ambient SOA could arise from limited oxidation aging in laboratory experiments. This study reveals that **SOA aging in laboratory chamber studies is highly dependent on NO_x levels.** SOA formed in HO_2-dominant experiments become more oxidized and less volatile as oxidation progresses. On the contrary, the composition of SOA in mixed experiments does not change substantially over time. Therefore, NO_x effects need to be taken into account in future laboratory aging studies.

6.1.3 Effects of Anthropogenic Emissions on Aerosol Formation from Isoprene and Monoterpenes in the Southeastern United States

We present direct observational evidence on the magnitude of anthropogenic influence on biogenic SOA formation based on comprehensive ambient measurements in the southeastern United States (US). Multiple high-time-resolution mass spectrometry organic aerosol measurements were obtained during different seasons at various locations, including urban and rural sites in the greater Atlanta area and Centreville in rural Alabama. Our results provide a quantitative understanding of the roles of anthropogenic SO_2 and NO_x in ambient SOA formation. **We show that isoprene-derived SOA is directly mediated by the abundance of sulfate, instead of the particle water content and/or particle acidity as suggested by prior laboratory studies**. **Anthropogenic NO_x is shown to enhance nighttime SOA formation via nitrate radical**

oxidation of monoterpenes, resulting in the formation of condensable organic nitrates. Together, **anthropogenic sulfate and NO_x can mediate 43-70% of total measured OA (29-49% of total PM_1) in the southeastern US during summer.**

Over the past 15 years, the OC at rural SEARCH sites in the SE US declined by about 38% as calculated from the trends shown in Hidy et al. (2014). During the same period, the emission of SO_2 and NO_x have also decreased by about 65% and 52%, respectively (Hidy et al., 2014), suggesting that our proposed mechanism about anthropogenic emissions mediating biogenic SOA formation contributes in a potentially significant way to the decrease in OC. As SO_2 and NO_x emissions continue to fall, other biogenic SOA formation pathways (e.g., isoprene SOA formation in the absence of sulfate and monoterpenes SOA from ozonolysis and photooxidation) may become more important, though these pathways have relatively lower SOA yields compared to the mechanisms discussed in this study (Surratt et al., 2010). The decreasing SO_2 and NO_x emissions may not only reduce the biogenic SOA burden, but also have impacts on climate and health. For example, while SOA from IEPOX uptake in the presence of sulfate (i.e., Isoprene-OA factor) is found to have the highest hygroscopicity (tendency to absorb water vapor) of all OA components (Cerully et al., 2015), biogenic SOA formed under lower sulfate and NO_x environments could have substantially different properties than those formed in polluted environments and warrants further studies.

Although isoprene OA formation via IEPOX uptake has been reported in several field campaigns, our study performs detailed analyses of particle water, particle acidity, and sulfate, and then provides comprehensive assessment to deconvolute their individual effects on isoprene OA formation in the atmosphere (Cerully et al., 2015; Guo et al., 2015).

Our observation in Centreville and the greater Atlanta area shows that it is sulfate, instead of particle water and acidity, that controls isoprene OA formation in the SE US during summer, though the exact mechanisms of this direct sulfate effect need further investigation. The influence of these parameters can vary regionally and globally. Therefore, SOA models need to carefully consider the fate of IEPOX and the complexity of isoprene OA formation under various atmospheric conditions. Moreover, our results reveal that the direct effect of sulfate may complicate the role of particle water in the partitioning of water-soluble organics. Finally, these findings emphasize the importance of careful calculations of both particle water content and particle acidity when investigating these SOA formation processes.

6.1.4 Enhanced formation of Isoprene-derived Organic Aerosol in Sulfur-rich Power Plant Plumes during Southeast Nexus (SENEX)

Although the rapid reactive uptake of IEPOX to acidic particles has been observed in laboratory studies (Gaston et al., 2014; Surratt et al., 2010; Liu et al., 2015b), **we report, for the first time, the rapid isoprene-OA formation via the IEPOX reactive uptake based on ambient measurements.** We show that the sulfate, which is an oxidation product of SO_2 emitted from power plants, can enhance IEPOX uptake and facilitate the subsequent SOA formation, because sulfate enhances both IEPOX uptake to particles (i.e., through particle surface area) and aqueous-phase reactions (i.e., through particle acidity).

Airborne measurements of power plant plumes provide an opportunity to elucidate the magnitude of sulfate influence on isoprene-OA formation. As the isoprene-OA was formed rapidly in the plumes that were sampled shortly after emission, we avoid challenges

encountered in the interpretation of surface measurements, such as long-range transport and chemical aging of aerosol. For the Harllee Branch plume, **we find that 1 μg sm^{-3} decrease in sulfate is associated with 0.23±0.08 μg sm^{-3} decrease in isoprene-OA**. The magnitude of the sulfate effect on isoprene-OA formation observed here is consistent with Blanchard et al. (2015), who estimated that the future decrease in sulfate concentration by 1 μg m^{-3} would reduce OA concentration by 0.2 to 0.35 μg m^{-3} (assuming OA/OC = 1.4) based on statistical analysis on 14 years of data collected at multiple sites in the southeastern United States. The magnitude in our study is also similar to Xu et al. (2015a), who reported that 1 μg m^{-3} decrease in sulfate would lead to 0.42 μg m^{-3} reduction of isoprene-OA at the ground site of the SOAS. However, it is important to note that the magnitude of sulfate on isoprene-OA reported in this study (i.e., 0.23 μg sm^{-3}) depends on the OH level. Plume OH is enhanced and reacts with IEPOX, which competes with IEPOX heterogeneous reaction. For example, while the sulfate concentration is enhanced in the Scherer plume (though weaker than Harllee Branch), the isoprene-OA is not enhanced, which is likely due to gas phase OH oxidation of IEPOX competing with IEPOX heterogeneous reaction.

The contrast in isoprene-OA concentration evolution between Harllee Branch (representative of older, inefficient, high NO_x and SO_2 emitting coal plants) and Scherer (representative of modern, more-efficient, lower NO_x and SO_2 emitting coal plants) shows one benefit to air quality by implementing the emission control system and subsequent reducing SO_2 emission. This benefit should be considered in the perspective of the environmental impacts of electric power generation (de Gouw et al., 2014). Hidy et al. (2014) showed that sulfate concentration in the southeastern United States has reduced by

~3 μg m^{-3} (average of all SEARCH sites) in summer during the past 15 years. This sulfate reduction could cause ~0.7 μg m^{-3} reduction in OA by applying the magnitude of sulfate effect on isoprene-OA obtained from this study. Considering that OA decreases by 2.8 μg m^{-3} (average of all SEARCH sites and assuming OA/OC ratio of 1.4) (Hidy et al., 2014), ~25% of the OA reduction could arise from the sulfate control over isoprene-OA formation. However, this estimation serves as an upper bound because the IEPOX concentration is expected to be lower in the past than the present, considering that ambient NO_x levels were substantially higher in the past and likely dominated the fate of RO_2. In the future, as the NO_x concentration is expected to keep decreasing due to emission regulations (Pye et al., 2015), the formation of IEPOX would be enhanced and could potentially increase the importance of sulfate in terms of mediating isoprene-OA formation during the summer.

6.2 Recommendations for future work

The scientific findings in this dissertation greatly improves our understanding of the sources and formation mechanisms of OA. However, several questions emerging from this study warrant future studies. Some recommendations for future work are summarized below.

1. MO-OOA is identified in both rural and urban sites throughout the year and it contributes 24-49% of total OA mass. Despite the ubiquitous and large abundance of MO-OOA, its sources are largely unknown. Possible sources of this factor have been proposed in the literature, but better understandings are required in order to further reduce the OA burden.

2. The identification of an Isoprene-OA factor at urban sites in the current study has interesting implications. The compound IEPOX is thought to be an oxidation product of

isoprene where the RO_2 react with HO_2 under low NO_x conditions. In urban areas, one would expect the majority of organic peroxy radicals to react with NO_x, considering the relatively high NO_x level (~15.4 ppb for JST_May). Thus, the sources of isoprene-OA in urban areas are unclear and warrants further studies.

3. Brown carbon can absorb light and cause warming effects in the atmosphere. We observed a large abundance of brown carbon in July in Yorkville, GA, but the brown carbon sources are unclear.

4. The nonlinear effects of NO_x on SOA formation need to be included in the SOA models in order to accurately predict the dynamics of SOA formation and composition in ambient environments where the fate of RO_2 varies considerably.

5. The parameter values in the IEPOX heterogeneous reaction parameterization are uncertain (such as α, H_{IEPOX}, and $k_{i,j}$'s), which highly limits quantitative understanding of the role of each factor in isoprene-OA formation. Further fundamental laboratory studies are needed to constrain these parameters and improve predictions of isoprene-OA.

6. As the anthropogenic emissions of SO_2 and NO_x keep decreasing, how the influence of anthropogenic emissions on biogenic SOA will change in the future?

APPENDIX A: WINTERTIME AEROSOL CHEMICAL COMPOSITION, VOLATILITY, AND SPATIAL VARIABILITY IN THE GREATER LONDON AREA

A.1 Background

Particulate matter (PM) concentration in the greater London area often exceeds European air quality limits, causing adverse effects on the health of habitants in this area (Harrison et al., 2012; Bohnenstengel et al., 2014). Therefore, it is critical to identify the PM sources in order to implement effective strategies to control ambient pollutants. The Clean Air for London (ClearfLo) project aimed to study boundary layer pollution in the greater London area through comprehensive measurements of meteorology, gaseous and particulate composition (Bohnenstengel et al., 2014). Multiple monitoring sites were set up in both urban and rural areas around London to quantify the urban increment in gas-phase and particle-phase pollutants.

Previous studies in the greater London area have repeatedly shown that the concentration of elemental carbon (EC) is higher in urban sites than rural sites due to elevated levels of primary emissions such as vehicle exhaust and wood smoke (Crilley et al., 2015; Yin et al., 2015). The origin of organic carbon (OC) at urban and rural sites is instead more challenging to elucidate considering the myriad of different OC sources. Based on the ratios among multiple tracers (e.g., EC/OC and levoglucosan/OC) from different sources, Crilley et al. (2015) estimated that the concentration of primary OC from vehicle emissions was higher in an urban area compared to a rural area in the UK. Many studies have applied the Chemical Mass Balance (CMB) model for OC apportionment (Yin

et al., 2010; Crilley et al., 2015; Yin et al., 2015). However, due to the uncertainties in the source profiles and the number of organic tracers included in the model, the concentration of secondary OC is highly uncertain. In addition, OC measurements based on filter samples on a daily basis limit the temporal resolution of rural vs. urban comparisons.

Factor analysis via Positive Matrix factorization (PMF) of aerosol mass spectrometer (AMS) measurements is another widely used method to identify sources of organic aerosol (OA) (Jimenez et al., 2009; Lanz et al., 2007; Ng et al., 2010; Xu et al., 2015a). Based on factor analysis of AMS measurements around the world, Zhang et al. (2007) observed that the contribution of hydrocarbon-like OA (a surrogate for primary OA) to total OA decreased from urban sites to rural sites, but the oxygenated OA (a surrogate for secondary OA), showed the opposite trend. The authors also showed that the average OA concentration is substantially lower in rural sites than urban sites (2.8 vs. 7.6 $\mu g\ m^{-3}$). However, the trend observed in Zhang et al. (2007) needs to be further verified since the urban vs. rural comparisons are not based on simultaneous measurements between paired locations.

Comparison based on simultaneous measurements between different sites, especially between rural and urban sites, is useful to identify regional and local sources of OA. For example, by comparing concurrent AMS measurements of OA at multiple sites in the greater Atlanta area, USA, Xu et al. (2015b) showed that the OA was spatially homogeneous and mainly regional in summer, but the OA showed substantial spatial variability in winter. Based on PMF analysis of AMS measurements, Crippa et al. (2013) investigated the correlation of various OA subtypes between three urban sites located in a 20km-radius region in Paris, France during winter 2010. The authors observed that the

secondary OA factor had substantially better correlation between different sites than the primary OA factors, including OA from vehicle, biomass burning, and cooking. However, a rural vs. urban comparison was not performed in Crippa et al. (2013).

In addition to OA sources, the volatility of OA is an important property since it directly determines the gas/particle partitioning. The thermal denuder (TD) has been used widely to measure the aerosol volatility (An et al., 2007; Huffman et al., 2008; Saleh et al., 2012). Many previous studies inferred the volatility from the mass fraction remaining (MFR) or volume fraction remaining (VFR), which is calculated as the ratio of the species mass (or volume) concentration after heating to an elevated temperature in the TD to the species mass (or volume) concentration without heating (An et al., 2007; Huffman et al., 2009b; Jonsson et al., 2007; Lee et al., 2011; Stanier et al., 2007; Grieshop et al., 2009b; Xu et al., 2014; Huffman et al., 2009a). Larger MFR is used as an indication for lower volatility of aerosol. However, Saleh et al. (2011) suggested that it is misleading to use MFR as an indication of volatility. This is mainly because the MFR is an extensive parameter (which explicitly depends on the initial mass concentration) while aerosol volatility is an intensive property (which depends only on chemical nature of the compounds in a mixture). Instead of MFR, Saleh et al. (2011) presented that that change in mass concentration when reaching equilibrium upon heating (i.e., ΔC) is an appropriate measure of volatility.

Although multiple previous studies have investigated the volatility of laboratory-generated OA (An et al., 2007; Huffman et al., 2009b; Jonsson et al., 2007; Lee et al., 2011; Stanier et al., 2007; Grieshop et al., 2009b; Xu et al., 2014), there are only limited studies on the volatility of ambient OA, especially on the volatility of OA from different sources

(Hildebrandt et al., 2010; Huffman et al., 2009a; Massoli et al., 2015; Paciga et al., 2015). Previous studies have showed the presence of non-volatile organics in the ambient aerosol even after heating to high temperatures (i.e., 230 - 300°C) (Huffman et al., 2009a; Häkkinen et al., 2012; Poulain et al., 2014; Massoli et al., 2015; Liu et al., 2015a). However, the sources of non-volatile organics are uncertain. Häkkinen et al. (2012) and Poulain et al. (2014) found that the non-volatile residuals correlated with anthropogenic tracers, such as BC and polycyclic aromatic hydrocarbons (PAHs), implying that the non-volatile species are possibly linked to anthropogenic emissions. However, in both studies, the thermal-denuder (TD) was only applied upstream of a scanning mobility particle sizer (SMPS); therefore the composition of remaining compounds was not directly measured but only conjectured. Massoli et al. (2015) coupled a TD with a soot-particle AMS (SP-AMS) during measurements in California. The authors observed the existence of refractory OA (i.e., detectable via laser vaporization in the SP-AMS, but not detectable by vaporization at 600°C in the standard AMS), which was present in the fresh urban air masses, but not in the aged air masses.

Many studies have used the degree of oxidation of OA, such as atomic O:C ratio and oxidation state (OS) as a proxy for volatility. For example, two oxygenated OA factors with high but different O:C ratio are often resolved from PMF analysis on AMS data. These two oxygenated OA factors are often named semi-volatile OOA (SVOOA) and low-volatility OOA (LVOOA) based on the volatility inferred from O:C values (Ng et al., 2010; Huang et al., 2010; Mohr et al., 2012; Jimenez et al., 2009). In a laboratory study on toluene SOA, Hildebrandt Ruiz et al. (2014) observed a linear relationship between OS and effective saturation concentration of the aerosol. However, for both ambient measurements

and laboratory studies, it is uncertain whether the O:C or OS of bulk OA is a good indicator of volatility. In Mexico City and Riverside, CA, Huffman et al. (2009a) showed that the O:C ratio of the thermally-denuded OA increased with TD heating temperature, which suggests that the O:C is inversely correlated with the volatility of organic aerosol (i.e., the residual OA with lower volatility after heating has a higher O:C). In contrast, only a weak correlation between O:C and volatility was observed in Hildebrandt et al. (2010), who measured the volatility of ambient OA in Finokalia, Greece. The authors found that between thermally-denuded OA and ambient OA, the mass spectrum was similar and the difference in f_{44} (i.e., fraction of organic signal at *m/z* 44, which has a linear correlation with O:C) was not statistically significant. This indicates that the degree of oxidation does not change after evaporation of relatively volatile species. In addition, various relationships between O:C and volatility (inferred from the MFR) have been observed in previous laboratory studies on different SOA systems (Grieshop et al., 2009b; Qi et al., 2010; Donahue et al., 2012; Kroll et al., 2009; Tritscher et al., 2011; Xu et al., 2014). For example, Xu et al. (2014) observed that while the O:C of isoprene SOA formed in the laboratory without additional NO remained fairly constant (~0.6) during photochemical aging, the VFR increased over time. Grieshop et al. (2009b) showed that during photochemical aging, OA from wood fires became more oxidized (i.e., O:C increases), but the MFR remained constant. Donahue et al. (2012) studied the photochemical aging of α-pinene ozonolysis SOA and observed that while the OA became more oxidized (i.e., O:C increases), the VFR decreased with aging. The authors proposed that the photochemical aging produced both relatively volatile products and more oxidized products, which broadened the volatility distribution of the OA (Donahue et al., 2012). In summary, while SOA becomes

progressively more oxidized (i.e., O:C increases) during aging, the MFR or VFR exhibits different trends (i.e., increases, stays constant, or decreases over time) for different SOA systems.

In this study, we performed simultaneous measurements at a rural site (Detling, Kent) and an urban site (North Kensington, London) in the greater London area in winter 2012 using two Aerodyne high resolution time-of-flight mass spectrometers (HR-ToF-AMS) (DeCarlo et al., 2006). The comparison of the simultaneous, high temporal resolution measurements and the OA source apportionment by PMF analysis provide insights into sources of wintertime OA in the greater London area. Since biogenic emissions are low in winter, these measurements allow a more direct evaluation of the contributions of anthropogenic emissions to OA formation. We also deployed a thermal denuder upstream of a suite of instruments to directly characterize the non-volatile residual at 250°C. Furthermore, we investigated the volatility of different OA sources and systematically evaluated the relationship between O:C and OA volatility.

A.2 Method

A.2.1 Sampling sites and meteorological conditions

Measurements were performed as part of the Clean Air for London (ClearfLo) project. An overview of the ClearfLo field campaign can be found in Bohnenstengel et al. (2014). The main goal of the ClearfLo project was to study boundary layer pollution in the greater London area by comprehensive measurements of meteorology, gaseous- and particulate composition. Multiple monitoring sites were set up in both urban and rural areas and at different elevations (street and elevated level) to perform year-long measurements

across London. In addition, two intensive observation periods (IOPs) were conducted during winter (January-February, 2012) and summer (July-August, 2012). Data presented in this paper were collected at the Detling site and the North Kensington (NK) site during the winter IOP. Figure A.1 shows the locations of both sites. The NK site (51.521055°N, 0.213432°W) is an urban background site located in a residential area, 7 km to the west of central London. The Detling site (51.301931°N, 0.589494°E) is a rural site located on a plateau (200 m a.s.l.), 45 km southeast of London. The closest road is about 150m (south), which carries ~42,000 vehicles per day (www.dft.gov.uk/traffic-counts). The typical meteorological data (temperature, relative humidity, and wind speed) at the Detling site are shown in Fig. S1a. The campaign-average temperature was 6°C. In the diurnal variation, the highest temperature was ~8°C at 14:00 and the lowest temperature was ~5°C at 07:00. The relative humidity was 83% on average. The wind speed was 5.8 m s^{-1} on average, but it reached 10 m s^{-1} occasionally. The wind rose plot is shown in Fig. S1b. The prevailing wind was from the northeast and the southwest.

A.2.2 Instrumentation

In the following discussions on instrumental setup and data analysis methods, we will focus on the rural Detling site. For instruments deployed at the urban NK site, only the high-resolution time-of-flight aerosol mass spectrometer (HR-ToF-AMS, Aerodyne) ambient measurements are included in this study. The data analysis of HR-ToF-AMS at the urban site is similar to that at the rural site, which will be discussed below. Details regarding the measurements at the NK site can be found in Young et al. (2015a).

A suite of instruments was deployed at the Detling site to characterize both the gas-phase and particle-phase composition. Instruments of interest to this study are shown in Fig. S2 and are described below. Ambient particles were sampled through a $PM_{2.5}$ cyclone and then directed through either a thermal denuder (denoted as TD line) or bypass line (denoted as bypass line) before being analyzed by downstream instruments. The thermal denuder (TD, Aerodyne), designed based on Huffman et al. (2008), consists of a 22" long stainless steel tube operated at elevated temperatures (i.e., heated section), followed by a 24" section of activated charcoal held at room temperature to adsorb the evaporated components from particles. The heating section was operated at 120 and 250°C. The aerosol residence time in the heating section of the TD was 5.3 s at the experimental flowrate rate (2.3 LPM determined by the sampling rate of instruments downstream of the TD). Caution is required when comparing the results between different studies with a TD because the TD configuration and residence times can be different. Particle loss in the TD was characterized based on the single particle soot photometer (SP2) refractory black carbon (rBC) mass measurement during the field campaign, since rBC does not evaporate even at 250°C. The transmission efficiency of TD is about 90% (Fig. S3), similar to the values reported in previous studies with similar TD configurations (Huffman et al., 2008; Massoli et al., 2015). The time scale to reach thermodynamic equilibrium in a given TD depends on a number of factors, such as TD temperature, aerosol mass concentration, aerosol diameter, and mass accommodation coefficient (Riipinen et al., 2010; An et al., 2007; Saleh et al., 2011). In this study, we calculate the characteristic time for aerosol equilibration by following the algorithm in Saleh et al. (2011). To evaluate the equilibration time scale in the TD, the authors started with the mass transfer equation (Eq. A.1) and then

obtained the characteristic time for aerosol equilibration (τ in Eq. A.2) by performing dimensional analysis.

$$\frac{dC_a}{dt} = -2\pi d_p DFN_{tot}(KC_{g,sat} - C_g) \quad \text{Eq. A.1}$$

$$\tau = \frac{1}{2\pi d_p DFN_{tot}} \quad \text{Eq. A.2}$$

$$F = \frac{1+Kn}{1+0.3773Kn+1.33Kn(1+Kn)/\partial} \quad \text{Eq. A.3}$$

In the equations, C_a, C_g, and $C_{g,sat}$ are the aerosol phase concentration, gas phase concentration, and gas phase saturation concentration, respectively. N_{tot} is the total number concentration, d_p is the particle size, D is the diffusion coefficient in the gas phase, K is the Kelvin effect correction, and F is the Fuchs-Sutugin correction, which is calculated by Eq. A.3. In Eq. A.3, Kn is the Knudsen number and α is the accommodation coefficient. D is on the order of 10^{-5} m^2 s^{-1} according to Tang et al. (2015) and α is on the order of 0.1 as shown in Saleh et al. (2012). By using the campaign-average particle number concentration (i.e., 4.28×10^3 cm^{-3}) and the mode of the particle number distribution (i.e., 87nm) in our study, we estimate that the characteristic equilibration time is about 1600s, which is orders of magnitude longer than that residence time (5s) in the TD. Since the evaporation process is likely far away from equilibrium, the gas phase saturation ratio is small and the particles are likely evaporating in a vapor-free environment. Under this assumption, the gas phase vapor concentration (i.e., C_g) in the mass transfer equation (Eq. A.1) can be neglected. After integration over the residence time in the TD, the change in mass concentration upon heating (ΔC_a) can be calculated by Eq. A.4, in which $t_{residence}$ is the residence time in TD

and the $\overline{C^*}$ is the evaporation-time-averaged saturation concentration. Thus, the ΔC_a for each component is proportional to its $\overline{C^*}$ because the other parameters are the same assuming the compounds are internally mixed.

$$\Delta C_a = C_{t=0} - C_{t_{residence}} = \int_0^{t_{residence}} \frac{KC_{g,sat}}{\tau} dt = \frac{t_{residence}}{\tau} K\overline{C^*} \qquad \text{Eq. A.4}$$

A high-resolution time-of-flight aerosol mass spectrometer (HR-ToF-AMS, Aerodyne), a soot-particle aerosol mass spectrometer (SP-AMS, Aerodyne), a single particle soot photometer (SP2, DMT), and a scanning mobility particle sizer (SMPS, TSI) were placed downstream of the TD. These four instruments alternated between sampling the bypass line (i.e., ambient) and the TD line (i.e., thermally-denuded) every 10 min. When the instruments were sampling through the bypass line, the heating section of TD was adjusted to the subsequent temperature setpoint. The MFR was determined by comparing the measurements between bypass line and TD line.

The HR-ToF-AMS provides real-time measurements of the chemical composition and size distribution of submicron non-refractory species (NR-PM_1) and has been described in detail previously (Canagaratna et al., 2007; DeCarlo et al., 2006). In brief, the HR-ToF-AMS samples particles through an aerodynamic lens and then impacts the focused particle beam on a heated tungsten surface (~600°C). The resultant vapors are ionized by electron impact ionization and the ions are analyzed using time-of-flight mass spectrometry. We used the ambient gas-phase CO_2 concentration (measured by a LI-COR CO_2 gas analyzer with 1 min resolution) to correct for the gas-phase interference in the particle-phase CO_2^+ signals for both the bypass line and TD line. The assumption behind

this correction for the TD line is that the CO_2 generated in the TD, if it exists, is negligible. Unless otherwise specified, the elemental ratios, such as atomic O:C and H:C, were calculated based on the latest recommendation by Canagaratna et al. (2015), who modified the original method developed for the HR-ToF-AMS (Aiken et al., 2007; Aiken et al., 2008). The HR-ToF-AMS data were analyzed using the standard AMS analysis toolkits SQUIRREL v1.56A and PIKA v1.15.

The SP-AMS measures the chemical composition of rBC containing particles by using an intracavity laser vaporizer (1064 nm). The detailed working principles of SP-AMS are extensively discussed in Onasch et al. (2012). In brief, after being focused through an aerodynamic lens, the rBC-containing particles are heated and vaporized by laser absorption. The chemical composition of both the rBC and any associated coatings are analyzed via high-resolution mass spectrometry. The SP-AMS data presented in this paper were obtained between 5 and 15 February, 2012, when the instrument was operated in the laser vaporizer only configuration, that is, only rBC-associated species were detected. Analysis and interpretation of the SP-AMS measurements for the entire deployment at Detling are presented in Williams et al. (2015).

The single particle soot photometer (SP2) measures rBC using laser-induced incandescence. The method has been described previously (Schwarz et al., 2006; Stephens et al., 2003). In brief, a 1064 nm Nd:YAG laser irradiates the particles as they enter the SP2, where upon vaporization and incandescence is induced in the particles containing rBC. The incandescence signal is proportional to the mass of rBC per particle, and with the sampling volume, rBC mass concentrations are quantified. The SP2 at the Detling site was calibrated using fullerene soot (Alfa Aesar, Inc., Ward Hill, Massachusetts; Stock# 40971,

Lot# L18U002). Fullerene soot is an rBC surrogate used for calibration of the SP2 due to its known density and similarities to ambient rBC (Baumgardner et al., 2012; Laborde et al., 2012). Data analysis was performed with the Paul Scherrer Institut Toolkit (PSI, Martin Gysel) developed for SP2 analysis within Igor Pro (Wavemetrics, Inc.).

A.2.3 Collection efficiency of the HR-ToF-AMS

In order to provide quantitative data from HR-ToF-AMS measurements, the particle collection efficiency (CE), which is largely due to particles bouncing on the vaporizer, needs to be evaluated. For the bypass line, we calculated the CE based on the composition-dependent algorithm proposed by Middlebrook et al. (2012) (i.e., CDCE). The CDCE for the bypass line ranges from 0.45 to 0.97, with the campaign-averaged value 0.52 ± 0.08 (one standard deviation). In order to validate the application of CDCE, we converted the mass concentrations of ambient non-refractory species measured by HR-ToF-AMS (after CDCE correction) together with the mass concentration of refractory species (i.e., rBC and crustal material) to volume using Eq. A.5 and then compared the calculated volume with SMPS measurements.

$$\text{volume} = \frac{[NO_3^-]+[SO_4^{2-}]+[NH_4^+]}{1.75} + \frac{[Cl^-]}{1.52} + \frac{[org]}{\rho_{org}} + \frac{[\text{crustal material}]}{2.7} + \frac{[BC]}{0.73} \quad \text{Eq. A.5}$$

In Eq. A.5, 1.75 g cm^{-3} was used as the density for inorganic nitrate, sulfate, and ammonium, and 1.52 g cm^{-3} was used as the density for chloride (Poulain et al., 2014). The density of ambient organics was estimated using atomic O:C and H:C ratios as suggested by Kuwata et al. (2012). It is noted that the O:C and H:C ratios calculated based on Aiken et al. (2008) were used in the density estimation in order to be consistent with Kuwata et al. (2012). The organic density was estimated to be 1.30, 1.42 and 1.68 g cm^{-3} for bypass

line, TD = 120°C and TD = 250°C, respectively. The estimated density values were within the literature range (Hallquist et al., 2009). The concentration of crustal material was estimated by summing the normal oxides (Na_2O, MgO, Al_2O_3, SiO_2, CaO, K_2O, FeO, Fe_2O_3, and TiO_2) of tracer elements (Malm et al., 1994). The tracer elements were measured by $PM_{1.0\text{-}0.3}$ rotating drum impactors and analyzed by synchrotron radiation-induced X-ray fluorescence spectrometry (Visser et al., 2015b). The density of crustal material (2.7 g cm^{-3}) was adapted from Lide (1991). The rBC concentration was measured by the SP2. For the rBC density, many previous studies have used 1.77 g cm^{-3} (Salcedo et al., 2006; Poulain et al., 2014; Huffman et al., 2009a). However, we note that 1.77 g cm^{-3} (adapted from Park et al. (2004)) is the inherent material density of diesel soot particles. If the inherent material density is used, one needs to consider the non-sphericity of rBC when comparing the calculated volume to the SMPS volume as the particles are assumed to be spherical when estimating the SMPS volume. In order to circumvent this issue, we used an effective density of rBC in this study. Park et al. (2003) measured the effective density of diesel soot particles in the 50-300nm range (mobility diameter) by using a Differential Mobility Analyzer - Aerosol Particle Mass analyzer (DMA - APM) system. The soot particles were firstly classified based on mobility diameter in DMA and the mass of classified particles was then measured by APM. The effective density was calculated with the following equation by assuming spherical particles:

$$\rho_{eff} = \frac{mass}{\frac{\pi}{6} d_{me}^{3}} \qquad \text{Eq. A.6}$$

where d_{me} is the mobility equivalent diameter. Thus, applying the effective density measured by a DMA-APM system allows one to convert BC mass to its apparent volume,

which is comparable to the SMPS volume. One factor that complicates the choice of rBC effective density is that this value decreases with increasing mobility diameter as shown in Park et al. (2003). Limited by the lack of knowledge of the size distribution (mobility diameter based) of rBC in our data, we calculated the average effective density based on all the values reported in Park et al. (2003) and used this average value (0.73 g cm^{-3}) in our study. This simplification is reasonable considering the following reasons. Firstly, Crilley et al. (2015) estimated that 70% of rBC at the Detling site is from traffic, which is similar to the BC types in Park et al. (2003). Secondly, the size distribution of total particles measured by SMPS in our study largely overlapped the size range studied in Park et al. (2003).

The calculated volume (based on HR-ToF-AMS + rBC + crustal material) was then compared with co-located SMPS measurements (Figure A.2). The SMPS measured the particle number distribution between 15.1 and 532.8 nm mobility diameter. The number distribution can be converted to a volume distribution assuming spherical particles. On average, the difference between the calculated volume and the SMPS volume was within 6%, which validates the application of CDCE for the bypass line (Figure A.2a).

However, the CDCE is not applicable for the TD line because the CDCE algorithm is parameterized based on aerosol neutralization (Eq. A.7), which depends strongly on the accuracy of the ammonium concentration measurement. The ammonium concentration decreased quickly upon heating and was close to the instrument detection limit at 250°C. Thus, we evaluated the CE for the TD line by comparing the calculated volume (based on HR-ToF-AMS + rBC + crustal material) and the SMPS volume (Salcedo et al., 2006).

$$\text{neutralization} = \frac{NH_{4,meas}}{NH_{4,predict}} = \frac{NH_{4,meas}}{18 \times \left(\frac{SO_4 \times 2}{96} + \frac{NO_3}{62} + \frac{Chl}{35.5}\right)} \quad \text{Eq. A.7}$$

We noted that the selection of the rBC density has a substantial effect on the TD line CE. For example, varying the rBC density from 1.77 to 0.60 g cm^{-3} (i.e., from the inherent material density to the effective density of 100 nm diesel soot particle reported in Park et al. (2003)) changed the CE at 250°C by a factor of 2 (Table S1). This sensitivity analysis highlighted the importance of the rBC density in applying this method to evaluate CE, especially for the TD line where rBC accounted for a large fraction of the mass concentration. In this study, since the TD line CE calculated with an rBC effective density of 0.73 g cm^{-3} (i.e., average value from Park et al. (2003)) was close to the default value for CE (i.e., 0.45), we used 0.45 as the TD line CE in our analysis. As shown in Figure A.2b and A.2c, the default CE results in a reasonable agreement between the calculated volume and the SMPS volume for the TD line. Specifically, the differences between the calculated volume and the SMPS volume are 14% and 11% at 120°C and 250°C, respectively, which are within the range of measurement uncertainties. Future studies are warranted to comprehensively investigate the change of AMS CE after heating of the aerosol.

A.2.4 Data analysis

A.2.4.1 Positive matrix factorization (PMF) analysis

Positive Matrix Factorization (PMF) analysis has been widely used for aerosol source apportionment in the AMS community. This technique represents the observed data as a linear combination of factors with constant mass spectra but varying concentrations

across time in the dataset (Paatero and Tapper, 1994; Paatero, 1997). Two solvers have been used for PMF analysis of AMS data, PMF2 and the multilinear engine (ME-2). The PMF2 solver does not require a priori information, which avoids some subjectivity. The ME-2 solver uses a priori information to reduce rotational ambiguity among possible solutions (Canonaco et al., 2013; Paatero, 1999).

For the ambient OA measurements, we used the standard PMF2 solver, which does not include any a priori information. This analysis is denoted as $PMF_{ambient}$ and was performed using the PMF Evaluation Toolkit (PET) software developed by Ulbrich et al. (2009). The error matrix was pre-treated based on the procedure in Ulbrich et al. (2009). *m/z*'s with signal-to-noise ratio in the range 0.2-2 were down weighted by a factor of 2, and *m/z*'s with signal-to-noise ratio smaller than 0.2 were removed. Also, the contributions of O^+, HO^+, H_2O^+, CO^+ and CO_2^+ were down weighted to avoid excessive weighting of CO_2^+ and related fragments. Following the detailed procedure listed in Zhang et al. (2011), the PMF solutions were evaluated by investigating the key diagnostic plots (Fig. S4), mass spectral signatures, correlations with external tracers, and the diurnal profiles. The rotational ambiguity of the optimal solution was examined by changing the FPEAK parameter from -1 to 1. In our case, an FPEAK value of 0 ($Q/Q_{exp} = 1.804$) was selected because the correlations between factors and external tracers were not improved for FPEAK values that were different from 0. We resolved three factors from $PMF_{ambient}$, i.e., hydrocarbon-like OA (HOA), solid fuel OA (SFOA), and oxygenated OA (OOA), which are discussed in section 3.1. The choice of a three-factor solution is discussed in detail in the SI (Fig. S5).

For the TD line measurements, we first tried the PMF2 solver on the combined ambient and thermally-denuded OA spectra (denoted as $PMF_{ambient+TD}$); this is the same approach applied in Huffman et al. (2009a). However, in this study, we encountered several issues in $PMF_{ambient+TD}$ analysis. The first issue we encountered is the "mixing" behavior of OA factors. For example, in the three-factor solution of $PMF_{ambient+TD}$, one factor has similar fragmentation patterns as HOA from $PMF_{ambient}$, but this factor also has substantial signal at $C_2H_4O_2^+$ (*m/z* 60, often used as a tracer marker for SFOA) (Fig. S6). In addition, another factor from $PMF_{ambient+TD}$ has similar time series as SFOA from $PMF_{ambient}$, but has similar mass spectrum as OOA from $PMF_{ambient}$. The second issue we encountered is that the mass loading of the OOA factor is occasionally higher in the TD runs compared to the preceding and succeeding bypass runs (Fig. S7). The reason for this behavior is not clear, but it is likely caused by the fact that only highly oxidized species remain upon heating and the mass spectrum of the remaining OA becomes more similar to the oxidized OA factors. Thus, PMF analysis might overestimate the concentrations of the oxidized OA factor. Overall, the PMF analysis on the combined bypass and TD line measurements by using the PMF2 solver without a priori information could not clearly separate OA factors. This is likely caused by the fact that including the thermally denuded data might distort the PMF results by introducing additional time variation in the mass spectra as pointed out by Huffman et al. (2009a).

Considering the above issues associated with $PMF_{ambient+TD}$, we performed PMF analysis using the ME-2 solver on the TD line measurements by applying the factor profiles determined from $PMF_{ambient}$ as a priori information, in order to improve the separation of OA factor. Data obtained at 120°C and 250°C were analyzed separately in order to account

for the variability of factor mass spectra at different temperatures. The analyses for 120°C and 250°C are denoted as ME-2_{120C} and ME-2_{250C}, respectively, and were performed using the toolkit Source Finder (SoFi v4.8) (Canonaco et al., 2013). The error matrix was pre-treated in the same way as for $PMF_{ambient}$. As recommended by Canonaco et al. (2013) and Crippa et al. (2014), secondary factors (i.e., OOA factor) were unconstrained and primary factors (i.e., HOA and SFOA) were constrained with a small *a* value (e.g., <0.1), which allows small variations of the resolved factors compared to the anchor profile in order to account for differences in ambient sources and avoid a mixing situation. We performed sensitivity tests and found that increasing the *a* value from 0 to 0.1 only reduced the fitting "residual" (i.e., Q/Q_{exp}) by <1% and had negligible influence on the factor profiles and factor concentrations (Figs. S8 and S9) for both ME-2_{120C} and ME-2_{250C}. Therefore, considering that 1) the small effect of the *a* value, and 2) the fact that the anchor profiles of HOA and SFOA resolved from $PMF_{ambient}$ were clearly separated, we selected 0 as the *a* value, which fully constrained the profile of HOA and SFOA. The mass spectra of thermally-denuded OOA at 120°C and 250°C, which were not constrained in ME-2_{120C} and ME-2_{250C}, change slightly compared to the ambient OOA mass spectrum (Fig. S10). The most discernable changes occur at f_{CHO+} (i.e., fraction of organic signal at CHO^+), f_{C2H3O+} and f_{CO2+}, suggesting that the composition of OOA is different at different denuding temperatures.

A.2.4.2 Retroplume analysis

Retroplume analysis was performed using the Numerical Atmospheric-Dispersion Modelling Environment (NAME) dispersion model (Jones et al., 2007) to identify the

origin of air masses. The NAME model used the Unified Model reanalysis of meteorological data and generated the surface level pathways of air masses arriving at the site after 1 day of transport (i.e., 1-day footprints). The domain of influence of the NAME run was divided into a number of geographical regions (i.e., Atlantic ocean, Benelux area, etc, shown in Fig. S11) as described in Fleming et al. (2012). For each 3-hour period, the fraction of air masses arriving from each region was calculated. According to Liu et al. (2013), for the time periods when the fraction of one region is greater than the 40th percentile of that region's air masses fraction, that region is deemed to have a strong influence on the sampling site. Regions can also be grouped into broader sectors. In this study, we focused on two broader sectors, the easterly sector (North France and Benelux area) and the westerly sector (Atlantic and Ireland). It is important to note that sometimes the sampling site is influenced by more than one sector.

In the following discussion, we first investigate the PM_1 composition and OA source apportionment at the Detling site (section 3.1). Then in section 3.2, we compare the measurements at the rural Detling site with the urban NK site to investigate the spatial variability of aerosol in the greater London area. Lastly, we examine the aerosol volatility based on measurements at the Detling site (section 3.3).

A.3 Results and Discussion

A.3.1 Aerosol characterization at the Detling site

Figure A.3a shows the time series of PM_1 composition measured by HR-ToF-AMS (i.e., non-refractory species) and SP2 (i.e., rBC). The campaign-average PM_1 concentration is 14 ± 12 μg m^{-3} (average ± one standard deviation). The chemical composition of PM_1 is

dominated by nitrate and organics, which on average accounts for 32% and 31% of total PM_1 mass, respectively. The other components include sulfate (17%), ammonium (14%), rBC (4.3%), and chloride (2.2%). Based on the fragmentation pattern of nitrate functionality in the AMS (i.e., NO^+/NO_2^+ ratio), one can determine whether the nitrate is of organic or inorganic origin (Farmer et al., 2010; Boyd et al., 2015; Fry et al., 2009; Xu et al., 2015c). At the Detling site, the measured NO^+/NO_2^+ ratio is close to the value of pure ammonium nitrate (Fig. S12), indicating that the majority of the measured nitrates are inorganic nitrates.

The PMF analysis on the ambient organic mass spectra (i.e., $PMF_{ambient}$) resolves three OA subtypes: oxygenated organic aerosol (OOA), solid fuel organic aerosol (SFOA), and hydrocarbon-like organic aerosol (HOA), which accounts for 54%, 23%, and 19% of total OA, respectively. The time series and mass spectra of the three factors are shown in Figure A.4. HOA is representative of primary OA from vehicle emissions as its mass spectrum is dominated by hydrocarbon-like ions (i.e., $C_xH_y^+$ ions). HOA is correlated with rBC and NO_x (Figure A.4a). SFOA is a surrogate for fresh OA from solid fuel combustion, including biomass burning (Young et al., 2015b). The mass spectrum of SFOA is characterized by prominent signals at $C_2H_4O_2^+$ (*m/z* 60) and $C_3H_5O_2^+$ (*m/z* 73), which are likely fragments from anhydrosugars such as levoglucosan and mannosan (tracers for biomass burning). The time series of SFOA correlates with particle-phase nitrated phenol compounds (Mohr et al., 2013), which are mainly associated with coal and wood combustion (Figure A.4b). OOA is the most oxidized (O:C = 0.92) among all three factors. At the Detling site, the OOA time series shows a good correlation with sulfate (Pearson's R=0.80, Figure A.4a) and acetaldehyde (R=0.78, Figure A.4a). Acetaldehyde could arise

from direct emissions, such as fossil fuel combustion and biomass burning, and secondary production by oxidation of various hydrocarbons (Langford et al., 2009). The observation that acetaldehyde correlates better with OOA than SFOA (R = 0.78 vs. 0.66) is consistent with previous studies which showed that acetaldehyde is dominated by secondary production after hours of photochemical processing (Hayes et al., 2013; Sommariva et al., 2011; de Gouw et al., 2005).

The identification of the sources of OOA is challenging because the mass spectrum of OA from different sources becomes more similar and resembles that of OOA with increasing photochemical aging (Ng et al., 2010; Jimenez et al., 2009). For the Detling data, we hypothesize that OOA is mainly from aged biomass burning. Liu et al. (2015a) combined the PMF results from our study with radiocarbon analysis and estimated that 73-90% of carbon in the OOA factor was non-fossil. Biogenic emissions and biomass burning are the major sources for non-fossil carbon. The large fraction of non-fossil carbon indicates that the OOA measured at the Detling site largely arises from aged biomass burning because the concentration of biogenic VOCs is low in winter due to cold temperature and reduced photosynthesis. For example, Yin et al. (2015) showed that the concentrations of isoprene SOA tracers (i.e., methyltetrols) and α-pinene SOA tracers (pinic acid and pinonic acid) at the NK site during the winter IOP are only 0.5 ng m^{-3} and 2.3 ng m^{-3}, respectively, which are substantially lower than the concentrations measured at US and European sites during warmer months. Both laboratory studies and ambient measurements have revealed that the oxidation of biomass burning OA is a rapid process (Hennigan et al., 2011; May et al., 2012; Bougiatioti et al., 2014; Zhao et al., 2015). During the oxidation process, the mass spectrum of biomass burning OA could lose its

characteristic signature (i.e., $C_2H_4O_2^+$ and $C_3H_5O_2^+$) and becomes progressively similar to that of OOA (Grieshop et al., 2009a; Hennigan et al., 2011). Thus, the aged biomass burning OA could be apportioned to the OOA by PMF analysis. With this, it is possible that the biomass burning OA contributes a larger fraction of ambient OA in winter than what previous field studies suggested, where this factor was typically identified based on the presence of larger signals at $C_2H_4O_2^+$ (*m/z* 60) and $C_3H_5O_2^+$ (*m/z* 73) alone.

Figure A.3b shows the aerosol composition when air masses come from the easterly sector (i.e., mainland Europe) and the westerly sector (i.e., Atlantic Ocean). The concentration of PM_1 is five times higher for the easterly sector compared to the westerly sector. This is consistent with previous studies which showed that elevated pollution levels in the southern UK were often associated with heavily polluted air masses transported from mainland Europe (Charron et al., 2013; Morgan et al., 2010; Morgan et al., 2015; Putaud et al., 2004). Similar to the greater London area, Beekmann et al. (2015) found that 70% of fine PM in the Paris megacity was also largely influenced by regional contribution from mainland Europe. A large fraction of OA from mainland Europe is highly oxidized organic aerosol (i.e., OOA). For example, while the concentrations of HOA and SFOA only double when the source of air masses switches from the Atlantic Ocean to mainland Europe, the OOA concentration increases from ~0.5 μg m^{-3} to ~3 μg m^{-3} (Figure A.3b). The higher contribution of OOA to total OA is consistent with the total OA from mainland Europe being more oxidized than that from the Atlantic Ocean. In Figure A.5, we compare the OA oxidation level for different air masses in the f_{44} (i.e., fraction of organic signal at *m/z* 44) vs. f_{43} (i.e., fraction of organic signal at *m/z* 43) plot (Ng et al., 2010). The OA for the easterly sector has a higher f_{44} compared to the westerly sector, suggesting that the air

masses advected from mainland Europe have undergone a larger extent of photochemical processing.

A.3.2 Comparison between London and Detling

In this section, we compare the two simultaneous HR-ToF-AMS measurements at the rural Detling site and the urban NK site. Only the sampling periods (hourly basis) when both instruments were operative from 20 January to 8 February, 2012 are included in the comparison, so that the concentrations reported in this section are different from those reported in section 3.1, where the whole data set at the Detling site (from 20 January to 15 February, 2012) is used.

A.3.2.1 Non-refractory species and OA factors comparison

The comparison between the Detling and NK sites in terms of concentration and diurnal variation of the five NR-PM_1 species is shown in Figure A.6 and Fig. S13, respectively. The concentration of nitrate is substantially higher at the urban NK site (i.e., 5.6 μg m^{-3}) than the rural Detling site (3.5 μg m^{-3}). This observation is consistent with McMeeking et al. (2012), who performed airborne measurements in the urban London region and observed an enhancement of nitrate concentration inside urban plumes. The elevated nitrate concentration (largely inorganic nitrate) at the urban site suggests that nitrate has a strong local contribution, likely due to the fact that nitrate formation occurs rapidly and its major sources (i.e., oxidation of NO_x) are much higher over inner London (Shaw et al., 2015). The sulfate concentration is well correlated between two sites (R = 0.82, Figure A.7), consistent with previous findings that sulfate has a strong regional contribution in the greater London area (Harrison et al., 2012; Yin et al., 2010). However,

the sulfate concentration is about 60% higher at the rural Detling site than the urban NK site. The comparison of sulfate concentration between the rural and urban site depends on the origin of air masses. As shown in Fig. S14, the sulfate concentrations agree well between the two sites when air masses come from Atlantic Ocean (i.e., westerly) compared to mainland Europe (i.e., easterly). The reason for the elevated sulfate concentration at the rural site will be discussed below.

Although the average concentration of total OA is comparable between NK (i.e., 4.3 μg m^{-3}) and Detling (4.0 μg m^{-3}) (Figure A.6), PMF analysis reveals that the contribution to total OA from different sources is distinctly different between the urban and rural sites. At the urban NK site, primary OA sources, including cooking, vehicle emission, and solid fuel combustion, account for about 70% of total OA. At the rural Detling site, in contrast, more than half of the total OA is aged secondary OA (i.e., OOA). Specifically, the cooking OA (i.e., COA), which accounts for 18% of total OA at the urban NK site, is not resolved at the rural Detling site. This is expected as there is no cooking activity near the rural Detling site. Hydrocarbon-like OA (i.e., HOA) only shows weak correlation between the two sites (R = 0.53) (Figure A.8f), which is because HOA is representative of primary OA and it is influenced by local vehicle emissions. The SFOA time series is moderately correlated (R = 0.65) between Detling and NK (Figure A.8d). The SFOA concentration at the urban NK site is almost twice as high at the rural Detling site, which is likely due to the elevated domestic space heating activities and related emissions in the urban London area during wintertime (Young et al., 2015b; Crilley et al., 2015).

Among all three OA factors, the OOA factor has the strongest correlation between the two sites (R = 0.81) (Figure A.8b), which suggests that OOA likely represents regional SOA. Crilley et al. (2015) also observed that the filter-based daily-average OC concentration is well correlated ($R^2 > 0.82$) between Detling and NK sites during the same period as our study. However, the good correlations of OOA and OC observed in our study and Crilley et al. (2015) are different from the observation in Charron et al. (2013), where the authors found that secondary organic carbon (SOC) was much less spatially homogeneous than nitrate and sulfate by comparing an urban (Birmingham site) and a rural site (Harwell site) in the greater London area between July and November 2010. The difference between this study and Charron et al. (2013) is likely due to the uncertainty in the SOC estimation method. In Charron et al. (2013), SOC is estimated from filter measured total OC by using the EC/OC method where a constant EC/CC ratio from primary sources is applied. As discussed in Charron et al. (2013), their estimation and the weak correlation of OC between different sites are affected by the uncertainties associated with the choice of source ratios and analytical procedure. In addition to SOC estimation uncertainty, the differences in sampling sites, sampling periods, and size cuts ($PM_{2.5}$ vs. PM_1) between Charron et al. (2013) and our study could also play a role.

Although the OOA is well-correlated between the two sites, the OOA concentration is almost twice as high at the rural Detling site than the urban NK site (Figure A.6). This observation is similar to the comparison of sulfate between the two sites, which is also usually considered to be regional, as discussed above. Based on atmospheric chemistry transport model, the higher OOA concentration at the rural site is a result of meteorological conditions, which cause a strong gradient of SOA concentration when air masses are

advected from polluted mainland Europe. For example, to simulate the SOA formation in the winter IOP, Ots et al. (2015) applied the regional EMEP4UK (European Monitoring and Evaluation Programme) model, which uses 5 km by 5 km British Isles grid nested within 50 km by 50 km greater Europe domain, 21 vertical levels, Weather Research and Forecasting (WRF) model meteorological reanalysis, and National Atmospheric Emissions Inventory (NAEI) for the UK, Centre on Emission Inventories and Projections (CEIP) emissions for other European countries. They observed a steep negative gradient of SOA concentration from near European continent to southern England. The steep gradient is a result of meteorological conditions (i.e., mainly wind direction), which causes that the pollution plume from mainland Europe largely passes over the rural site, but not the urban site.

A.3.2.2 OA oxidation level

Figure A.5 compares the OA oxidation level between Detling and NK. Compared to the NK site, the average OA at the Detling site has higher f_{44}, indicating that the OA at the Detling site is more oxidized than that at the NK site. The difference in OA oxidation level between the Detling and the NK sites are due to different OA compositions. As shown in Figure A.6, the OA at the NK site is dominated by primary OA (~70% of total OA) from cooking, vehicle emissions, and solid fuel combustion, whose O:C is much lower than OOA. In contrast, more than half of OA at the Detling site is OOA, which is highly oxidized.

A.3.3 Aerosol volatility analysis

A.3.3.1 Volatility of non-refractory species and OA factors

Figure A.9a and c show the thermograms and the change in concentration after heating (ΔC) of non-refractory (NR) species as measured by the HR-ToF-AMS. The MFR is calculated as the ratio of the species mass concentration through the TD to the average mass concentration of the preceding and succeeding bypass runs. The ΔC is calculated as the concentration difference between the bypass and TD runs (Eq. A.4). Both the MFR and the ΔC have been corrected for the particle loss in the thermal denuder (TD) by using the TD transmission efficiency as discussed in section 2.2. The MFR of NR species is consistent with previous ambient measurements (Huffman et al., 2009a). Nitrate has the largest average ΔC and the smallest MFR among all NR species. The MFR of nitrate decreases to 0.15 at 120°C and it volatilizes completely at 250°C (i.e., MFR < 0.05). Sulfate is the least volatile species at 120°C, which has the smallest average ΔC and an MFR equal to 0.89. The sulfate MFR is higher than that of ammonium sulfate from laboratory studies, which has been attributed to particle mixing state affecting the sulfate volatility (Huffman et al., 2009a; Massoli et al., 2015). For OA, the MFR is about 0.16 at 250°C. On average, 0.88 μg m^{-3} OA remains after heating, implying the existence of non-volatile organic compounds. Figure A.9d shows that the ΔC's of three OA factors are not statistically different at 120°C. This suggests that although the O:C of OOA (O:C = 0.92) is substantially larger than that of HOA (O:C = 0.22) and SFOA (O:C = 0.37), the volatilities of the three factors are similar at 120°C. Thus, the O:C may not be a good indicator of the volatility of the OA factors. At 250°C, both HOA and SFOA fully evaporate (MFR < 0.05) so that the volatility cannot be compared under this temperature.

A.3.3.2 Sources of residual organics at 250°C

Figure A.10 shows the chemical composition of the residual PM_1 after heating to 250°C. The major components of the residual PM_1 are OA (90% of OA is OOA), rBC, and sulfate. rBC accounts for about 30% of the remaining mass. This value is smaller than that reported in Poulain et al. (2014) (i.e., 47% in summer and 59% in winter for TD temperature 300°C) and in Häkkinen et al. (2012) (i.e., 55-87% depending on season for TD temperature 280°C). The differences are likely due to 1) the density of rBC used in previous studies when converting SMPS volume concentration to mass concentration, 2) different TD temperatures and residence times, 3) techniques to measure rBC concentration, and 4) sampling locations.

At 250°C, OA has the largest contribution (~40%) to the residual mass. The existence of highly oxidized, non-volatile organic compounds is consistent with previous ambient measurements and model studies. For example, Cappa and Jimenez (2010) used a kinetic model to simulate the volatility of OA factors measured by Huffman et al. (2009a) in the MILAGRO field campaign and the authors estimated that a large fraction of OA was non-volatile and would not evaporate under any atmospheric conditions.

The sources of non-volatile organics are uncertain, but appear to be related to anthropogenic emissions. A previous study by Häkkinen et al. (2012) showed that the MFR (excluding rBC) at 280°C correlated well with anthropogenic tracers (i.e., polycyclic aromatic hydrocarbons), indicating that the non-volatile species may be affected by anthropogenic emissions. In this study, we investigate the sources of the non-volatile organics by comparing the measurements of HR-ToF-AMS and SP-AMS after heating at 250°C. While the HR-ToF-AMS measures the bulk total non-refractory organics, SP-AMS

only detects the organics associated with rBC when the SP-AMS is operated with the laser vaporizer only (i.e., no tungsten vaporizer) (Onasch et al., 2012). Figure A.11 shows that after heating at 250°C, the residual organics associated with rBC correlate well with the residual organics in the bulk measurements, and they only account for <10% of the bulk measurements. Therefore, this good correlation is not caused by a large contribution from rBC-associated species, but is possibly caused by the fact that the non-volatile organics in the bulk measurements have similar sources or have undergone similar chemical processing as rBC in the atmosphere. Denkenberger et al. (2007) suggested that the non-volatile organics may be oligomers formed within the TD based on the observation that oligomer intensity increased after heating ambient particles in a TD. In our study, the signals at high *m/z* (100 – 180), which are potential indicators for oligomers, decrease with TD temperature (Fig. S15). This suggests that the non-volatile organics are unlikely to be oligomers formed within the TD.

A.3.3.3 OA MFR and O:C ratio

To examine the relationship between O:C and MFR, the O:C of thermally-denuded OA is plotted as a function of TD temperature. As shown in Figure A.12a, the O:C of thermally-denuded OA increases with increasing TD temperature, indicating that the residual OA with lower volatility is more oxidized, which is consistent with previous observations (Huffman et al., 2009a; Huffman et al., 2009b). Thus, it appears that the OA oxidation level (i.e., O:C) is correlated with MFR. If so, one would expect that ambient OA with higher O:C should have larger MFR. However, as shown in Figure A.12b to e, the MFR increases only slightly with the bypass O:C (or OS) over a wide range of O:C (or

OS). In addition, the correlation between MFR and bypass O:C (or OS) is weak (i.e., $R < 0.4$), suggesting that the volatility of OA cannot be readily inferred by its O:C or OS.

The lack of correlation between OA MFR and O:C is likely due to the distributions of volatility and O:C in bulk OA, that is, one population of particles with a higher bulk O:C could have lower MFR after heating compared to another population of particles with a lower bulk O:C, if the volatility and O:C distributions are different between two populations. In the following discussion, we use a simple model to illustrate our point (Figure A.13). Two populations of particles are comprised of three compounds (i.e., A, B, and C), but with different amounts. These three compounds have the same molecular weight, but different volatility and O:C. The assumed properties of the three compounds and the compositions of two populations of particles are atmospherically relevant and are summarized in Figure A.13. Although the average O:C of population #2 (i.e., 0.75) is higher than that of population #1 (i.e., 0.61), population #2 has the same MFR as population #1 after heating, which is consistent with the trend in Figure A.12b-e. On the other hand, the O:C of each population always increases after heating, which is consistent with the observation in Figure A.12a. We note that the example described here is specific; however, it clearly illustrates that the distributions of volatility and O:C largely influence the relationship between O:C and MFR of bulk OA. This also helps to explain the various types of relationship between O:C and MFR observed in laboratory studies (Grieshop et al., 2009b; Qi et al., 2010; Donahue et al., 2012; Kroll et al., 2009; Tritscher et al., 2011; Xu et al., 2014). In previous laboratory studies, while the SOA generally becomes progressively more oxidized (i.e., O:C increases) during the chemical aging, the volatility distribution evolves differently for different SOA systems, which results in various types

of MFR trend (i.e., increases, or stays constant, or decreases over time). Our analysis emphasizes the importance of understanding the distribution of volatility and O:C in bulk OA and reveals the potential weakness of using one averaged O:C value to describe the degree of oxidation, which is in line with the two-dimensional volatility-oxidation modeling framework proposed by Donahue et al. (2011). In addition to the distribution of O:C and volatility, the fact that MFR depends on the initial concentration of OA, which is different between studies, may also contribute to the various relationships between O:C and MFR.

Hildebrandt et al. (2010) proposed that the lack of correlation between O:C and volatility in Finokalia, Greece was caused by the OA being highly oxidized with an average O:C of 0.8 (estimated from the measured f_{44}). In order to test this hypothesis, we plot the O:C enhancement (i.e., ratio between O:C of thermally denuded OA and O:C of ambient OA) vs. O:C of ambient OA (Figure A.14a) to show the O:C enhancement after heating. By extrapolating the linear fit under different temperatures, we find that if the O:C of ambient OA is about 1, the enhancement is negligible even after heating at 250°C. It is important to note that the O:C reported in Figure A.14a is calculated based on the recent formulation in Canagaratna et al. (2015). The improved O:C calculation method in Canagaratna et al. (2015) results in higher O:C compared to the values based on Aiken et al. (2008), which was used in Hildebrandt et al. (2010). By using the method in Aiken et al. (2008), we found that the O:C threshold for no enhancement is 0.8 (Fig. S16), which is the same as the O:C of ambient OA in Hildebrandt et al. (2010). In addition, the campaign-average f_{44} of ambient OA in Hildebrandt et al. (2010) is 0.182, which is close to f_{44} of TD OA under 250°C (i.e., 0.188) in our study (Figure A.14b). To conclude, this analysis

provides a specific case in which the average O:C ratio might not be a good indicator of OA volatility.

A.4 Conclusions

In this study, we deployed a suite of instruments to characterize the composition of PM_1 at a rural site (Detling, Kent) near London during the Clean Air for London (ClearfLo) project in 2012 winter. Nitrate and organics are two major components in PM_1, each of which accounts for ~30% of total PM_1 mass concentration. Retroplume analysis reveals that the PM_1 concentration in the greater London area is largely influenced by the origin of the air masses. When air masses are advected from mainland Europe, the PM_1 concentration is elevated and the organic aerosol is more oxidized. Oxygenated organic aerosol (OOA) accounts for ~50% of total OA. Taking advantage of measurements in winter when the biogenic emissions are low, we hypothesize that the OOA in the current study is likely aged OA from biomass burning. The hypothesis is based on the combined PMF and radiocarbon analysis where more than 70% of carbon in OOA is estimated to be non-fossil (Liu et al., 2015a) and cannot be explained by the small amount of biogenic SOA in winter.

With simultaneous HR-ToF-AMS measurements taking place at the rural Detling site and the urban North Kensington site, we have a unique opportunity to investigate the spatial variability of PM_1 in the greater London area. The nitrate concentration is markedly higher at the urban site compared to the rural site (i.e., 5.6 vs 3.5 $\mu g\ m^{-3}$). The high nitrate concentration at the rural site together with the urban excess of nitrate imply that the nitrate in the greater London area has a high regional background overlaid by important

contributions from local production. Although the OA concentration is comparable between the rural and urban sites, PMF analysis suggests distinctly different contribution from different sources between the two sites. Similar to previous studies, we find that OA at the urban site mainly arises from primary sources, while OA at the rural site is mainly secondary. Vehicle emission, solid fuel combustion, and cooking together account for ~70% of OA at the urban NK site. In contrast, OOA contributes more than half of total OA at the rural Detling site. Among all OA factors, OOA has the best correlation between the two sites (R = 0.81), which suggests that this factor is largely regional. We find that the OOA concentration is almost twice as high at the rural Detling site than the urban NK site. This is a result of meteorological conditions, which cause a strong gradient of SOA concentration when air masses are advected from polluted mainland Europe. The observation that the OOA concentration is higher at the rural site than urban site is opposite to the trend shown in Zhang et al. (2007). However, the trend reported in Zhang et al. (2007) is not based on simultaneous measurements at paired rural and urban sites. Thus, our observation highlights the importance of meteorology in determining the OA spatial distribution.

A TD was deployed to investigate the volatility of PM_1 species at the Detling site. We find that although OOA has substantial larger O:C than HOA and SFOA, the volatilities of these three factors are similar at 120°C, which is inferred from the change in mass concentration after heating at 120°C. This suggests that the O:C may not be a good proxy of OA factor volatility. We note that 16% of total OA remains even after heating at 250°C, suggesting the existence of non-volatile organics. PMF analysis reveals that the majority of the remaining organics are oxygenated OA. At 250°C, the time series of the residual

organics measured by HR-ToF-AMS correlate well with the residual organics associated with rBC measured by SP-AMS. The good correlation suggests that the non-volatile organics likely have similar sources or have undergone similar chemical processing as rBC in the atmosphere, considering that rBC-associated organics only account for <10% of bulk organics.

We evaluate the relationship between the volatility (using the MFR) and degree of oxidation (using the O:C or OS) of bulk OA. We found that, on the one hand, the O:C of thermally denuded OA is higher than that of ambient OA, indicating that less-volatile compounds have higher O:C. On the other hand, the MFR of OA shows a weak correlation with O:C of ambient OA, indicating that the average O:C of bulk OA may not be a good indicator for volatility. One possible explanation for the seemingly contradictory observations lies in the broad distribution of volatility and O:C in bulk OA. For example, different O:C distributions could result in the same bulk O:C but different volatility distributions, which may cause that particles with the same O:C to have different MFR. Thus, it is important to understand and use the distribution of properties (i.e., volatility and O:C) to describe the complexity of OA.

Figure A.1. Geographical locations of the sampling sites (i.e., North Kensington and Detling) in this study. The region circled by the M25 motorway is the greater London area. The map is adapted from Google Maps.

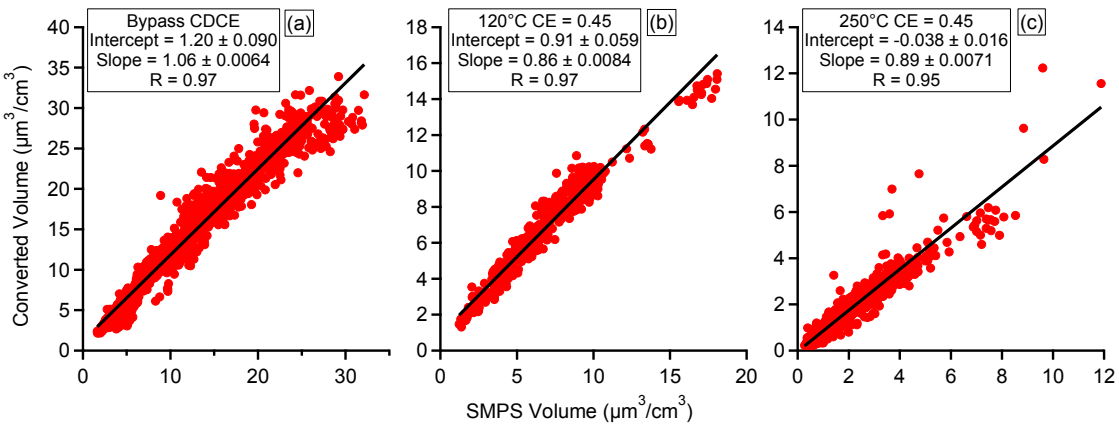

Figure A.2. Scatter plot of converted volume (based on HR-ToF-AMS total + BC + crustal material) vs. the apparent volume estimated from SMPS measurement for (a) the bypass line and the TD line at (b) 120°C and (c) 250°C. The composition-dependent CE is applied to the bypass line HR-ToF-AMS measurements and CE = 0.45 is applied to the TD line HR-ToF-AMS measurements. The slopes and intercepts are obtained by orthogonal distance regression (ODR). The Pearson's R is obtained by linear least-squares fit.

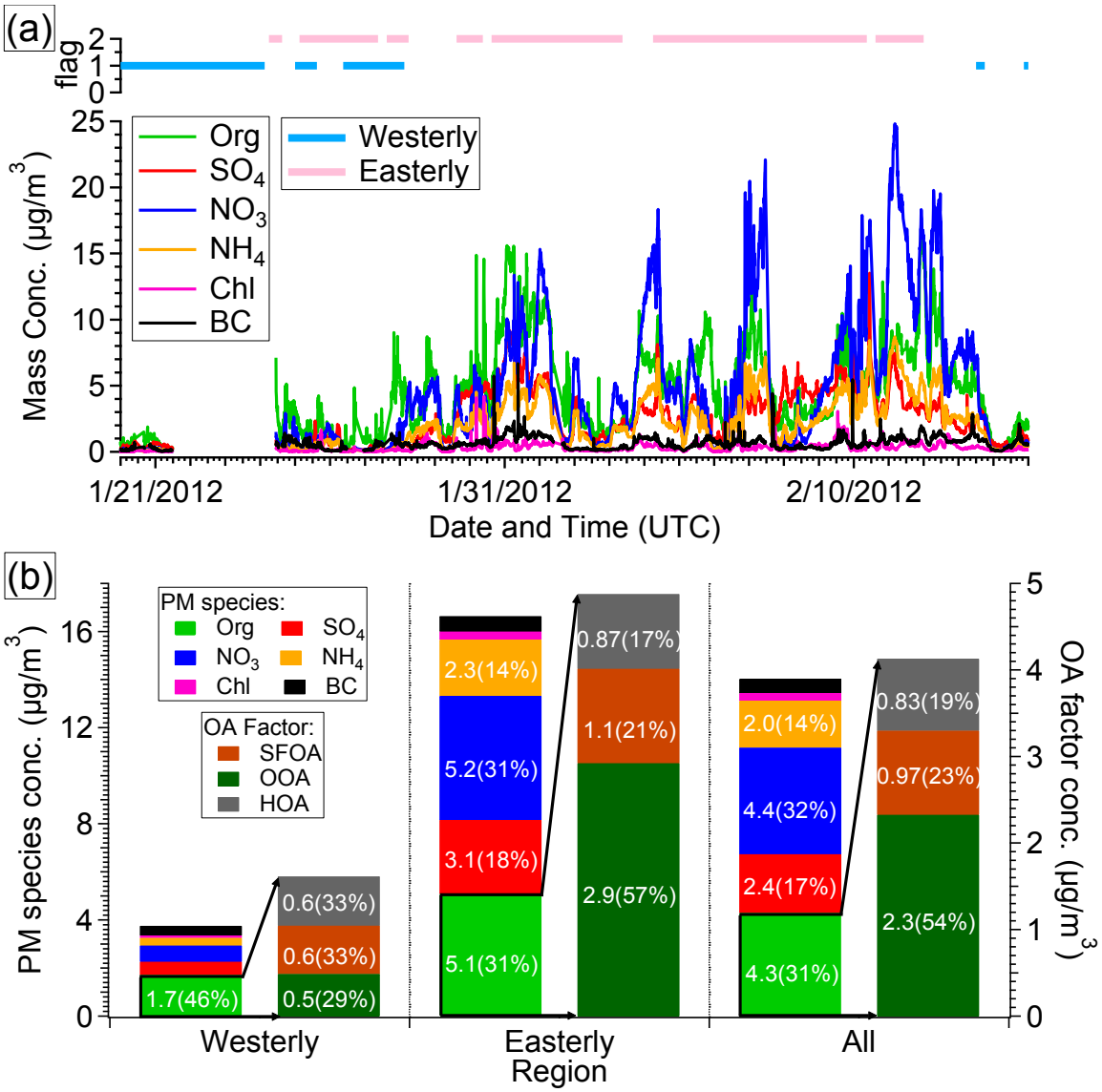

Figure A.3. (a) Time series of non-refractory species and black carbon in addition to the flag waves of dominant air mass origin based on the NAME model. (b) Average concentration of non-refractory species, black carbon, and OA factors resolved by PMF analysis for the easterly sector, westerly sector, and the whole campaign. The unexplained mass by PMF analysis is less than 6% of total OA and not shown in the figure. The gap between 1/22 and 1/25 is due to a clogged instrument inlet.

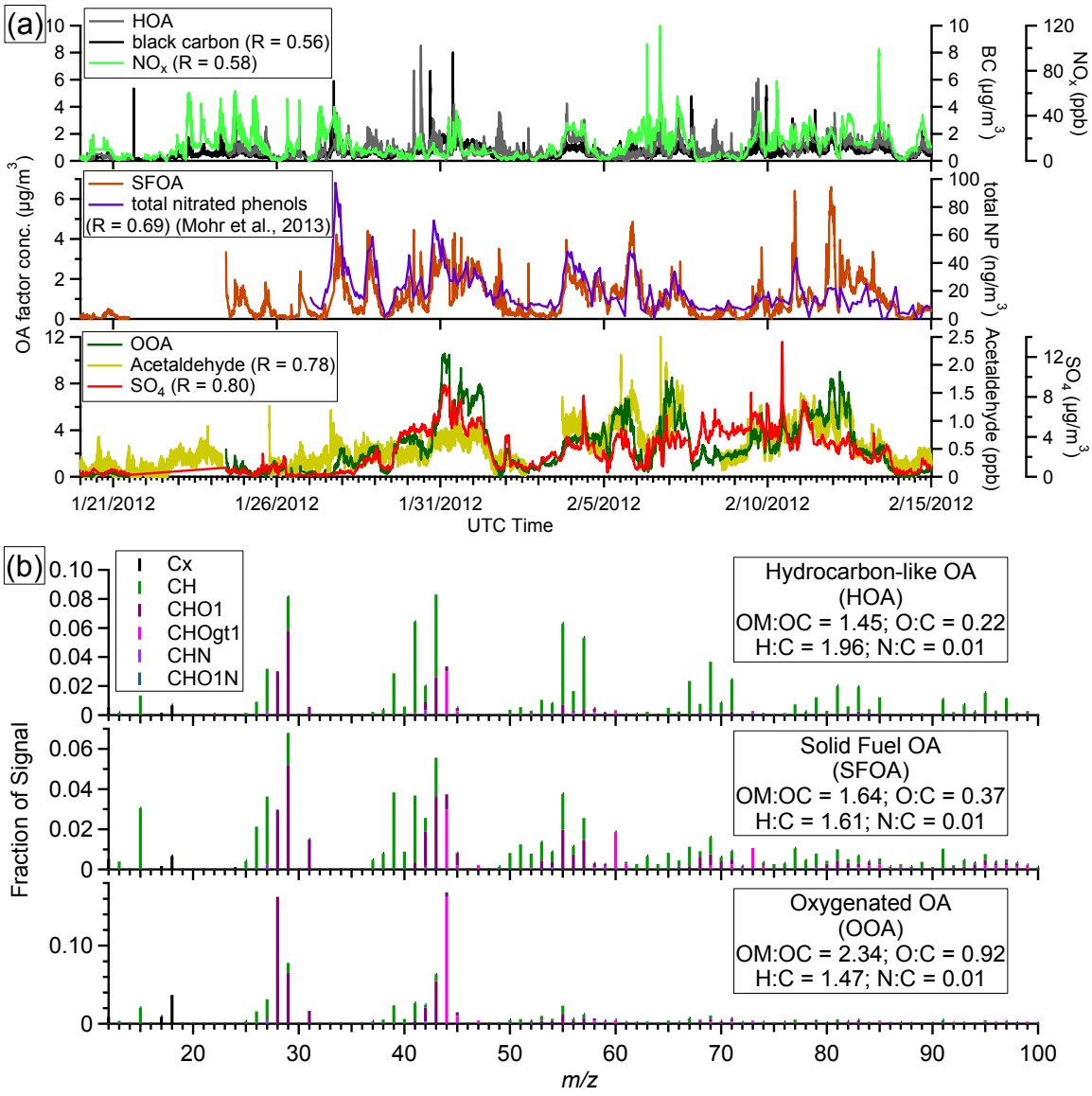

Figure A.4. (a) Time series of OA factors resolved from the unconstrained PMF analysis on the ambient data (i.e. $PMF_{ambient}$) and corresponding external tracers. (b) Mass spectra of OA factors, which are colored by the ion type. The time series of total nitrated phenols is from Mohr et al. (2013).

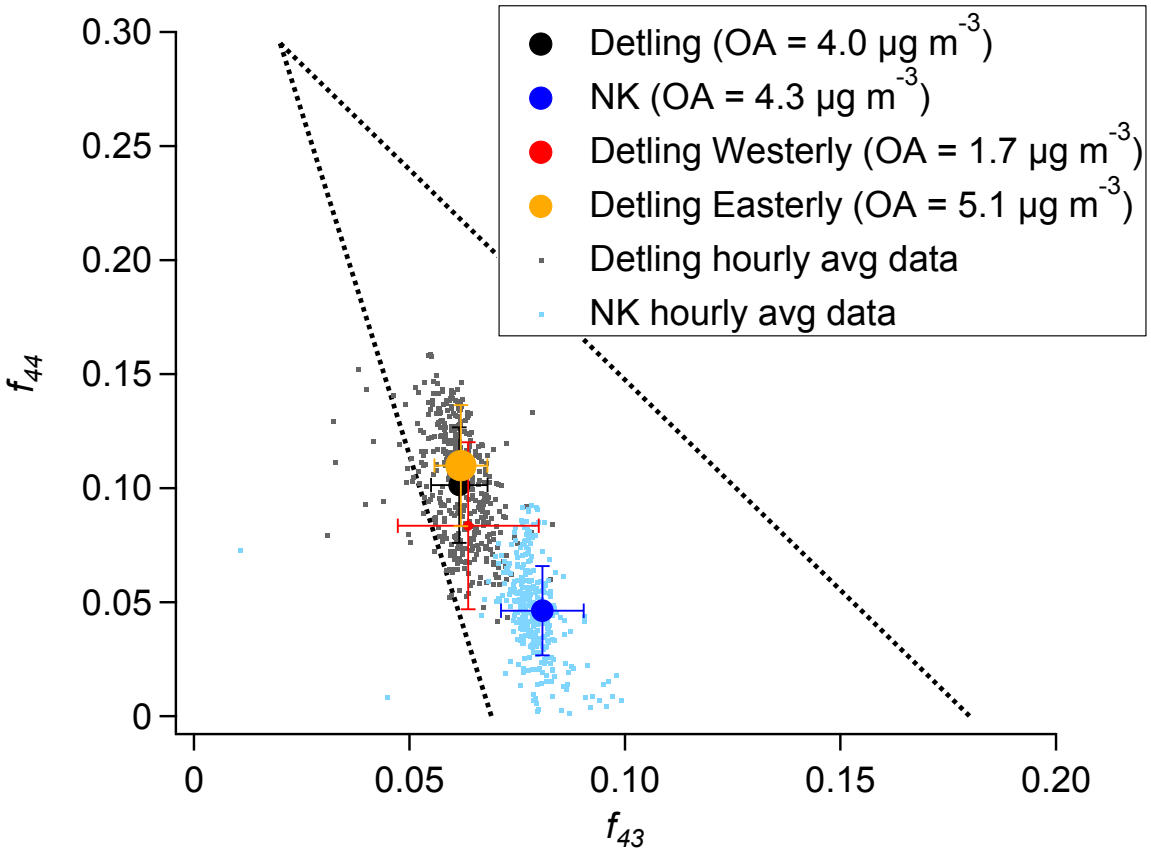

Figure A.5. f_{44} vs. f_{43} for Detling and NK sites, as well as for the westerly sector and easterly sector of the Detling site. The dotted lines were adapted from Ng et al. (2010). The averages are sized by average organic loading. The error bars indicate one standard deviation. The average OA concentration at the Detling site is different from the value in Figure A.3. due to different sampling periods.

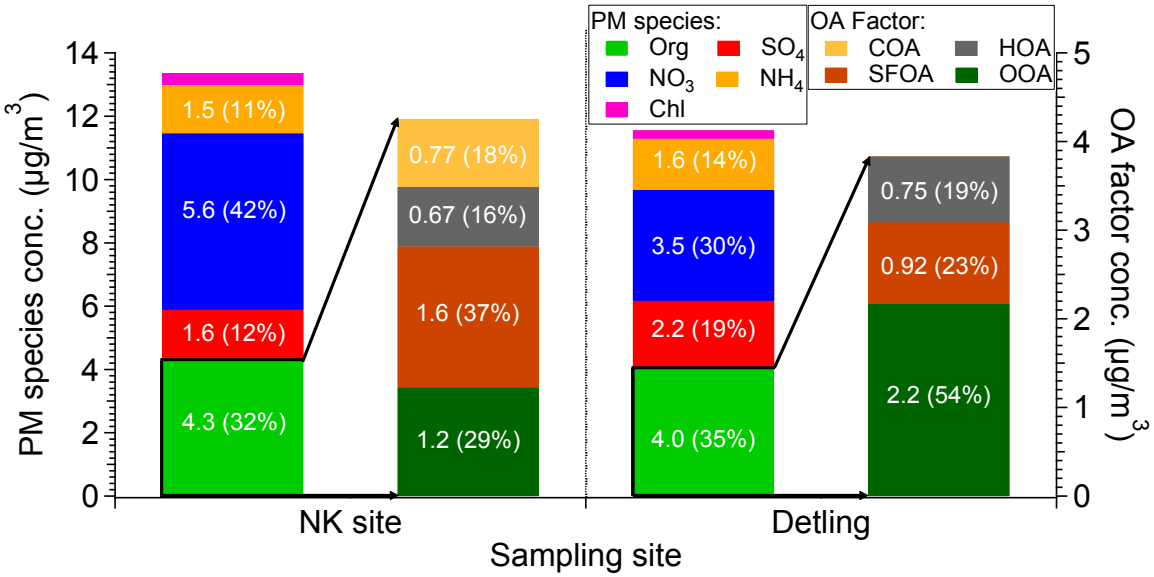

Figure A.6. Comparison between NK and Detling sites in terms of the campaign-averaged concentration and mass fraction of non-refractory species and OA factors. The unexplained mass by PMF analysis is less than 6% of total OA and not shown in the figure.

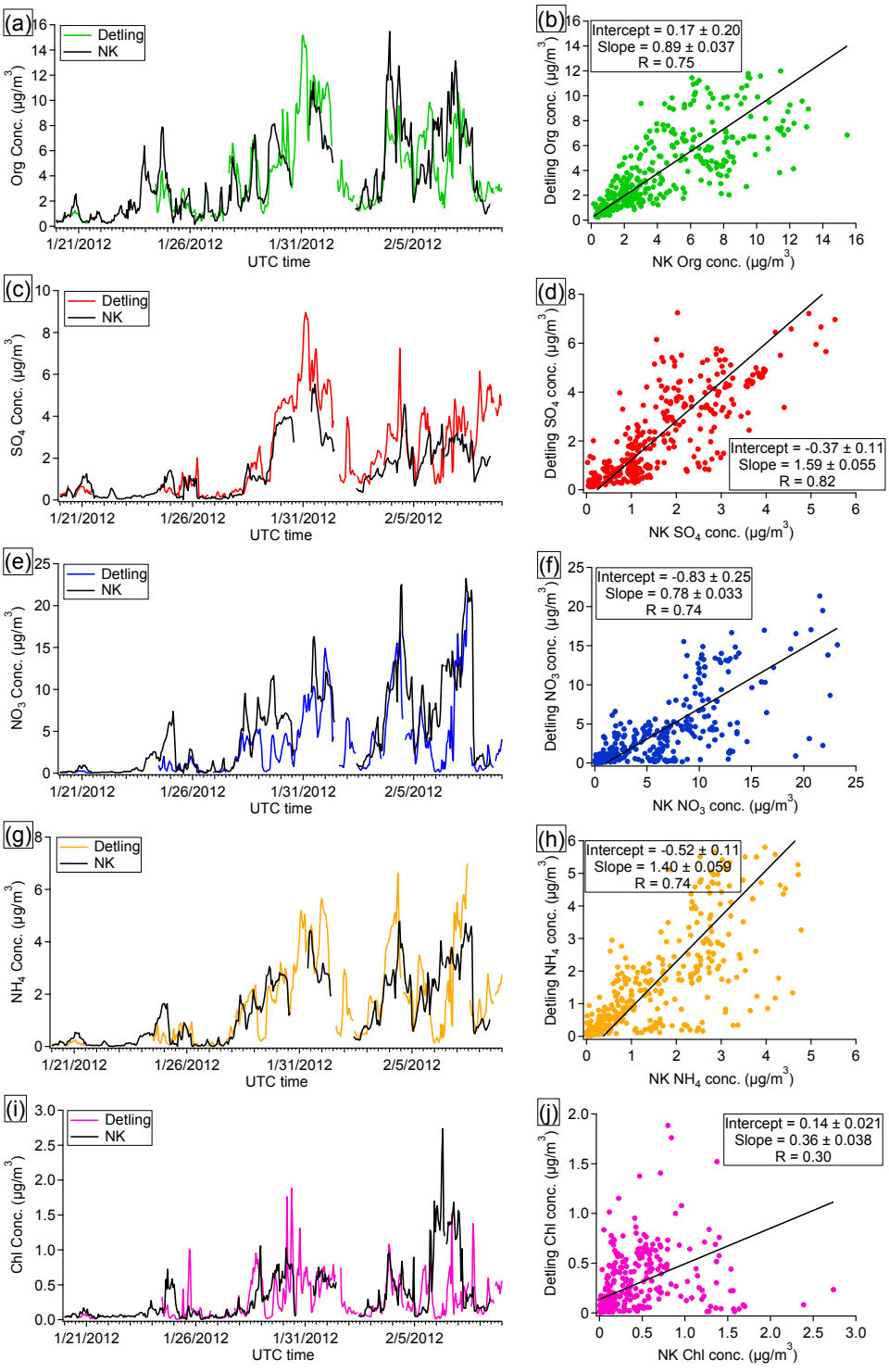

Figure A.7. Comparison of non-refractory species time series between NK and Detling sites. The intercept and slope are obtained by orthogonal distance regression. The Pearson's R is obtained by linear least-squares fit.

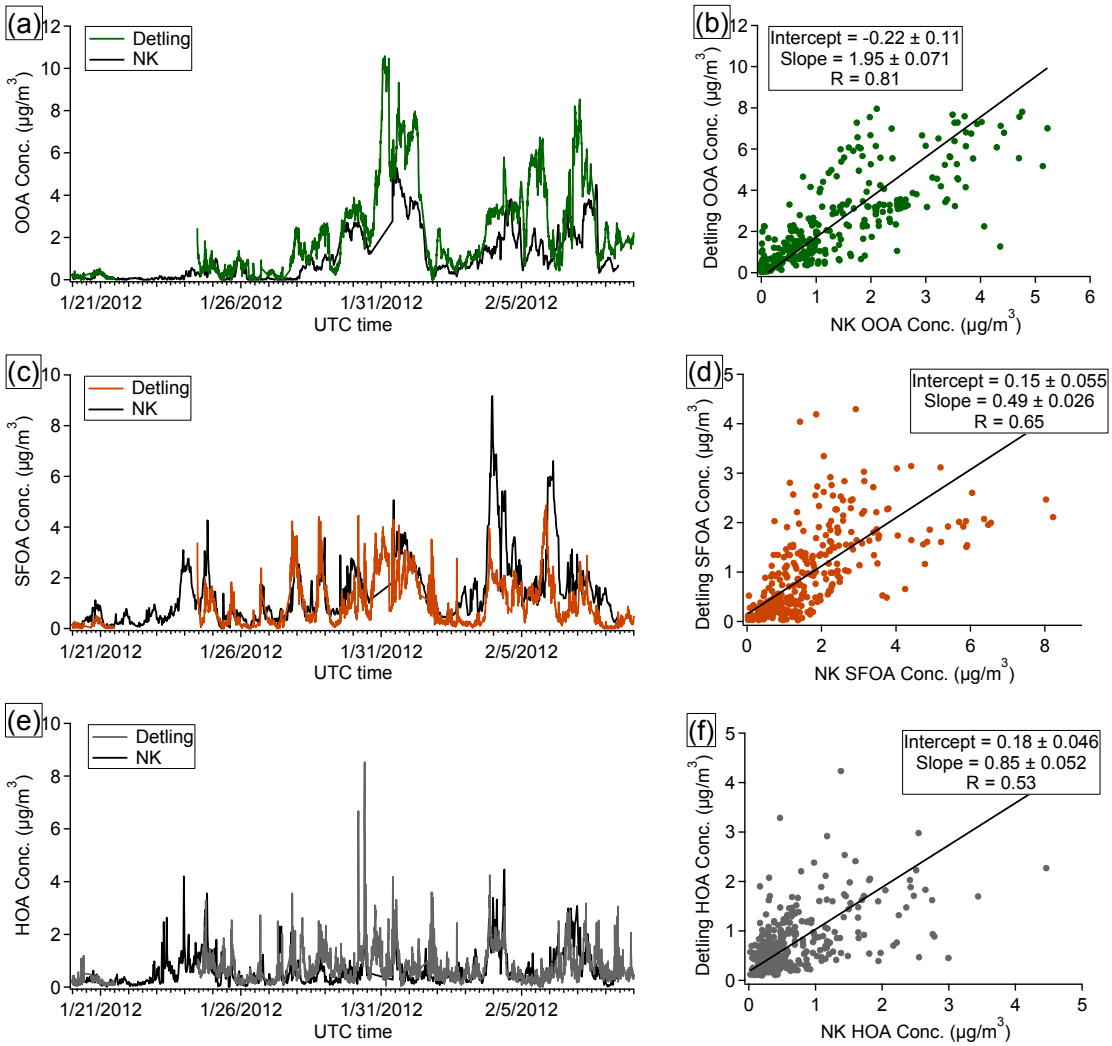

Figure A.8. Comparison of OA factors time series between NK and Detling sites. The intercept and slope are obtained by orthogonal distance regression. The Pearson's R is obtained by linear least-squares fit.

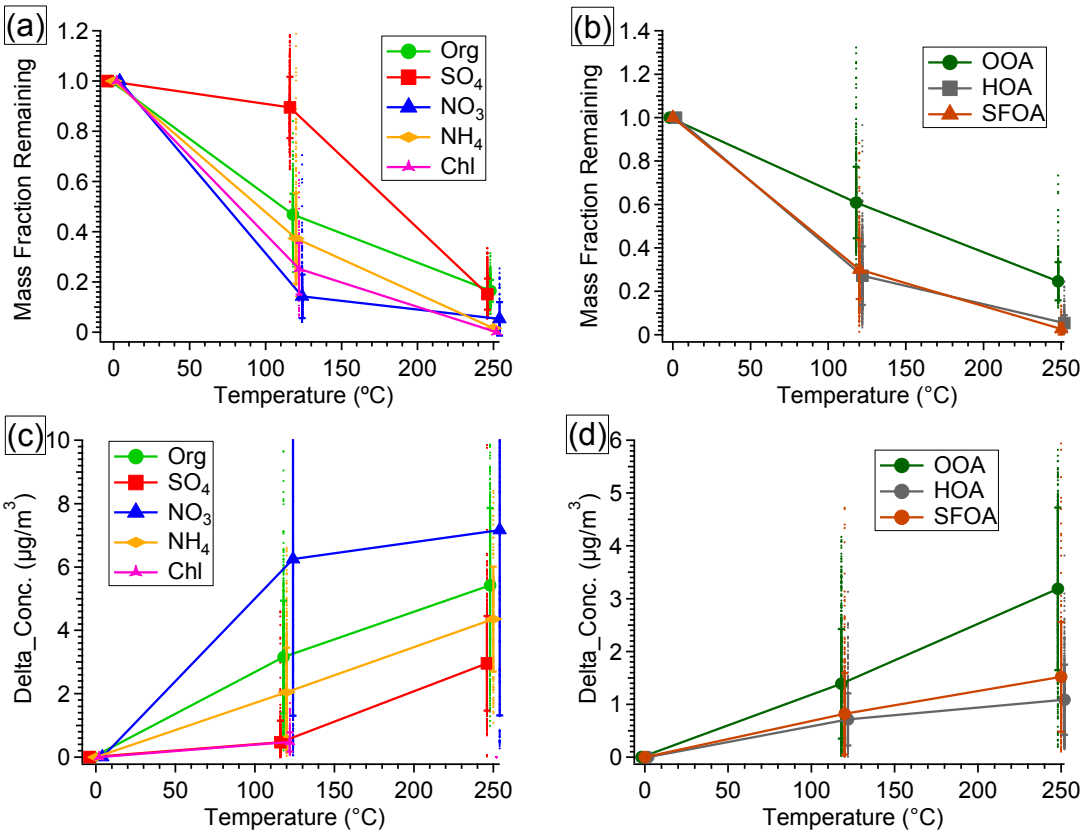

Figure A.9. Thermogram of (a) non-refractory species and (b) OA factors. The change in mass concentration after heating in the TD (i.e., ΔC) of (c) non-refractory species and (d) OA factors. Error bars indicate one standard deviation. The average values are connected by lines to guide the eyes.

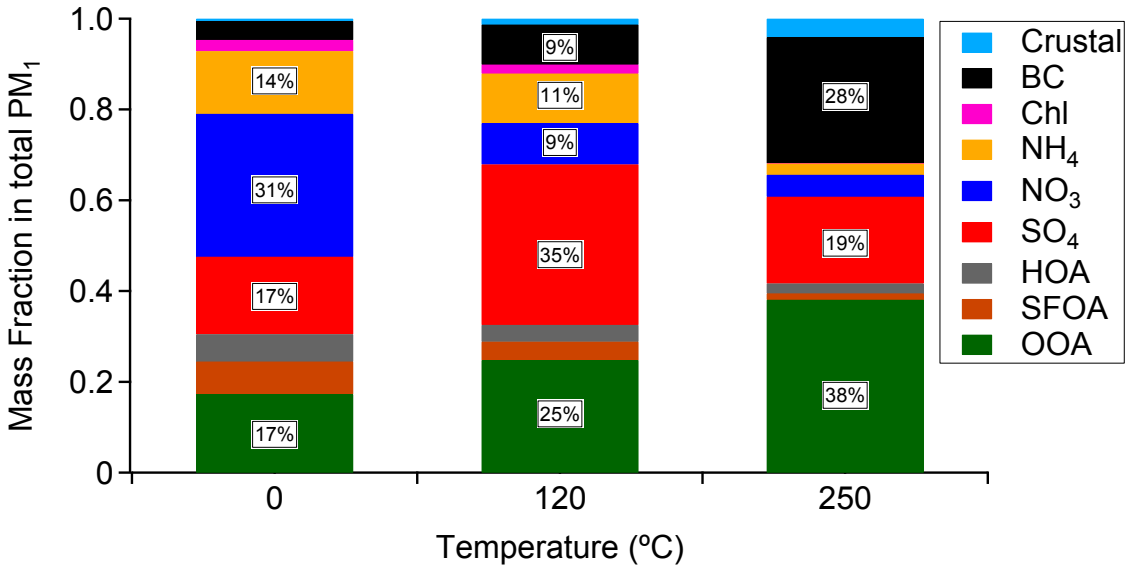

Figure A.10. Mass fraction of PM_1 species for bypass line and TD line (i.e., 120°C and 250°C). The mass fractions larger than 9% are labeled in the figure.

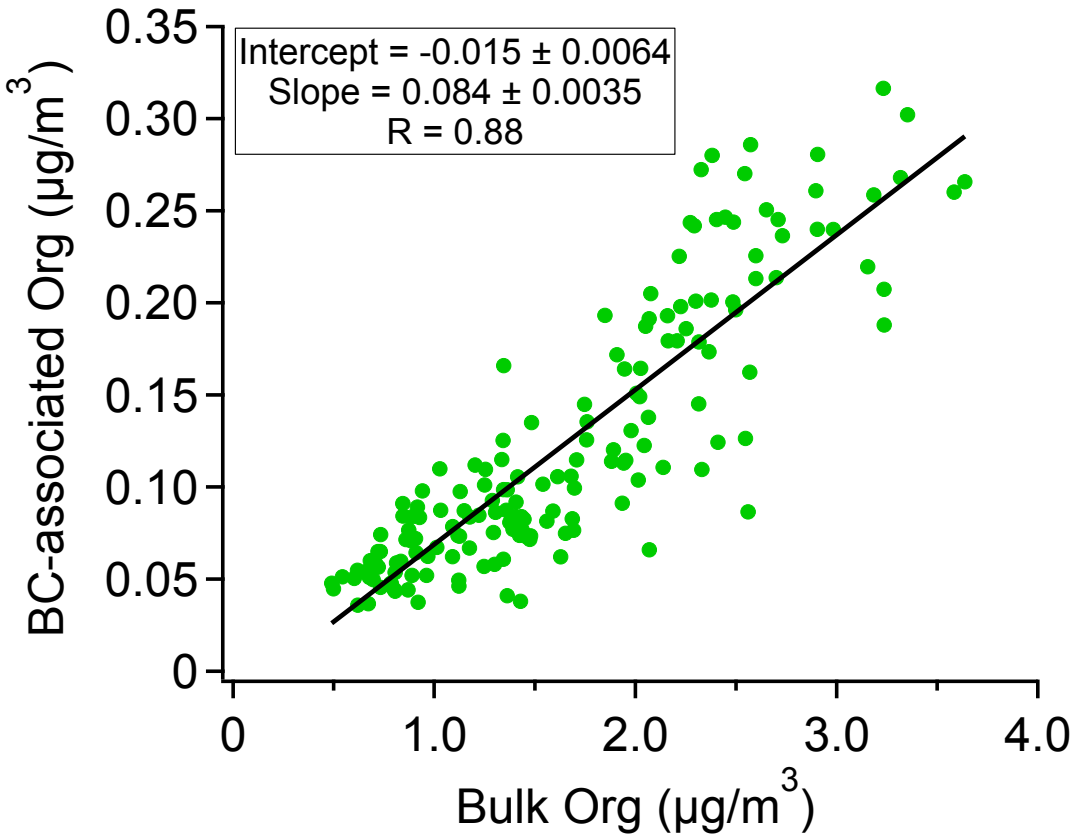

Figure A.11. Comparison between organics associated with rBC (measured by SP-AMS with laser vaporizer only) and the non-refractory organics in the bulk measurement (by HR-ToF-AMS) after heating at 250°C.

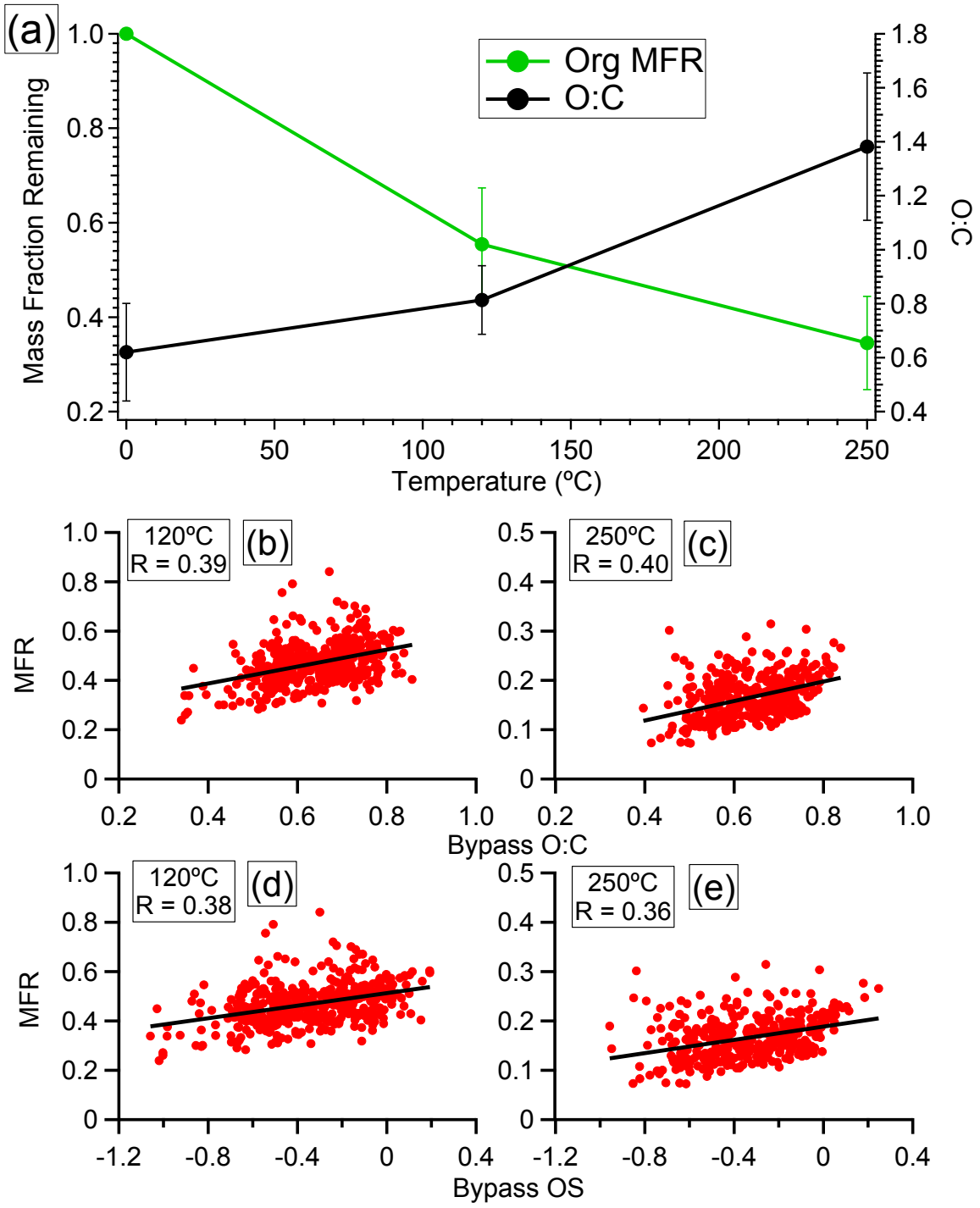

Figure A.12. (a) Organic mass fraction remaining (MFR) and O:C as a function of TD temperature; (b) – (e) organic MFR at 120°C and 250°C as a function of bypass line organic O:C and oxidation state.

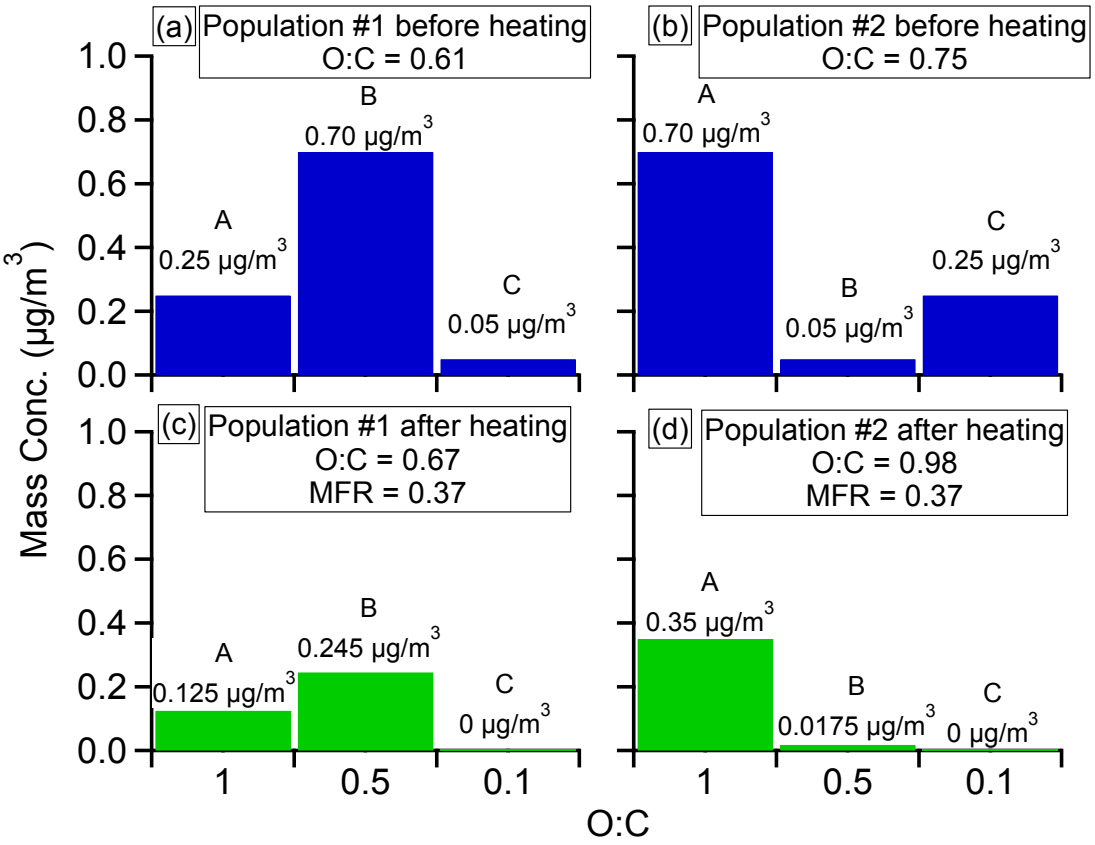

Figure A.13. The properties (O:C and volatility) of three model compounds and the composition of two populations of particles used in the simple model to illustrate the relationship between bulk OA O:C and volatility. The O:C is 1, 0.5, and 0.1 for compound A, B, and C, respectively. Upon heating at temperature T0, 50%, 65% and 100% of A, B, and C would evaporate. Population #1 is comprised of 0.25, 0.7, and 0.05 µg m^{-3} of A, B, and C, respectively, and population #2 is comprised of 0.7, 0.05, and 0.25 µg m^{-3} of A, B, and C, respectively.

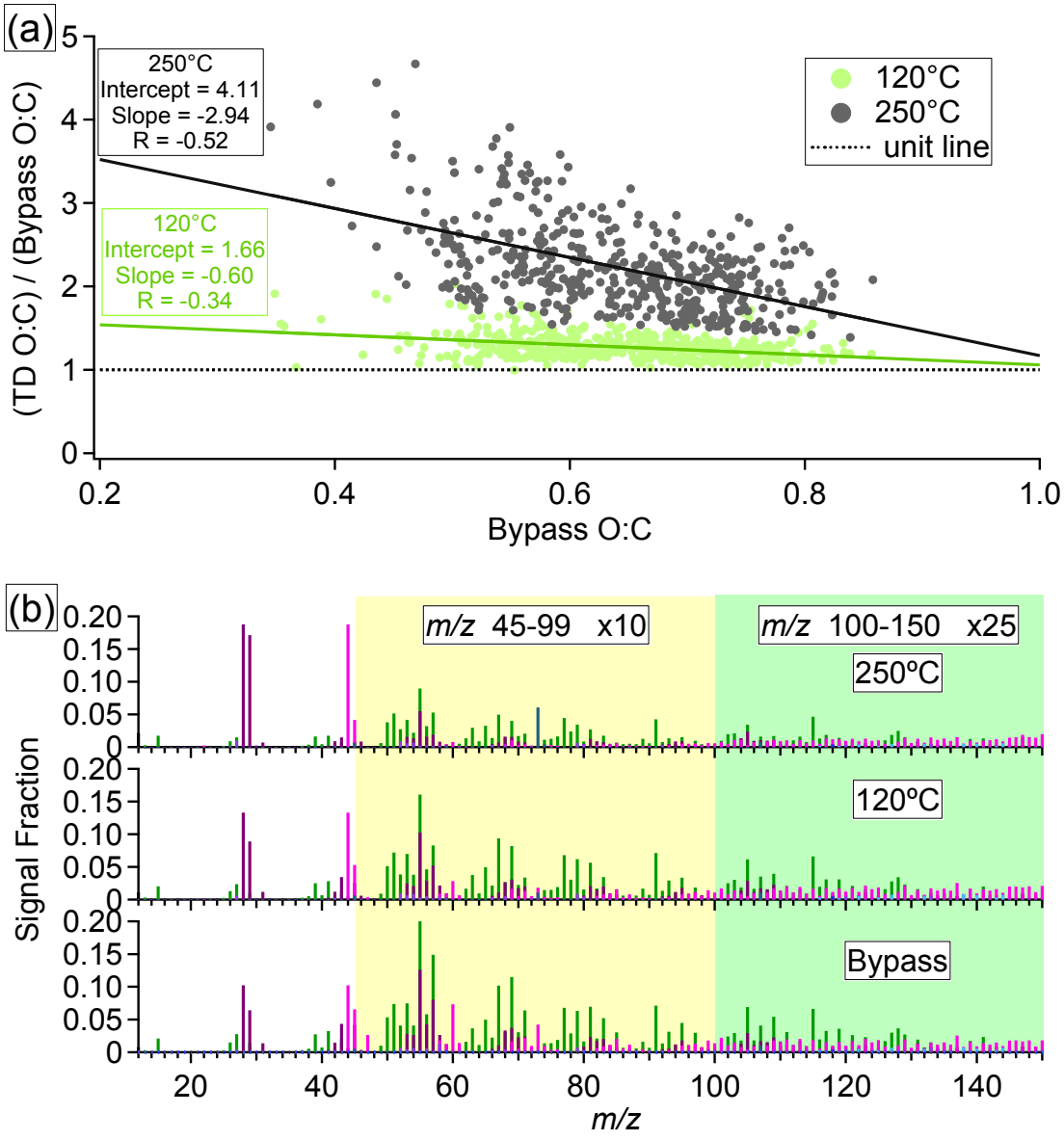

Figure A.14. (a) O:C enhancement (i.e., ratio of TD line O:C to bypass line O:C) as a function of bypass line O:C. (b) Mass spectra of OA under different TD temperatures. The signals between *m/z* 45 and 99 are multiplied by 10 and the signals between *m/z* 100 and 150 are multiplied by 25 for clarity. The mass spectra are colored by the ion type in the same way as Figure A.4b.

REFERENCES

Aiken, A. C., DeCarlo, P. F., and Jimenez, J. L.: Elemental Analysis of Organic Species with Electron Ionization High-Resolution Mass Spectrometry, Anal Chem, 79, 8350-8358, 10.1021/ac071150w, 2007.

Aiken, A. C., Decarlo, P. F., Kroll, J. H., Worsnop, D. R., Huffman, J. A., Docherty, K. S., Ulbrich, I. M., Mohr, C., Kimmel, J. R., Sueper, D., Sun, Y., Zhang, Q., Trimborn, A., Northway, M., Ziemann, P. J., Canagaratna, M. R., Onasch, T. B., Alfarra, M. R., Prevot, A. S. H., Dommen, J., Duplissy, J., Metzger, A., Baltensperger, U., and Jimenez, J. L.: O/C and OM/OC ratios of primary, secondary, and ambient organic aerosols with high-resolution time-of-flight aerosol mass spectrometry, Environ Sci Technol, 42, 4478-4485, Doi 10.1021/Es703009q, 2008.

Aiken, A. C., Salcedo, D., Cubison, M. J., Huffman, J. A., DeCarlo, P. F., Ulbrich, I. M., Docherty, K. S., Sueper, D., Kimmel, J. R., Worsnop, D. R., Trimborn, A., Northway, M., Stone, E. A., Schauer, J. J., Volkamer, R. M., Fortner, E., de Foy, B., Wang, J., Laskin, A., Shutthanandan, V., Zheng, J., Zhang, R., Gaffney, J., Marley, N. A., Paredes-Miranda, G., Arnott, W. P., Molina, L. T., Sosa, G., and Jimenez, J. L.: Mexico City aerosol analysis during MILAGRO using high resolution aerosol mass spectrometry at the urban supersite (T0) – Part 1: Fine particle composition and organic source apportionment, Atmos. Chem. Phys., 9, 6633-6653, 10.5194/acp-9-6633-2009, 2009.

Alfarra, M. R., Coe, H., Allan, J. D., Bower, K. N., Boudries, H., Canagaratna, M. R., Jimenez, J. L., Jayne, J. T., Garforth, A. A., Li, S. M., and Worsnop, D. R.: Characterization of urban and rural organic particulate in the lower Fraser valley using two aerodyne aerosol mass spectrometers, Atmospheric Environment, 38, 5745-5758, DOI 10.1016/j.atmosenv.2004.01.054, 2004.

Allan, J. D., Bower, K. N., Coe, H., Boudries, H., Jayne, J. T., Canagaratna, M. R., Millet, D. B., Goldstein, A. H., Quinn, P. K., Weber, R. J., and Worsnop, D. R.: Submicron aerosol composition at Trinidad Head, California, during ITCT 2K2: Its relationship with gas phase volatile organic carbon and assessment of instrument performance, Journal of Geophysical Research: Atmospheres, 109, D23S24, 10.1029/2003JD004208, 2004.

Allan, J. D., Williams, P. I., Morgan, W. T., Martin, C. L., Flynn, M. J., Lee, J., Nemitz, E., Phillips, G. J., Gallagher, M. W., and Coe, H.: Contributions from transport, solid fuel burning and cooking to primary organic aerosols in two UK cities, Atmos. Chem. Phys., 10, 647-668, 10.5194/acp-10-647-2010, 2010.

Allan, J. D., Morgan, W. T., Darbyshire, E., Flynn, M. J., Williams, P. I., Oram, D. E., Artaxo, P., Brito, J., Lee, J. D., and Coe, H.: Airborne observations of IEPOX-

derived isoprene SOA in the Amazon during SAMBBA, Atmos. Chem. Phys., 14, 11393-11407, 10.5194/acp-14-11393-2014, 2014.

An, W. J., Pathak, R. K., Lee, B. H., and Pandis, S. N.: Aerosol volatility measurement using an improved thermodenuder: Application to secondary organic aerosol, J Aerosol Sci, 38, 305-314, DOI 10.1016/j.jaerosci.2006.12.002, 2007.

Andreae, M. O., and Gelencsér, A.: Black carbon or brown carbon? The nature of light-absorbing carbonaceous aerosols, Atmos. Chem. Phys., 6, 3131-3148, 10.5194/acp-6-3131-2006, 2006.

Atkinson, R.: Gas-phase tropospheric chemistry of volatile organic compounds .1. Alkanes and alkenes, J Phys Chem Ref Data, 26, 215-290, 1997.

Atkinson, R., and Arey, J.: Atmospheric degradation of volatile organic compounds, Chemical Reviews, 103, 4605-4638, 2003a.

Atkinson, R., and Arey, J.: Gas-phase tropospheric chemistry of biogenic volatile organic compounds: a review, Atmospheric Environment, 37, S197-S219, Doi 10.1016/S1352-2310(03)00391-1, 2003b.

Atkinson, R.: Rate constants for the atmospheric reactions of alkoxy radicals: An updated estimation method, Atmospheric Environment, 41, 8468-8485, DOI 10.1016/j.atmosenv.2007.07.002, 2007.

Baasandorj, M., Papanastasiou, D. K., Talukdar, R. K., Hasson, A. S., and Burkholder, J. B.: (CH3)(3)COOH (tert-butyl hydroperoxide): OH reaction rate coefficients between 206 and 375 K and the OH photolysis quantum yield at 248 nm, Phys Chem Chem Phys, 12, 12101-12111, Doi 10.1039/C0cp00463d, 2010.

Bae, M. S., Schwab, J. J., Zhang, Q., Hogrefe, O., Demerjian, K. L., Weimer, S., Rhoads, K., Orsini, D., Venkatachari, P., and Hopke, P. K.: Interference of organic signals in highly time resolved nitrate measurements by low mass resolution aerosol mass spectrometry, J Geophys Res-Atmos, 112, Artn D22305 Doi 10.1029/2007jd008614, 2007.

Bahreini, R., Dunlea, E. J., Matthew, B. M., Simons, C., Docherty, K. S., DeCarlo, P. F., Jimenez, J. L., Brock, C. A., and Middlebrook, A. M.: Design and Operation of a Pressure-Controlled Inlet for Airborne Sampling with an Aerodynamic Aerosol Lens, Aerosol Sci Tech, 42, 465-471, 10.1080/02786820802178514, 2008.

Bahreini, R., Ervens, B., Middlebrook, A. M., Warneke, C., de Gouw, J. A., DeCarlo, P. F., Jimenez, J. L., Brock, C. A., Neuman, J. A., Ryerson, T. B., Stark, H., Atlas, E., Brioude, J., Fried, A., Holloway, J. S., Peischl, J., Richter, D., Walega, J., Weibring, P., Wollny, A. G., and Fehsenfeld, F. C.: Organic aerosol formation in urban and

industrial plumes near Houston and Dallas, Texas, Journal of Geophysical Research: Atmospheres, 114, D00F16, 10.1029/2008JD011493, 2009.

Bates, K. H., Crounse, J. D., St. Clair, J. M., Bennett, N. B., Nguyen, T. B., Seinfeld, J. H., Stoltz, B. M., and Wennberg, P. O.: Gas Phase Production and Loss of Isoprene Epoxydiols, The Journal of Physical Chemistry A, 118, 1237-1246, 10.1021/jp4107958, 2014.

Baumgardner, D., Popovicheva, O., Allan, J., Bernardoni, V., Cao, J., Cavalli, F., Cozic, J., Diapouli, E., Eleftheriadis, K., Genberg, P. J., Gonzalez, C., Gysel, M., John, A., Kirchstetter, T. W., Kuhlbusch, T. A. J., Laborde, M., Lack, D., Muller, T., Niessner, R., Petzold, A., Piazzalunga, A., Putaud, J. P., Schwarz, J., Sheridan, P., Subramanian, R., Swietlicki, E., Valli, G., Vecchi, R., and Viana, M.: Soot reference materials for instrument calibration and intercomparisons: a workshop summary with recommendations, Atmos Meas Tech, 5, 1869-1887, DOI 10.5194/amt-5-1869-2012, 2012.

Beddows, D. C. S., Harrison, R. M., Green, D. C., and Fuller, G. W.: Receptor modelling of both particle composition and size distribution from a background site in London, UK, Atmos. Chem. Phys. Discuss., 15, 10123-10162, 10.5194/acpd-15-10123-2015, 2015.

Beekmann, M., Prévôt, A. S. H., Drewnick, F., Sciare, J., Pandis, S. N., Denier van der Gon, H. A. C., Crippa, M., Freutel, F., Poulain, L., Ghersi, V., Rodriguez, E., Beirle, S., Zotter, P., von der Weiden-Reinmüller, S. L., Bressi, M., Fountoukis, C., Petetin, H., Szidat, S., Schneider, J., Rosso, A., El Haddad, I., Megaritis, A., Zhang, Q. J., Michoud, V., Slowik, J. G., Moukhtar, S., Kolmonen, P., Stohl, A., Eckhardt, S., Borbon, A., Gros, V., Marchand, N., Jaffrezo, J. L., Schwarzenboeck, A., Colomb, A., Wiedensohler, A., Borrmann, S., Lawrence, M., Baklanov, A., and Baltensperger, U.: In situ, satellite measurement and model evidence on the dominant regional contribution to fine particulate matter levels in the Paris megacity, Atmos. Chem. Phys., 15, 9577-9591, 10.5194/acp-15-9577-2015, 2015.

Bertman, S. B., and Roberts, J. M.: A Pan Analog from Isoprene Photooxidation, Geophysical Research Letters, 18, 1461-1464, Doi 10.1029/91gl01852, 1991.

Bethel, H. L., Atkinson, R., and Arey, J.: Hydroxycarbonyl products of the reactions of selected diols with the OH radical, J Phys Chem A, 107, 6200-6205, Doi 10.1021/Jp0276931, 2003.

Bin Lim, Y., and Ziemann, P. J.: Kinetics of the heterogeneous conversion of 1,4-hydroxycarbonyls to cyclic hemiacetals and dihydrofurans on organic aerosol particles, Phys Chem Chem Phys, 11, 8029-8039, Doi 10.1039/B904333k, 2009.

Blanchard, C. L., Hidy, G. M., Tanenbaum, S., Edgerton, E., Hartsell, B., and Jansen, J.: Carbon in southeastern U.S. aerosol particles: Empirical estimates of secondary organic aerosol formation, Atmospheric Environment, 42, 6710-6720, dx.doi.org/10.1016/j.atmosenv.2008.04.011, 2008.

Blanchard, C. L., Hidy, G. M., Tanenbaum, S., and Edgerton, E. S.: NMOC, ozone, and organic aerosol in the southeastern United States, 1999-2007: 3. Origins of organic aerosol in Atlanta, Georgia, and surrounding areas, Atmospheric Environment, 45, 1291-1302, DOI 10.1016/j.atmosenv.2010.12.004, 2011.

Blanchard, C. L., Hidy, G. M., Tanenbaum, S., Edgerton, E. S., and Hartsell, B. E.: The Southeastern Aerosol Research and Characterization (SEARCH) study: Spatial variations and chemical climatology, 1999–2010, J Air Waste Manage, 63, 260-275, 10.1080/10962247.2012.749816, 2013.

Blanchard, C. L., Hidy, G. M., Shaw, S., Baumann, K., and Edgerton, E. S.: Effects of emission reductions on organic aerosol in the southeastern United States, Atmos. Chem. Phys. Discuss., 15, 17051-17092, 10.5194/acpd-15-17051-2015, 2015.

Bohnenstengel, S. I., Belcher, S. E., Aiken, A., Allan, J. D., Allen, G., Bacak, A., Bannan, T. J., Barlow, J. F., Beddows, D. C. S., Bloss, W. J., Booth, A. M., Chemel, C., Coceal, O., Di Marco, C. F., Dubey, M. K., Faloon, K. H., Fleming, Z. L., Furger, M., Gietl, J. K., Graves, R. R., Green, D. C., Grimmond, C. S. B., Halios, C. H., Hamilton, J. F., Harrison, R. M., Heal, M. R., Heard, D. E., Helfter, C., Herndon, S. C., Holmes, R. E., Hopkins, J. R., Jones, A. M., Kelly, F. J., Kotthaus, S., Langford, B., Lee, J. D., Leigh, R. J., Lewis, A. C., Lidster, R. T., Lopez-Hilfiker, F. D., McQuaid, J. B., Mohr, C., Monks, P. S., Nemitz, E., Ng, N. L., Percival, C. J., Prévôt, A. S. H., Ricketts, H. M. A., Sokhi, R., Stone, D., Thornton, J. A., Tremper, A. H., Valach, A. C., Visser, S., Whalley, L. K., Williams, L. R., Xu, L., Young, D. E., and Zotter, P.: Meteorology, Air Quality, and Health in London: The ClearfLo Project, B Am Meteorol Soc, 96, 779-804, 10.1175/BAMS-D-12-00245.1, 2014.

Bougiatioti, A., Stavroulas, I., Kostenidou, E., Zarmpas, P., Theodosi, C., Kouvarakis, G., Canonaco, F., Prévôt, A. S. H., Nenes, A., Pandis, S. N., and Mihalopoulos, N.: Processing of biomass-burning aerosol in the eastern Mediterranean during summertime, Atmos. Chem. Phys., 14, 4793-4807, 10.5194/acp-14-4793-2014, 2014.

Boyd, C. M., Sanchez, J., Xu, L., Eugene, A. J., Nah, T., Tuet, W. Y., Guzman, M. I., and Ng, N. L.: Secondary Organic Aerosol (SOA) formation from the β-pinene + NO3 system: effect of humidity and peroxy radical fate, Atmos. Chem. Phys. Discuss., 15, 2679-2744, 10.5194/acpd-15-2679-2015, 2015.

Brock, C. A., Washenfelder, R. A., Trainer, M., Ryerson, T. B., Wilson, J. C., Reeves, J. M., Huey, L. G., Holloway, J. S., Parrish, D. D., Hübler, G., and Fehsenfeld, F. C.: Particle growth in the plumes of coal-fired power plants, Journal of Geophysical Research: Atmospheres, 107, AAC 9-1-AAC 9-14, 10.1029/2001JD001062, 2002.

Brock, C. A., Trainer, M., Ryerson, T. B., Neuman, J. A., Parrish, D. D., Holloway, J. S., Nicks, D. K., Frost, G. J., Hubler, G., Fehsenfeld, F. C., Wilson, J. C., Reeves, J. M., Lafleur, B. G., Hilbert, H., Atlas, E. L., Donnelly, S. G., Schauffler, S. M., Stroud, V. R., and Wiedinmyer, C.: Particle growth in urban and industrial plumes in Texas, J Geophys Res-Atmos, 108, Artn 4111
Doi 10.1029/2002jd002746, 2003.

Brock, C. A., Wagner, N. L., Anderson, B. E., Attwood, A. R., Beyersdorf, A., Campuzano-Jost, P., Carlton, A. G., Day, D. A., Diskin, G. S., Gordon, T. D., Jimenez, J. L., Lack, D. A., Liao, J., Markovic, M. Z., Middlebrook, A. M., Ng, N. L., Perring, A. E., Richardson, M. S., Schwarz, J. P., Washenfelder, R. A., Welti, A., Xu, L., Ziemba, L. D., and Murphy, D. M.: Aerosol optical properties in the southeastern United States in summer – Part 1: Hygroscopic growth, Atmos. Chem. Phys. Discuss., 15, 25695-25738, 10.5194/acpd-15-25695-2015, 2015.

Bruns, E. A., Perraud, V., Zelenyuk, A., Ezell, M. J., Johnson, S. N., Yu, Y., Imre, D., Finlayson-Pitts, B. J., and Alexander, M. L.: Comparison of FTIR and Particle Mass Spectrometry for the Measurement of Particulate Organic Nitrates, Environ Sci Technol, 44, 1056-1061, 10.1021/es9029864, 2010.

Budisulistiorini, S. H., Canagaratna, M. R., Croteau, P. L., Marth, W. J., Baumann, K., Edgerton, E. S., Shaw, S. L., Knipping, E. M., Worsnop, D. R., Jayne, J. T., Gold, A., and Surratt, J. D.: Real-Time Continuous Characterization of Secondary Organic Aerosol Derived from Isoprene Epoxydiols in Downtown Atlanta, Georgia, Using the Aerodyne Aerosol Chemical Speciation Monitor, Environ Sci Technol, 47, 5686-5694, Doi 10.1021/Es400023n, 2013.

Budisulistiorini, S. H., Li, X., Bairai, S. T., Renfro, J., Liu, Y., Liu, Y. J., McKinney, K. A., Martin, S. T., McNeill, V. F., Pye, H. O. T., Nenes, A., Neff, M. E., Stone, E. A., Mueller, S., Knote, C., Shaw, S. L., Zhang, Z., Gold, A., and Surratt, J. D.: Examining the effects of anthropogenic emissions on isoprene-derived secondary organic aerosol formation during the 2013 Southern Oxidant and Aerosol Study (SOAS) at the Look Rock, Tennessee ground site, Atmos. Chem. Phys., 15, 8871-8888, 10.5194/acp-15-8871-2015, 2015.

Canagaratna, M. R., Jayne, J. T., Jimenez, J. L., Allan, J. D., Alfarra, M. R., Zhang, Q., Onasch, T. B., Drewnick, F., Coe, H., Middlebrook, A., Delia, A., Williams, L. R., Trimborn, A. M., Northway, M. J., DeCarlo, P. F., Kolb, C. E., Davidovits, P., and Worsnop, D. R.: Chemical and microphysical characterization of ambient aerosols

with the aerodyne aerosol mass spectrometer, Mass Spectrometry Reviews, 26, 185-222, 10.1002/mas.20115, 2007.

Canagaratna, M. R., Jimenez, J. L., Kroll, J. H., Chen, Q., Kessler, S. H., Massoli, P., Hildebrandt Ruiz, L., Fortner, E., Williams, L. R., Wilson, K. R., Surratt, J. D., Donahue, N. M., Jayne, J. T., and Worsnop, D. R.: Elemental ratio measurements of organic compounds using aerosol mass spectrometry: characterization, improved calibration, and implications, Atmos. Chem. Phys., 15, 253-272, 10.5194/acp-15-253-2015, 2015.

Canonaco, F., Crippa, M., Slowik, J. G., Baltensperger, U., and Prévôt, A. S. H.: SoFi, an IGOR-based interface for the efficient use of the generalized multilinear engine (ME-2) for the source apportionment: ME-2 application to aerosol mass spectrometer data, Atmos. Meas. Tech., 6, 3649-3661, 10.5194/amt-6-3649-2013, 2013.

Cappa, C. D., and Jimenez, J. L.: Quantitative estimates of the volatility of ambient organic aerosol, Atmos. Chem. Phys., 10, 5409-5424, 10.5194/acp-10-5409-2010, 2010.

Carlton, A. G., Wiedinmyer, C., and Kroll, J. H.: A review of Secondary Organic Aerosol (SOA) formation from isoprene, Atmos Chem Phys, 9, 4987-5005, 2009.

Carlton, A. G., Pinder, R. W., Bhave, P. V., and Pouliot, G. A.: To What Extent Can Biogenic SOA be Controlled?, Environ Sci Technol, 44, 3376-3380, Doi 10.1021/Es903506b, 2010.

Carlton, A. G., and Turpin, B. J.: Particle partitioning potential of organic compounds is highest in the Eastern US and driven by anthropogenic water, Atmos. Chem. Phys., 13, 10203-10214, 10.5194/acp-13-10203-2013, 2013.

Cerully, K. M., Bougiatioti, A., Hite Jr, J. R., Guo, H., Xu, L., Ng, N. L., Weber, R., and Nenes, A.: On the link between hygroscopicity, volatility, and oxidation state of ambient and water-soluble aerosols in the southeastern United States, Atmos. Chem. Phys., 15, 8679-8694, 10.5194/acp-15-8679-2015, 2015.

Chameides, W. L., Lindsay, R. W., Richardson, J., and Kiang, C. S.: The Role of Biogenic Hydrocarbons in Urban Photochemical Smog - Atlanta as a Case-Study, Science, 241, 1473-1475, DOI 10.1126/science.3420404, 1988.

Chan, A. W. H., Kroll, J. H., Ng, N. L., and Seinfeld, J. H.: Kinetic modeling of secondary organic aerosol formation: effects of particle- and gas-phase reactions of semivolatile products, Atmos Chem Phys, 7, 4135-4147, 2007.

Chan, A. W. H., Chan, M. N., Surratt, J. D., Chhabra, P. S., Loza, C. L., Crounse, J. D., Yee, L. D., Flagan, R. C., Wennberg, P. O., and Seinfeld, J. H.: Role of aldehyde

chemistry and NOx concentrations in secondary organic aerosol formation, Atmos Chem Phys, 10, 7169-7188, DOI 10.5194/acp-10-7169-2010, 2010a.

Chan, M. N., Surratt, J. D., Claeys, M., Edgerton, E. S., Tanner, R. L., Shaw, S. L., Zheng, M., Knipping, E. M., Eddingsaas, N. C., Wennberg, P. O., and Seinfeld, J. H.: Characterization and Quantification of Isoprene-Derived Epoxydiols in Ambient Aerosol in the Southeastern United States, Environ Sci Technol, 44, 4590-4596, Doi 10.1021/Es100596b, 2010b.

Charron, A., Degrendele, C., Laongsri, B., and Harrison, R. M.: Receptor modelling of secondary and carbonaceous particulate matter at a southern UK site, Atmos. Chem. Phys., 13, 1879-1894, 10.5194/acp-13-1879-2013, 2013.

Chen, Q., Farmer, D. K., Rizzo, L. V., Pauliquevis, T., Kuwata, M., Karl, T. G., Guenther, A., Allan, J. D., Coe, H., Andreae, M. O., Pöschl, U., Jimenez, J. L., Artaxo, P., and Martin, S. T.: Fine-mode organic mass concentrations and sources in the Amazonian wet season (AMAZE-08), Atmos. Chem. Phys. Discuss., 14, 16151-16186, 10.5194/acpd-14-16151-2014, 2014.

Chen, Q., Farmer, D. K., Rizzo, L. V., Pauliquevis, T., Kuwata, M., Karl, T. G., Guenther, A., Allan, J. D., Coe, H., Andreae, M. O., Pöschl, U., Jimenez, J. L., Artaxo, P., and Martin, S. T.: Submicron particle mass concentrations and sources in the Amazonian wet season (AMAZE-08), Atmos. Chem. Phys., 15, 3687-3701, 10.5194/acp-15-3687-2015, 2015.

Claeys, M., Graham, B., Vas, G., Wang, W., Vermeylen, R., Pashynska, V., Cafmeyer, J., Guyon, P., Andreae, M. O., Artaxo, P., and Maenhaut, W.: Formation of secondary organic aerosols through photooxidation of isoprene, Science, 303, 1173-1176, DOI 10.1126/science.1092805, 2004a.

Claeys, M., Wang, W., Ion, A. C., Kourtchev, I., Gelencser, A., and Maenhaut, W.: Formation of secondary organic aerosols from isoprene and its gas-phase oxidation products through reaction with hydrogen peroxide, Atmospheric Environment, 38, 4093-4098, DOI 10.1016/j.atmosenv.2004.06.001, 2004b.

Cohan, D., Boylan, J., Marmur, A., and Khan, M.: An Integrated Framework for Multipollutant Air Quality Management and Its Application in Georgia, Environmental Management, 40, 545-554, 10.1007/s00267-006-0228-4, 2007.

Crilley, L. R., Bloss, W. J., Yin, J., Beddows, D. C. S., Harrison, R. M., Allan, J. D., Young, D. E., Flynn, M., Williams, P., Zotter, P., Prevot, A. S. H., Heal, M. R., Barlow, J. F., Halios, C. H., Lee, J. D., Szidat, S., and Mohr, C.: Sources and contributions of wood smoke during winter in London: assessing local and regional influences, Atmos. Chem. Phys., 15, 3149-3171, 10.5194/acp-15-3149-2015, 2015.

Crippa, M., DeCarlo, P. F., Slowik, J. G., Mohr, C., Heringa, M. F., Chirico, R., Poulain, L., Freutel, F., Sciare, J., Cozic, J., Di Marco, C. F., Elsasser, M., Nicolas, J. B., Marchand, N., Abidi, E., Wiedensohler, A., Drewnick, F., Schneider, J., Borrmann, S., Nemitz, E., Zimmermann, R., Jaffrezo, J. L., Prévôt, A. S. H., and Baltensperger, U.: Wintertime aerosol chemical composition and source apportionment of the organic fraction in the metropolitan area of Paris, Atmos. Chem. Phys., 13, 961-981, 10.5194/acp-13-961-2013, 2013.

Crippa, M., Canonaco, F., Lanz, V. A., Äijälä, M., Allan, J. D., Carbone, S., Capes, G., Ceburnis, D., Dall'Osto, M., Day, D. A., DeCarlo, P. F., Ehn, M., Eriksson, A., Freney, E., Hildebrandt Ruiz, L., Hillamo, R., Jimenez, J. L., Junninen, H., Kiendler-Scharr, A., Kortelainen, A. M., Kulmala, M., Laaksonen, A., Mensah, A. A., Mohr, C., Nemitz, E., O'Dowd, C., Ovadnevaite, J., Pandis, S. N., Petäjä, T., Poulain, L., Saarikoski, S., Sellegri, K., Swietlicki, E., Tiitta, P., Worsnop, D. R., Baltensperger, U., and Prévôt, A. S. H.: Organic aerosol components derived from 25 AMS data sets across Europe using a consistent ME-2 based source apportionment approach, Atmos. Chem. Phys., 14, 6159-6176, 10.5194/acp-14-6159-2014, 2014.

Crounse, J. D., Knap, H. C., Ornso, K. B., Jorgensen, S., Paulot, F., Kjaergaard, H. G., and Wennberg, P. O.: Atmospheric Fate of Methacrolein. 1. Peroxy Radical Isomerization Following Addition of OH and O-2, J Phys Chem A, 116, 5756-5762, Doi 10.1021/Jp211560u, 2012.

Day, D. A., Wooldridge, P. J., Dillon, M. B., Thornton, J. A., and Cohen, R. C.: A thermal dissociation laser-induced fluorescence instrument for in situ detection of NO2, peroxy nitrates, alkyl nitrates, and HNO3, Journal of Geophysical Research: Atmospheres, 107, ACH 4-1-ACH 4-14, 10.1029/2001JD000779, 2002.

de Gouw, Parrish, D. D., Frost, G. J., and Trainer, M.: Reduced emissions of CO2, NOx, and SO2 from U.S. power plants owing to switch from coal to natural gas with combined cycle technology, Earth's Future, 2, 75-82, 10.1002/2013EF000196, 2014.

de Gouw, Trainer, M., Brown, S. S., Edwards, P., Gilman, J. B., Graus, M., Hanisco, T., Kaiser, J., Keutsch, F. N., Kim, S.-W., Lerner, B. M., Neuman, J. A., Parrish, D. D., Pollack, B., Roberts, J. M., Ryerson, T. R., Veres, P. R., Warneke, C., and Wolfe, G. M.: Enhanced Removal of Biogenic Hydrocarbons in Power Plant Plumes Constrains the Dependence of Atmospheric Hydroxyl Concentrations on Nitrogen Oxides, In preparation, 2016.

de Gouw, J. A., Middlebrook, A. M., Warneke, C., Goldan, P. D., Kuster, W. C., Roberts, J. M., Fehsenfeld, F. C., Worsnop, D. R., Canagaratna, M. R., Pszenny, A. A. P., Keene, W. C., Marchewka, M., Bertman, S. B., and Bates, T. S.: Budget of organic carbon in a polluted atmosphere: Results from the New England Air Quality Study

in 2002, J Geophys Res-Atmos, 110, Artn D16305 Doi 10.1029/2004jd005623, 2005.

DeCarlo, P. F.: Field-Deployable, High-Resolution, Time-of-Flight Aerosol Mass Spectrometer, Anal. Chem., 78, 14, 2006.

DeCarlo, P. F., Kimmel, J. R., Trimborn, A., Northway, M. J., Jayne, J. T., Aiken, A. C., Gonin, M., Fuhrer, K., Horvath, T., Docherty, K. S., Worsnop, D. R., and Jimenez, J. L.: Field-Deployable, High-Resolution, Time-of-Flight Aerosol Mass Spectrometer, Anal Chem, 78, 8281-8289, 10.1021/ac061249n, 2006.

Denkenberger, K. A., Moffet, R. C., Holecek, J. C., Rebotier, T. P., and Prather, K. A.: Real-Time, Single-Particle Measurements of Oligomers in Aged Ambient Aerosol Particles, Environ Sci Technol, 41, 5439-5446, 10.1021/es070329l, 2007.

DeWitt, H. L., Hellebust, S., Temime-Roussel, B., Ravier, S., Polo, L., Jacob, V., Buisson, C., Charron, A., André, M., Pasquier, A., Besombes, J. L., Jaffrezo, J. L., Wortham, H., and Marchand, N.: Direct measurements of near-highway emissions in a high diesel environment, Atmos. Chem. Phys. Discuss., 14, 27373-27424, 10.5194/acpd-14-27373-2014, 2014.

Ding, X., Zheng, M., Yu, L. P., Zhang, X. L., Weber, R. J., Yan, B., Russell, A. G., Edgerton, E. S., and Wang, X. M.: Spatial and seasonal trends in biogenic secondary organic aerosol tracers and water-soluble organic carbon in the southeastern United States, Environ Sci Technol, 42, 5171-5176, Doi 10.1021/Es7032636, 2008.

Dommen, J., Metzger, A., Duplissy, J., Kalberer, M., Alfarra, M. R., Gascho, A., Weingartner, E., Prevot, A. S. H., Verheggen, B., and Baltensperger, U.: Laboratory observation of oligomers in the aerosol from isoprene/NO(x) photooxidation, Geophysical Research Letters, 33, Artn L13805
Doi 10.1029/2006gl026523, 2006.

Donahue, N. M., Epstein, S. A., Pandis, S. N., and Robinson, A. L.: A two-dimensional volatility basis set: 1. organic-aerosol mixing thermodynamics, Atmos. Chem. Phys., 11, 3303-3318, 10.5194/acp-11-3303-2011, 2011.

Donahue, N. M., Henry, K. M., Mentel, T. F., Kiendler-Scharr, A., Spindler, C., Bohn, B., Brauers, T., Dorn, H. P., Fuchs, H., Tillmann, R., Wahner, A., Saathoff, H., Naumann, K. H., Mohler, O., Leisner, T., Muller, L., Reinnig, M. C., Hoffmann, T., Salo, K., Hallquist, M., Frosch, M., Bilde, M., Tritscher, T., Barmet, P., Praplan, A. P., DeCarlo, P. F., Dommen, J., Prevot, A. S. H., and Baltensperger, U.: Aging of biogenic secondary organic aerosol via gas-phase OH radical reactions, P Natl Acad Sci USA, 109, 13503-13508, DOI 10.1073/pnas.1115186109, 2012.

Eddingsaas, N. C., VanderVelde, D. G., and Wennberg, P. O.: Kinetics and Products of the Acid-Catalyzed Ring-Opening of Atmospherically Relevant Butyl Epoxy Alcohols, J Phys Chem A, 114, 8106-8113, Doi 10.1021/Jp103907c, 2010.

Edgerton, E. S., Hartsell, B. E., Saylor, R. D., Jansen, J. J., Hansen, D. A., and Hidy, G. M.: The southeastern aerosol research and characterization study: Part II. Filter-based measurements of fine and coarse particulate matter mass and composition, J Air Waste Manage, 55, 1527-1542, 2005.

Ehn, M., Thornton, J. A., Kleist, E., Sipila, M., Junninen, H., Pullinen, I., Springer, M., Rubach, F., Tillmann, R., Lee, B., Lopez-Hilfiker, F., Andres, S., Acir, I.-H., Rissanen, M., Jokinen, T., Schobesberger, S., Kangasluoma, J., Kontkanen, J., Nieminen, T., Kurten, T., Nielsen, L. B., Jorgensen, S., Kjaergaard, H. G., Canagaratna, M., Maso, M. D., Berndt, T., Petaja, T., Wahner, A., Kerminen, V.-M., Kulmala, M., Worsnop, D. R., Wildt, J., and Mentel, T. F.: A large source of low-volatility secondary organic aerosol, Nature, 506, 476-479, 10.1038/nature13032, 2014.

El Haddad, I., D'Anna, B., Temime-Roussel, B., Nicolas, M., Boreave, A., Favez, O., Voisin, D., Sciare, J., George, C., Jaffrezo, J. L., Wortham, H., and Marchand, N.: Towards a better understanding of the origins, chemical composition and aging of oxygenated organic aerosols: case study of a Mediterranean industrialized environment, Marseille, Atmos. Chem. Phys., 13, 7875-7894, 10.5194/acp-13-7875-2013, 2013.

Farmer, D. K., Matsunaga, A., Docherty, K. S., Surratt, J. D., Seinfeld, J. H., Ziemann, P. J., and Jimenez, J. L.: Response of an aerosol mass spectrometer to organonitrates and organosulfates and implications for atmospheric chemistry, Proceedings of the National Academy of Sciences, 107, 6670-6675, 10.1073/pnas.0912340107, 2010.

Feng, Y., Ramanathan, V., and Kotamarthi, V. R.: Brown carbon: a significant atmospheric absorber of solar radiation?, Atmos. Chem. Phys., 13, 8607-8621, 10.5194/acp-13-8607-2013, 2013.

Fierz, M., Vernooij, M. G. C., and Burtscher, H.: An improved low-flow thermodenuder, J Aerosol Sci, 38, 1163-1168, DOI 10.1016/j.jaerosci.2007.08.006, 2007.

Fleming, Z. L., Monks, P. S., and Manning, A. J.: Review: Untangling the influence of air-mass history in interpreting observed atmospheric composition, Atmos Res, 104–105, 1-39, doi.org/10.1016/j.atmosres.2011.09.009, 2012.

Ford, B., and Heald, C. L.: Aerosol loading in the Southeastern United States: reconciling surface and satellite observations, Atmos Chem Phys, 13, 9269-9283, DOI 10.5194/acp-13-9269-2013, 2013.

Fountoukis, C., and Nenes, A.: ISORROPIA II: a computationally efficient thermodynamic equilibrium model for K+-Ca2+-Mg2+-NH(4)(+)-Na+-SO42--NO3--Cl--H2O aerosols, Atmos Chem Phys, 7, 4639-4659, 2007.

Froyd, K. D., Murphy, S. M., Murphy, D. M., de Gouw, J. A., Eddingsaas, N. C., and Wennberg, P. O.: Contribution of isoprene-derived organosulfates to free tropospheric aerosol mass, P Natl Acad Sci USA, 107, 21360-21365, DOI 10.1073/pnas.1012561107, 2010.

Fry, J. L., Kiendler-Scharr, A., Rollins, A. W., Wooldridge, P. J., Brown, S. S., Fuchs, H., Dube, W., Mensah, A., dal Maso, M., Tillmann, R., Dorn, H. P., Brauers, T., and Cohen, R. C.: Organic nitrate and secondary organic aerosol yield from NO3 oxidation of beta-pinene evaluated using a gas-phase kinetics/aerosol partitioning model, Atmos Chem Phys, 9, 1431-1449, 2009.

Fry, J. L., Kiendler-Scharr, A., Rollins, A. W., Brauers, T., Brown, S. S., Dorn, H. P., Dubé, W. P., Fuchs, H., Mensah, A., Rohrer, F., Tillmann, R., Wahner, A., Wooldridge, P. J., and Cohen, R. C.: SOA from limonene: role of NO3 in its generation and degradation, Atmos. Chem. Phys., 11, 3879-3894, 10.5194/acp-11-3879-2011, 2011.

Fry, J. L., Draper, D. C., Zarzana, K. J., Campuzano-Jost, P., Day, D. A., Jimenez, J. L., Brown, S. S., Cohen, R. C., Kaser, L., Hansel, A., Cappellin, L., Karl, T., Roux, A. H., Turnipseed, A., Cantrell, C., Lefer, B. L., and Grossberg, N.: Observations of gas- and aerosol-phase organic nitrates at BEACHON-RoMBAS 2011, Atmos Chem Phys, 13, 8585-8605, DOI 10.5194/acp-13-8585-2013, 2013.

Fry, J. L., Draper, D. C., Barsanti, K. C., Smith, J. N., Ortega, J., Winkler, P. M., Lawler, M. J., Brown, S. S., Edwards, P. M., Cohen, R. C., and Lee, L.: Secondary Organic Aerosol Formation and Organic Nitrate Yield from NO3 Oxidation of Biogenic Hydrocarbons, Environ. Sci. Technol., 48, 11944-11953, 10.1021/es502204x, 2014.

Gaston, C. J., Riedel, T. P., Zhang, Z., Gold, A., Surratt, J. D., and Thornton, J. A.: Reactive Uptake of an Isoprene-Derived Epoxydiol to Submicron Aerosol Particles, Environ Sci Technol, 48, 11178-11186, 10.1021/es5034266, 2014.

Geron, C., Rasmussen, R., Arnts, R. R., and Guenther, A.: A review and synthesis of monoterpene speciation from forests in the United States, Atmospheric Environment, 34, 1761-1781, Doi 10.1016/S1352-2310(99)00364-7, 2000.

Gharagheizi, F., Eslamimanesh, A., Mohammadi, A. H., and Richon, D.: Representation and Prediction of Molecular Diffusivity of Nonelectrolyte Organic Compounds in Water at Infinite Dilution Using the Artificial Neural Network-Group Contribution

Method, Journal of Chemical & Engineering Data, 56, 1741-1750, 10.1021/je101190p, 2011.

Goldstein, A. H., and Galbally, I. E.: Known and unexplored organic constituents in the earth's atmosphere, Environ Sci Technol, 41, 1514-1521, Doi 10.1021/Es072476p, 2007.

Goldstein, A. H., Koven, C. D., Heald, C. L., and Fung, I. Y.: Biogenic carbon and anthropogenic pollutants combine to form a cooling haze over the southeastern United States, P Natl Acad Sci USA, 106, 8835-8840, DOI 10.1073/pnas.0904128106, 2009.

Grieshop, A. P., Donahue, N. M., and Robinson, A. L.: Laboratory investigation of photochemical oxidation of organic aerosol from wood fires 2: analysis of aerosol mass spectrometer data, Atmos. Chem. Phys., 9, 2227-2240, 10.5194/acp-9-2227-2009, 2009a.

Grieshop, A. P., Logue, J. M., Donahue, N. M., and Robinson, A. L.: Laboratory investigation of photochemical oxidation of organic aerosol from wood fires 1: measurement and simulation of organic aerosol evolution, Atmos. Chem. Phys., 9, 1263-1277, 10.5194/acp-9-1263-2009, 2009b.

Griffin, R. J., Cocker, D. R., Flagan, R. C., and Seinfeld, J. H.: Organic aerosol formation from the oxidation of biogenic hydrocarbons, J Geophys Res-Atmos, 104, 3555-3567, Doi 10.1029/1998jd100049, 1999.

Guenther, A., Karl, T., Harley, P., Wiedinmyer, C., Palmer, P. I., and Geron, C.: Estimates of global terrestrial isoprene emissions using MEGAN (Model of Emissions of Gases and Aerosols from Nature), Atmos Chem Phys, 6, 3181-3210, 2006.

Guo, H., Xu, L., Bougiatioti, A., Cerully, K. M., Capps, S. L., Hite, J. R., Carlton, A. G., Lee, S. H., Bergin, M. H., Ng, N. L., Nenes, A., and Weber, R. J.: Particle water and pH in the southeastern United States, Atmos. Chem. Phys. Discuss., 14, 27143-27193, 10.5194/acpd-14-27143-2014, 2014.

Guo, H., Xu, L., Bougiatioti, A., Cerully, K. M., Capps, S. L., Hite Jr, J. R., Carlton, A. G., Lee, S. H., Bergin, M. H., Ng, N. L., Nenes, A., and Weber, R. J.: Fine-particle water and pH in the southeastern United States, Atmos. Chem. Phys., 15, 5211-5228, 10.5194/acp-15-5211-2015, 2015.

Häkkinen, S. A. K., Äijälä, M., Lehtipalo, K., Junninen, H., Backman, J., Virkkula, A., Nieminen, T., Vestenius, M., Hakola, H., Ehn, M., Worsnop, D. R., Kulmala, M., Petäjä, T., and Riipinen, I.: Long-term volatility measurements of submicron atmospheric aerosol in Hyytiälä, Finland, Atmos. Chem. Phys., 12, 10771-10786, 10.5194/acp-12-10771-2012, 2012.

Hallquist, M., Wangberg, I., Ljungstrom, E., Barnes, I., and Becker, K. H.: Aerosol and product yields from NO3 radical-initiated oxidation of selected monoterpenes, Environ. Sci. Technol., 33, 553-559, 10.1021/es980292s, 1999.

Hallquist, M., Wenger, J. C., Baltensperger, U., Rudich, Y., Simpson, D., Claeys, M., Dommen, J., Donahue, N. M., George, C., Goldstein, A. H., Hamilton, J. F., Herrmann, H., Hoffmann, T., Iinuma, Y., Jang, M., Jenkin, M. E., Jimenez, J. L., Kiendler-Scharr, A., Maenhaut, W., McFiggans, G., Mentel, T. F., Monod, A., Prevot, A. S. H., Seinfeld, J. H., Surratt, J. D., Szmigielski, R., and Wildt, J.: The formation, properties and impact of secondary organic aerosol: current and emerging issues, Atmos Chem Phys, 9, 5155-5236, 2009.

Hansen, D. A., Edgerton, E. S., Hartsell, B. E., Jansen, J. J., Kandasamy, N., Hidy, G. M., and Blanchard, C. L.: The southeastern aerosol research and characterization study: Part 1-overview, J Air Waste Manage, 53, 1460-1471, 2003.

Hao, L. Q., Kortelainen, A., Romakkaniemi, S., Portin, H., Jaatinen, A., Leskinen, A., Komppula, M., Miettinen, P., Sueper, D., Pajunoja, A., Smith, J. N., Lehtinen, K. E. J., Worsnop, D. R., Laaksonen, A., and Virtanen, A.: Atmospheric submicron aerosol composition and particulate organic nitrate formation in a boreal forestland–urban mixed region, Atmos. Chem. Phys., 14, 13483-13495, 10.5194/acp-14-13483-2014, 2014.

Harrison, R. M., Dall'Osto, M., Beddows, D. C. S., Thorpe, A. J., Bloss, W. J., Allan, J. D., Coe, H., Dorsey, J. R., Gallagher, M., Martin, C., Whitehead, J., Williams, P. I., Jones, R. L., Langridge, J. M., Benton, A. K., Ball, S. M., Langford, B., Hewitt, C. N., Davison, B., Martin, D., Petersson, K. F., Henshaw, S. J., White, I. R., Shallcross, D. E., Barlow, J. F., Dunbar, T., Davies, F., Nemitz, E., Phillips, G. J., Helfter, C., Di Marco, C. F., and Smith, S.: Atmospheric chemistry and physics in the atmosphere of a developed megacity (London): an overview of the REPARTEE experiment and its conclusions, Atmos. Chem. Phys., 12, 3065-3114, 10.5194/acp-12-3065-2012, 2012.

Hasson, A. S., Tyndall, G. S., and Orlando, J. J.: A product yield study of the reaction of HO2 radicals with ethyl peroxy (C2H5O2), acetyl peroxy (CH3C(O)O-2), and acetonyl peroxy (CH3C(O)CH2O2) radicals, J Phys Chem A, 108, 5979-5989, Doi 10.1021/Jp048873t, 2004.

Hatakeyama, S., Izumi, K., Fukuyama, T., and Akimoto, H.: Reactions of Ozone with Alpha-Pinene and Beta-Pinene in Air - Yields of Gaseous and Particulate Products, J Geophys Res-Atmos, 94, 13013-13024, Doi 10.1029/Jd094id10p13013, 1989.

Hatakeyama, S., Izumi, K., Fukuyama, T., Akimoto, H., and Washida, N.: Reactions of Oh with Alpha-Pinene and Beta-Pinene in Air - Estimate of Global Co Production from

the Atmospheric Oxidation of Terpenes, J Geophys Res-Atmos, 96, 947-958, Doi 10.1029/90jd02341, 1991.

Hayes, P. L., Ortega, A. M., Cubison, M. J., Froyd, K. D., Zhao, Y., Cliff, S. S., Hu, W. W., Toohey, D. W., Flynn, J. H., Lefer, B. L., Grossberg, N., Alvarez, S., Rappenglueck, B., Taylor, J. W., Allan, J. D., Holloway, J. S., Gilman, J. B., Kuster, W. C., De Gouw, J. A., Massoli, P., Zhang, X., Liu, J., Weber, R. J., Corrigan, A. L., Russell, L. M., Isaacman, G., Worton, D. R., Kreisberg, N. M., Goldstein, A. H., Thalman, R., Waxman, E. M., Volkamer, R., Lin, Y. H., Surratt, J. D., Kleindienst, T. E., Offenberg, J. H., Dusanter, S., Griffith, S., Stevens, P. S., Brioude, J., Angevine, W. M., and Jimenez, J. L.: Organic aerosol composition and sources in Pasadena, California, during the 2010 CalNex campaign, J Geophys Res-Atmos, 118, 9233-9257, Doi 10.1002/Jgrd.50530, 2013.

Healy, R. M., Temime, B., Kuprovskyte, K., and Wenger, J. C.: Effect of Relative Humidity on Gas/Particle Partitioning and Aerosol Mass Yield in the Photooxidation of p-Xylene, Environ Sci Technol, 43, 1884-1889, Doi 10.1021/Es802404z, 2009.

Hecobian, A., Zhang, X., Zheng, M., Frank, N., Edgerton, E. S., and Weber, R. J.: Water-Soluble Organic Aerosol material and the light-absorption characteristics of aqueous extracts measured over the Southeastern United States, Atmos. Chem. Phys., 10, 5965-5977, 10.5194/acp-10-5965-2010, 2010.

Hennigan, C. J., Sullivan, A. P., Fountoukis, C. I., Nenes, A., Hecobian, A., Vargas, O., Peltier, R. E., Case Hanks, A. T., Huey, L. G., Lefer, B. L., Russell, A. G., and Weber, R. J.: On the volatility and production mechanisms of newly formed nitrate and water soluble organic aerosol in Mexico City, Atmos. Chem. Phys., 8, 3761-3768, 10.5194/acp-8-3761-2008, 2008.

Hennigan, C. J., Bergin, M. H., Russell, A. G., Nenes, A., and Weber, R. J.: Gas/particle partitioning of water-soluble organic aerosol in Atlanta, Atmos Chem Phys, 9, 3613-3628, 2009.

Hennigan, C. J., Miracolo, M. A., Engelhart, G. J., May, A. A., Presto, A. A., Lee, T., Sullivan, A. P., McMeeking, G. R., Coe, H., Wold, C. E., Hao, W. M., Gilman, J. B., Kuster, W. C., de Gouw, J., Schichtel, B. A., Collett Jr, J. L., Kreidenweis, S. M., and Robinson, A. L.: Chemical and physical transformations of organic aerosol from the photo-oxidation of open biomass burning emissions in an environmental chamber, Atmos. Chem. Phys., 11, 7669-7686, 10.5194/acp-11-7669-2011, 2011.

Hennigan, C. J., Izumi, J., Sullivan, A. P., Weber, R. J., and Nenes, A.: A critical evaluation of proxy methods used to estimate the acidity of atmospheric particles, Atmos. Chem. Phys., 15, 2775-2790, 10.5194/acp-15-2775-2015, 2015.

Henry, K. M., and Donahue, N. M.: Photochemical Aging of alpha-Pinene Secondary Organic Aerosol: Effects of OH Radical Sources and Photolysis, J Phys Chem A, 116, 5932-5940, Doi 10.1021/Jp210288s, 2012.

Heringa, M. F., DeCarlo, P. F., Chirico, R., Tritscher, T., Dommen, J., Weingartner, E., Richter, R., Wehrle, G., Prévôt, A. S. H., and Baltensperger, U.: Investigations of primary and secondary particulate matter of different wood combustion appliances with a high-resolution time-of-flight aerosol mass spectrometer, Atmos. Chem. Phys., 11, 5945-5957, 10.5194/acp-11-5945-2011, 2011.

Hiatt, R. R., and Strachan, W. M.: Effect of Structure on Thermal Stability of Hydroperoxides, J Org Chem, 28, 1893-&, Doi 10.1021/Jo01042a041, 1963.

Hidy, G. M., Blanchard, C. L., Baumann, K., Edgerton, E., Tanenbaum, S., Shaw, S., Knipping, E., Tombach, I., Jansen, J., and Walters, J.: Chemical climatology of the southeastern United States, 1999–2013, Atmos. Chem. Phys., 14, 11893-11914, 10.5194/acp-14-11893-2014, 2014.

Hildebrandt, L., Engelhart, G. J., Mohr, C., Kostenidou, E., Lanz, V. A., Bougiatioti, A., DeCarlo, P. F., Prevot, A. S. H., Baltensperger, U., Mihalopoulos, N., Donahue, N. M., and Pandis, S. N.: Aged organic aerosol in the Eastern Mediterranean: the Finokalia Aerosol Measurement Experiment-2008, Atmos Chem Phys, 10, 4167-4186, DOI 10.5194/acp-10-4167-2010, 2010.

Hildebrandt Ruiz, L., Paciga, A. L., Cerully, K., Nenes, A., Donahue, N. M., and Pandis, S. N.: Aging of secondary organic aerosol from small aromatic VOCs: changes in chemical composition, mass yield, volatility and hygroscopicity, Atmos. Chem. Phys. Discuss., 14, 31441-31481, 10.5194/acpd-14-31441-2014, 2014.

Hoyle, C. R., Boy, M., Donahue, N. M., Fry, J. L., Glasius, M., Guenther, A., Hallar, A. G., Hartz, K. H., Petters, M. D., Petaja, T., Rosenoern, T., and Sullivan, A. P.: A review of the anthropogenic influence on biogenic secondary organic aerosol, Atmos Chem Phys, 11, 321-343, DOI 10.5194/acp-11-321-2011, 2011.

Hu, K. S., Darer, A. I., and Elrod, M. J.: Thermodynamics and kinetics of the hydrolysis of atmospherically relevant organonitrates and organosulfates, Atmos. Chem. Phys., 11, 8307-8320, 10.5194/acp-11-8307-2011, 2011.

Hu, W. W., Campuzano-Jost, P., Palm, B. B., Day, D. A., Ortega, A. M., Hayes, P. L., Krechmer, J. E., Chen, Q., Kuwata, M., Liu, Y. J., de Sá, S. S., McKinney, K., Martin, S. T., Hu, M., Budisulistiorini, S. H., Riva, M., Surratt, J. D., St. Clair, J. M., Isaacman-Van Wertz, G., Yee, L. D., Goldstein, A. H., Carbone, S., Brito, J., Artaxo, P., de Gouw, J. A., Koss, A., Wisthaler, A., Mikoviny, T., Karl, T., Kaser, L., Jud, W., Hansel, A., Docherty, K. S., Alexander, M. L., Robinson, N. H., Coe, H., Allan, J. D., Canagaratna, M. R., Paulot, F., and Jimenez, J. L.: Characterization

of a real-time tracer for isoprene epoxydiols-derived secondary organic aerosol (IEPOX-SOA) from aerosol mass spectrometer measurements, Atmos. Chem. Phys., 15, 11807-11833, 10.5194/acp-15-11807-2015, 2015.

Huang, X. F., He, L. Y., Hu, M., Canagaratna, M. R., Sun, Y., Zhang, Q., Zhu, T., Xue, L., Zeng, L. W., Liu, X. G., Zhang, Y. H., Jayne, J. T., Ng, N. L., and Worsnop, D. R.: Highly time-resolved chemical characterization of atmospheric submicron particles during 2008 Beijing Olympic Games using an Aerodyne High-Resolution Aerosol Mass Spectrometer, Atmos Chem Phys, 10, 8933-8945, DOI 10.5194/acp-10-8933-2010, 2010.

Huffman, J. A., Ziemann, P. J., Jayne, J. T., Worsnop, D. R., and Jimenez, J. L.: Development and Characterization of a Fast-Stepping/Scanning Thermodenuder for Chemically-Resolved Aerosol Volatility Measurements, Aerosol Sci Tech, 42, 395-407, 10.1080/02786820802104981, 2008.

Huffman, J. A., Docherty, K. S., Aiken, A. C., Cubison, M. J., Ulbrich, I. M., DeCarlo, P. F., Sueper, D., Jayne, J. T., Worsnop, D. R., Ziemann, P. J., and Jimenez, J. L.: Chemically-resolved aerosol volatility measurements from two megacity field studies, Atmos Chem Phys, 9, 7161-7182, 2009a.

Huffman, J. A., Docherty, K. S., Mohr, C., Cubison, M. J., Ulbrich, I. M., Ziemann, P. J., Onasch, T. B., and Jimenez, J. L.: Chemically-Resolved Volatility Measurements of Organic Aerosol from Different Sources, Environ Sci Technol, 43, 5351-5357, 10.1021/es803539d, 2009b.

Ion, A. C., Vermeylen, R., Kourtchev, I., Cafmeyer, J., Chi, X., Gelencser, A., Maenhaut, W., and Claeys, M.: Polar organic compounds in rural PM(2.5) aerosols from K-puszta, Hungary, during a 2003 summer field campaign: Sources and diel variations, Atmos Chem Phys, 5, 1805-1814, 2005.

Isaacman, G., Kreisberg, N. M., Yee, L. D., Worton, D. R., Chan, A. W. H., Moss, J. A., Hering, S. V., and Goldstein, A. H.: Online derivatization for hourly measurements of gas- and particle-phase semi-volatile oxygenated organic compounds by thermal desorption aerosol gas chromatography (SV-TAG), Atmos. Meas. Tech., 7, 4417-4429, 10.5194/amt-7-4417-2014, 2014.

Jacobs, M. I., Darer, A. I., and Elrod, M. J.: Rate Constants and Products of the OH Reaction with Isoprene-Derived Epoxides, Environ Sci Technol, 47, 12868-12876, Doi 10.1021/Es403340g, 2013.

Jacobs, M. I., Burke, W. J., and Elrod, M. J.: Kinetics of the reactions of isoprene-derived hydroxynitrates: gas phase epoxide formation and solution phase hydrolysis, Atmos. Chem. Phys., 14, 8933-8946, 10.5194/acp-14-8933-2014, 2014.

Jaeckels, J. M., Bae, M.-S., and Schauer, J. J.: Positive Matrix Factorization (PMF) Analysis of Molecular Marker Measurements to Quantify the Sources of Organic Aerosols, Environ Sci Technol, 41, 5763-5769, 10.1021/es062536b, 2007.

Janssen, R. H. H., Vilà-Guerau de Arellano, J., Jimenez, J. L., Ganzeveld, L. N., Robinson, N. H., Allan, J. D., Coe, H., and Pugh, T. A. M.: Influence of boundary layer dynamics and isoprene chemistry on the organic aerosol budget in a tropical forest, Journal of Geophysical Research: Atmospheres, 118, 9351-9366, 10.1002/jgrd.50672, 2013.

Jathar, S. H., Gordon, T. D., Hennigan, C. J., Pye, H. O. T., Pouliot, G., Adams, P. J., Donahue, N. M., and Robinson, A. L.: Unspeciated organic emissions from combustion sources and their influence on the secondary organic aerosol budget in the United States, P Natl Acad Sci USA, 111, 10473-10478, DOI 10.1073/pnas.1323740111, 2014.

Jayne, J. T., Leard, D. C., Zhang, X. F., Davidovits, P., Smith, K. A., Kolb, C. E., and Worsnop, D. R.: Development of an aerosol mass spectrometer for size and composition analysis of submicron particles, Aerosol Sci Tech, 33, 49-70, Doi 10.1080/027868200410840, 2000.

Jimenez, J. L., Canagaratna, M. R., Donahue, N. M., Prevot, A. S. H., Zhang, Q., Kroll, J. H., DeCarlo, P. F., Allan, J. D., Coe, H., Ng, N. L., Aiken, A. C., Docherty, K. S., Ulbrich, I. M., Grieshop, A. P., Robinson, A. L., Duplissy, J., Smith, J. D., Wilson, K. R., Lanz, V. A., Hueglin, C., Sun, Y. L., Tian, J., Laaksonen, A., Raatikainen, T., Rautiainen, J., Vaattovaara, P., Ehn, M., Kulmala, M., Tomlinson, J. M., Collins, D. R., Cubison, M. J., Dunlea, E. J., Huffman, J. A., Onasch, T. B., Alfarra, M. R., Williams, P. I., Bower, K., Kondo, Y., Schneider, J., Drewnick, F., Borrmann, S., Weimer, S., Demerjian, K., Salcedo, D., Cottrell, L., Griffin, R., Takami, A., Miyoshi, T., Hatakeyama, S., Shimono, A., Sun, J. Y., Zhang, Y. M., Dzepina, K., Kimmel, J. R., Sueper, D., Jayne, J. T., Herndon, S. C., Trimborn, A. M., Williams, L. R., Wood, E. C., Middlebrook, A. M., Kolb, C. E., Baltensperger, U., and Worsnop, D. R.: Evolution of Organic Aerosols in the Atmosphere, Science, 326, 1525-1529, DOI 10.1126/science.1180353, 2009.

Johnson, D., Jenkin, M. E., Wirtz, K., and Martin-Reviejo, M.: Simulating the Formation of Secondary Organic Aerosol from the Photooxidation of Toluene, Environ Chem, 1, 150-165, Doi 10.1071/En04069, 2004.

Jones, A., Thomson, D., Hort, M., and Devenish, B.: The U.K. Met Office's Next-Generation Atmospheric Dispersion Model, NAME III, in: Air Pollution Modeling and Its Application XVII, edited by: Borrego, C., and Norman, A.-L., Springer US, 580-589, 2007.

Jonsson, A. M., Hallquist, M., and Saathoff, H.: Volatility of secondary organic aerosols from the ozone initiated oxidation of alpha-pinene and limonene, J Aerosol Sci, 38, 843-852, DOI 10.1016/j.jaerosci.2007.06.008, 2007.

Kampf, C. J., Waxman, E. M., Slowik, J. G., Dommen, J., Pfaffenberger, L., Praplan, A. P., Prevot, A. S. H., Baltensperger, U., Hoffmann, T., and Volkamer, R.: Effective Henry's Law Partitioning and the Salting Constant of Glyoxal in Aerosols Containing Sulfate, Environ Sci Technol, 47, 4236-4244, Doi 10.1021/Es400083d, 2013.

Kanakidou, M., Seinfeld, J. H., Pandis, S. N., Barnes, I., Dentener, F. J., Facchini, M. C., Van Dingenen, R., Ervens, B., Nenes, A., Nielsen, C. J., Swietlicki, E., Putaud, J. P., Balkanski, Y., Fuzzi, S., Horth, J., Moortgat, G. K., Winterhalter, R., Myhre, C. E. L., Tsigaridis, K., Vignati, E., Stephanou, E. G., and Wilson, J.: Organic aerosol and global climate modelling: a review, Atmos Chem Phys, 5, 1053-1123, 2005.

Keywood, M. D., Varutbangkul, V., Bahreini, R., Flagan, R. C., and Seinfeld, J. H.: Secondary organic aerosol formation from the ozonolysis of cycloalkenes and related compounds, Environ Sci Technol, 38, 4157-4164, Doi 10.1021/Es.035363o, 2004.

King, S. M., Rosenoern, T., Shilling, J. E., Chen, Q., Wang, Z., Biskos, G., McKinney, K. A., Poschl, U., and Martin, S. T.: Cloud droplet activation of mixed organic-sulfate particles produced by the photooxidation of isoprene, Atmos Chem Phys, 10, 3953-3964, 2010.

Kjaergaard, H. G., Knap, H. C., Ornso, K. B., Jorgensen, S., Crounse, J. D., Paulot, F., and Wennberg, P. O.: Atmospheric Fate of Methacrolein. 2. Formation of Lactone and Implications for Organic Aerosol Production, J Phys Chem A, 116, 5763-5768, Doi 10.1021/Jp210853h, 2012.

Kleindienst, T. E., Lewandowski, M., Offenberg, J. H., Jaoui, M., and Edney, E. O.: Ozone-isoprene reaction: Re-examination of the formation of secondary organic aerosol, Geophysical Research Letters, 34, Artn L01805
Doi 10.1029/2006gl027485, 2007.

Kleindienst, T. E., Lewandowski, M., Offenberg, J. H., Jaoui, M., and Edney, E. O.: The formation of secondary organic aerosol from the isoprene plus OH reaction in the absence of NOx, Atmos Chem Phys, 9, 6541-6558, 2009.

Kostenidou, E., Lee, B. H., Engelhart, G. J., Pierce, J. R., and Pandis, S. N.: Mass Spectra Deconvolution of Low, Medium, and High Volatility Biogenic Secondary Organic Aerosol, Environ Sci Technol, 43, 4884-4889, Doi 10.1021/Es803676g, 2009.

Kroll, J. H.: Secondary organic aerosol formation from isoprene photooxidation under high-NOx conditions, GEOPHYSICAL RESEARCH LETTERS, 32, 4, 2005.

Kroll, J. H.: Secondary Organic Aerosol Formation from Isoprene Photooxidation, Environ. Sci. Technol., 9, 2006.

Kroll, J. H., Ng, N. L., Murphy, S. M., Flagan, R. C., and Seinfeld, J. H.: Secondary organic aerosol formation from isoprene photooxidation, Environ Sci Technol, 40, 1869-1877, Doi 10.1021/Es0524301, 2006.

Kroll, J. H., and Seinfeld, J. H.: Chemistry of secondary organic aerosol: Formation and evolution of low-volatility organics in the atmosphere, Atmospheric Environment, 42, 3593-3624, DOI 10.1016/j.atmosenv.2008.01.003, 2008.

Kroll, J. H., Smith, J. D., Che, D. L., Kessler, S. H., Worsnop, D. R., and Wilson, K. R.: Measurement of fragmentation and functionalization pathways in the heterogeneous oxidation of oxidized organic aerosol, Phys Chem Chem Phys, 11, 8005-8014, Doi 10.1039/B905289e, 2009.

Kroll, J. H., Donahue, N. M., Jimenez, J. L., Kessler, S. H., Canagaratna, M. R., Wilson, K. R., Altieri, K. E., Mazzoleni, L. R., Wozniak, A. S., Bluhm, H., Mysak, E. R., Smith, J. D., Kolb, C. E., and Worsnop, D. R.: Carbon oxidation state as a metric for describing the chemistry of atmospheric organic aerosol, Nat Chem, 3, 133-139, Doi 10.1038/Nchem.948, 2011.

Kuwata, M., Zorn, S. R., and Martin, S. T.: Using Elemental Ratios to Predict the Density of Organic Material Composed of Carbon, Hydrogen, and Oxygen, Environ Sci Technol, 46, 787-794, 10.1021/es202525q, 2012.

Laborde, M., Mertes, P., Zieger, P., Dommen, J., Baltensperger, U., and Gysel, M.: Sensitivity of the Single Particle Soot Photometer to different black carbon types, Atmos Meas Tech, 5, 1031-1043, DOI 10.5194/amt-5-1031-2012, 2012.

Lack, D. A., Bahreini, R., Langridge, J. M., Gilman, J. B., and Middlebrook, A. M.: Brown carbon absorption linked to organic mass tracers in biomass burning particles, Atmos. Chem. Phys., 13, 2415-2422, 10.5194/acp-13-2415-2013, 2013.

Lamb, B., Guenther, A., Gay, D., and Westberg, H.: A National Inventory of Biogenic Hydrocarbon Emissions, Atmospheric Environment, 21, 1695-1705, Doi 10.1016/0004-6981(87)90108-9, 1987.

Lamb, B., Gay, D., Westberg, H., and Pierce, T.: A Biogenic Hydrocarbon Emission Inventory for the USA Using a Simple Forest Canopy Model, Atmos Environ a-Gen, 27, 1673-1690, Doi 10.1016/0960-1686(93)90230-V, 1993.

Lane, T. E., Donahue, N. M., and Pandis, S. N.: Effect of NO(x) on secondary organic aerosol concentrations, Environ Sci Technol, 42, 6022-6027, Doi 10.1021/Es703225a, 2008.

Langford, B., Davison, B., Nemitz, E., and Hewitt, C. N.: Mixing ratios and eddy covariance flux measurements of volatile organic compounds from an urban canopy (Manchester, UK), Atmos. Chem. Phys., 9, 1971-1987, 10.5194/acp-9-1971-2009, 2009.

Langford, B., Misztal, P. K., Nemitz, E., Davison, B., Helfter, C., Pugh, T. A. M., MacKenzie, A. R., Lim, S. F., and Hewitt, C. N.: Fluxes and concentrations of volatile organic compounds from a South-East Asian tropical rainforest, Atmos Chem Phys, 10, 8391-8412, DOI 10.5194/acp-10-8391-2010, 2010.

Lanz, V. A., Alfarra, M. R., Baltensperger, U., Buchmann, B., Hueglin, C., and Prevot, A. S. H.: Source apportionment of submicron organic aerosols at an urban site by factor analytical modelling of aerosol mass spectra, Atmos Chem Phys, 7, 1503-1522, 2007.

Lee, B. H., Pierce, J. R., Engelhart, G. J., and Pandis, S. N.: Volatility of secondary organic aerosol from the ozonolysis of monoterpenes, Atmospheric Environment, 45, 2443-2452, DOI 10.1016/j.atmosenv.2011.02.004, 2011.

Lee, B. H., Lopez-Hilfiker, F. D., Mohr, C., Kurtén, T., Worsnop, D. R., and Thornton, J. A.: An Iodide-Adduct High-Resolution Time-of-Flight Chemical-Ionization Mass Spectrometer: Application to Atmospheric Inorganic and Organic Compounds, Environ Sci Technol, 48, 6309-6317, 10.1021/es500362a, 2014.

Lee, M. H., Heikes, B. G., and O'Sullivan, D. W.: Hydrogen peroxide and organic hydroperoxide in the troposphere: A review, Atmospheric Environment, 34, 3475-3494, Doi 10.1016/S1352-2310(99)00432-X, 2000.

Li, Q. F., Hu, D., Leungsakul, S., and Kamens, R. M.: Large outdoor chamber experiments and computer simulations: (I) Secondary organic aerosol formation from the oxidation of a mixture of d-limonene and alpha-pinene, Atmospheric Environment, 41, 9341-9352, DOI 10.1016/j.atmosenv.2007.09.017, 2007.

Li, Y. J., Lee, B. P., Su, L., Fung, J. C. H., and Chan, C. K.: Seasonal characteristics of fine particulate matter (PM) based on high-resolution time-of-flight aerosol mass spectrometric (HR-ToF-AMS) measurements at the HKUST Supersite in Hong Kong, Atmos. Chem. Phys., 15, 37-53, 10.5194/acp-15-37-2015, 2015.

Liao, H., Henze, D. K., Seinfeld, J. H., Wu, S., and Mickley, L. J.: Biogenic secondary organic aerosol over the United States: Comparison of climatological simulations

with observations, Journal of Geophysical Research: Atmospheres, 112, n/a-n/a, 10.1029/2006JD007813, 2007.

Liao, J., Froyd, K. D., Murphy, D. M., Keutsch, F. N., Yu, G., Wennberg, P. O., St. Clair, J. M., Crounse, J. D., Wisthaler, A., Mikoviny, T., Jimenez, J. L., Campuzano-Jost, P., Day, D. A., Hu, W., Ryerson, T. B., Pollack, I. B., Peischl, J., Anderson, B. E., Ziemba, L. D., Blake, D. R., Meinardi, S., and Diskin, G.: Airborne measurements of organosulfates over the continental U.S, Journal of Geophysical Research: Atmospheres, 120, 2990-3005, 10.1002/2014JD022378, 2015.

Lide, D. R.: CRC Handbook of Chemistry and Physics, CRC Press Inc, 1991.

Lim, H.-J., and Turpin, B. J.: Origins of Primary and Secondary Organic Aerosol in Atlanta: Results of Time-Resolved Measurements during the Atlanta Supersite Experiment, Environ Sci Technol, 36, 4489-4496, 10.1021/es0206487, 2002.

Lin, Y.-H., Budisulistiorini, S. H., Chu, K., Siejack, R. A., Zhang, H., Riva, M., Zhang, Z., Gold, A., Kautzman, K. E., and Surratt, J. D.: Light-Absorbing Oligomer Formation in Secondary Organic Aerosol from Reactive Uptake of Isoprene Epoxydiols, Environ Sci Technol, 48, 12012-12021, 10.1021/es503142b, 2014.

Lin, Y. H., Zhang, Z. F., Docherty, K. S., Zhang, H. F., Budisulistiorini, S. H., Rubitschun, C. L., Shaw, S. L., Knipping, E. M., Edgerton, E. S., Kleindienst, T. E., Gold, A., and Surratt, J. D.: Isoprene Epoxydiols as Precursors to Secondary Organic Aerosol Formation: Acid-Catalyzed Reactive Uptake Studies with Authentic Compounds, Environ Sci Technol, 46, 250-258, Doi 10.1021/Es202554c, 2012.

Lin, Y. H., Knipping, E. M., Edgerton, E. S., Shaw, S. L., and Surratt, J. D.: Investigating the influences of SO2 and NH3 levels on isoprene-derived secondary organic aerosol formation using conditional sampling approaches, Atmos. Chem. Phys., 13, 8457-8470, 10.5194/acp-13-8457-2013, 2013a.

Lin, Y. H., Zhang, H. F., Pye, H. O. T., Zhang, Z. F., Marth, W. J., Park, S., Arashiro, M., Cui, T. Q., Budisulistiorini, H., Sexton, K. G., Vizuete, W., Xie, Y., Luecken, D. J., Piletic, I. R., Edney, E. O., Bartolotti, L. J., Gold, A., and Surratt, J. D.: Epoxide as a precursor to secondary organic aerosol formation from isoprene photooxidation in the presence of nitrogen oxides, P Natl Acad Sci USA, 110, 6718-6723, DOI 10.1073/pnas.1221150110, 2013b.

Liu, D., Allan, J., Whitehead, J., Young, D., Flynn, M., Coe, H., McFiggans, G., Fleming, Z. L., and Bandy, B.: Ambient black carbon particle hygroscopic properties controlled by mixing state and composition, Atmos. Chem. Phys., 13, 2015-2029, 10.5194/acp-13-2015-2013, 2013.

Liu, J., Scheuer, E., Dibb, J., Ziemba, L. D., Thornhill, K. L., Anderson, B. E., Wisthaler, A., Mikoviny, T., Devi, J. J., Bergin, M., and Weber, R. J.: Brown carbon in the continental troposphere, Geophysical Research Letters, 41, 2013GL058976, 10.1002/2013GL058976, 2014.

Liu, S., Day, D. A., Shields, J. E., and Russell, L. M.: Ozone-driven daytime formation of secondary organic aerosol containing carboxylic acid groups and alkane groups, Atmos Chem Phys, 11, 8321-8341, DOI 10.5194/acp-11-8321-2011, 2011.

Liu, S., Shilling, J. E., Song, C., Hiranuma, N., Zaveri, R. A., and Russell, L. M.: Hydrolysis of Organonitrate Functional Groups in Aerosol Particles, Aerosol Sci Tech, 46, 1359-1369, Doi 10.1080/02786826.2012.716175, 2012.

Liu, S., Aiken, A. C., Gorkowski, K., Dubey, M. K., Cappa, C. D., Williams, L. R., Herndon, S. C., Massoli, P., Fortner, E. C., Chhabra, P. S., Brooks, W. A., Onasch, T. B., Jayne, J. T., Worsnop, D. R., China, S., Sharma, N., Mazzoleni, C., Xu, L., Ng, N. L., Liu, D., Allan, J. D., Lee, J. D., Fleming, Z. L., Mohr, C., Zotter, P., Szidat, S., and Prevot, A. S. H.: Enhanced light absorption by mixed source black and brown carbon particles in UK winter, Nat Commun, 6, 10.1038/ncomms9435, 2015a.

Liu, Y., Kuwata, M., Strick, B. F., Geiger, F. M., Thomson, R. J., McKinney, K. A., and Martin, S. T.: Uptake of Epoxydiol Isomers Accounts for Half of the Particle-Phase Material Produced from Isoprene Photooxidation via the HO2 Pathway, Environ Sci Technol, 49, 250-258, 10.1021/es5034298, 2015b.

Loza, C. L., Chan, A. W. H., Galloway, M. M., Keutsch, F. N., Flagan, R. C., and Seinfeld, J. H.: Characterization of Vapor Wall Loss in Laboratory Chambers, Environ Sci Technol, 44, 5074-5078, Doi 10.1021/Es100727v, 2010.

Loza, C. L., Chhabra, P. S., Yee, L. D., Craven, J. S., Flagan, R. C., and Seinfeld, J. H.: Chemical aging of m-xylene secondary organic aerosol: laboratory chamber study, Atmos Chem Phys, 12, 151-167, DOI 10.5194/acp-12-151-2012, 2012.

M.R.Canagaratna: CHEMICAL AND MICROPHYSICAL CHARACTERIZATION OF AMBIENT AEROSOLS WITH THE AERODYNE AEROSOL MASS SPECTROMETER, Mass Spectrometry Reviews, 26, 38, 2007.

Malm, W. C., Sisler, J. F., Huffman, D., Eldred, R. A., and Cahill, T. A.: Spatial and seasonal trends in particle concentration and optical extinction in the United States, Journal of Geophysical Research: Atmospheres, 99, 1347-1370, 10.1029/93JD02916, 1994.

Mao, J., Ren, X., Zhang, L., Van Duin, D. M., Cohen, R. C., Park, J. H., Goldstein, A. H., Paulot, F., Beaver, M. R., Crounse, J. D., Wennberg, P. O., DiGangi, J. P., Henry,

S. B., Keutsch, F. N., Park, C., Schade, G. W., Wolfe, G. M., Thornton, J. A., and Brune, W. H.: Insights into hydroxyl measurements and atmospheric oxidation in a California forest, Atmos. Chem. Phys., 12, 8009-8020, 10.5194/acp-12-8009-2012, 2012.

Marais, E. A., Jacob, D. J., Jimenez, J. L., Campuzano-Jost, P., Day, D. A., Hu, W., Krechmer, J., Zhu, L., Kim, P. S., Miller, C. C., Fisher, J. A., Travis, K., Yu, K., Hanisco, T. F., Wolfe, G. M., Arkinson, H. L., Pye, H. O. T., Froyd, K. D., Liao, J., and McNeill, V. F.: Aqueous-phase mechanism for secondary organic aerosol formation from isoprene: application to the Southeast United States and co-benefit of SO2 emission controls, Atmos. Chem. Phys. Discuss., 15, 32005-32047, 10.5194/acpd-15-32005-2015, 2015.

Massoli, P., Onasch, T. B., Cappa, C. D., Nuamaan, I., Hakala, J., Hayden, K., Li, S.-M., Sueper, D. T., Bates, T. S., Quinn, P. K., Jayne, J. T., and Worsnop, D. R.: Characterization of black carbon-containing particles from soot particle aerosol mass spectrometer measurements on the R/V Atlantis during CalNex 2010, Journal of Geophysical Research: Atmospheres, 120, 2575-2593, 10.1002/2014JD022834, 2015.

Matsunaga, A., and Ziemann, P. J.: Gas-Wall Partitioning of Organic Compounds in a Teflon Film Chamber and Potential Effects on Reaction Product and Aerosol Yield Measurements, Aerosol Sci Tech, 44, 881-892, Doi 10.1080/02786826.2010.501044, 2010.

Matthew, B. M., Middlebrook, A. M., and Onasch, T. B.: Collection efficiencies in an Aerodyne Aerosol Mass Spectrometer as a function of particle phase for laboratory generated aerosols, Aerosol Sci Tech, 42, 884-898, Doi 10.1080/02786820802356797, 2008.

May, A. A., Saleh, R., Hennigan, C. J., Donahue, N. M., and Robinson, A. L.: Volatility of Organic Molecular Markers Used for Source Apportionment Analysis: Measurements and Implications for Atmospheric Lifetime, Environ Sci Technol, 46, 12435-12444, 10.1021/es302276t, 2012.

McMeeking, G. R., Bart, M., Chazette, P., Haywood, J. M., Hopkins, J. R., McQuaid, J. B., Morgan, W. T., Raut, J. C., Ryder, C. L., Savage, N., Turnbull, K., and Coe, H.: Airborne measurements of trace gases and aerosols over the London metropolitan region, Atmos. Chem. Phys., 12, 5163-5187, 10.5194/acp-12-5163-2012, 2012.

Middlebrook, A. M., Bahreini, R., Jimenez, J. L., and Canagaratna, M. R.: Evaluation of Composition-Dependent Collection Efficiencies for the Aerodyne Aerosol Mass Spectrometer using Field Data, Aerosol Sci Tech, 46, 258-271, Doi 10.1080/02786826.2011.620041, 2012.

Mohr, C., Huffman, J. A., Cubison, M. J., Aiken, A. C., Docherty, K. S., Kimmel, J. R., Ulbrich, I. M., Hannigan, M., and Jimenez, J. L.: Characterization of Primary Organic Aerosol Emissions from Meat Cooking, Trash Burning, and Motor Vehicles with High-Resolution Aerosol Mass Spectrometry and Comparison with Ambient and Chamber Observations, Environ Sci Technol, 43, 2443-2449, 10.1021/es8011518, 2009.

Mohr, C., DeCarlo, P. F., Heringa, M. F., Chirico, R., Slowik, J. G., Richter, R., Reche, C., Alastuey, A., Querol, X., Seco, R., Peñuelas, J., Jiménez, J. L., Crippa, M., Zimmermann, R., Baltensperger, U., and Prévôt, A. S. H.: Identification and quantification of organic aerosol from cooking and other sources in Barcelona using aerosol mass spectrometer data, Atmos. Chem. Phys., 12, 1649-1665, 10.5194/acp-12-1649-2012, 2012.

Mohr, C., Lopez-Hilfiker, F. D., Zotter, P., Prévôt, A. S. H., Xu, L., Ng, N. L., Herndon, S. C., Williams, L. R., Franklin, J. P., Zahniser, M. S., Worsnop, D. R., Knighton, W. B., Aiken, A. C., Gorkowski, K. J., Dubey, M. K., Allan, J. D., and Thornton, J. A.: Contribution of Nitrated Phenols to Wood Burning Brown Carbon Light Absorption in Detling, United Kingdom during Winter Time, Environ Sci Technol, 47, 6316-6324, 10.1021/es400683v, 2013.

Morgan, W. T., Allan, J. D., Bower, K. N., Highwood, E. J., Liu, D., McMeeking, G. R., Northway, M. J., Williams, P. I., Krejci, R., and Coe, H.: Airborne measurements of the spatial distribution of aerosol chemical composition across Europe and evolution of the organic fraction, Atmos. Chem. Phys., 10, 4065-4083, 10.5194/acp-10-4065-2010, 2010.

Morgan, W. T., Ouyang, B., Allan, J. D., Aruffo, E., Di Carlo, P., Kennedy, O. J., Lowe, D., Flynn, M. J., Rosenberg, P. D., Williams, P. I., Jones, R., McFiggans, G. B., and Coe, H.: Influence of aerosol chemical composition on N2O5 uptake: airborne regional measurements in northwestern Europe, Atmos. Chem. Phys., 15, 973-990, 10.5194/acp-15-973-2015, 2015.

Murphy, J. G., Oram, D. E., and Reeves, C. E.: Measurements of volatile organic compounds over West Africa, Atmos Chem Phys, 10, 5281-5294, DOI 10.5194/acp-10-5281-2010, 2010.

Ng, N. L., Kroll, J. H., Keywood, M. D., Bahreini, R., Varutbangkul, V., Flagan, R. C., Seinfeld, J. H., Lee, A., and Goldstein, A. H.: Contribution of first- versus second-generation products to secondary organic aerosols formed in the oxidation of biogenic hydrocarbons, Environ Sci Technol, 40, 2283-2297, Doi 10.1021/Es052269u, 2006.

Ng, N. L.: Effect of NOx level on secondary organic aerosol (SOA) formation from the photooxidation of terpenes, Atmos. Chem. Phys., 7, 16, 2007.

Ng, N. L., Chhabra, P. S., Chan, A. W. H., Surratt, J. D., Kroll, J. H., Kwan, A. J., McCabe, D. C., Wennberg, P. O., Sorooshian, A., Murphy, S. M., Dalleska, N. F., Flagan, R. C., and Seinfeld, J. H.: Effect of NO(x) level on secondary organic aerosol (SOA) formation from the photooxidation of terpenes, Atmos Chem Phys, 7, 5159-5174, 2007.

Ng, N. L.: Secondary organic aerosol (SOA) formation from reaction of isoprene with nitrate radicals (NO3), Atmos. Chem. Phys., 8, 25, 2008.

Ng, N. L., Kwan, A. J., Surratt, J. D., Chan, A. W. H., Chhabra, P. S., Sorooshian, A., Pye, H. O. T., Crounse, J. D., Wennberg, P. O., Flagan, R. C., and Seinfeld, J. H.: Secondary organic aerosol (SOA) formation from reaction of isoprene with nitrate radicals (NO(3)), Atmos Chem Phys, 8, 4117-4140, 2008.

Ng, N. L., Canagaratna, M. R., Zhang, Q., Jimenez, J. L., Tian, J., Ulbrich, I. M., Kroll, J. H., Docherty, K. S., Chhabra, P. S., Bahreini, R., Murphy, S. M., Seinfeld, J. H., Hildebrandt, L., Donahue, N. M., DeCarlo, P. F., Lanz, V. A., Prevot, A. S. H., Dinar, E., Rudich, Y., and Worsnop, D. R.: Organic aerosol components observed in Northern Hemispheric datasets from Aerosol Mass Spectrometry, Atmos Chem Phys, 10, 4625-4641, DOI 10.5194/acp-10-4625-2010, 2010.

Ng, N. L., Herndon, S. C., Trimborn, A., Canagaratna, M. R., Croteau, P. L., Onasch, T. B., Sueper, D., Worsnop, D. R., Zhang, Q., Sun, Y. L., and Jayne, J. T.: An Aerosol Chemical Speciation Monitor (ACSM) for Routine Monitoring of the Composition and Mass Concentrations of Ambient Aerosol, Aerosol Sci Tech, 45, 780-794, Pii 934555189 Doi 10.1080/02786826.2011.560211, 2011.

Nguyen, T. B., Bateman, A. P., Bones, D. L., Nizkorodov, S. A., Laskin, J., and Laskin, A.: High-resolution mass spectrometry analysis of secondary organic aerosol generated by ozonolysis of isoprene, Atmospheric Environment, 44, 1032-1042, DOI 10.1016/j.atmosenv.2009.12.019, 2010.

Nguyen, T. B., Laskin, J., Laskin, A., and Nizkorodov, S. A.: Nitrogen-Containing Organic Compounds and Oligomers in Secondary Organic Aerosol Formed by Photooxidation of Isoprene, Environ Sci Technol, 45, 6908-6918, Doi 10.1021/Es201611n, 2011.

Nguyen, T. B., Coggon, M. M., Bates, K. H., Zhang, X., R. H. Schwantes, Schilling, K. A., Loza, C. L., Flagan, R. C., Wennberg, P. O., and Seinfeld, J. H.: Organic aerosol formation from the reactive uptake of isoprene epoxydiols (IEPOX) onto non-acidified inorganic seeds, Atmospheric Chemistry and Physics Discuss, 27677 - 27716, 2013.

Nguyen, T. B., Coggon, M. M., Bates, K. H., Zhang, X., Schwantes, R. H., Schilling, K. A., Loza, C. L., Flagan, R. C., Wennberg, P. O., and Seinfeld, J. H.: Organic aerosol formation from the reactive uptake of isoprene epoxydiols (IEPOX) onto non-acidified inorganic seeds, Atmos. Chem. Phys., 14, 3497-3510, 10.5194/acp-14-3497-2014, 2014.

Nordin, E. Z., Eriksson, A. C., Roldin, P., Nilsson, P. T., Carlsson, J. E., Kajos, M. K., Hellén, H., Wittbom, C., Rissler, J., Löndahl, J., Swietlicki, E., Svenningsson, B., Bohgard, M., Kulmala, M., Hallquist, M., and Pagels, J. H.: Secondary organic aerosol formation from idling gasoline passenger vehicle emissions investigated in a smog chamber, Atmos. Chem. Phys., 13, 6101-6116, 10.5194/acp-13-6101-2013, 2013.

Odum, J. R.: Gas/Particle Partitioning and Secondary Organic Aerosol Yields, Environ. Sci. Technol., 30, 6, 1996.

Onasch, T. B., Trimborn, A., Fortner, E. C., Jayne, J. T., Kok, G. L., Williams, L. R., Davidovits, P., and Worsnop, D. R.: Soot Particle Aerosol Mass Spectrometer: Development, Validation, and Initial Application, Aerosol Sci Tech, 46, 804-817, 10.1080/02786826.2012.663948, 2012.

Orlando, J. J., Tyndall, G. S., and Paulson, S. E.: Mechanism of the OH-initiated oxidation of methacrolein, Geophysical Research Letters, 26, 2191-2194, Doi 10.1029/1999gl900453, 1999.

Orsini, D. A., Ma, Y. L., Sullivan, A., Sierau, B., Baumann, K., and Weber, R. J.: Refinements to the particle-into-liquid sampler (PILS) for ground and airborne measurements of water soluble aerosol composition, Atmospheric Environment, 37, 1243-1259, Doi 10.1016/S1352-2310(02)01015-4, 2003.

Ots, R., Young, D. E., Vieno, M., Xu, L., Dunmore, R. E., Allan, J. D., Coe, H., Williams, L. R., Herndon, S. C., Ng, N. L., Hamilton, J. F., Bergström, R., Marco, C. D., Nemitz, E., Mackenzie, I. A., Kuenen, J. J. P., Green, D. C., Reis, S., and Heal, M. R. H.: Simulating secondary organic aerosol from missing diesel-related intermediate-volatility organic compound emissions during the Clean Air for London (ClearfLo) campaign, Submitted to Atmos. Chem. Phys. , 2015.

Paatero, P., and Tapper, U.: Positive Matrix Factorization - a Nonnegative Factor Model with Optimal Utilization of Error-Estimates of Data Values, Environmetrics, 5, 111-126, DOI 10.1002/env.3170050203, 1994.

Paatero, P.: A weighted non-negative least squares algorithm for three-way 'PARAFAC' factor analysis, Chemometr Intell Lab, 38, 223-242, Doi 10.1016/S0169-7439(97)00031-2, 1997.

Paatero, P.: The Multilinear Engine—A Table-Driven, Least Squares Program for Solving Multilinear Problems, Including the n-Way Parallel Factor Analysis Model, Journal of Computational and Graphical Statistics, 8, 854-888, 10.1080/10618600.1999.10474853, 1999.

Paciga, A., Karnezi, E., Kostenidou, E., Hildebrandt, L., Psichoudaki, M., Engelhart, G. J., Lee, B. H., Crippa, M., Prévôt, A. S. H., Baltensperger, U., and Pandis, S. N.: Volatility of organic aerosol and its components in the Megacity of Paris, Atmos. Chem. Phys. Discuss., 15, 22263-22289, 10.5194/acpd-15-22263-2015, 2015.

Paglione, M., Kiendler-Scharr, A., Mensah, A. A., Finessi, E., Giulianelli, L., Sandrini, S., Facchini, M. C., Fuzzi, S., Schlag, P., Piazzalunga, A., Tagliavini, E., Henzing, J. S., and Decesari, S.: Identification of humic-like substances (HULIS) in oxygenated organic aerosols using NMR and AMS factor analyses and liquid chromatographic techniques, Atmos. Chem. Phys., 14, 25-45, 10.5194/acp-14-25-2014, 2014.

Park, K., Cao, F., Kittelson, D. B., and McMurry, P. H.: Relationship between Particle Mass and Mobility for Diesel Exhaust Particles, Environ Sci Technol, 37, 577-583, 10.1021/es025960v, 2003.

Park, K., Kittelson, D., Zachariah, M., and McMurry, P.: Measurement of Inherent Material Density of Nanoparticle Agglomerates, J Nanopart Res, 6, 267-272, 10.1023/B:NANO.0000034657.71309.e6, 2004.

Paulot, F., Crounse, J. D., Kjaergaard, H. G., Kroll, J. H., Seinfeld, J. H., and Wennberg, P. O.: Isoprene photooxidation: new insights into the production of acids and organic nitrates, Atmos Chem Phys, 9, 1479-1501, 2009a.

Paulot, F., Crounse, J. D., Kjaergaard, H. G., Kurten, A., St Clair, J. M., Seinfeld, J. H., and Wennberg, P. O.: Unexpected Epoxide Formation in the Gas-Phase Photooxidation of Isoprene, Science, 325, 730-733, DOI 10.1126/science.1172910, 2009b.

Perring, A. E., Pusede, S. E., and Cohen, R. C.: An Observational Perspective on the Atmospheric Impacts of Alkyl and Multifunctional Nitrates on Ozone and Secondary Organic Aerosol, Chem Rev, 113, 5848-5870, Doi 10.1021/Cr300520x, 2013.

Petters, M. D., and Kreidenweis, S. M.: A single parameter representation of hygroscopic growth and cloud condensation nucleus activity, Atmos. Chem. Phys., 7, 1961-1971, 10.5194/acp-7-1961-2007, 2007.

Piletic, I. R., Edney, E. O., and Bartolotti, L. J.: A computational study of acid catalyzed aerosol reactions of atmospherically relevant epoxides, Phys Chem Chem Phys, 15, 18065-18076, 10.1039/C3CP52851K, 2013.

Platt, S. M., El Haddad, I., Zardini, A. A., Clairotte, M., Astorga, C., Wolf, R., Slowik, J. G., Temime-Roussel, B., Marchand, N., Jezek, I., Drinovec, L., Mocnik, G., Mohler, O., Richter, R., Barmet, P., Bianchi, F., Baltensperger, U., and Prevot, A. S. H.: Secondary organic aerosol formation from gasoline vehicle emissions in a new mobile environmental reaction chamber, Atmos Chem Phys, 13, 9141-9158, DOI 10.5194/acp-13-9141-2013, 2013.

Poulain, L., Birmili, W., Canonaco, F., Crippa, M., Wu, Z. J., Nordmann, S., Spindler, G., Prévôt, A. S. H., Wiedensohler, A., and Herrmann, H.: Chemical mass balance of 300 °C non-volatile particles at the tropospheric research site Melpitz, Germany, Atmos. Chem. Phys., 14, 10145-10162, 10.5194/acp-14-10145-2014, 2014.

Presto, A. A.: Secondary Organic Aerosol Production from Terpene Ozonolysis. 2. Effect of NOx Concentration, Environ. Sci. Technol., 9, 2005a.

Presto, A. A.: Secondary Organic Aerosol Production from Terpene Ozonolysis. 1. Effect of UV Radiation, Environ. Sci. Technol., 39, 10, 2005b.

Presto, A. A., and Donahue, N. M.: Investigation of alpha-pinene plus ozone secondary organic aerosol formation at low total aerosol mass, Environ Sci Technol, 40, 3536-3543, Doi 10.1021/Es052203z, 2006.

Presto, A. A., Gordon, T. D., and Robinson, A. L.: Primary to secondary organic aerosol: evolution of organic emissions from mobile combustion sources, Atmos. Chem. Phys., 14, 5015-5036, 10.5194/acp-14-5015-2014, 2014.

Putaud, J.-P., Raes, F., Van Dingenen, R., Brüggemann, E., Facchini, M. C., Decesari, S., Fuzzi, S., Gehrig, R., Hüglin, C., Laj, P., Lorbeer, G., Maenhaut, W., Mihalopoulos, N., Müller, K., Querol, X., Rodriguez, S., Schneider, J., Spindler, G., Brink, H. t., Tørseth, K., and Wiedensohler, A.: A European aerosol phenomenology—2: chemical characteristics of particulate matter at kerbside, urban, rural and background sites in Europe, Atmospheric Environment, 38, 2579-2595, http://dx.doi.org/10.1016/j.atmosenv.2004.01.041, 2004.

Pye, Pinder, R. W., Piletic, I. R., Xie, Y., Capps, S. L., Lin, Y. H., Surratt, J. D., Zhang, Z. F., Gold, A., Luecken, D. J., Hutzell, W. T., Jaoui, M., Offenberg, J. H., Kleindienst, T. E., Lewandowski, M., and Edney, E. O.: Epoxide Pathways Improve Model Predictions of Isoprene Markers and Reveal Key Role of Acidity in Aerosol Formation, Environ Sci Technol, 47, 11056-11064, Doi 10.1021/Es402106h, 2013.

Pye, Luecken, D. J., Xu, L., Boyd, C. M., Ng, N. L., Baker, K. R., Ayres, B. R., Bash, J. O., Baumann, K., Carter, W. P. L., Edgerton, E., Fry, J. L., Hutzell, W. T., Schwede, D. B., and Shepson, P. B.: Modeling the Current and Future Roles of Particulate Organic Nitrates in the Southeastern United States, Environ Sci Technol, 49, 14195-14203, 10.1021/acs.est.5b03738, 2015.

Pye, H. O. T., Chan, A. W. H., Barkley, M. P., and Seinfeld, J. H.: Global modeling of organic aerosol: the importance of reactive nitrogen (NOx and NO3), Atmos Chem Phys, 10, 11261-11276, DOI 10.5194/acp-10-11261-2010, 2010.

Qi, L., Nakao, S., Malloy, Q., Warren, B., and Cocker, D. R.: Can secondary organic aerosol formed in an atmospheric simulation chamber continuously age?, Atmospheric Environment, 44, 2990-2996, DOI 10.1016/j.atmosenv.2010.05.020, 2010.

Raatikainen, T., Vaattovaara, P., Tiitta, P., Miettinen, P., Rautiainen, J., Ehn, M., Kulmala, M., Laaksonen, A., and Worsnop, D. R.: Physicochemical properties and origin of organic groups detected in boreal forest using an aerosol mass spectrometer, Atmos. Chem. Phys., 10, 2063-2077, 10.5194/acp-10-2063-2010, 2010.

Riedel, Lin, Y.-H., Budisulistiorini, S. H., Gaston, C. J., Thornton, J. A., Zhang, Z., Vizuete, W., Gold, A., and Surratt, J. D.: Heterogeneous Reactions of Isoprene-Derived Epoxides: Reaction Probabilities and Molar Secondary Organic Aerosol Yield Estimates, Environmental Science & Technology Letters, 10.1021/ez500406f, 2015.

Riedel, Lin, Y. H., Zhang, Z., Chu, K., Thornton, J. A., Vizuete, W., Gold, A., and Surratt, J. D.: Constraining condensed-phase formation kinetics of secondary organic aerosol components from isoprene epoxydiols, Atmos. Chem. Phys., 16, 1245-1254, 10.5194/acp-16-1245-2016, 2016.

Riipinen, I., Pierce, J. R., Donahue, N. M., and Pandis, S. N.: Equilibration time scales of organic aerosol inside thermodenuders: Evaporation kinetics versus thermodynamics, Atmospheric Environment, 44, 597-607, http://dx.doi.org/10.1016/j.atmosenv.2009.11.022, 2010.

Robinson, A. L., Donahue, N. M., Shrivastava, M. K., Weitkamp, E. A., Sage, A. M., Grieshop, A. P., Lane, T. E., Pierce, J. R., and Pandis, S. N.: Rethinking organic aerosols: Semivolatile emissions and photochemical aging, Science, 315, 1259-1262, DOI 10.1126/science.1133061, 2007.

Robinson, N. H., Hamilton, J. F., Allan, J. D., Langford, B., Oram, D. E., Chen, Q., Docherty, K., Farmer, D. K., Jimenez, J. L., Ward, M. W., Hewitt, C. N., Barley, M. H., Jenkin, M. E., Rickard, A. R., Martin, S. T., McFiggans, G., and Coe, H.: Evidence for a significant proportion of Secondary Organic Aerosol from isoprene

above a maritime tropical forest, Atmos Chem Phys, 11, 1039-1050, DOI 10.5194/acp-11-1039-2011, 2011a.

Robinson, N. H., Newton, H. M., Allan, J. D., Irwin, M., Hamilton, J. F., Flynn, M., Bower, K. N., Williams, P. I., Mills, G., Reeves, C. E., McFiggans, G., and Coe, H.: Source attribution of Bornean air masses by back trajectory analysis during the OP3 project, Atmos. Chem. Phys., 11, 9605-9630, 10.5194/acp-11-9605-2011, 2011b.

Rollins, A. W., Kiendler-Scharr, A., Fry, J. L., Brauers, T., Brown, S. S., Dorn, H. P., Dube, W. P., Fuchs, H., Mensah, A., Mentel, T. F., Rohrer, F., Tillmann, R., Wegener, R., Wooldridge, P. J., and Cohen, R. C.: Isoprene oxidation by nitrate radical: alkyl nitrate and secondary organic aerosol yields, Atmos. Chem. Phys., 9, 6685-6703, 2009.

Rollins, A. W., Fry, J. L., Hunter, J. F., Kroll, J. H., Worsnop, D. R., Singaram, S. W., and Cohen, R. C.: Elemental analysis of aerosol organic nitrates with electron ionization high-resolution mass spectrometry, Atmos Meas Tech, 3, 301-310, 2010.

Rollins, A. W., Browne, E. C., Min, K.-E., Pusede, S. E., Wooldridge, P. J., Gentner, D. R., Goldstein, A. H., Liu, S., Day, D. A., Russell, L. M., and Cohen, R. C.: Evidence for NOx Control over Nighttime SOA Formation, Science, 337, 1210-1212, 10.1126/science.1221520, 2012.

Russell, A., Holmes, H., Friberg, M., Ivey, C., Hu, Y., Balachandran, S., Mulholland, J., Tolbert, P., Sarnat, J., Sarnat, S., Strickland, M., Chang, H., and Liu, Y.: Use of Air Quality Modeling Results in Health Effects Research, in: Air Pollution Modeling and its Application XXIII, edited by: Steyn, D., and Mathur, R., Springer Proceedings in Complexity, Springer International Publishing, 1-5, 2014.

Salcedo, D., Onasch, T. B., Dzepina, K., Canagaratna, M. R., Zhang, Q., Huffman, J. A., DeCarlo, P. F., Jayne, J. T., Mortimer, P., Worsnop, D. R., Kolb, C. E., Johnson, K. S., Zuberi, B., Marr, L. C., Volkamer, R., Molina, L. T., Molina, M. J., Cardenas, B., Bernabé, R. M., Márquez, C., Gaffney, J. S., Marley, N. A., Laskin, A., Shutthanandan, V., Xie, Y., Brune, W., Lesher, R., Shirley, T., and Jimenez, J. L.: Characterization of ambient aerosols in Mexico City during the MCMA-2003 campaign with Aerosol Mass Spectrometry: results from the CENICA Supersite, Atmos. Chem. Phys., 6, 925-946, 10.5194/acp-6-925-2006, 2006.

Saleh, R., Shihadeh, A., and Khlystov, A.: On transport phenomena and equilibration time scales in thermodenuders, Atmos. Meas. Tech., 4, 571-581, 10.5194/amt-4-571-2011, 2011.

Saleh, R., Khlystov, A., and Shihadeh, A.: Determination of Evaporation Coefficients of Ambient and Laboratory-Generated Semivolatile Organic Aerosols from Phase Equilibration Kinetics in a Thermodenuder, Aerosol Sci Tech, 46, 22-30, 10.1080/02786826.2011.602762, 2012.

Sato, K., Takami, A., Isozaki, T., Hikida, T., Shimono, A., and Imamura, T.: Mass spectrometric study of secondary organic aerosol formed from the photo-oxidation of aromatic hydrocarbons, Atmospheric Environment, 44, 1080-1087, dx.doi.org/10.1016/j.atmosenv.2009.12.013, 2010.

Sato, K., Nakao, S., Clark, C. H., Qi, L., and Cocker, D. R.: Secondary organic aerosol formation from the photooxidation of isoprene, 1,3-butadiene, and 2,3-dimethyl-1,3-butadiene under high NOx conditions, Atmos Chem Phys, 11, 7301-7317, DOI 10.5194/acp-11-7301-2011, 2011.

Schichtel, B. A., Malm, W. C., Bench, G., Fallon, S., McDade, C. E., Chow, J. C., and Watson, J. G.: Fossil and contemporary fine particulate carbon fractions at 12 rural and urban sites in the United States, Journal of Geophysical Research: Atmospheres, 113, D02311, 10.1029/2007JD008605, 2008.

Schneider, J., Weimer, S., Drewnick, F., Borrmann, S., Helas, G., Gwaze, P., Schmid, O., Andreae, M. O., and Kirchner, U.: Mass spectrometric analysis and aerodynamic properties of various types of combustion-related aerosol particles, Int J Mass Spectrom, 258, 37-49, dx.doi.org/10.1016/j.ijms.2006.07.008, 2006.

Schwantes, R. H., Teng, A. P., Nguyen, T. B., Coggon, M. M., Crounse, J. D., St. Clair, J. M., Zhang, X., Schilling, K. A., Seinfeld, J. H., and Wennberg, P. O.: Isoprene NO3 Oxidation Products from the RO2 + HO2 Pathway, The Journal of Physical Chemistry A, 10.1021/acs.jpca.5b06355, 2015.

Schwarz, J. P., Gao, R. S., Fahey, D. W., Thomson, D. S., Watts, L. A., Wilson, J. C., Reeves, J. M., Darbeheshti, M., Baumgardner, D. G., Kok, G. L., Chung, S. H., Schulz, M., Hendricks, J., Lauer, A., Karcher, B., Slowik, J. G., Rosenlof, K. H., Thompson, T. L., Langford, A. O., Loewenstein, M., and Aikin, K. C.: Single-particle measurements of midlatitude black carbon and light-scattering aerosols from the boundary layer to the lower stratosphere, J Geophys Res-Atmos, 111, Doi 10.1029/2006jd007076, 2006.

Setyan, A., Zhang, Q., Merkel, M., Knighton, W. B., Sun, Y., Song, C., Shilling, J. E., Onasch, T. B., Herndon, S. C., Worsnop, D. R., Fast, J. D., Zaveri, R. A., Berg, L. K., Wiedensohler, A., Flowers, B. A., Dubey, M. K., and Subramanian, R.: Characterization of submicron particles influenced by mixed biogenic and anthropogenic emissions using high-resolution aerosol mass spectrometry: results from CARES, Atmos Chem Phys, 12, 8131-8156, DOI 10.5194/acp-12-8131-2012, 2012.

Shaw, M. D., Lee, J. D., Davison, B., Vaughan, A., Purvis, R. M., Harvey, A., Lewis, A. C., and Hewitt, C. N.: Airborne determination of the temporo-spatial distribution of benzene, toluene, nitrogen oxides and ozone in the boundary layer across Greater

London, UK, Atmos. Chem. Phys., 15, 5083-5097, 10.5194/acp-15-5083-2015, 2015.

Shilling, J. E., Chen, Q., King, S. M., Rosenoern, T., Kroll, J. H., Worsnop, D. R., DeCarlo, P. F., Aiken, A. C., Sueper, D., Jimenez, J. L., and Martin, S. T.: Loading-dependent elemental composition of alpha-pinene SOA particles, Atmos Chem Phys, 9, 771-782, 2009.

Shilling, J. E., Zaveri, R. A., Fast, J. D., Kleinman, L., Alexander, M. L., Canagaratna, M. R., Fortner, E., Hubbe, J. M., Jayne, J. T., Sedlacek, A., Setyan, A., Springston, S., Worsnop, D. R., and Zhang, Q.: Enhanced SOA formation from mixed anthropogenic and biogenic emissions during the CARES campaign, Atmos Chem Phys, 13, 2091-2113, DOI 10.5194/acp-13-2091-2013, 2013.

Sillman, S.: Ozone production efficiency and loss of NOx in power plant plumes: Photochemical model and interpretation of measurements in Tennessee, J Geophys Res-Atmos, 105, 9189-9202, Doi 10.1029/1999jd901014, 2000.

Slowik, J. G., Vlasenko, A., McGuire, M., Evans, G. J., and Abbatt, J. P. D.: Simultaneous factor analysis of organic particle and gas mass spectra: AMS and PTR-MS measurements at an urban site, Atmos Chem Phys, 10, 1969-1988, 2010.

Slowik, J. G., Brook, J., Chang, R. Y. W., Evans, G. J., Hayden, K., Jeong, C. H., Li, S. M., Liggio, J., Liu, P. S. K., McGuire, M., Mihele, C., Sjostedt, S., Vlasenko, A., and Abbatt, J. P. D.: Photochemical processing of organic aerosol at nearby continental sites: contrast between urban plumes and regional aerosol, Atmos Chem Phys, 11, 2991-3006, DOI 10.5194/acp-11-2991-2011, 2011.

Sommariva, R., de Gouw, J. A., Trainer, M., Atlas, E., Goldan, P. D., Kuster, W. C., Warneke, C., and Fehsenfeld, F. C.: Emissions and photochemistry of oxygenated VOCs in urban plumes in the Northeastern United States, Atmos. Chem. Phys., 11, 7081-7096, 10.5194/acp-11-7081-2011, 2011.

Song, C., Na, K., Warren, B., Malloy, Q., and Cocker, D. R.: Impact of propene on secondary organic aerosol formation from m-xylene, Environ Sci Technol, 41, 6990-6995, Doi 10.1021/Es062279a, 2007.

Spittler, M., Barnes, I., Bejan, I., Brockmann, K. J., Benter, T., and Wirtz, K.: Reactions of NO3 radicals with limonene and alpha-pinene: Product and SOA formation, Atmospheric Environment, 40, S116-S127, 10.1016/j.atmosenv.2005.09.093, 2006.

Spracklen, D. V., Jimenez, J. L., Carslaw, K. S., Worsnop, D. R., Evans, M. J., Mann, G. W., Zhang, Q., Canagaratna, M. R., Allan, J., Coe, H., McFiggans, G., Rap, A., and Forster, P.: Aerosol mass spectrometer constraint on the global secondary organic

aerosol budget, Atmos. Chem. Phys., 11, 12109-12136, 10.5194/acp-11-12109-2011, 2011.

Sprengnether, M., Demerjian, K. L., Donahue, N. M., and Anderson, J. G.: Product analysis of the OH oxidation of isoprene and 1,3-butadiene in the presence of NO, J Geophys Res-Atmos, 107, Artn 4269 Doi 10.1029/2001jd000716, 2002.

Stanier, C. O., Pathak, R. K., and Pandis, S. N.: Measurements of the volatility of aerosols from alpha-piniene ozonolysis, Environ Sci Technol, 41, 2756-2763, Doi 10.1021/Es0519280, 2007.

Stephens, M., Turner, N., and Sandberg, J.: Particle identification by laser-induced incandescence in a solid-state laser cavity, Appl Optics, 42, 3726-3736, Doi 10.1364/Ao.42.003726, 2003.

Sullivan, A. P., Peltier, R. E., Brock, C. A., de Gouw, J. A., Holloway, J. S., Warneke, C., Wollny, A. G., and Weber, R. J.: Airborne measurements of carbonaceous aerosol soluble in water over northeastern United States: Method development and an investigation into water-soluble organic carbon sources, Journal of Geophysical Research: Atmospheres, 111, n/a-n/a, 10.1029/2006JD007072, 2006.

Sun, Y. L., Zhang, Q., Schwab, J. J., Chen, W. N., Bae, M. S., Hung, H. M., Lin, Y. C., Ng, N. L., Jayne, J., Massoli, P., Williams, L. R., and Demerjian, K. L.: Characterization of near-highway submicron aerosols in New York City with a high-resolution aerosol mass spectrometer, Atmos. Chem. Phys., 12, 2215-2227, 10.5194/acp-12-2215-2012, 2012a.

Sun, Y. L., Zhang, Q., Schwab, J. J., Yang, T., Ng, N. L., and Demerjian, K. L.: Factor analysis of combined organic and inorganic aerosol mass spectra from high resolution aerosol mass spectrometer measurements, Atmos. Chem. Phys., 12, 8537-8551, 10.5194/acp-12-8537-2012, 2012b.

Surratt, J. D., Murphy, S. M., Kroll, J. H., Ng, N. L., Hildebrandt, L., Sorooshian, A., Szmigielski, R., Vermeylen, R., Maenhaut, W., Claeys, M., Flagan, R. C., and Seinfeld, J. H.: Chemical composition of secondary organic aerosol formed from the photooxidation of isoprene, J Phys Chem A, 110, 9665-9690, Doi 10.1021/Jp061734m, 2006.

Surratt, J. D., Lewandowski, M., Offenberg, J. H., Jaoui, M., Kleindienst, T. E., Edney, E. O., and Seinfeld, J. H.: Effect of acidity on secondary organic aerosol formation from isoprene, Environ Sci Technol, 41, 5363-5369, Doi 10.1021/Es0704176, 2007.

Surratt, J. D., Gomez-Gonzalez, Y., Chan, A. W. H., Vermeylen, R., Shahgholi, M., Kleindienst, T. E., Edney, E. O., Offenberg, J. H., Lewandowski, M., Jaoui, M.,

Maenhaut, W., Claeys, M., Flagan, R. C., and Seinfeld, J. H.: Organosulfate formation in biogenic secondary organic aerosol, J Phys Chem A, 112, 8345-8378, Doi 10.1021/Jp802310p, 2008.

Surratt, J. D., Chan, A. W. H., Eddingsaas, N. C., Chan, M. N., Loza, C. L., Kwan, A. J., Hersey, S. P., Flagan, R. C., Wennberg, P. O., and Seinfeld, J. H.: Reactive intermediates revealed in secondary organic aerosol formation from isoprene, P Natl Acad Sci USA, 107, 6640-6645, DOI 10.1073/pnas.0911114107, 2010.

Tang, M. J., Shiraiwa, M., Pöschl, U., Cox, R. A., and Kalberer, M.: Compilation and evaluation of gas phase diffusion coefficients of reactive trace gases in the atmosphere: Volume 2. Diffusivities of organic compounds, pressure-normalised mean free paths, and average Knudsen numbers for gas uptake calculations, Atmos. Chem. Phys., 15, 5585-5598, 10.5194/acp-15-5585-2015, 2015.

Tanner, R. L., Olszyna, K. J., Edgerton, E. S., Knipping, E., and Shaw, S. L.: Searching for evidence of acid-catalyzed enhancement of secondary organic aerosol formation using ambient aerosol data, Atmospheric Environment, 43, 3440-3444, DOI 10.1016/j.atmosenv.2009.03.045, 2009.

Tritscher, T., Dommen, J., DeCarlo, P. F., Gysel, M., Barmet, P. B., Praplan, A. P., Weingartner, E., Prévôt, A. S. H., Riipinen, I., Donahue, N. M., and Baltensperger, U.: Volatility and hygroscopicity of aging secondary organic aerosol in a smog chamber, Atmos. Chem. Phys., 11, 11477-11496, 10.5194/acp-11-11477-2011, 2011.

Tsigaridis, K., Daskalakis, N., Kanakidou, M., Adams, P. J., Artaxo, P., Bahadur, R., Balkanski, Y., Bauer, S. E., Bellouin, N., Benedetti, A., Bergman, T., Berntsen, T. K., Beukes, J. P., Bian, H., Carslaw, K. S., Chin, M., Curci, G., Diehl, T., Easter, R. C., Ghan, S. J., Gong, S. L., Hodzic, A., Hoyle, C. R., Iversen, T., Jathar, S., Jimenez, J. L., Kaiser, J. W., Kirkevåg, A., Koch, D., Kokkola, H., Lee, Y. H., Lin, G., Liu, X., Luo, G., Ma, X., Mann, G. W., Mihalopoulos, N., Morcrette, J. J., Müller, J. F., Myhre, G., Myriokefalitakis, S., Ng, N. L., O'Donnell, D., Penner, J. E., Pozzoli, L., Pringle, K. J., Russell, L. M., Schulz, M., Sciare, J., Seland, Ø., Shindell, D. T., Sillman, S., Skeie, R. B., Spracklen, D., Stavrakou, T., Steenrod, S. D., Takemura, T., Tiitta, P., Tilmes, S., Tost, H., van Noije, T., van Zyl, P. G., von Salzen, K., Yu, F., Wang, Z., Wang, Z., Zaveri, R. A., Zhang, H., Zhang, K., Zhang, Q., and Zhang, X.: The AeroCom evaluation and intercomparison of organic aerosol in global models, Atmos. Chem. Phys., 14, 10845-10895, 10.5194/acp-14-10845-2014, 2014.

Tuazon, E. C., and Atkinson, R.: A Product Study of the Gas-Phase Reaction of Isoprene with the Oh Radical in the Presence of Nox, Int J Chem Kinet, 22, 1221-1236, DOI 10.1002/kin.550221202, 1990.

Tuazon, E. C., Atkinson, R., and Aschmann, S. M.: Kinetics and Products of the Gas-Phase Reactions of the Oh Radical and O3 with Allyl Chloride and Benzyl-Chloride at Room-Temperature, Int J Chem Kinet, 22, 981-998, DOI 10.1002/kin.550220909, 1990.

Ulbrich, I. M., Canagaratna, M. R., Zhang, Q., Worsnop, D. R., and Jimenez, J. L.: Interpretation of organic components from Positive Matrix Factorization of aerosol mass spectrometric data, Atmos. Chem. Phys., 9, 2891-2918, 10.5194/acp-9-2891-2009, 2009.

Verma, V., Fang, T., Guo, H., King, L., Bates, J. T., Peltier, R. E., Edgerton, E., Russell, A. G., and Weber, R. J.: Reactive oxygen species associated with water-soluble PM2.5 in the southeastern United States: spatiotemporal trends and source apportionment, Atmos. Chem. Phys., 14, 12915-12930, 10.5194/acp-14-12915-2014, 2014.

Verma, V., Fang, T., Xu, L., Peltier, R. E., Russell, A. G., Ng, N. L., and Weber, R. J.: Organic Aerosols Associated with the Generation of Reactive Oxygen Species (ROS) by Water-Soluble PM2.5, Environ Sci Technol, 10.1021/es505577w, 2015.

Villenave, E., Lesclaux, R., Seefeld, S., and Stockwell, W. R.: Kinetics and atmospheric implications of peroxy radical cross reactions involving the CH3C(O)O-2 radical, J Geophys Res-Atmos, 103, 25273-25285, Doi 10.1029/98jd00926, 1998.

Virkkula, A., Mäkelä, T., Hillamo, R., Yli-Tuomi, T., Hirsikko, A., Hämeri, K., and Koponen, I. K.: A Simple Procedure for Correcting Loading Effects of Aethalometer Data, J Air Waste Manage, 57, 1214-1222, 10.3155/1047-3289.57.10.1214, 2007.

Visser, S., Slowik, J. G., Furger, M., Zotter, P., Bukowiecki, N., Canonaco, F., Flechsig, U., Appel, K., Green, D. C., Tremper, A. H., Young, D. E., Williams, P. I., Allan, J. D., Coe, H., Williams, L. R., Mohr, C., Xu, L., Ng, N. L., Nemitz, E., Barlow, J. F., Halios, C. H., Fleming, Z. L., Baltensperger, U., and Prévôt, A. S. H.: Advanced source apportionment of size-resolved trace elements at multiple sites in London during winter, Atmos. Chem. Phys. Discuss., 15, 14733-14781, 10.5194/acpd-15-14733-2015, 2015a.

Visser, S., Slowik, J. G., Furger, M., Zotter, P., Bukowiecki, N., Dressler, R., Flechsig, U., Appel, K., Green, D. C., Tremper, A. H., Young, D. E., Williams, P. I., Allan, J. D., Herndon, S. C., Williams, L. R., Mohr, C., Xu, L., Ng, N. L., Detournay, A., Barlow, J. F., Halios, C. H., Fleming, Z. L., Baltensperger, U., and Prévôt, A. S. H.: Kerb and urban increment of highly time-resolved trace elements in PM10, PM2.5 and PM1.0 winter aerosol in London during ClearfLo 2012, Atmos. Chem. Phys., 15, 2367-2386, 10.5194/acp-15-2367-2015, 2015b.

Wang, W., Kourtchev, I., Graham, B., Cafmeyer, J., Maenhaut, W., and Claeys, M.: Characterization of oxygenated derivatives of isoprene related to 2-methyltetrols in Amazonian aerosols using trimethylsilylation and gas chromatography/ion trap mass spectrometry, Rapid Commun Mass Sp, 19, 1343-1351, Doi 10.1002/Rcm.1940, 2005.

Warneke, C., Trainer, M., de Gouw, J. A., Parrish, D. D., Fahey, D. W., Ravishankara, A. R., Middlebrook, A. M., Brock, C. A., Roberts, J. M., Brown, S. S., Neuman, J. A., Lerner, B. M., Lack, D., Law, D., Huebler, G., Pollack, I., Sjostedt, S., Ryerson, T. B., Gilman, J. B., Liao, J., Holloway, J., Peischl, J., Nowak, J. B., Aikin, K., Min, K. E., Washenfelder, R. A., Graus, M. G., Richardson, M., Markovic, M. Z., Wagner, N. L., Welti, A., Veres, P. R., Edwards, P., Schwarz, J. P., Gordon, T., Dube, W. P., McKeen, S., Brioude, J., Ahmadov, R., Bougiatioti, A., Lin, J., Nenes, A., Wolfe, G. M., Hanisco, T. F., Lee, B. H., Lopez-Hilfiker, F. D., Thornton, J. A., Keutsch, F. N., Kaiser, J., Mao, J., and Hatch, C.: Instrumentation and Measurement Strategy for the NOAA SENEX Aircraft Campaign as Part of the Southeast Atmosphere Study 2013, Atmos. Meas. Tech. Discuss., 2016, 1-39, 10.5194/amt-2015-388, 2016.

Washenfelder, R. A., Attwood, A. R., Brock, C. A., Guo, H., Xu, L., Weber, R. J., Ng, N. L., Allen, H. M., Ayres, B. R., Baumann, K., Cohen, R. C., Draper, D. C., Duffey, K. C., Edgerton, E., Fry, J. L., Hu, W. W., Jimenez, J. L., Palm, B. B., Romer, P., Stone, E. A., Wooldridge, P. J., and Brown, S. S.: Biomass burning dominates brown carbon absorption in the rural southeastern United States, Geophysical Research Letters, 2014GL062444, 10.1002/2014GL062444, 2015.

Weber, R.: Short-Term Temporal Variation in PM2.5 Mass and Chemical Composition during the Atlanta Supersite Experiment, 1999, J Air Waste Manage, 53, 84-91, 10.1080/10473289.2003.10466123, 2003.

Weber, R., Orsini, D., Duan, Y., Baumann, K., Kiang, C. S., Chameides, W., Lee, Y. N., Brechtel, F., Klotz, P., Jongejan, P., ten Brink, H., Slanina, J., Boring, C. B., Genfa, Z., Dasgupta, P., Hering, S., Stolzenburg, M., Dutcher, D. D., Edgerton, E., Hartsell, B., Solomon, P., and Tanner, R.: Intercomparison of near real time monitors of PM2.5 nitrate and sulfate at the U.S. Environmental Protection Agency Atlanta Supersite, Journal of Geophysical Research: Atmospheres, 108, 8421, 10.1029/2001JD001220, 2003.

Weber, R. J., Orsini, D., Daun, Y., Lee, Y. N., Klotz, P. J., and Brechtel, F.: A particle-into-liquid collector for rapid measurement of aerosol bulk chemical composition, Aerosol Sci Tech, 35, 718-727, Doi 10.1080/02786820152546761, 2001.

Weber, R. J., Sullivan, A. P., Peltier, R. E., Russell, A., Yan, B., Zheng, M., de Gouw, J., Warneke, C., Brock, C., Holloway, J. S., Atlas, E. L., and Edgerton, E.: A study of secondary organic aerosol formation in the anthropogenic-influenced southeastern

United States, J Geophys Res-Atmos, 112, Artn D13302 Doi 10.1029/2007jd008408, 2007.

Wennberg, P.: Let's abandon the high NOx and low NOx terminology, IGACnews, 2013.

Wert, B. P., Trainer, M., Fried, A., Ryerson, T. B., Henry, B., Potter, W., Angevine, W. M., Atlas, E., Donnelly, S. G., Fehsenfeld, F. C., Frost, G. J., Goldan, P. D., Hansel, A., Holloway, J. S., Hubler, G., Kuster, W. C., Nicks, D. K., Neuman, J. A., Parrish, D. D., Schauffler, S., Stutz, J., Sueper, D. T., Wiedinmyer, C., and Wisthaler, A.: Signatures of terminal alkene oxidation in airborne formaldehyde measurements during TexAQS 2000, J Geophys Res-Atmos, 108, Artn 4104
10.1029/2002jd002502, 2003.

Whalen, D. L.: Buffer catalysis in epoxide hydrolyses, J Am Chem Soc, 95, 3432-3434, 10.1021/ja00791a086, 1973.

Williams, L., Herndon, S., Jayne, J., Freedman, A., Brooks, B., Franklin, J. P., Massoli, P., Fortner, E., Chhabra, P. S., Zahniser, M. S., Stark, H., canagaratna, M., Onasch, T., Worsnop, D., Ng, N. L., Xu, L., Knighton, B., Aiken, A., Gorkowski, K. J., Liu, S., Martin, A. T., Coulter, R., Lopez-Hilfiker, F. D., Mohr, C., Thornton, J., Visser, S., Furger, M., Zotter, P., and Prevot, A. S. H.: Characterization of black carbon containing particles in rural wintertime UK with an Aerodyne soot particle aerosol mass spectrometer (SP-AMS), Atmos. Chem. Phys. Discuss., in preparation, 2015.

Winquist, A., Kirrane, E., Klein, M., Strickland, M., Darrow, L. A., Sarnat, S. E., Gass, K., Mulholland, J., Russell, A., and Tolbert, P.: Joint Effects of Ambient Air Pollutants on Pediatric Asthma Emergency Department Visits in Atlanta, 1998–2004, Epidemiology, 25, 666-673, 10.1097/ede.0000000000000146, 2014.

Wolfe, G. M., Kaiser, J., Hanisco, T. F., Keutsch, F. N., de Gouw, J. A., Gilman, J. B., Graus, M., Hatch, C. D., Holloway, J., Horowitz, L. W., Lee, B. H., Lerner, B. M., Lopez-Hilifiker, F., Mao, J., Marvin, M. R., Peischl, J., Pollack, I. B., Roberts, J. M., Ryerson, T. B., Thornton, J. A., Veres, P. R., and Warneke, C.: Formaldehyde production from isoprene oxidation across NOx regimes, Atmos. Chem. Phys. Discuss., 15, 31587-31620, 10.5194/acpd-15-31587-2015, 2015.

Worton, D. R., Goldstein, A. H., Farmer, D. K., Docherty, K. S., Jimenez, J. L., Gilman, J. B., Kuster, W. C., de Gouw, J., Williams, B. J., Kreisberg, N. M., Hering, S. V., Bench, G., McKay, M., Kristensen, K., Glasius, M., Surratt, J. D., and Seinfeld, J. H.: Origins and composition of fine atmospheric carbonaceous aerosol in the Sierra Nevada Mountains, California, Atmos. Chem. Phys., 11, 10219-10241, 10.5194/acp-11-10219-2011, 2011.

Worton, D. R., Surratt, J. D., LaFranchi, B. W., Chan, A. W. H., Zhao, Y. L., Weber, R. J., Park, J. H., Gilman, J. B., de Gouw, J., Park, C., Schade, G., Beaver, M., St Clair,

J. M., Crounse, J., Wennberg, P., Wolfe, G. M., Harrold, S., Thornton, J. A., Farmer, D. K., Docherty, K. S., Cubison, M. J., Jimenez, J. L., Frossard, A. A., Russell, L. M., Kristensen, K., Glasius, M., Mao, J. Q., Ren, X. R., Brune, W., Browne, E. C., Pusede, S. E., Cohen, R. C., Seinfeld, J. H., and Goldsteint, A. H.: Observational Insights into Aerosol Formation from Isoprene, Environ Sci Technol, 47, 11403-11413, Doi 10.1021/Es4011064, 2013.

Xu, L., Kollman, M. S., Song, C., Shilling, J. E., and Ng, N. L.: Effects of NOx on the Volatility of Secondary Organic Aerosol from Isoprene Photooxidation, Environ Sci Technol, 48, 2253-2262, 10.1021/es404842g, 2014.

Xu, L., Guo, H., Boyd, C. M., Klein, M., Bougiatioti, A., Cerully, K. M., Hite, J. R., Isaacman-VanWertz, G., Kreisberg, N. M., Knote, C., Olson, K., Koss, A., Goldstein, A. H., Hering, S. V., de Gouw, J., Baumann, K., Lee, S.-H., Nenes, A., Weber, R. J., and Ng, N. L.: Effects of anthropogenic emissions on aerosol formation from isoprene and monoterpenes in the southeastern United States, Proceedings of the National Academy of Sciences, 112, 37-42, 10.1073/pnas.1417609112, 2015a.

Xu, L., Suresh, S., Guo, H., Weber, R. J., and Ng, N. L.: Aerosol characterization over the southeastern United States using high-resolution aerosol mass spectrometry: spatial and seasonal variation of aerosol composition and sources with a focus on organic nitrates, Atmos. Chem. Phys., 15, 7307-7336, 10.5194/acp-15-7307-2015, 2015b.

Xu, L., Suresh, S., Guo, H., Weber, R. J., and Ng, N. L.: Aerosol characterization over the southeastern United States using high resolution aerosol mass spectrometry: spatial and seasonal variation of aerosol composition, sources, and organic nitrates, Atmos. Chem. Phys. Discuss., 15, 10479-10552, 10.5194/acpd-15-10479-2015, 2015c.

Yee, L. D., Craven, J. S., Loza, C. L., Schilling, K. A., Ng, N. L., Canagaratna, M. R., Ziemann, P. J., Flagan, R. C., and Seinfeld, J. H.: Secondary Organic Aerosol Formation from Low-NOx Photooxidation of Dodecane: Evolution of Multigeneration Gas-Phase Chemistry and Aerosol Composition, J Phys Chem A, 116, 6211-6230, Doi 10.1021/Jp211531h, 2012.

Yin, J., Harrison, R. M., Chen, Q., Rutter, A., and Schauer, J. J.: Source apportionment of fine particles at urban background and rural sites in the UK atmosphere, Atmospheric Environment, 44, 841-851, http://dx.doi.org/10.1016/j.atmosenv.2009.11.026, 2010.

Yin, J., Cumberland, S. A., Harrison, R. M., Allan, J., Young, D. E., Williams, P. I., and Coe, H.: Receptor modelling of fine particles in southern England using CMB including comparison with AMS-PMF factors, Atmos. Chem. Phys., 15, 2139-2158, 10.5194/acp-15-2139-2015, 2015.

Young, D. E., Allan, J. D., Williams, P. I., Green, D. C., Flynn, M. J., Harrison, R. M., Yin, J., Gallagher, M. W., and Coe, H.: Investigating the annual behaviour of submicron secondary inorganic and organic aerosols in London, Atmos. Chem. Phys., 15, 6351-6366, 10.5194/acp-15-6351-2015, 2015a.

Young, D. E., Allan, J. D., Williams, P. I., Green, D. C., Harrison, R. M., Yin, J., Flynn, M. J., Gallagher, M. W., and Coe, H.: Investigating a two-component model of solid fuel organic aerosol in London: processes, PM1 contributions, and seasonality, Atmos. Chem. Phys., 15, 2429-2443, 10.5194/acp-15-2429-2015, 2015b.

Zhang, Q., Alfarra, M. R., Worsnop, D. R., Allan, J. D., Coe, H., Canagaratna, M. R., and Jimenez, J. L.: Deconvolution and Quantification of Hydrocarbon-like and Oxygenated Organic Aerosols Based on Aerosol Mass Spectrometry, Environ Sci Technol, 39, 4938-4952, 10.1021/es048568l, 2005.

Zhang, Q., Jimenez, J. L., Canagaratna, M. R., Allan, J. D., Coe, H., Ulbrich, I., Alfarra, M. R., Takami, A., Middlebrook, A. M., Sun, Y. L., Dzepina, K., Dunlea, E., Docherty, K., DeCarlo, P. F., Salcedo, D., Onasch, T., Jayne, J. T., Miyoshi, T., Shimono, A., Hatakeyama, S., Takegawa, N., Kondo, Y., Schneider, J., Drewnick, F., Borrmann, S., Weimer, S., Demerjian, K., Williams, P., Bower, K., Bahreini, R., Cottrell, L., Griffin, R. J., Rautiainen, J., Sun, J. Y., Zhang, Y. M., and Worsnop, D. R.: Ubiquity and dominance of oxygenated species in organic aerosols in anthropogenically-influenced Northern Hemisphere midlatitudes, Geophysical Research Letters, 34, Artn L13801 Doi 10.1029/2007gl029979, 2007.

Zhang, Q., Jimenez, J. L., Canagaratna, M. R., Ulbrich, I. M., Ng, N. L., Worsnop, D. R., and Sun, Y. L.: Understanding atmospheric organic aerosols via factor analysis of aerosol mass spectrometry: a review, Anal Bioanal Chem, 401, 3045-3067, DOI 10.1007/s00216-011-5355-y, 2011.

Zhang, X., Hecobian, A., Zheng, M., Frank, N. H., and Weber, R. J.: Biomass burning impact on PM 2.5 over the southeastern US during 2007: integrating chemically speciated FRM filter measurements, MODIS fire counts and PMF analysis, Atmos. Chem. Phys., 10, 6839-6853, 10.5194/acp-10-6839-2010, 2010.

Zhang, X., Liu, Z., Hecobian, A., Zheng, M., Frank, N. H., Edgerton, E. S., and Weber, R. J.: Spatial and seasonal variations of fine particle water-soluble organic carbon (WSOC) over the southeastern United States: implications for secondary organic aerosol formation, Atmos. Chem. Phys., 12, 6593-6607, 10.5194/acp-12-6593-2012, 2012.

Zhao, R., Mungall, E. L., Lee, A. K. Y., Aljawhary, D., and Abbatt, J. P. D.: Aqueous-phase photooxidation of levoglucosan – a mechanistic study using aerosol

time-of-flight chemical ionization mass spectrometry (Aerosol ToF-CIMS), Atmos. Chem. Phys., 14, 9695-9706, 10.5194/acp-14-9695-2014, 2014.

Zhao, R., Lee, A. K. Y., Huang, L., Li, X., Yang, F., and Abbatt, J. P. D.: Photochemical processing of aqueous atmospheric brown carbon, Atmos. Chem. Phys., 15, 6087-6100, 10.5194/acp-15-6087-2015, 2015.

Zheng, M., Cass, G. R., Schauer, J. J., and Edgerton, E. S.: Source Apportionment of PM2.5 in the Southeastern United States Using Solvent-Extractable Organic Compounds as Tracers, Environ Sci Technol, 36, 2361-2371, 10.1021/es011275x, 2002.

Zheng, M., Ke, L., Edgerton, E. S., Schauer, J. J., Dong, M., and Russell, A. G.: Spatial distribution of carbonaceous aerosol in the southeastern United States using molecular markers and carbon isotope data, Journal of Geophysical Research: Atmospheres, 111, D10S06, 10.1029/2005JD006777, 2006.

Zotter, P., El-Haddad, I., Zhang, Y., Hayes, P. L., Zhang, X., Lin, Y.-H., Wacker, L., Schnelle-Kreis, J., Abbaszade, G., Zimmermann, R., Surratt, J. D., Weber, R., Jimenez, J. L., Szidat, S., Baltensperger, U., and Prévôt, A. S. H.: Diurnal cycle of fossil and nonfossil carbon using radiocarbon analyses during CalNex, Journal of Geophysical Research: Atmospheres, 119, 2013JD021114, 10.1002/2013JD021114, 2014.